Delivery and Immunogenicity of Biopharmaceuticals for Vaccination or Therapy

Anne Marit de Groot

colofon

The research leading to these results has received support from the Innovative Medicines Initiative Joint Undertaking under grant agreement no. [115363], resources of which are composed of financial contribution from the European Union's Seventh Framework Programme (FP7/2007-2013) and EFPIA companies' in kind contribution.

Printing of this thesis was financially supported by the Infection & Immunity Center Utrecht.

layout, cover design: proefschrift-aio.nl

ISBN: 978-90-393-6887-9

Delivery and Immunogenicity of Biopharmaceuticals for Vaccination or Therapy

Aflevering en immunogeniciteit van biofarmaceutica voor vaccinatie en voor therapie

(met een samenvatting in het Nederlands)

Proefschrift

ter verkrijging van de graad van doctor aan de Universiteit Utrecht op gezag van de rector magnificus, prof.dr. G.J. van der Zwaan, ingevolge het besluit van het college voor promoties in het openbaar te verdedigen op donderdag 7 december 2017 des middags te 2.30 uur

door

Anne Marit de Groot

geboren op 2 juni 1988
te Naarden

Promotor:	Prof.dr. W. van Eden
Copromotoren:	Dr. E.J.A.M. Sijts
	Dr. F. Broere

Table of content

Ch1: **General Introduction** 9

Part I: Delivery and Immunogenicity of Biopharmaceuticals for Vaccination 23

Ch2: **Nanoporous Microneedle Arrays to Efficiently Induce Antibody Responses against Diphtheria and Tetanus Toxoid** 25

Ch3: **Hollow microneedle-mediated intradermal delivery of model vaccine antigen-loaded PLGA nanoparticles elicits protective T cell-mediated immunity to an intracellular bacterium** 45

Ch4: **Strategies to enhance immunogenicity of cDNA vaccine encoded antigens by modulation of antigen processing** 71

Part II: Delivery and Immunogenicity of Biopharmaceuticals for Therapy 95

Ch5: **Overcoming lipidoid-mediated TLR4 activation with lipidoid-polymer nanoparticles: *In silico* modelling and *in vitro* testing** 97

Ch6: **Surface coating of siRNA–peptidomimetic nano-self-assemblies with anionic lipid bilayers: enhanced gene silencing and reduced adverse effects *in vitro*** 127

Ch7: **Conjugation of Cell-Penetrating Peptides to Parathyroid Hormone Affects Its Structure, Potency, and Transepithelial Permeation** 155

Ch8: **Summarizing Discussion** 185

Ch9: **Addendum** 203
Abbreviations 204
Samenvatting in het Nederlands 205
Dankwoord / Acknowledgements 210
CV 213
List of Publications 214


1

General Introduction

1

Biopharmaceuticals

Biopharmaceuticals (or biologicals) are a new class of drugs produced by the biotechnology field and offer many advantages compared to classical small molecule synthetic drugs.[1] Biopharmaceuticals (BP) are from biological origine and may consist of proteins or peptides, nucleic acids such as RNA and DNA structures or other parts of microorganisms and cells.[2] The main difference between BP and small molecules is the complexity of the structure. BP offer more specificity on a variety of purposes. BPs show high specificity at receptor level or they can have a selective mode of action at gene level. Together this makes it possible to effectively intervene in disease pathways and makes it possible to either avoid or enhance immune activation.

When looking at therapeutic use, BP proteins such as monoclonal-antibodies are used to treat autoimmune diseases,[3] and insulin is used in diabetes patients. Next to that, BP nucleic acids such as small interfering RNAs (siRNA) are able to selectively silence expression of a variety proteins by capturing messenger RNA's before translation. Nucleic acids can be used in both anti-inflammatory therapy by silencing of Tumor Necrosis Factor α (TNFα) in autoimmune diseases or can act as antiviral mechanism by interference with viral reproduction. Multiple siRNAs have already entered clinical trials.[4]

On the other hand, when looking at immune activation, the use of proteins or peptides in vaccination has been established for quite some time. Most vaccines on the market are indeed based on either adjuvanted proteins, in subunit vaccines, or whole inactivated or attenuated pathogens. Next to that, research is done on using nucleic acids like DNA plasmid for vaccination purposes as well.

Delivery of biopharmaceuticals

Although the BPs have many advantages in specificity, this class of medicine also has some challenges. First, the biologics are larger in size and are not able to easily cross cell- or tissue membranes. Second, they have poor stability in solution or liquid phase and are subjected to enzymatic degradation, especially when taken orally.[5] Therefore, the main route of administration for BPs in development is currently parenteral injection, which often requires more organization and trained health care workers than oral application. And last, they could be recognized by the innate or adaptive immune system when corresponding to non-human structure. This is indeed desired when developing for vaccination purposes. On the other hand, the BP can lack immunogenicity, which is desired for therapeutic purposes. While many challenges lay in delivery and immunogenicity of BPs, it also gives opportunities in tuning the use of BPs.

In order to overcome delivery challenges and to prolong circulation time, new delivery mechanisms are necessary. For this purpose, drug delivery systems (DDS) are designed to protect the BP structure and to facilitate barrier crossing. These delivery systems are used to enhance uptake by cells and release their cargo (the BP) to the cytosol or over tissue

membranes. Many types of DDS are being designed, such as lipid liposomes, polymer structures, cell penetrating peptides or other micro- or nanoparticles.[6-8] Examples are depicted in **Figure 1.**

The current application route of BP is via injection, either intravenously or perhaps subcutaneously or intramuscularly and these routes will lead to fast distribution through the body, by bloodstream or lymphatic system. However, this also leads through the liver and large proportions of the administered cargo and DDS end in the liver and/or are secreted from the body. A way to circumvent clearance from the body, is by delivering the DDS with cargo directly to the target organ. For instance, by delivering anti-inflammatory medicine like anti-TNFα directly to the lungs via respiratory route when used for chronic asthma. Or by using another injection free route, such as delivering insulin protein via the oral route[9, 10]; and also vaccination strategies via the skin are in development.[11]

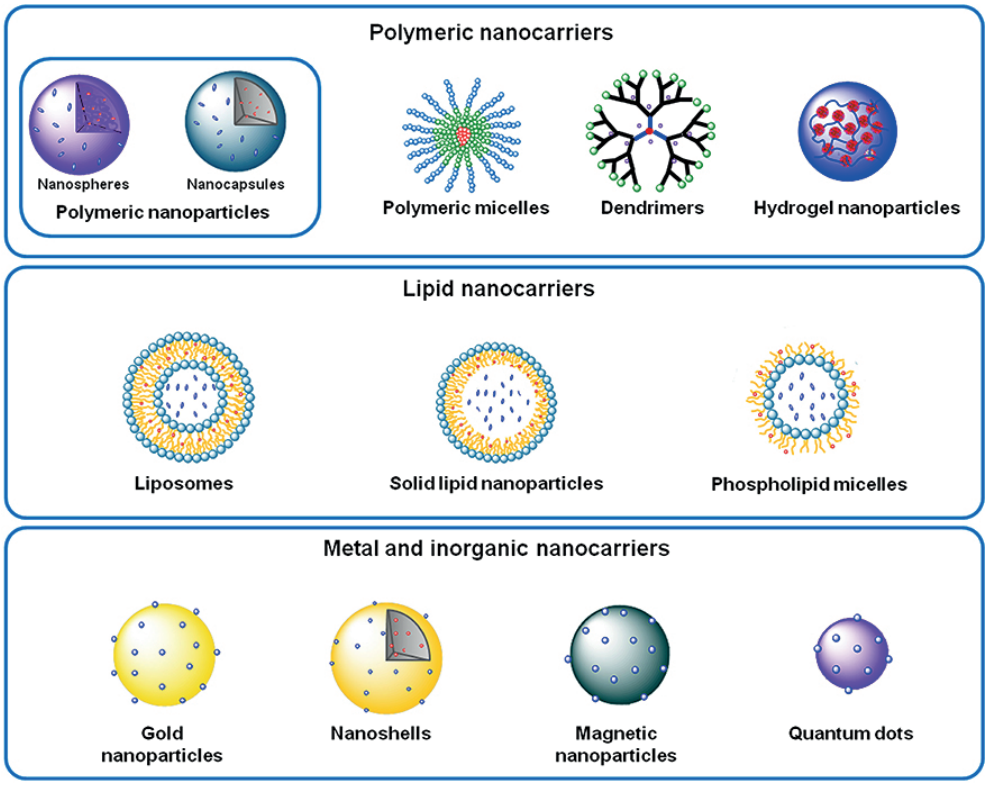

Figure 1: Example structures of drug delivery systems for delivery of biopharmaceuticals.
Adapted from Conniot et al.[12]

Immunogenicity of BP for therapeutic use

The use of DDS for delivery of BPs can, however, also alter interaction with the immune system. Activation or alteration is an unwanted effect when BPs are used for therapeutic end use, because several risks are to be considered. The uptake by antigen presenting cells leads to reduced bioavailability. The activation of either the innate or adaptive system can lead to production of inflammatory cytokines, leading to inflammation or even sepsis. The activation of the adaptive immune system can lead to production of antibodies towards either a protein-based cargo or towards the delivery system itself. And these antibodies could neutralize therapeutic effects (**Figure 2**). Overall, the interaction of the DDS or cargo with the immune system could change the pharmacokinetics and have possible side-effects.[13-15] All these risks could be enhanced when BPs in DDS are delivered repeatedly, and hypersensitivity could occur.

Immunogenicity assessment for therapeutic use

During the development of DDS, the assessment of immunogenicity is an important step in optimization. Looking directly via clinical trials at efficacy and safety in humans is, although effective and currently the only step required,[16] for ethical reasons not possible for the many BP formulations, in development phase. Therefore, immunogenicity assessment in earlier stages seems necessary. Via *in vivo* studies in animal models, the biodistribution, bioavailability and effect of the cargo could be assessed, and also possible side effects like inflammation could hopefully be detected. However, going directly *in vivo,* in murine models, for every optimization step in DDS optimization is costly, time consuming and ethically suboptimal. Thus, the use of *in vitro* systems as a first line screening for immunogenicity is necessary. With such assays one could select lead candidates in research phase of BP development. While effects on the total body, such as distribution or effects on a complex system like the adaptive immune system, are difficult to simulate *in vitro*, the initial activation of the immune system could be reproduced *in vitro*.

The first defense of the immune system is the innate immune system, consisting of phagocytic cells such as macrophages, dendritic cells and neutrophils. They have a variety of pathogen recognition receptors (PRR) on their surface in order to detect non-autologous structures. The Toll-Like-Receptor (TLR) family is one of the PRR families and upon recognition of foreign structures, like single stranded RNA, Lipopolysaccharide or CpG island in DNA, TLRs activate transcription factors. These transcription factors, NFκB and AP1, in turn activate the production of inflammatory cytokines, which either activate other innate phagocytic cells, or enhance maturation of antigen presenting cells. Professional antigen presenting cells (pAPC) are dendritic cells, macrophages and B cells. pAPC take up pathogens or foreign structures, process these into smaller antigens, and then present these antigens to the adaptive immune system. Activation of the adaptive immune system can occur when co-stimulatory molecules, such as CD40 or CD86, have

been upregulated on -, and cytokines are released by pAPCs. Lymphocytes of the adaptive immune system in turn enhance production and class switching of neutralizing antibodies, or may have direct lytic effects. While production of antibodies or activation of larger parts of the adaptive system cannot be measured in a simple high throughput *in vitro* assay, individual cells of the innate system can be cultured. In this thesis immunogenicity of DDS or their cargo is assessed by their ability to either activate human TLRs and their downstream transcription factors, or upregulate costimulatory markers on murine derived pAPCs. While this pAPC assessment measures a brother range of activation possibilities, i.e. there are multiple PRR families that can activate an APC, the human TLR assessment assay measures activation of a direct human receptor repertoire, and gives insight into the specific structures, able to activate specific TLR.

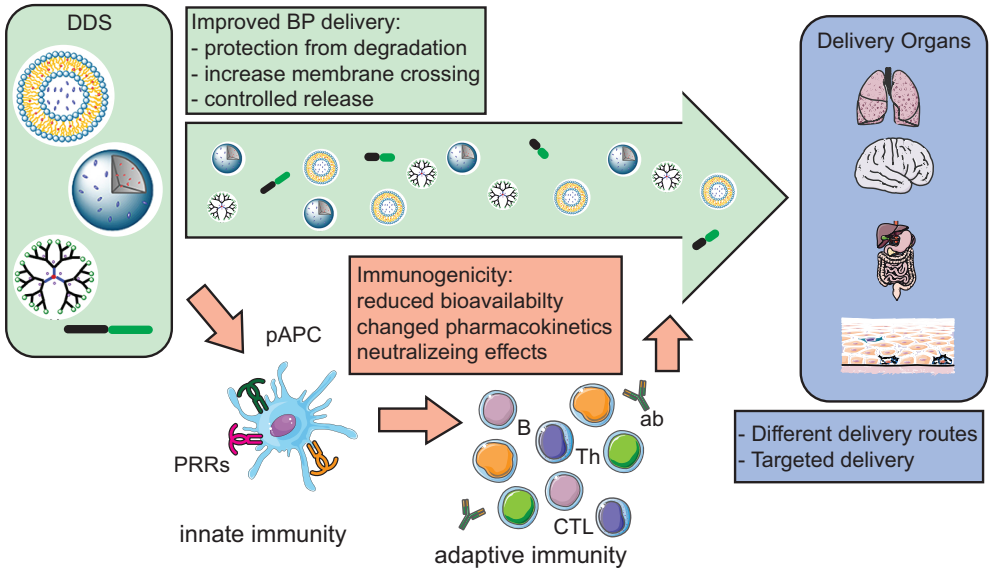

Figure 2: Graphical representation of delivery system, delivery routes and immunogenicity as investigated by EFPIA IMI funded consortium COMPACT. *Delivery systems include from top to bottom: liposomes, polymeric nanospheres, dendrimers, cell penetrating peptide. Scale is not appropriate and figure is adapted from Habraken.*[17] *DDS: drug delivery system, BP: biopharmaceutical, pAPC: professional antigen presenting cell, PRR: pathogen recognition receptors, CTL: cytotoxic T cell, Th: T helper cell, ab: antibody, B: B cell*

Immunogenicity of BP for vaccination

As mentioned before, BPs are not only used for therapeutics but also in vaccine design. The subunit vaccines currently available (for instance Diphtheria Tetanus Polio (DTP) in the Netherlands) consist of structures derived from micro-organisms. Here, an immune response against the BP is the desired effect and immunogenicity is of high importance. Most vaccines on the market are vaccines that depend on the induction of antibodies, e.g. a humoral response is necessary to clear the pathogens they are designed against. However, for intracellular pathogens and highly variable or mutating pathogens, a cellular cytotoxic T cell response is needed to eliminate the infected cells in order to clear the intruder from the body.

In order to activate memory $CD8^+$ T cells that could clear a pathogen, naïve $CD8^+$ T cells need to be activated during vaccination or immunization. Naïve $CD8^+$ T cells are activated after recognition of an epitope presented by pAPC, in context of appropriate costimulatory signals. Antigens and epitopes derive from pathogens that are processed by the cell and pathogens can either be endogenous or exogenous. Exogenous pathogens can be taken up by the pAPCs via endocytosis and the pathogens will be digested in the lysosomes by proteases. Now, the antigens produced from exogenous pathogens are exchanged with Clip-peptide, loaded in the presenting molecule MHCII present in the endosome, and the formed MHC-II-peptide-complex is directed from the endosome to the cell surface. In contrast, when a pathogen is intracellular (i.e. virus, intracellular bacterium), antigen processing occurs via the proteasome. The proteasome cleaves the antigens into smaller peptides that, after additional trimming in the ER or cytosol, now fit into the groove of presenting MHC-I molecules, if containing an appropriate MHC-I binding motif.[18-20] Only MHC-I-peptide epitope complexes are able to activate $CD8^+$ T cell responses , therefore, MHC-I presentation allows $CD8^+$ T cells to monitor the cellular content and react to foreign antigens (i.e. to infection). Indeed, $CD8^+$ T cell responses are necessary to clear pathogens that are in the cytosol (**Figure 3**).

When vaccinating with subunit vaccines, an extracellular protein is used for immunization. This would classically lead to degradation in the endosome and presentation via MHC-II on the surface. When aiming for cellular cytotoxic $CD8^+$ T cell responses, the subunit protein needs to escape the endosome into the cytosol, to be degraded by the proteasome and presented via MHC-I. One way to achieve this is by the use of DDS that are able to cross cellular membranes. DDS structures are larger than proteins and will be faster recognized by pAPCs, leading to enhanced phagocytosis, enhanced degradation and prolonged presentation of encapsulated antigens, in comparison to naked antigens, on the cell surface.[22, 23] Therefore DDS, such as PLGA nanoparticles, can be used as vaccine adjuvants to induce $CD8^+$ T cell responses.[24-26]

When vaccinating with nucleic acid structures, these need to be intracellular, or even in the nucleus, as well. The DNA or RNA structures used for vaccination will not be presented on the surface, but the proteins they encode will be presented similar as described above. Transcription and translation of DNA will occur inside the cell, thus intracellular delivery is necessary. Thus, DDS can also be used for delivery of DNA over the cell membrane, but other mechanisms to enhance uptake of DNA or enhance cross-presentation of encoded proteins are also described and include non DDS adjuvants or mechanic inflammation induction.

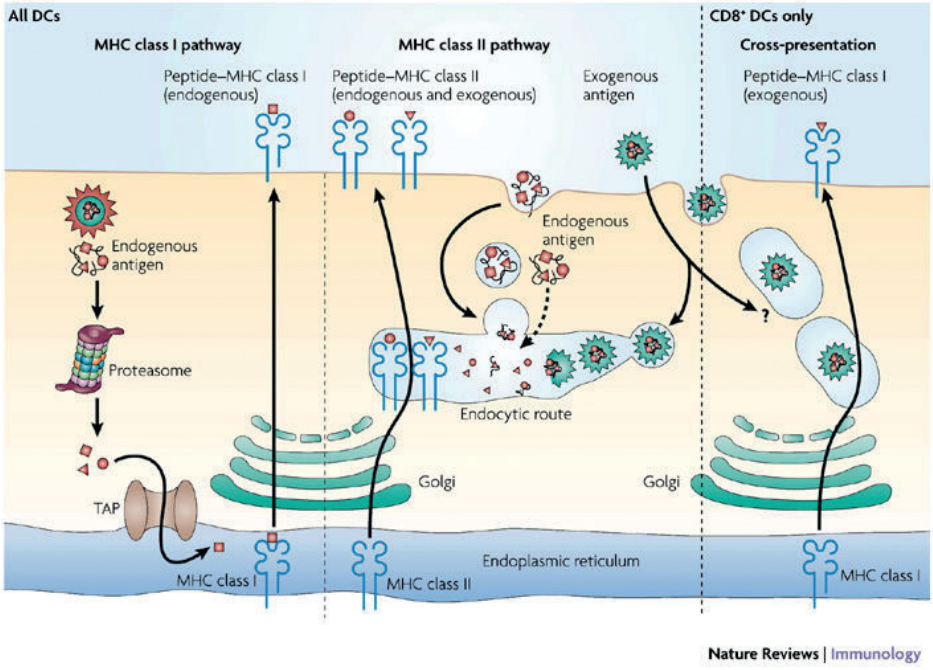

Figure 3: Antigen presentation pathway in dendritic cells.
Adapted from Villadangos et al.[21]

Intradermal immunization

Current vaccines are delivered intramuscularly or subcutaneously, but also other parenteral routes are being investigated for vaccine delivery. The skin has great potential as a delivery site, because it has a large surface, it is easy to reach, and delivery over the skin avoids degradation disadvantages from the gastro-intestinal tract.[27] Furthermore, many immune cells like pAPCs lay within the epidermis and dermis of the skin.[28, 29] However, the skin carefully protects the body from intruders via the stratum corneum. This outer layer forms a barrier towards all pathogens, unfortunately it forms also a barrier towards vaccine antigens. Crossing this barrier is essential for immune activation. The most widely used way to circumvent the stratum corneum to date is by intradermal injection (ID) using hypodermic needles, and this is applied already in clinical trials.[30, 31] However, traditional ID injection requires well-trained health care workers for precise and reproducible injections and the long needles will reach the nociceptors in the dermis, leading to pain induction. A minimal-invasive manner for barrier crossing is more desirable.[32] Using microneedles for the delivery of the vaccine antigens into the skin, as minimal invasive manner to cross the stratum corneum, shows great potential (**Figure 4**). After the release of the antigen for vaccination into the skin, the antigen is taken up by the Langerhans cells or dermal dendritic cells in the skin[28, 29] and the activated pAPCs will migrate to draining lymph nodes.[33] Here, the activation of lymphocytes occurs and an antibody response and cytotoxic T cell response can be induced. The activated T cells can migrate back to the site of immunization or later infection (tissue resident memory or effector memory), or the memory T cells can circulate systemically (central memory). [34]

Microneedles for intradermal immunization

Microneedles with needles in the micrometer range are being developed for vaccine delivery.[36] If they are combined in an array with multiple needle structures they are called microneedle arrays. Microneedles have the ability to penetrate the skin, either by pressing of the finger top to the array[34, 37] or by use of an applicator,[38] of which the latter gives more precise injections. After skin penetration, the antigens will be released into the skin. The use of microneedles for injection into the skin has the advantage of possible painless vaccination, because the nociceptors that register pain in the dermis will not be reached. Much research is done on different types of microneedles. They consist of either solid, dissolving, hollow or porous needle structures, all with their own mechanisms for antigen release.[11, 32, 36, 39, 40] The use of microneedles for dermal delivery of vaccines is investigated in many studies[11, 40] and for instance for subunit vaccines[41] and viral vaccines[42] induction of humoral responses has been described in experimental setting. Even first steps with DNA vaccination in the skin using microneedles are being set.[43, 44]

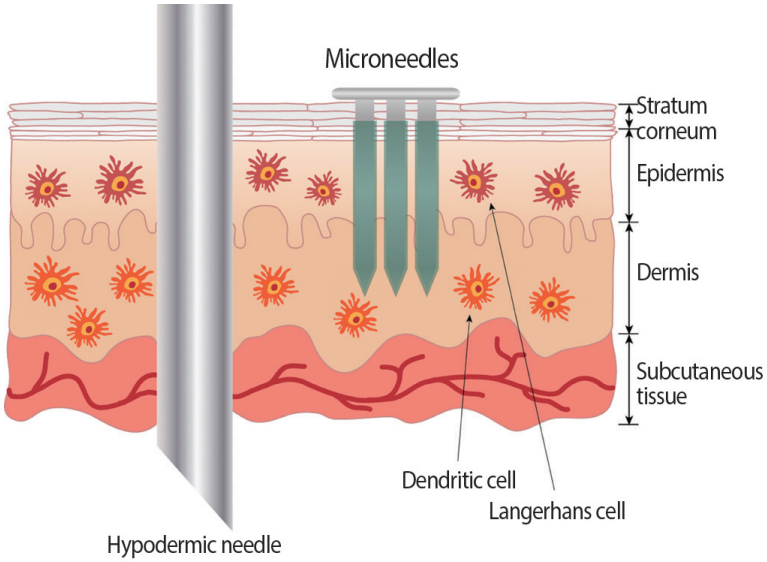

Figure 4: graphical representation of microneedle versus hypodermic traditional needle.
Adapted from Suh et al.[35]

Other methods for intradermal immunization

In addition, the use of a tattooing device to deliver formulations into the skin has also been described.[45] The vaccine formulation is coated on the small needles of a tattoo-device which forms pores in the skin at a certain speed. This will lead to the delivery of vaccine formulations into the skin. Modified tattooing devices have been used in medical research for the delivery of various materials to the skin for different purposes, and indeed also for the delivery of DNA for vaccination.[46-48]

Scope of this thesis

BP have expanded the range of options available for the treatment of complex diseases and DDS are designed to protect the BP structure and to facilitate barrier crossing. This thesis focuses on the challenges in delivery and imposed by immunogenicity of BPs and how this can be altered by the use of DDS.

Part one of this thesis is focusing on delivery and immunogenicity of BPs for intradermal vaccination. In **Chapter 2** a recently developed porous microneedle array is described and this chapter shows the successful induction of antibody responses towards two subunit vaccine antigens of the DTP vaccine. Inducing a Cytotoxic T cell response requires the presence of vaccine antigens in the cytosol of the cell and the use of a DDS could induce this membrane crossing. In **Chapter 3** nanoparticles loaded with a model antigen and a TLR agonist adjuvant are delivered using hollow microneedles. Here, a cytotoxic T cell response was induced that was protective against an intracellular bacterium.

Further, vaccine efficiency can be increased if the intracellular antigens become more immunogenic, i.e. would be more efficiently processed and presented to the adaptive immune system. Strategies to increase immunogenicity of vaccine antigens are described in **Chapter 4** and include introducing activating helper proteins and proteasome-favorable cleavage sites in vaccine formulations.

Part two of this thesis focuses on delivery and immunogenicity of BPs for therapeutic use. While effects on the adaptive immune system are difficult to determine, the initial activation of the innate immune system can be assessed *in vitro*. In chapters 5-7, three different delivery system are developed. In **Chapter 6 and 7**, two new DDS show full immune compatibility. One DDS is for the delivery of siRNA and one for the delivery of a therapeutic hormone. While in chapter 6 the DDS consisted of peptide-polymer hybrid nanoparticles, in **Chapter 5** a lipid-polymer hybrid combination was used for the delivery of siRNA. Combining the lipidoid structures with a polymer-based nanoparticle prevented the lipidoid-mediated activation of the innate immune system.

The results of this thesis are summarized and discussed in **Chapter 8**.

References

1 Walsh G. Biopharmaceuticals and biotechnology medicines: an issue of nomenclature. Eur J Pharm Sci. 2002;15(2):135-8.

2 Rader R. (Re)defining biopharmaceutical. Nat Biotechnol. 2008;26(7):743-51.

3 Johnson Leger C, El Proudfoot A, Johnson Léger C, Power C, Shomade G, Shaw J. Protein therapeutics--lessons learned and a view of the future. Expert Opin Biol Ther. 2006;6(1):1-7.

4 Castanotto D, Rossi J. The promises and pitfalls of RNA-interference-based therapeutics. Nature. 2009;457(7228):426-33.

5 Lipinski C, Lombardo F, Dominy B, Feeney P. Experimental and computational approaches to estimate solubility and permeability in drug discovery and development settings. Adv Drug Deliv Rev. 2012;64(supplement):4-17.

6 Chang H, Yeh M. Clinical development of liposome-based drugs: formulation, characterization, and therapeutic efficacy. Int J Nanomedicine. 2012;7:49-60.

7 Onoue S, Yamada S, Chan H. Nanodrugs: pharmacokinetics and safety. Int J Nanomedicine. 2014;9:1025-37.

8 Foged C, Nielsen H. Cell-penetrating peptides for drug delivery across membrane barriers. Expert Opin Drug Deliv. 2008;5(1):105-17.

9 Heinemann L, Jacques Y. Oral Insulin and Buccal Insulin: A Critical Reappraisal. J Diabetes Sci Technol. 2009;3((3)):568,-584.

10 Antosova Z, Mackova M, Kral V, Macek T. Therapeutic application of peptides and proteins: parenteral forever? Trends Biotechnol. 2009;27(11):628-35.

11 Kim Y, Park J, Prausnitz M. Microneedles for drug and vaccine delivery. Adv Drug Deliv Rev. 2012;64(14):1547-68.

12 Conniot J, Silva J, Fernandes J, Silva L, Gaspar R, Brocchini S, et al. Cancer immunotherapy: nanodelivery approaches for immune cell targeting and tracking. Front Chem. 2014;2:105-.

13 Weber RW. Adverse reactions to biological modifiers. Current Opinion Allergy Clinical Immunology. 2004;4(4):277,-83.

14 Jiskoot W, van Schie, Rianne M F, Carstens M, Schellekens H. Immunological risk of injectable drug delivery systems. Pharm Res. 2009;26(6):1303-14.

15 Sethu S, Govindappa K, Alhaidari M, Pirmohamed M, Park K, Sathish J. Immunogenicity to biologics: mechanisms, prediction and reduction. Arch Immunol Ther Exp (Warsz). 2012;60(5):331-44.

16 Committee for Medicinal Products for Human Use (CHMP). Guideline on Immunogenicity assessment of biotechnology-derived therapeutic proteins. European Medicine Agency; 2008. Report No.: EMEA/CHMP/BMWP/14327/2006.

17 Habraken T. Assessing the immunogenicity of Drug Delivery Systems. 2014.

18 Kloetzel PM. Antigen processing by the proteasome. Nat Rev Mol Cell Biol. 2001;2(3):179-87.

19 Rock K, York I, Saric T, Goldberg A. Protein degradation and the generation of MHC class I-presented peptides. Adv Immunol. 2002;80:1-70.

20 Sijts EJ, Kloetzel PM. The role of the proteasome in the generation of MHC class I ligands and immune responses. Cell Mol Life Sci. 2011 May;68(9):1491-502.

21 Villadangos J, Schnorrer P. Intrinsic and cooperative antigen-presenting functions of dendritic-cell subsets in vivo. Nat Rev Immunol. 2007;7(7):543-55.

22 Shen H, Ackerman A, Cody V, Giodini A, Hinson E, Cresswell P, et al. Enhanced and prolonged cross-presentation following endosomal escape of exogenous antigens encapsulated in biodegradable nanoparticles. Immunology. 2006;117(1):78-88.

23 Waeckerle Men Y, Allmen EU, Gander B, Scandella E, Schlosser E, Schmidtke G, et al. Encapsulation of proteins and peptides into biodegradable poly(D,L-lactide-co-glycolide) microspheres prolongs and enhances antigen presentation by human dendritic cells. Vaccine. 2006;24(11):1847-57.

24 Varypataki E, Silva A, Barnier Quer C, Collin N, Ossendorp F, Jiskoot W. Synthetic long peptide-based vaccine formulations for induction of cell mediated immunity: A comparative study of cationic liposomes and PLGA nanoparticles. J Control Release. 2016;226:98-106.

[25] Hamdy S, Molavi O, Ma Z, Haddadi A, Alshamsan A, Gobti Z, et al. Co-delivery of cancer-associated antigen and Toll-like receptor 4 ligand in PLGA nanoparticles induces potent CD8+ T cell-mediated anti-tumor immunity. Vaccine. 2008;26(39):5046-57.

[26] Waeckerle Men Y, Groettrup M. PLGA microspheres for improved antigen delivery to dendritic cells as cellular vaccines. Adv Drug Deliv Rev. 2005;57(3):475-82.

[27] Levin C, Perrin H, Combadiere B. Tailored immunity by skin antigen-presenting cells. Hum Vaccin Immunother. 2015;11(1):27-36.

[28] Fehres C, Garcia Vallejo J, Unger WWJ, van Kooyk Y. Skin-resident antigen-presenting cells: instruction manual for vaccine development. Front Immunol. 2013;4:157-.

[29] Zaric M, Lyubomska O, Poux C, Hanna ML, McCrudden MT, Malissen B, et al. Dissolving microneedle delivery of nanoparticle-encapsulated antigen elicits efficient cross-priming and th1 immune responses by murine langerhans cells. J Invest Dermatol. 2015;135(2):425-34.

[30] Van Damme P, Oosterhuis Kafeja F, Van der Wielen M, Almagor Y, Sharon O, Levin Y. Safety and efficacy of a novel microneedle device for dose sparing intradermal influenza vaccination in healthy adults. Vaccine. 2009;27(3):454-9.

[31] Kenney R, Frech S, Muenz L, Villar C, Glenn G. Dose sparing with intradermal injection of influenza vaccine. N Engl J Med. 2004;351(22):2295-301.

[32] Bal S, Ding Z, van Riet E, Jiskoot W, Bouwstra J. Advances in transcutaneous vaccine delivery: do all ways lead to Rome? J Control Release. 2010;148(3):266-82.

[33] Harvey A, Kaestner S, Sutter D, Harvey N, Mikszta J, Pettis R. Microneedle-based intradermal delivery enables rapid lymphatic uptake and distribution of protein drugs. Pharm Res. 2011;28(1):107-16.

[34] Zaric M, Lyubomska O, Touzelet O, Poux C, Al Zahrani S, Fay F, et al. Skin dendritic cell targeting via microneedle arrays laden with antigen-encapsulated poly-D,L-lactide-co-glycolide nanoparticles induces efficient antitumor and antiviral immune responses. ACS Nano. 2013;7(3):2042-55.

[35] Suh H, Shin J, Kim Y. Microneedle patches for vaccine delivery. Clin Exp Vaccine Res. 2014;3(1):42,-49.

[36] van der Maaden K, Jiskoot W, Bouwstra J. Microneedle technologies for (trans)dermal drug and vaccine delivery. J Control Release. 2012;161(2):645-55.

[37] Boks MA, Unger WWJ, Engels S, Ambrosini M, Kooyk YV, Luttge R. Controlled release of a model vaccine by nanoporous ceramic microneedle arrays. Int J Pharm. 2015;491(1-2):375-83.

[38] Van Der Maaden K, Trietsch SJ, Kraan H, Varypataki EM, Romeijn S, Zwier R, et al. Novel hollow microneedle technology for depth-controlled microinjection-mediated dermal vaccination: A study with polio vaccine in rats. Pharm Res. 2014;31(7):1846-54.

[39] van der Maaden K, Luttge R, Vos P, Bouwstra J, Kersten G, Ploemen I. Microneedle-based drug and vaccine delivery via nanoporous microneedle arrays. Drug Deliv Transl Res. 2015;5(4):397-406.

[40] Larraneta E, McCrudden MTC, Courtenay A, Donnelly R, Larrañeta E. Microneedles: A New Frontier in Nanomedicine Delivery. Pharm Res. 2016;33(5):1055-73.

[41] Widera G, Johnson J, Kim L, Libiran L, Nyam K, Daddona P, et al. Effect of delivery parameters on immunization to ovalbumin following intracutaneous administration by a coated microneedle array patch system. Vaccine. 2006;24(10):1653-64.

[42] Kim Y, Quan F, Yoo D, Compans R, Kang S, Prausnitz M. Improved influenza vaccination in the skin using vaccine coated microneedles. Vaccine. 2009;27(49):6932-8.

[43] McCaffrey J, McCrudden C, Ali A, Massey A, McBride J, McCarthy HO, et al. Transcending epithelial and intracellular biological barriers; a prototype DNA delivery device. J Control Release. 2016;226:238-47.

[44] Seok HY, Suh H, Baek S, Kim YC. Microneedle applications for DNA vaccine delivery to the skin. Methods Mol Biol. 2014;1143:141,-58.

[45] Bins AD, Jorritsma A, Wolkers MC, Hung CF, Wu TC, Schumacher TNM, et al. A rapid and potent DNA vaccination strategy defined by in vivo monitoring of antigen expression. Nat Med. 2005;11(8):899-904.

[46] Baxby D. Smallpox vaccination techniques; from knives and forks to needles and pins. Vaccine. 2002;20(16):2140-9.

[47] Pokorna D, Rubio I, Muller M. DNA-vaccination via tattooing induces stronger humoral and cellular immune responses than intramuscular delivery supported by molecular adjuvants. Genet Vaccines Ther. 2008 feb 7;6:4.

[48] Chiu Y, Sampson J, Jiang X, Zolla Pazner S, Kong X. Skin Tattooing As A Novel Approach For DNA Vaccine Delivery. Journal of Visualized Experiments (JoVE). 2012(68).

Part I

Delivery and Immunogenicity of Biopharmaceuticals for Vaccination


2

Nanoporous Microneedle Arrays to Efficiently Induce Antibody Responses against Diphtheria and Tetanus Toxoid

In review

Anne Marit de Groot[a*]
Anouk C.M. Platteel[a*]
Nico Kuijt[b]
Peter J.S. van Kooten[a]
Pieter Jan Vos[b]
Alice J.A.M. Sijts[a]
Koen van der Maaden[b]

[a] *Department of Infectious Diseases and Immunology, Faculty of Veterinary Sciences, Utrecht University, the Netherlands*
[b] *MyLife Technologies B.V., Leiden, the Netherlands*

*Equal contribution

Abstract

The skin is immunologically very potent because of the high number of antigen presenting cells in the dermis and epidermis, and is therefore considered to be very suitable for vaccination. However, the skin's physical barrier, the stratum corneum, prevents foreign substances, including vaccines, from entering the skin. Microneedles, which are needle-like structures with dimensions in the micrometer range, form a relatively new approach to circumvent the stratum corneum, allowing for minimally-invasive and pain free vaccination. In this study we tested ceramic nanoporous microneedle arrays (npMNAs), representing a novel microneedle-based drug delivery technology, for their ability to deliver the subunit vaccines diphtheria toxoid (DT) and tetanus toxoid (TT) intradermally. First, the piercing ability of the ceramic (alumina) npMNAs, which contained over 100 microneedles per array, a length of 475 μm, and an average pore size of 80 nm, was evaluated in mouse skin. Then, the hydrodynamic diameters of DT and TT and the loading of DT, TT and imiquimod into -, and subsequent release from the npMNAs were assessed *in vitro*. It was shown that DT and TT were successfully loaded into the tips of the ceramic nanoporous microneedles, and by using near-infrared fluorescently-labeled antigens we found that DT and TT were released following piercing of the antigen-loaded npMNAs into *ex vivo* murine skin. Finally, the application of DT- and TT-loaded npMNAs onto mouse skin *in vivo* led to the induction of antigen-specific antibodies, with titers similar to these obtained upon subcutaneous immunization with a similar dose. In conclusion, we show for the first time the potential of nanoporous microneedle arrays for intradermal immunization with subunit vaccines, which opens possibilities for future intradermal vaccination designs.

Keywords

nanoporous microneedles
intradermal vaccination
antigen release
humoral immune response
diphtheria
tetanus

1. Introduction

The skin has great potential for vaccine delivery, because it is a large organ that is easy to reach. Delivery via the skin circumvents degradation challenges to biomacromolecules, as posed for example by the gastro-intestinal delivery route.[1, 2] The skin, with the stratum corneum as outer barrier, is designed to keep foreign materials including pathogens outside. Besides, the skin is immunologically very potent, with a variety of professional antigen presenting cells, such as dermal dendritic cells and Langerhans cells,[3, 4] present in the dermis and epidermis, respectively. To circumvent the barrier function of the stratum corneum and reach antigen presenting cells for vaccination purposes, microneedles can be used. Microneedles are needle-like structures with a length in the micrometer range, and are a promising tool to deliver drugs and vaccines across the barrier. Furthermore, they represent a possible painless vaccination method,[5] they present reduced contamination risks compared to traditional needles, they allow for injection by less trained personnel, and even have potential for self-administration.[6] However, microneedles need to be sufficiently long and strong enough to pierce the stratum corneum, but also preferably short enough to not reach the nociceptors. A variety of microneedles are under development which are either hollow-, solid-, dissolving- or less known porous-structured.[6-10] For all types, multiple strategies have been tested for the delivery of vaccine agents into the skin, as reviewed in van der Maaden *et al*.[10]

Porous microneedles, which may be used as a single-unit-drug delivery system, can be prepared from pore-forming materials,[11] from (nano)particles,[12, 13] or by making solid microneedle material porous.[14, 15] Porous microneedle arrays (MNAs) can be loaded with a drug, by loading the formulation into the pores of the MNAs. The drug is released when the microneedles are pierced into the skin, via diffusion from the pores. To date, several materials have been used for the production of porous MNAs. Amongst these, biodegradable polymeric porous MNA, with a porosity of 75%, lacked strength to penetrate the skin[11]. Use of the already brittle material silicon for porous microneedles asks for high porosity but small pore-sizes to provide enough strength and biocompatibility[14, 15] and, therefore, is limited to the delivery of low-molecular-weight drugs.[10] Using self-setting ceramics for production of porous MNA increases MNA strength. However, drug loading into these MNAs requires circumstances that are unfavorable for biotherapeutical drug formulations, such as an exothermic reaction or ethanol as a solvent.[16]

In this study, microneedles composed of a biocompatible ceramic, alumina (Al_2O_3),[12] were tested for their suitability for intradermal vaccination. With an average pore-size of 80 nm and an estimated porosity of 40%, these microneedles allow for encapsulation of large biomacromolecules post production.[10, 13] In previous studies, it was shown that alumina nanoporous MNAs (npMNA) can be successfully loaded with small molecules or nanoparticles with sizes up to 100 nm in solution or dispersion via absorption (via

capillary forces), and to release these substances *in vitro* by diffusion. The npMNAs had sufficient strength to reproducibly pierce human skin *ex vivo* without breaking,[10] and have shown to activate immune cells upon dermal application of a peptide-loaded npMNA in a murine model.[17] However, characterization of ceramic alumina npMNA loaded with larger, more relevant molecules, such as subunit vaccine antigens, had not been performed.

In this study, characterization and application of alumina npMNA are described. Loading of npMNAs with DT and TT, antigen release in murine skin *ex vivo*, and *in vivo* immunogenicity of npMNA-delivered antigen were examined. We show that npMNA-mediated vaccine delivery elicits TT- and DT-specific antibody responses in mice, comparable to those induced by subcutaneous immunization with a similar dose. This is the first report showing the potential of porous microneedles in dermal immunization with subunit vaccines.

2. Material and Methods

2.1 Materials

DT and TT were obtained from Staten Serum Institute (Copenhagen, Denmark) and Imiquimod Vaccigrade was obtained from Invivogen. Trifluoroacetic acid (TFA), 3,3',5,5'-Tetramethylbenzidine (TMB) and Bovine Serum Albumin (BSA), and 0.4% (w/v) were obtained from Sigma Aldrich. High-performance liquid chromatography (HPLC)-R grade acetonitrile (ACN) was from Biosolve and phosphate buffered saline (PBS; pH 7.2, 1.5 mM KH_2PO_4, 2.7 mM Na_2HPO_4-7H2O, and 155 mM NaCl) was from Gibco (ThermoFisher Scientific). IRdye800cw carboxylic acid N-hydroxy succinimide ester (IRdye800cw-NHS) was purchased from Li-cor (Lincoln, NE, USA). Dexdormitor was purchased from Orion Corporation, Narketan ketamine from Vétoquinol, and Atipam was purchased from Dechra. Goat-anti-Mouse IgG total horseradish peroxidase (GaM-IgG total HRP), Goat anti mouse IgG1 HRP (GaM-IgG1 HRP) and Goat anti mouse IgG2a HRP (GaM-IgG2a HRP) were obtained from Southern Biotech and microtiter plates 9610 used for ELISA were from Corning Costar.

2.2 Preparation and characterization of npMNA

npMNAs were produced by using a double replication technology as previously described.[12] In brief, from an inverse silicon master a first positive PDMS mold was created, from which a second inverse PDMS mold was produced. Alumina npMNAs were fabricated at LouwersHanique from the second PDMS mold according to MyLife Technologies' manufacturing procedure,[18] using a slurry that contains alumina nanoparticles with an average size of 300 nm and a plasticizer. After controlled drying, the resulting microneedles were removed from the PDMS mold and were sintered at 1450°C. This results in removal of the plasticizer and the formation of nanoporous

alumina material with an average pore size of 80 nm and a porosity of approximately 40%.[10, 12] Microneedles used in this study had a length of 475 µm and a density of 150 microneedles/cm^2 on a back plate of 0.7 mm^2 (105 microneedles/array; **Figure 1A, -B)**. The total volume in the nanopores of only the tips of the microneedles of a single microneedle array was calculated to be 0.25 µL. To characterize the geometry of npMNAs Burker Nano Surface analysis was performed.

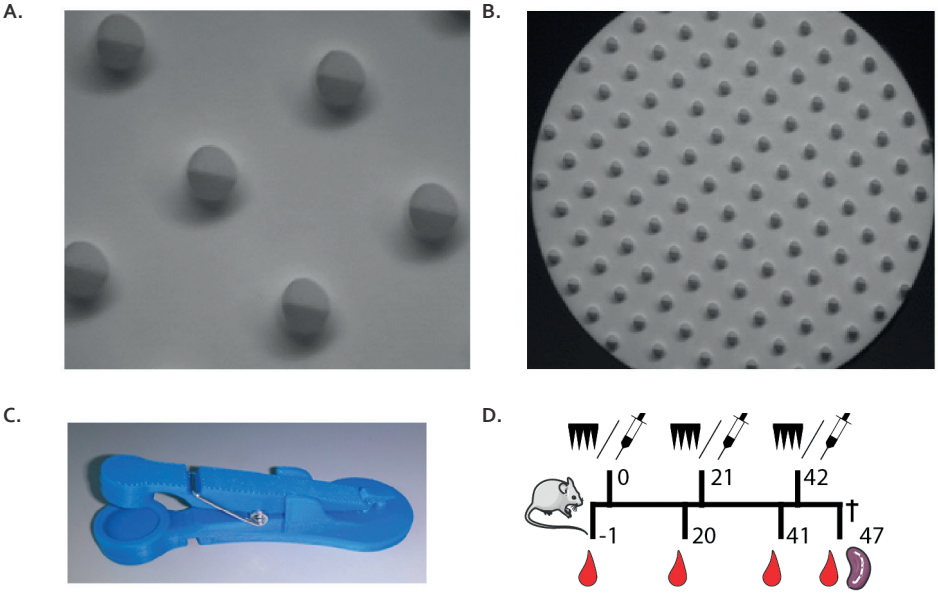

Figure 1: *(A+B) Brightfield microscopy images of a npMNA from the needle-side with microneedles with a length of 475 µm and a density of 105 microneedles/array. (C) Microneedle applicator design that was used to apply npMNAs onto mouse ears. Upon lowering the applicator lid, a microneedle array is pierced into the skin by impact application and the npMNA is subsequently held onto the skin by force (4 Newton). (D) Experimental setup for immunization studies. Immunization with either npMNA or hydrodermic needle on day 0, 21 and 42. Blood samples for serum were collected on d -1, 20, 41 and 47, at which the experiment was terminated and subsequently, spleens were collected.*

2.3 Preparation of npMNAs with antigen-loaded microneedle tips

In order to only load the tips of the microneedles, microneedles were pierced through a foil (Parafilm®) by using a UAFM-V1 electrical applicator (uPRAX Microsolutions) at a velocity of 65 cm/sec. Next, a drop of 5 µL drug formulation was applied onto the foil-pierced npMNAs to absorb a drug/vaccine formulation into the microneedle tips. After 5 seconds the surplus drop of drug formulation and the foil were sequentially removed from the npMNAs. To confirm that only the microneedle tips can be loaded with

a drug formulation, the tips of npMNAs were loaded with a 0.4% trypan blue solution as described above.

2.4 Skin penetration

To test the piercing ability, a npMNA was applied trice on the dorsal side of ex vivo murine ears (balb/C), which were collected from surplus mice, by using 3D-printed uPRAX impact applicators (Figure 1C) having an average holding force of 4.08±0.75 Newton (mean±SD, n=19). Subsequently, the three pierced ex vivo mice ears were incubated with 50 µL of a 0.4% trypan blue solution at room temperature. After 30 minutes the trypan blue was removed and the ears were washed in 10 mL PBS. Finally, the blue dots (piercings) were counted, from which the penetration efficiency was calculated.

2.5 Hydrodynamic diameter and size distribution of antigens

To determine whether the npMNAs are suitable devices to load and release subunit antigens DT and TT, the hydrodynamic diameter and size distribution of DT and TT were determined by using dynamic light scattering on a Zetasizer Nano (Malvern Instruments). For these measurements DT and TT were at a concentration of 0.8 and 0.4 mg/mL, respectively.

2.6 Release of imiquimod and antigen from nanoporous alumina *in vitro*

Imiquimod has the potential to enhance the immunogenicity of antigens in the skin.[19] To evaluate how imiquimod is released from imiquimod-loaded nanoporous material in the presence of DT and TT, npMNAs were loaded by applying a drop (on the microneedle side of a npMNA that were not pierced through a foil) of 5 µL PBS containing only 2.5 µg imiquimod, or 2.5 µg imiquimod and 2.5 Lf DT or TT. Such a drop is absorbed into a npMNA within seconds because of capillary forces. Next, the imiquimod-loaded npMNAs were incubated in 2.5 mL release buffer (PBS) under shaking at 300 rpm and samples of 75 µL were taken in duplicate at different time points (1, 5, 10, 30, 60, 120, and 240 minutes). The imiquimod concentration in the release buffer was determined by using high-performance liquid chromatography (HPLC) on an Agilent 1100 series HPLC equipped with a UV detector using a Phenomenex Kinetex 150*4,6 mm 2.6µ EVO C18 column. A linear gradient of 5% solvent A (acetonitrile with 0.1% TFA) to 68% solvent B (milliQ with 0.1% TFA) from 0-12 min was detected at a wavelength of 242 nm at a retention time of 9.8 min.

To assess the release of antigen from antigen-loaded nanoporous material, npMNAs (that were not pierced through a foil) were loaded with 15 µL PBS that contained 5 Lf DT or TT as described above. Next, antigen-loaded npMNAs were incubated in 4 mL release buffer while shaking at 300 rpm. At different time points (1, 5, 10, 30, 60, 120,

and 240 minutes) samples of 500 µL were taken in which the released amount of antigen was quantified by measuring the intrinsic fluorescence (emission wavelength of 348 nm) at an excitation wavelength of 280 nm and using standard concentrations of DT and TT ranging from 0.01 ng/mL to 50 ng/mL on a Tecan Infinite M1000 plate reader. The release of antigen in the presence of imiquimod was not investigated, because imiquimod is fluorescent at similar wavelengths (excitation at 260 nm and emission at 340 nm) that are used to measure the intrinsic fluorescence of the antigens.[20]

2.7 Fluorescently labelling of antigens

In order to quantify the amount of DT and TT that is delivered from DT- and TT-loaded npMNAs into skin, DT and TT were labeled with a near infrared fluorescent dye (IRdye800cw-NHS). To this end, 1 mg/mL solutions of DT and TT in a 100 mM carbonate buffer pH 8.5 were prepared. Subsequently, 1 mL of each of these solutions was added to 500 µg of IRdye800cw-NHS. After one hour shaking (300 rpm) at 37°C, the free dye was removed and the carbonate buffer was exchanged by PBS using a Zeba™ spin desalting column with a molecular weight cut-off (MWCO) of 7 KDa (Thermo Fisher Scientific). Next, IRdye800cw-labeled antigens were concentrated approximately 50 times by using 0.5 mL Amicon (Millipore) 10 kDa MWCO filters. Finally, the concentration of IRdye800cw-labeled DT and TT were determined by using a calibration curve of non-labeled antigens and measuring the intrinsic fluorescence (as described above).

2.8 Quantification of antigen in *ex vivo* mouse ears

To quantify the delivered amount of DT and TT into murine skin, npMNAs of which only the tips were loaded (using foil piercing) with fluorescently-labeled antigen were prepared by using 5 µL of 12 Lf/µL (DT) and 6 Lf/µL (TT), as described above. The microneedles were applied by impact application and retained onto the skin by using a uPRAX 3D printed applicator. After 30 minutes at room temperature the antigen-loaded npMNAs were removed from the ears and their fluorescence was compared to the fluorescence of standard solutions having known amounts of fluorescently-labeled DT and TT, by using a IVIS® lumina II equipped with an ICG filter set. The intradermally-delivered amounts of DT and TT were quantified by using Living Image® Software (version 4.3.1).

2.9 Preparation of vaccine formulations for loading npMNAs for immunization

Subunit vaccine formulations of DT and TT for loading the microneedle tips were prepared from antigen stock solutions (2.0 and 0.7 Lf/µL, respectively). Antigen stock solutions were concentrated (6-30 X) by using 0.5 mL Amicon (Millipore) 10 kDa MWCO filters. Next, the concentration of the concentrates was determined by measuring the intrinsic fluorescence as described above. Finally, the antigen concentration was adjusted

by diluting the concentrates in PBS to a concentration of 12 Lf/μL and 6 Lf/μL for DT and TT, respectively.

2.10 Immunization of mice

Seven-week old Balb/C female mice (10 mice per group) obtained from Charles River (France) were immunized with 1.2 Lf (~0.50 μg) DT and 1.5 Lf (~0.77 μg) TT, or with 0.6 Lf DT and 0.75 Lf TT adjuvanted with 0.5 μg imiquimod, on day 0, 21 and 42. The vaccine was administered via a subcutaneous injection of 100 μL in the neck using traditional hypodermic needles, or by dermal administration in the ear pinnae by using microneedles of which only the tips were loaded with vaccine formulation. Prior to each microneedle-based immunization, mice were anaesthetized with 30 mg/kg ketamine and 0.1 mg/kg Dexdormitor by intraperitoneal injection. After the microneedles were removed, the anaesthetic was antagonized with 0.4 mg/kg Atipam. On each ear a DT- and TT-loaded npMNA was applied for 30 minutes by using a uPRAX applicator (**Figure 1C**). As a negative control mice were mock immunized via a PBS-loaded npMNA. Blood samples were collected from the tail vein one day prior to each immunization and serum was obtained by centrifugation; spleens were collected at day 47 (**Figure 1D**). Prior ethical approval was obtained from Animal Ethics Committee from Utrecht University, the Netherlands (DEC #2014.II.11.080).

2.11 DT and TT – specific IgG total, IgG1 and IgG2a titers

DT and TT specific antibody titers were determined using ELISA. ELISA plates were coated with 0.2 μg DT or 0.2 μg TT for 30 min and then blocked with 1% BSA in PBS for 15 minutes. Thereafter, 50 μL of serum sample at dilutions ranging from 1:25 until 1:200 (day 0), or from 1:200 until 1:25.000 (day 20, 41 and 47) were added, for 30 min. After extensive washing with 0.01 % Tween 20 in PBS (PBST), wells were incubated for 30 min with GaM-IgG total HRP (1:5000), GaM-IgG1 HRP (1:3000) or GaM-IgG2a HRP (1:5000). After extensive washing with PBST, antibody titers were quantified by adding 50 μL of stock TMB. Reactions were stopped after 60 sec, with 100 μL of 1 M H_2SO_4, and absorption was measured at a wavelength of 450 nm, with a reference wavelength of 650 nm, on a Microplate reader 550 (Biorad). Titers of all animals at all time points for each isotype were measured in one experiment per antigen.

2.12 Statistical analysis

From 4 optical density (OD) values (at a wavelength of 450 nm) of diluted serum samples, the EC_{50} midpoint titers were determined using GraphPad Prism (GraphPad Software Inc, San Diego, v6.05). Immunized mice showing OD values below the mean OD values ± 3 × SD measured for PBS treated mice were considered as non-responders and were given an arbitrary value of 0, equal to ^{10}Log = 1. Statistical differences between immunization

groups were determined using a non-parametric one-way ANOVA Kruskal-Wallis test with a Dunn's test for multiple comparisons And statistical significance was presented as: P<0.05 = *; p<0.01 = **; p<0.001 = ***, and ns=not significant. Ratio of IgG1:IgG2a were determined by dividing midpoint titers of individual isotypes and if animals were considered as non-responders for one of the isotypes (see above), they were excluded from ratio analysis.

3. Results

3.1 Characteristics of npMNA

npMNAs fabricated from alumina nanoparticles as previously reported,[10] were characterized for geometry via surface Bruker analysis, which showed that the ceramic microneedles had an average length of 475 µm and a needle shaft diameter of 275 µm (**Figure 2A**). For economic reasons loading of only the tip of the microneedle with vaccine is an advantage, as residual vaccine quantities in the npMNAs will be strongly reduced. To test for this possibility, npMNAs were pierced through foil, and tips were then loaded with a trypan blue solution for visualization. Brightfield microscopy showed successful tip loading and no loading of the backplate of the npMNA (**Figure 2B**).

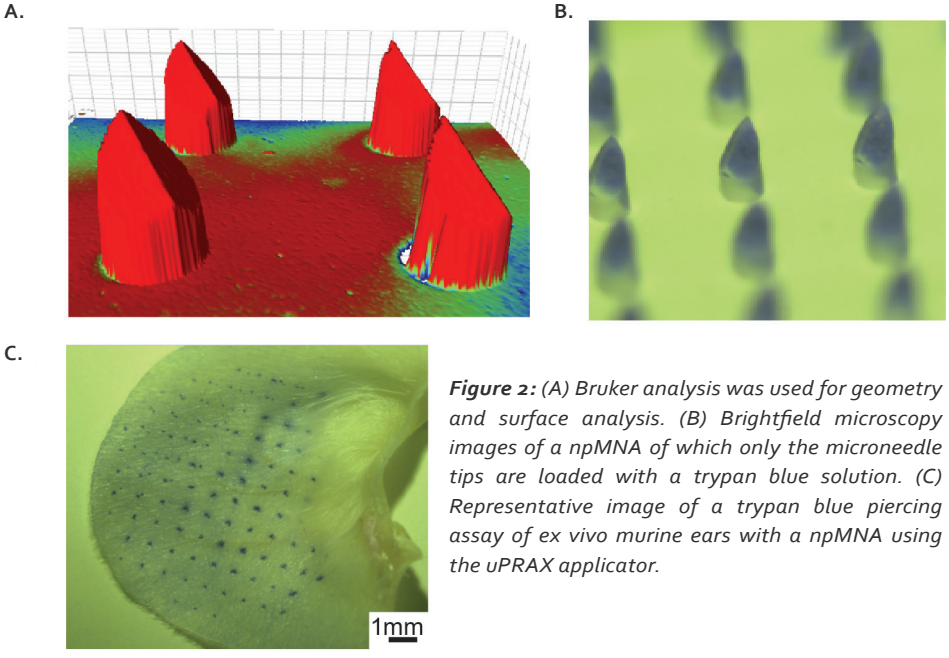

Figure 2: *(A) Bruker analysis was used for geometry and surface analysis. (B) Brightfield microscopy images of a npMNA of which only the microneedle tips are loaded with a trypan blue solution. (C) Representative image of a trypan blue piercing assay of ex vivo murine ears with a npMNA using the uPRAX applicator.*

3.2 Strength of npMNA by skin penetration

The ability of npMNAs to penetrate the skin is essential for intradermal antigen delivery. To determine whether the npMNAs are strong enough to penetrate the skin effectively and reproducibly, skin piercing was evaluated in *ex vivo* murine ear skin using a trypan blue assay (**Figure 2C**). Using the npMNAs resulted in an average piercing efficiency of 87 ± 17% (mean ± SD, n=3). No visual breakage or reduction in strength or sharpness were observed. Together, these data show that the developed npMNA can be used to repeatedly penetrate the skin without breakage. To determine whether the npMNAs, having an average pore size of 80 nm, are suitable to be loaded with the subunit vaccine antigens, the hydrodynamic diameter of DT and TT were determined by using DLS. This revealed that DT and TT had a hydrodynamic diameter of 8.7 ± 2.8 nm (mean ± SD, n=3) and 13.5 ± 5.6 nm (mean ± SD, n=3), respectively, (**Figure 3A, B**). Therefore, the npMNAs should be suitable to be loaded with DT and TT into their nanopores.

3.3 Antigen and adjuvant loading and release *in vitro*

After the npMNAs were loaded with either one of the antigens, the release of these antigens from the npMNAs in a release buffer was determined by measuring the intrinsic fluorescence of the antigens. After 30 min of incubation of npMNAs loaded with either DT or TT in release buffer, 30% of both DT and TT were released from the npMNAs (**Figure 3C**). Besides, the release of imiquimod from imiquimod-loaded npMNAs was quantified after incubating them in a release buffer and using HPLC with UV detection. This revealed that approximately 50% of the npMNA-loaded imiquimod was released after 30 min. Furthermore, it was observed that the co-delivery of imiquimod and DT or TT resulted, not statistically significant, in a slightly lower release rate (**Figure 3D**). The release of imiquimod reached a plateau at 60%, which indicates that imiquimod partially adsorbes onto the npMNA. This was confirmed by incubating non-loaded npMNAs in an imiquimod-containing buffer, having the same amount of imiquimod as the imiquimod-loaded npMNAs. The concentration of imiquimod in the buffer decreased from 100% to 60% over time, showing that 0.2 μg imiquimod was adsorbed onto the npMNA surface (data not shown). The effect of imiquimod on the release of DT or TT could not be assessed due to interference with the fluorescence of imiquimod.[20] Together these data showed that ceramic alumina npMNAs are suitable to be loaded with the subunit vaccine proteins DT and TT and the adjuvant imiquimod, and that the antigens and adjuvant are released *in vitro*.

3.4 Release of antigen into *ex vivo* skin

Next, the delivery of fluorescently-labeled antigens from npMNAs in *ex vivo* murine skin was investigated. The antigen dose delivered into the skin was quantified after the application of fluorescent-labelled antigen-loaded npMNAs onto mouse ears. The delivery of the

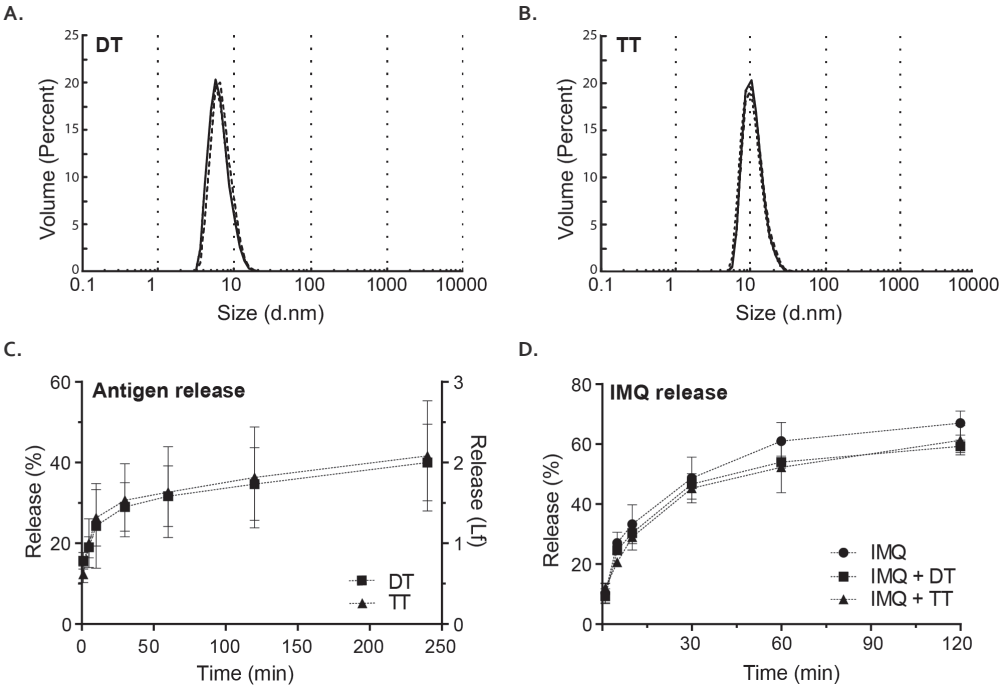

Figure 3: *(A) Hydrodynamic diameter of diphtheria toxoid (8.72 ± 2.83 nm, mean ± SD, n=3). (B) Hydrodynamic diameter of tetanus toxoid (13.5 ± 5.6 nm, mean ± SD, n=3). (C) Release of DT and TT in release buffer measured by intrinsic fluorescence (D) release of imiquimod (IMQ) from npMNA in PBS measured by HPLC.*

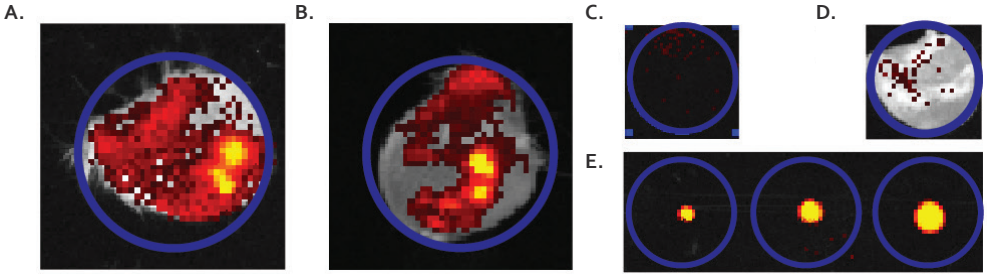

Figure 4: *Representative quantification image of the delivery of fluorescently-labelled antigen into mouse ears. (A+B) an overlay of picture of the mouse ear and infrared fluorescence imaging. Two independent ear piercing experiments are shown for DT (A) and TT (B). (C+D) background fluorescence without and with mouse ear. (E) Gradient of solution containing 0.24, 0.6, and 1,2 Lf DT. Blue circles all indicate region of interest and have an equal diameter in all cases.*

antigens into the ears was quantified by using infrared fluorescence imaging (**Figure 4A, -B**) and was compared to a gradient of known amounts of fluorescently-labeled antigens (**Figure 4E**). The delivery of DT was 0.61±0.44 Lf (which corresponds with ~0.25±0.18 μg) per MNA (**Figure 4A**) and the delivery of TT was 0.77±0.23 Lf (~0.38±0.11 μg) per MNA (**Figure 4B**).

Delivery efficiencies of DT and TT from the npMNAs were calculated by using the geometric values of the npMNAs. With an estimated total tip pore volume of 0.25 μL, the loaded amount of DT was calculated as 0.25 μL 12 Lf/μL = 3 Lf/MNA. With a release of 0.61 Lf out of 3 Lf loaded, 20% delivery efficiency was achieved for DT, after 30 min of application onto the skin. For TT, an amount of 0.25 μL 6 Lf/μL = 1.5 Lf/MNA was loaded and with a release of 0.77 Lf, the delivery efficiency was 0.77 Lf / 1.5 Lf = 51%, after 30 min. For immunization studies, two arrays per mouse were used per antigen and this resulted in a delivery of 1.25 Lf (~0.5 μg) DT and a delivery of 1.53 Lf (~0.77 μg) TT. These values of delivered doses correspond with 26% and 31%, respectively, of the currently used human vaccination dose (5 Lf).

3.5 Immune response after dermal immunization

To determine whether npMNA-mediated intradermal delivery induces antigen-specific immunity, mice were immunized with both DT (1.2 Lf) and TT (1.5 Lf) using antigen-loaded npMNAs (intradermal administration) or using a needle and a syringe (subcutaneous injection). After each immunization, antibody titers in the serum were determined (**Figure 1D**). As expected, no DT- and TT-specific antibodies were detected one day before the 1st immunization (data not shown). At day 20 after immunization, approximately 50% of the immunized mice showed detectable IgG titers against DT, which were increased after the 1st boost measured at day 41. After the 2nd boost (measured at day 47), all mice produced antibodies against DT (**Figure 5A-C**). IgG titers against TT were slightly higher compared to DT specific titers (**Figure 5D-F**). When comparing intradermal administration with subcutaneous injection, no statistical differences were found for DT-specific titers. IgG titers against TT were slightly higher upon subcutaneous delivery as compared to microneedle-mediated delivery (significant after the boost and second boost) (**Figure 5D-F**).

Besides, 50% of the antigen dose (0.6 Lf DT and 0.75 Lf TT) adjuvanted with 0.5 μg TLR7 agonist imiquimod[19] was administered via npMNAs or via a needle and syringe. Despite the lower antigen dose, in general similar antibody titers were detected in mice immunized with adjuvanted compared to unadjuvanted vaccine (**Figure 5**). This with the exception of DT-specific responses measured at day 41 where 3/10 in the adjuvanted group compared to 1/10 mice in the unadjuvanted group had failed to respond (**Figure 5B**). Overall, observing TT-specific antibody titers, the subcutaneously-injected mice showed slightly higher titers than the intradermally-immunized mice. Moreover, mice immunized

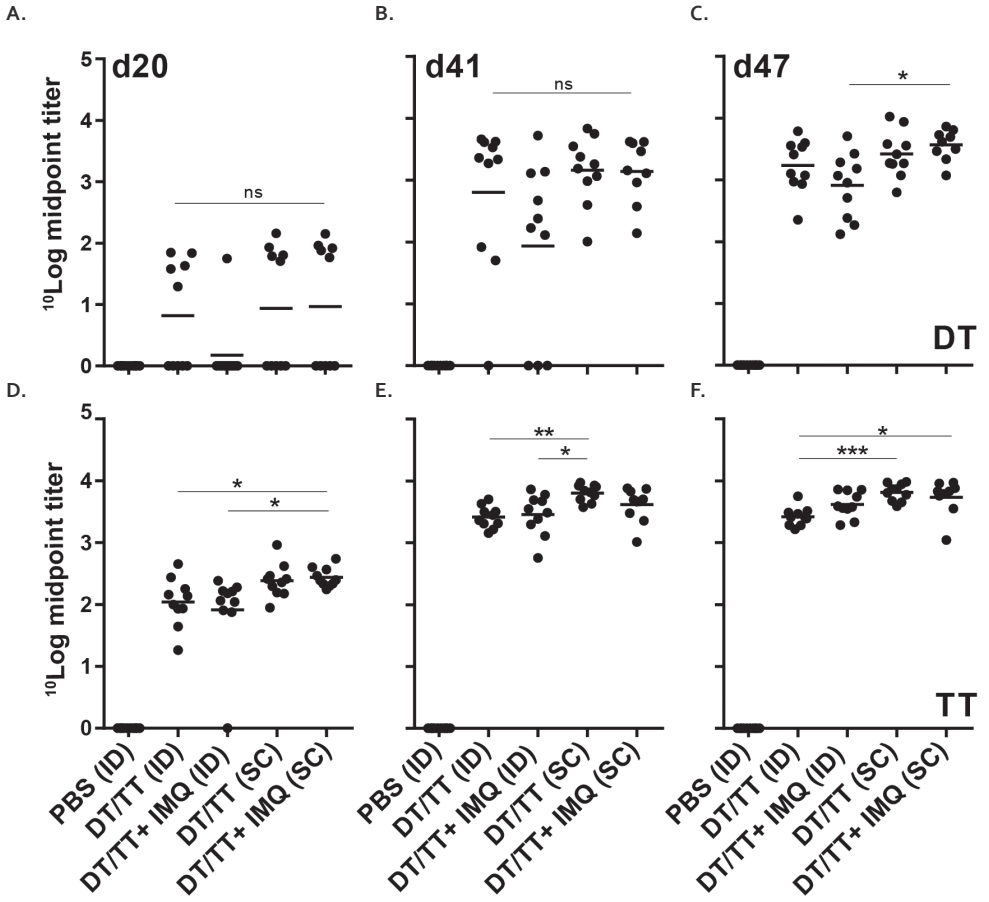

Figure 5: *Serum IgG responses (mean + individual results) after immunization with PBS or 1.2 Lf DT and 1.5 Lf TT ID loaded onto npMNA or SC, both routes with or without Imiquimod. IgG responses were detected against DT antigens (A-C) and TT antigens(D-F). Kruskall-Wallis test with Dunns post-hoc test were performed to determine statistical differences between midpoint titers determined using 4 different titers dilutions.*

with 50% of the vaccine dose (adjuvanted) resulted in similar immune responses as compared to the 100% vaccine dose (non-adjuvanted) (**Figure 5D-F**).

Next to total IgG levels, relative quantities of the IgG isotypes IgG2a and IgG1, which serve as markers for T helper 1 and T helper 2 type lymphocytes, respectively, were determined after boost immunizations. Relative quantities could not be calculated after prime immunization because of non-responders. Overall, ratios between DT and TT-specific IgG1:IgG2a, after first and second boost immunization, indicated that IgG1,

and thus Th2 cell responses, prevailed **(Supplementary Figure 1A, -B**). Remarkably, addition of imiquimod enhanced vaccine-induced DT-specific IgG1 responses (day 41) in subcutaneous but not in intradermal immunized mice. After the second booster immunization (day 47) these differences disappeared, and similar ratios between DT-specific IgG1:IgG2a were observed in all four immunization groups **(Supplementary Figure 1A, -B**). For TT specific isotypes the kinetics were different. While after the first boost immunization, in all mouse groups, ratios between IgG1 and IgG2a were similar, both intradermal immunized mice receiving the adjuvanted vaccine and subcutaneous immunized mice receiving the unadjuvanted vaccine showed increased IgG1:IgG2a ratios after boost (**Supplementary Figure 1C, -D)**. Taken together, although no major differences in IgG isotype ratios between groups were observed, these data demonstrate that followed vaccination regimen induces a predominantly Th2 skewed lymphocyte response.

4. Discussion

Nowadays, many microneedle technologies are investigated for their potential future application in intradermal immunization, because they can be used to deliver drugs and vaccines in a minimally-invasive and potentially pain-free manner into the skin. In the landscape of microneedle technologies, nanoporous microneedles are relatively new and pose an immunization method that enables the loading of drug formulations into the pores of the microneedle arrays, which are released via diffusion upon piercing of the microneedles into the skin. In this study we show that ceramic alumina npMNAs can be used for intradermal immunization with subunit vaccines, aimed to elicit humoral responses.

npMNA strength is an important characteristic contributing to the efficiency of skin piercing, but is closely related to the porosity of the material.[15] High porosity can weaken the material resulting in breaking of the needle tips in the skin and thereby resulting in less efficient piercing of the skin . When designing npMNAs for the delivery of proteins or subunit vaccines, larger pores are necessary. The use of Alumina (Al_2O_3) AKP30 particles for the production of npMNAs results in approximately 40% porosity, with an average pore size of 80 nm[13] and such npMNAs have sufficient strength to repeatedly penetrate the skin without breaking (10). Furthermore, it was previously shown that nanoporous microneedles can be loaded with small molecules and nanoparticles with sizes up to 100 nm.[10] Alumina npMNAs, although with a different geometry, have previously been loaded with small molecules[10] and short peptides,[17] however, peptides are in general not ideal for prophylactic vaccination, because they contain only one minimal T or B cell epitope. Here, we show for the first time successful loading of npMNAs with the subunit vaccine proteins DT and TT, and subsequent release of these antigens from npMNAs into skin, which potentially give rise to a variety of epitopes.

npMNAs have an interconnected porous structured network throughout both the backplate reservoir and the microneedles -seamlessly connected to the backplate of the MNA[21]- and this allows for loading of formulation in both the microneedles as well as the backplate reservoir. While relatively high formulation contents in the npMNA can have advantages, because of the potential for release of high vaccine doses in the skin, high formulation contents are disadvantageous when approached from financial or availability perspective. Furthermore, diffusion of vaccines, or other biomacromolecules, from the backplate via the tips into the skin is a time consuming process. In this study we successfully achieved to load only the tips of the npMNAs, post production of the npMNA, resulting in relatively efficient use of vaccine formulations and allowing for limited application time on the skin. In addition, absorption of a formulation (by porous microneedles) could be favorable over adsorption onto (or coating of) the surface of, for instance, solid microneedles, because 1) the microneedle tip sharpness is retained, and 2) potentially less excipients are required to retain the immunogenicity of a vaccine. Coating of solid MNAs generally requires a thick drug-containing layer to achieve the required amounts of drug/vaccine loading and this could reduce the sharpness of the tips and thereby their skin piercing ability[22, 23] and several excipients are required to adsorb the coating onto the microneedle surface and retain the immunogenicity of vaccines.[24, 25] On the other hand, dissolving microneedles, wherein the drug/vaccine is embedded in the microneedle matrix require a more complex loading strategy in which the vaccine and excipients are added during the preparation phase. Therefore, using dissolving microneedle technologies to only load the microneedle tips with a drug/vaccine is more challenging as compared to using porous microneedles. Therefore, npMNAs can be advantageous over coated and dissolving MNAs.

The release of DT, TT, and imiquimod from drug-loaded npMNAs, was determined after incubating the drug-loaded npMNAs in release buffer *in vitro*. Indeed, around 30% of the vaccine antigens that were loaded into the npMNAs were released in buffer after 30 min. To establish if the vaccine subunit antigens were also released from the npMNA after they penetrated the skin and to quantify the amount of antigen delivered, *ex vivo* mice ears were pierced with fluorescently-labeled antigen-loaded npMNA. The amount of delivered antigen was quantified, from which the release- and delivery efficiency were calculated. The intradermal delivery efficiency of DT was around 20%, and about 50% for TT. When the amounts of antigens that were released into the skin are correlated to the human vaccination dose,[26, 27] the estimated diameter of the circular npMNA that needs to be used for human application should be 2.3 cm and 2.5 cm for DT and TT, respectively. This indicates a feasible size to deliver the corresponding vaccine doses.

The Toll-like receptor 7 agonist imiquimod is extensively researched for its adjuvanticity,[19, 28, 29] as TLR agonists hold promise as novel adjuvants in vaccination approaches, because upon activation, pro-inflammatory cytokines are released.[30, 31] The

cytokine profile induced by imiquimod specifically favors Th1 over Th2 type responses,[32, 33] and thereby the induction of a cellular immune response. Imiquimod 5% cream (Aldara) already has FDA approval for topical use for the treatment of wraths, actinic keratinosis and superficial basal cell carnicoma. Together this makes imiquimod a potent and attractive adjuvant for intradermal immunization. However, one study shows that mainly topical application, rather than intradermal injection, activated antigen presenting cells in skin explants.[34] This is in line with our findings that after prime and 1st boost immunization, no differences in specific antibody titers are observed between mice receiving unadjuvanted or imiquimod-adjuvanted vaccine formulation. In addition, after the 3rd immunization we observed enhanced TT-specific IgG1:IgG2a ratios in intradermal immunized mice that received the imiquimod-adjuvanted compared to the non-adjuvanted vaccine. This indicates that npMNA-mediated intradermal immunization with imiquimod-adjuvanted vaccine predominantly induces Th2, and not Th1 responses.

5. Conclusion

Taken together, in this study we show that ceramic nanoporous microneedles are strong enough to repeatedly penetrate the skin and that they can be loaded with protein subunit vaccines such as DT and TT. After skin piercing the antigen dose delivered intradermally can be assessed and we show that the delivery of DT and TT via npMNAs induces antigen-specific antibody responses. This opens the possibility for the application of npMNAs in intradermal vaccination approaches and further improved loading and release strategies.

Funding

This work was financially supported by the European Union's Seventh Framework Program - Grant No. 280873 ADITEC acronym: NaPoVacs to AS and KM

Conflict of interest

KM is co-owner of uPRAX Microsolutions. The other authors declare that they have no commercial or financial relationships that could be construed as a potential conflict of interest.

Author contributions

Substantial contributions to the conception was done by KM, PV and AS and design of the work by KM, AS, AP. Acquisition, analysis, and interpretation of data by AP, KM, MG, NK and PK. Drafting the manuscript by MG and KM. All authors revised the work and gave final approval of the version to be published.

References

1. Levin C, Perrin H, Combadiere B. Tailored immunity by skin antigen-presenting cells. Hum Vaccin Immunother. 2015;11(1):27-36.
2. Antosova Z, Mackova M, Kral V, Macek T. Therapeutic application of peptides and proteins: parenteral forever? Trends Biotechnol. 2009;27(11):628-35.
3. Fehres C, Garcia Vallejo J, Unger WWJ, van Kooyk Y. Skin-resident antigen-presenting cells: instruction manual for vaccine development. Front Immunol. 2013;4:157-.
4. Zaric M, Lyubomska O, Poux C, Hanna ML, McCrudden MT, Malissen B, et al. Dissolving microneedle delivery of nanoparticle-encapsulated antigen elicits efficient cross-priming and th1 immune responses by murine langerhans cells. J Invest Dermatol. 2015;135(2):425-34.
5. Gupta J, Park S, Bondy B, Felner E, Prausnitz M. Infusion pressure and pain during microneedle injection into skin of human subjects. Biomaterials. 2011;32(28):6823-31.
6. van der Maaden K, Jiskoot W, Bouwstra J. Microneedle technologies for (trans)dermal drug and vaccine delivery. J Control Release. 2012;161(2):645-55.
7. Kim Y, Park J, Prausnitz M. Microneedles for drug and vaccine delivery. Adv Drug Deliv Rev. 2012;64(14):1547-68.
8. Larraneta E, McCrudden MTC, Courtenay A, Donnelly R, Larrañeta E. Microneedles: A New Frontier in Nanomedicine Delivery. Pharm Res. 2016;33(5):1055-73.
9. Bal S, Ding Z, Kersten GFA, Jiskoot W, Bouwstra J. Microneedle-based transcutaneous immunisation in mice with N-trimethyl chitosan adjuvanted diphtheria toxoid formulations. Pharm Res. 2010;27(9):1837-47.
10. van der Maaden K, Luttge R, Vos P, Bouwstra J, Kersten G, Ploemen I. Microneedle-based drug and vaccine delivery via nanoporous microneedle arrays. Drug Deliv Transl Res. 2015;5(4):397-406.
11. Park J, Choi S, Kamath R, Yoon Y, Allen M, Prausnitz M. Polymer particle-based micromolding to fabricate novel microstructures. Biomed Microdevices. 2007;9(2):223-34.
12. Bystrova S, Luttge R. Micromolding for ceramic microneedle arrays. Microelectronic Engineering. 2011 8;88(8):1681-4.
13. Verhoeven M, Bystrova S, Winnubst L, Qureshi H, de Gruijl T. Applying ceramic nanoporous microneedle arrays as a transport interface in egg plants and an ex-vivo human skin model. Microelectronic engineering. 2012;98:659-62.
14. Klyshko A, Balucani M, Ferrari A. Mechanical strength of porous silicon and its possible applications. Superlattices and microstructures. 2008;44(4-5):374-7.
15. Ji J, Tay FEH, Miao J, Iliescu C. Microfabricated microneedle with porous tip for drug delivery. J Micromech Microengineering. 2006;16(5):958-64.
16. Cai B, Xia W, Bredenberg S, Engqvist H. Self-setting bioceramic microscopic protrusions for transdermal drug delivery. Journal of Materials Chemistry B: Materials for biology and medicine. 2014;2(36):5992-8.
17. Boks MA, Unger WWJ, Engels S, Ambrosini M, Kooyk YV, Luttge R. Controlled release of a model vaccine by nanoporous ceramic microneedle arrays. Int J Pharm. 2015;491(1-2):375-83.
18. Lüttge R, Bystrova SN, van Bennekom JG, Domanski M, Loeters PWH, Lammertink RGH, et al., inventors; Integrated microneedle array and a method for manufacturing thereof. 2009 .
19. Johnston D, Bystryn J. Topical imiquimod is a potent adjuvant to a weakly-immunogenic protein prototype vaccine. Vaccine. 2006 3/10;24(11):1958-65.
20. Donnelly R, McCarron P, Zawislak A, Woolfson AD. Design and physicochemical characterisation of a bioadhesive patch for dose-controlled topical delivery of imiquimod. Int J Pharm. 2006;307(2):318-25.
21. Liu L, Kai H, Nagamine K, Ogawa Y, Nishizawa M. Porous polymer microneedles with interconnecting microchannels for rapid fluid transport. RSC Advances. 2016;6(54):48630-5.
22. Chen X, Prow T, Crichton M, Jenkins DWK, Roberts M, Frazer I. Dry-coated microprojection array patches for targeted delivery of immunotherapeutics to the skin. J Control Release. 2009;139(3):212-20.
23. Ameri M, Daddona P, Maa Y. Demonstrated solid-state stability of parathyroid hormone PTH(1-34) coated on a novel transdermal microprojection delivery system. Pharm Res. 2009;26(11):2454-63.

24. Choi H, Yoo D, Bondy B, Quan F, Compans R, Kang S, et al. Stability of influenza vaccine coated onto microneedles. Biomaterials. 2012;33(14):3756-69.
25. Gill H, Prausnitz M. Coated microneedles for transdermal delivery. J Control Release. 2007;117(2):227-37.
26. Sanofi Pasteur Europe. SAMENVATTING VAN DE PRODUCTKENMERKEN - REVAXIS. Medicines Evaluation Board, Netherlands; 2000, rev 2016.
27. GlaxoSmithKline BV. Samenvatting van de Productkenmerken - Boostrix. Bijsluiter. Medicines Evaluation Board Netherlands; 2009, rev 2017.
28. Zuber A, Bråve A, Engström G, Zuber B, Ljungberg K, Fredriksson M, et al. Topical delivery of imiquimod to a mouse model as a novel adjuvant for human immunodeficiency virus (HIV) DNA. Vaccine. 2004;22(13-14):1791-8.
29. Adams S, O'Neill D, Nonaka D, Hardin E, Chiriboga L, Siu K, et al. Immunization of malignant melanoma patients with full-length NY-ESO-1 protein using TLR7 agonist imiquimod as vaccine adjuvant. J Immunol. 2008;181(1):776-84.
30. Kawai T, Akira S. The role of pattern-recognition receptors in innate immunity: update on Toll-like receptors. Nat Immunol. 2010;11(5):373-84.
31. Manicassamy S, Pulendran B. Modulation of adaptive immunity with Toll-like receptors. Semin Immunol. 2009 8;21(4):185-93.
32. Wagner TL, Ahonen CL, Couture AM, Gibson SJ, Miller RL, Smith RM, et al. Modulation of TH1 and TH2 cytokine production with the immune response modifiers, R-848 and imiquimod. Cell Immunol. 1999;191(1):10-9.
33. Doxsee C, Riter T, Reiter M, Gibson S, Vasilakos J, Kedl R. The immune response modifier and Toll-like receptor 7 agonist S-27609 selectively induces IL-12 and TNF-alpha production in CD11c+CD11b+CD8- dendritic cells. J Immunol. 2003;171(3):1156-63.
34. Fehres C, Bruijns SCM, van Beelen A, Kalay H, Ambrosini M, Unger WWJ, et al. Topical rather than intradermal application of the TLR7 ligand imiquimod leads to human dermal dendritic cell maturation and CD8+ T-cell cross-priming. Eur J Immunol. 2014;44(8):2415-24.

Supplementary information

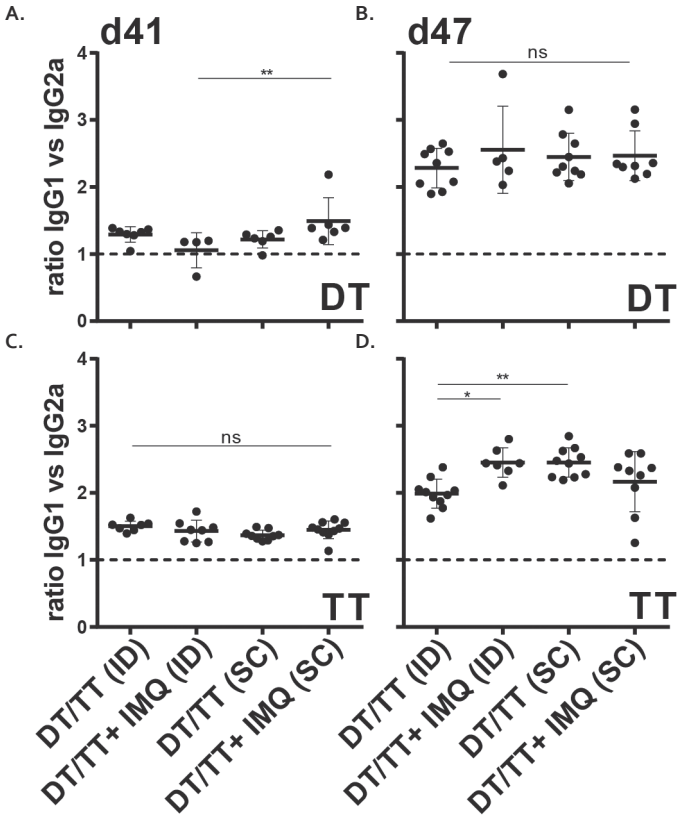

Supplementary Figure 1: *Ratio of IgG1:IgG2a serum responses after ID or SC immunization with PBS or 1.2 Lf DT and 1.5 Lf TT ID , both routes with or without Imiquimod. IgG responses were detected against DT antigens after 1st boost (A) or after 2nd boost (B) and TT antigens (C+D). Kruskall-Wallis test with Dunn's post-hoc test were performed to determine statistical differences of midpoint titers determined using 4 different titers dilutions. Titers of either IgG1 or IgG2a with value of 0 were excluded from graph, because no ratio could be determined.*


3

Hollow microneedle-mediated intradermal delivery of model vaccine antigen-loaded PLGA nanoparticles elicits protective T cell-mediated immunity to an intracellular bacterium

Journal of Controlled Release 266 (2017) 27–35

Anne Marit de Groot[a*]
Guangsheng Du[b*]
Juha Mönkäre[b]
Anouk C.M. Platteel[a]
Femke Broere[a]
Joke A. Bouwstra[b]
Alice J.A.M. Sijts[a]

[1] Department of Infectious diseases and Immunology, Faculty of Veterinary Medicine, Utrecht University, Utrecht, The Netherlands
[2] Division of Drug Delivery Technology, Cluster Bio-Therapeutics, Leiden Academic Centre for Drug Research, Leiden University, Leiden, The Netherlands

*Equal contribution

Graphical abstract

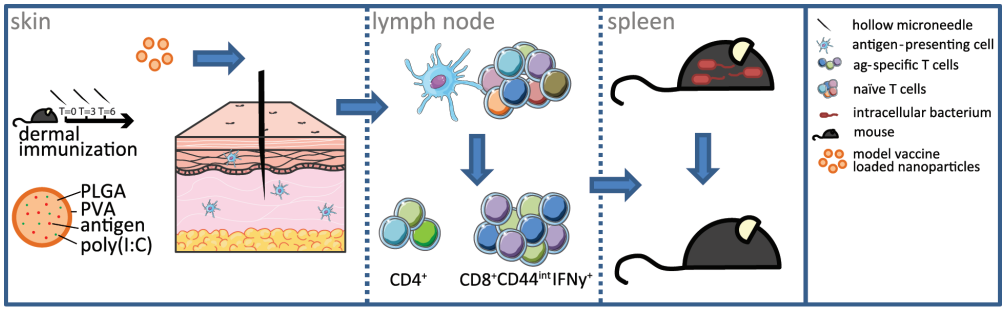

Abstract

The skin is an attractive organ for immunization due to the presence of a large number of epidermal and dermal antigen-presenting cells. Hollow microneedles allow for precise and non-invasive intradermal delivery of vaccines. In this study, ovalbumin (OVA)-loaded poly(lactic-co-glycolic acid) (PLGA) nanoparticles with and without TLR3 agonist poly(I:C) were prepared and administered intradermally by hollow microneedles. The capacity of the PLGA nanoparticles to induce a cytotoxic T cell response, contributing to protection against intracellular pathogens, was examined. We show that a single injection of OVA-loaded PLGA nanoparticles, compared to soluble OVA, primed both adoptively transferred antigen-specific naïve transgenic $CD8^+$ and $CD4^+$ T cells with markedly high efficiency. Applying a triple immunization protocol, PLGA nanoparticles primed also endogenous OVA-specific $CD8^+$ T cells. Immune response, following immunization with in particular anionic PLGA nanoparticles co-encapsulated with OVA and poly(I:C), provided protection against a recombinant strain of the intracellular bacterium *Listeria monocytogenes*, secreting OVA. Taken together, we show that PLGA nanoparticle formulation is an excellent delivery system for protein antigen into the skin and that protective cellular immune responses can be induced using hollow microneedles for intradermal immunizations.

Keywords

protein vaccine
hollow microneedles
intradermal immunization
PLGA nanoparticles
cytotoxic T cell response

1. Introduction

The skin is an organ with many immune cells and is considered a potent organ for immunizations.[1] However, the challenge is to deliver high-molecular-weight antigens across the stratum corneum, which is the outermost layer of the skin and acts as an effective natural barrier for penetration of pathogens and allergens into the skin. One of the methods to circumvent the skin barrier is the use of microneedles. Microneedles are miniaturized needles that provide the possibility of minimally invasive vaccination in the dermis and epidermis of the skin. There are other benefits in using microneedles compared to traditional hypodermic needles, like possible painless vaccination, the requirement of less trained personnel and reduced contamination risk.[2] Nowadays a wide variety of these microneedles exist, including solid, coated, dissolving and hollow microneedles.[3, 4]

Hollow microneedles have multiple benefits, for instance they can be used to inject a wide variety of fluids into the skin at different pressure-driven flow rates[3, 5, 6] and offer the highest precision in dose delivery among all microneedle types. Furthermore, they offer the possibility to screen formulations without time-consuming design and preparation of microneedles, as in case of coated and dissolving microneedles. Recently, hollow microneedles and an applicator for them were developed in our laboratory to inject formulations in precise manner into the skin. These microneedles were successfully used for formulations with inactivated polio virus vaccine in rats resulting in effective humoral immune responses.[7-9] However, whether hollow microneedle-mediated delivery may also induce $CD8^+$ T cell responses towards vaccine antigens is presently unclear.

Cytotoxic $CD8^+$ T cells play an important role in cellular immune protection against intracellular pathogens or tumor growth. To induce such $CD8^+$ T cell responses, an antigen needs to be processed in the cell and presented by MHC-I molecules on professional antigen-presenting cells (pAPC) to the immune system. Delivery of vaccine protein antigens over the cellular membrane can be achieved using delivery systems and over the past decades different types of them, such as polymeric nanoparticles, emulsions and lipid-based nanoparticles have been developed.[10-12] Nano-encapsulation of antigens has several advantages, such as stabilization of antigens *in vivo*, enhancement of the uptake by pAPC and also reduction of antigen release into systemic circulation.[4, 13] The immune outcome can be potentially shaped by using nanoparticles with difference size[14] and surface charge,[15] and by co-encapsulating antigen and adjuvant into the nanoparticles.[16, 17]

For the production of polymeric nanoparticles, poly(lactic-*co*-glycolic acid) (PLGA) is the most commonly used polymer, because of its superior biocompatibility and biodegradability.[18-20] Previous studies have shown that model antigen- and adjuvant-loaded PLGA nanoparticles used for vaccination were able to improve the induction of cell-mediated immune response in mice.[17, 21-23] However, relatively little is known about how encapsulation in PLGA nanoparticles modifies T cell responses to antigen/adjuvant

combinations that are delivered intradermally by different novel types of microneedles. One recent study reported that PLGA nanoparticles, delivered intradermally using dissolving microneedles arrays,[24] induced cellular immune responses and protection against viral infection and tumor growth.

In this study, nanoparticles were prepared and characterized in terms of size, surface charge and antigen/adjuvant release profiles. We investigated the ability of hollow microneedle-delivered protein antigens, encapsulated in either anionic or cationic PLGA nanoparticles without and with co-encapsulated TLR 3 agonist poly(I:C) to induce a protective, cellular immune response towards an intracellular pathogen in a mouse model.

2. Materials and Methods

2.1 Materials

PLGA (acid terminated, lactide glycolide 50:50, Mw 24.000 - 38.000), polyethylenimine (PEI, linear, average M_n 10,000), Roswell Park Memorial Institute medium (RPMI) and Fetal bovine serum (FBS) were purchased from Sigma-Aldrich (Zwijndrecht, The Netherlands). PVA 4-88 (31 kDa) was obtained from Fluka (Steinheim, Germany). Endotoxin-free ovalbumin (OVA), polyinosinic-polycytidylic acid (poly(I:C)) (low molecular weight) and its rhodamine-labelled version were obtained from Invivogen (Toulouse, France). Alexa647 labelled OVA (OVA-Alexa647) was ordered from Thermo-Fischer Scientific (Waltham, MA). Dimethylsulfoxide (DMSO) was obtained from Biosolve BV (Valkenswaard, The Netherlands). Sodium dodecyl sulfate (SDS) was obtained from Merck Millipore (Hohenbrunn, Germany). Ammonium-Chloride-Potassium (ACK) lysis buffer (150 mM NH_4CL, 1 mM $NaHCO_3$; pH 7.40) and 1 mM phosphate buffer (PB; pH 7.4) were prepared in the lab. Milli-Q water (18.2 MΩ/cm, Millipore Co., USA) was used for the preparation of solutions. Sterile phosphate buffered saline (PBS) was obtained from Braun (Oss, The Netherlands). All other chemicals used are of analytical grade.

Purification antibodies used for DynaBeads® selection were all made in house and included the following antibody clones: αCD11b (clone M1/70), αMHC-II (M5/114), αB220 (RA3-6B2), αCD4 (GK1.4), αCD8 (YTS169) and αCD25 (PC61). Purification antibodies for sorting via flow cytometry were αCD8-APC (53-6.7; eBioscience), CD44-FITC (IM7; eBioscience) and CD62L-PE (MEL-14; BD Bioscience) using a BD influx (BD Biosciences). For the detection of the adoptively transferred T cells the antibodies αCD45.2-PerCPCy5.5 (104; eBioscience), αCD4-PE (GK1.5; eBioscience) and αCD8-APC (53-6.7; BD Bioscience) were used. Detection of the endogenous T cells was measured using the antibodies αCD8-APC (53-6.7; eBioscience), αCD4-eFluor450 (GK1.5; eBioscience), αCD62L-Horizon B510 or αCD44-FITC (IM7; eBioscience), αCD16/CD32-unstained (2.4G2; made in house) and αIFNγ-PE (XMG1.2; eBioscience).

2.2 Preparation of PLGA nanoparticles

OVA-loaded PLGA nanoparticles were prepared by double emulsion with solvent evaporation method as previously reported with modifications.[25] Briefly, 75 µl OVA (20 mg/ml) in PBS was dispersed in 1 ml PLGA (25 mg/ml) in ethyl acetate by a Branson sonifier 250 (Danbury, USA) for 15 s with a power of 20 W. To prepare anionic OVA-loaded PLGA nanoparticles (anPLGA-OVA), the obtained water-in-oil emulsion was emulsified with 2 ml 2% (w/v) PVA with the sonifier (15 s, 20 W) to get a water-in-oil-in-water double emulsion. In case of cationic OVA-loaded PLGA nanoparticles (catPLGA-OVA), the single emulsion was emulsified with 2 ml 2% (w/v) PVA and 4% (w/v) PEI solution. The double emulsion was added dropwise into 25 ml 0.3% (w/v) PVA (40 °C) under stirring. The ethyl acetate was evaporated by a rotary evaporator (Buchi rotavapor R210, Switzerland) for 3 h (150 mbar, 40 °C). The nanoparticle suspension was centrifugated (Avanti™ J-20XP centrifuge, Beckman Coulter, Brea, CA) at 35000 g for 10 min, washed twice with 1 mM PB to remove the excess OVA and PVA, and dried in a Alpha1-2 freeze dryer (Osterode, Germany, -49 °C, 90 mbar) overnight. To prepare OVA and poly(I:C) co-encapsulated PLGA nanoparticles (anPLGA-OVA-PIC), 18.75 µl OVA (40 mg/ml) and 75 µl poly(I:C) (46.7 mg/ml, including 0.03% fluorescently labelled equivalent) were emulsified with 1 ml PLGA (25 mg/ml) in ethyl acetate to obtain the water-in-oil emulsion. The remaining of the procedure was identical to that of anPLGA-OVA. The obtained nanoparticles were stored at 4 °C for analysis and further use. To prepare the PLGA nanoparticles for release study, 10% of total OVA was replaced with OVA-Alexa647 the preparation.

2.3 Characterization of PLGA nanoparticles

The size (Z-average) and polydispersity index (PDI) of nanoparticles were measured by dynamic light scattering and the zeta potential of nanoparticles was measured by laser doppler velocimetry using a Nano ZS® zetasizer (Malvern Instruments, Worcestershire, U.K.). The samples were diluted with 1 mM PB buffer to a nanoparticle concentration of 25 µg/ml before each measurement. To determine the loading efficiency of OVA and poly(I:C) in PLGA nanoparticles, approximately 1 mg of nanoparticles were dissolved in a mixture of 15% (v/v) DMSO and 85% (v/v) 0.05 M NaOH and 0.5% SDS. The amount of OVA was determined by MicroBCA method following the manufacturer's instructions. The amount of poly(I:C) was quantified by the fluorescence intensity of rhodamine labelled poly(I:C) (λ_{ex} 545 nm/ λ_{em} 576 nm). The encapsulation efficiency (EE) and loading capacity (LC) of OVA and poly(I:C) in the nanoparticles were calculated as below:

$$EE\ \% = \frac{M_{loaded\ OVA\ /poly(I:C)}}{M_{totoal\ ova\ /poly(I:C)}} \times 100\% \quad (1)$$

$$LC\ \% = \frac{M_{loaded\ OVA\ /\ poly(I:C)}}{M_{nanoparticles}} \times 100\% \quad (2)$$

Where $M_{\text{loaded OVA/poly(I:C)}}$ represents the mass of loaded OVA or poly(I:C), $M_{\text{total OVA/poly (I:C)}}$ is the total amount of OVA or poly(I:C) added to the formulation and $M_{\text{nanoparticles}}$ is the weight of nanoparticles.

2.4 Release of OVA and poly(I:C) from PLGA nanoparticles

Nanoparticles were prepared in triplicate as described above. To study the release of OVA and poly(I:C) from PLGA nanoparticles, 3 mg anPLGA-OVA, catPLGA-OVA or anPLGA-OVA-PIC were dispered into 1 ml RPMI supplemented with 10% FBS and incubated at 37 °C with a shaking speed of 350 rpm. At different time points, the suspensions were centrifugated (9000 g, 5 min) with Sigma 1-15 centrifuge (Osterode, Germany). A release sample of 600 µl of the supernatant was collected and replaced by fresh medium. The released amount of OVA and poly(I:C) was determined by fluoresence intensity of OVA-Alexa647 (λ_{ex} 647 nm/λ_{em} 671 nm) and rhodamine labelled poly(I:C) (λ_{ex} 545 nm/ λ_{em} 576 nm), respectively.

2.5 Mice and intradermal immunizations

8-18 week old male B6.SJL/ptprcaPep3b/BoyCrl (B6.SJL) wild type mice and 8-30 week old transgenic (tg) mice that express $pOVA_{323-339}$-specific T cell receptor (OT-II mice) or $pOVA_{257-264}$-specific T cell receptor (OT-I mice) were initially obtained from Charles River and were bred in house. Abdomen of mice were shaved prior to immunization on both flanks and intradermal immunization was done using a single hollow microneedle as reported previously[8, 9]. The hollow microneedle was inserted into the abdomen of mice using an applicator controlling precisely the depth, volume and rate of the injections. The injections were performed at a depth of 120 µm, with a volume of 40 µl in 3 injections (2 right flank, 1 left flank) and with a rate of 10 µl/min. The depth was increased up to 200 µm if leakage was observed at the beginning of injection. In all experiments a total of 5 µg OVA or 50 µg OVA peptides were injected per immunization. In case of anPLGA-OVA-PIC, the dose of poly(I:C) was also 5 µg. Ethical approval was given by the Animal Ethics Committee from Utrecht University, The Netherlands.

2.6 Adoptive transfer of OVA T Cell Receptor (TCR) tg T Cells

OVA-specific T cell transferred mice were obtained by injecting OT-I $CD8^+$ and OT-II $CD4^+$ T cells into wildtype B6.SJL mice. In order to obtain OT-I and OT-II cells, spleens were isolated from OT-I and OT-II mice and erythrocyte-depleted splenocytes were obtained as follows. Single cell suspensions were prepared by passage over a 70 µM cell strainer after homogenizing the spleens with a syringe plunger, in RPMI 1640 GlutaMAX supplemented with 8.5% fetal calf serum (Bodinco), 30 µM 2-mercaptoethanol and penicillin/streptomycin (complete RPMI medium). The erythrocytes were depleted by lysis with ACK lysis buffer. Transgenic naïve $CD4^+$ (OT-II) cells and transgenic

$CD8^+$ (OT-I) cells were isolated from splenocytes by negative selection using Magnetic DynaBeads® (Thermo Fisher Scientific, Waltham, MA). Antibodies used were αCD11b, αMHC-II, αB220 and either αCD4 for CD8 (OT-I) T cell purification or αCD8 and αCD25 for naïve $CD4^+$ (OT-II) T cell purification. After negative selection by magnetic beads, a purity around 70% was achieved for naïve tg $CD4^+$ (OT-II) T cells. An additional sorting was necessary to separate naïve from non-naïve tg $CD8^+$ (OT-I) T cells. After selection on $CD8^+$, $CD44^{low}$ and $CD62L^{high}$ using a BD influx, 100% purity of naïve tg $CD8^+$ (OT-I) T cells was obtained. Naïve tg $CD4^+$ (OT-II) T cells were stained with carboxy-fluorescein succinimidyl ester (CFSE; 0.5 μM, Invitrogen) and naïve tg $CD8^+$ (OT-I) T cells were stained with Cell trace violet (CTV; 5 μM, Invitrogen) for 10 min at 37°C. A total of 2×10^6 CFSE-labelled naïve tg $CD4^+$ T cells and 1×10^6 CTV-labelled naïve tg $CD8^+$ cells were injected into the tail vein of recipient mice, one day before immunization to obtain OVA-specific T cell transferred mice.

2.7 *In vivo* proliferation of adoptively transferred T cells

OVA-specific T cell transferred mice were immunized with OVA, anPLGA-OVA and catPLGA-OVA at day 0. PBS and OVA peptide immunizations were used as negative and positive controls, respectively. Proliferation of tg T cells was studied at day 3, 5 and 7. Next, 2.5×10^6 erythrocyte depleted splenocytes or draining (inguinal) lymph node cells were stained with αCD45.2-, αCD4 and αCD8 and transferred cells were measured as a percentage of $CD45.2^+$ and either $CD8^+$ or $CD4^+$ cells of total cells using a FACSCanto II (BD Biosciences) and FlowJo (TriStar) analysis software. Percentages of fully *proliferated* (> 6 division) transferred cells were measured by similar antibody staining, but as $CD45.2^+$ and either CTV^-CD4^+ and $CFSE^{low}$ or as $CFSE^-CD8^+$ and CTV^{low}, all after gating on live cells on FSC-A/SSC-A and single cells in FSC-A/FSC-H.

2.8 Endogenous $CD4^+$ and $CD8^+$ T cell response

B6.SJL mice were immunized with OVA, OVA+poly(I:C), anPLGA-OVA, catPLGA-OVA or anPLGA-OVA-PIC at day 0, 3, 6 and T cell responses were analyzed at day 13. The endogenous $CD4^+$ T cell response was measured by ^3H thymidine incorporation. For this 0.2×10^6 erythrocyte-depleted splenocytes or inguinal lymph node cells were plated in complete RPMI medium in a 96 well round bottom plate for 72 h with or without 10 μg/mL OVA Endo-Fit (Worthigton) or ConA, at 37 °C in a humidified incubator. After 72 h, ^3H-Thymidine (0.4 μCi/well; Amersham Biosciences Europe GmbH) was added for an additional 18 h and incorporation into DNA was measured by liquid scintillation counting (Microbeta, Perkin-Elmer Inc.).

$CD8^+$ T cell activation was measured using intracellular IFNγ staining as described previously[26]. In short, 2.5×10^6 erythrocyte-depleted splenocytes were incubated in complete RPMI medium with 1 μg/ml $pOVA_{257\text{-}264}$ (Genscript) or complete RPMI medium

and 10 μM monensin (eBioscience) for 6 h at 37 °C in 6% humidified incubator. Cells were stained with either αCD8 antibody, αCD4, αCD62L or αCD44 in the presence of αCD16/CD32 to block Fc-receptors. Next, they were fixed with 2% paraformaldehyde and stained with αIFNγ antibody in the presence of 0.05% saponin. Samples were measured on a FACSCanto II (BD Biosciences) and analyzed using FlowJo software (Tree Star).

2.9 CFU counts in bacterial challenge study

B6.SJL mice were immunized with OVA, OVA+PIC, anPLGA-OVA, catPLGA-OVA or anPLGA-OVA-PIC at day 0, 3 and 6. Mice were challenged with recombinant *Listeria monocytogenes* secreting OVA (rLM-OVA) 21 days after final immunization. Mice immunized with 10.000 CFU rLM-OVA at day 6 were used as positive control and unimmunized mice served as negative control. rLM-OVA[27, 28] were cultured in Brain Hart Infusion broth (BHI; Sigma-Aldrich) with 5 μg/mL erythromycin and to challenge the mice 100.000 bacteria from a LOG-phase culture were injected in 200 μl/mouse in the tail vain. To study the elimination of bacteria, three days after challenge spleens were isolated and single cell suspensions were made in RPMI medium. Serial dilutions were plated on BHI agar plates and CFU counts were determined after approximately 36 h in a 37 °C incubator. The remaining mice were sacrificed 5 days after the challenge to study the $CD4^+$ and $CD8^+$ T cell response. The specific T cell response was determined in spleen using intracellular IFN-γ staining method as described in section 8. To determine the memory phenotype of the $CD8^+$ T cells, CD62L and CD44 antibodies were used. First, in the gate of the total $CD8^+$ T cells, three different populations were gated (**Supplement Figure 1B;** solid lines). $CD44^-$ were considered naïve T cells, $CD44^+CD62L^+$ are T central memory cells and $CD44^+CD62L^-$ are T effector and T effector memory cells. Second, in order to determine the antigen specific memory phenotype, the gates that were set on all $CD8^+$ T cells were copied in the $CD8^+IFN\gamma^+$ population.

2.10 Statistics

Statistical significance was determined using Krukal-Wallis and multiple comparison/post hoc analysis was done with Dunn's correction, *=$p<0.05$, **=$p<0.01$, ***=$p<0.001$.

3 Results

3.1 Preparation and characterization of PLGA nanoparticles

The physicochemical characteristics of PLGA nanoparticles are shown in **Table 1.** PLGA nanoparticles had a size of approximately 150 nm with a low PDI ranging from 0.032 to 0.100. AnPLGA-OVA had a negative surface charge with a zeta potential of approximately -18 mV and catPLGA-OVA possessed a positive surface charge with an

opposite zeta potential around +10 mV. The EE% of OVA was approximately 50% in both anPLGA-OVA and anPLGA-OVA-PIC, and catPLGA-OVA showed a significantly higher EE%. CatPLGA-OVA had also a higher LC% (10.4%) of OVA than anPLGA-OVA (6.6%) and anPLGA-OVA-PIC (2.8%). The ratio between the initial amounts of OVA and poly(I:C) in the formulations during the preparation procedure was adjusted in order to prepare anPLGA-OVA-PIC with similar LC% of OVA (2.8%) and poly(I:C) (2.7%).

Nanoparticles	Size (nm)	PDI	ZP (mV)	EE%		LC%	
				OVA	Poly(I:C)	OVA	Poly(I:C)
anPLGA-OVA	155.0±6.2	0.064±0.010	-18.2±1.7	54.8±1.0	-	6.6±0.1	-
catPLGA-OVA	147.3±2.1	0.100±0.029	9.9±0.5	87.0±4.8	-	10.4±0.6	-
anPLGA-OVA-PIC	148.4±8.4	0.032±0.007	-17.4±0.8	47.2±16.2	9.6±2.8	2.8±1.0	2.7±0.8

Table 1: Physicochemical characteristics of PLGA nanoparticles

The formulations are characterized in terms of size (diameter) and poly disperse index (PDI), zeta potential (ZP), and encapsulation efficiency (EE) and loading capacity (LC) of OVA and poly(I:C). The EE% of OVA or poly(I:C) was defined as the percentage of encapsulated amount of OVA or poly(I:C) compared to the added amount of OVA or poly(I:C). The LC% of OVA or poly(I:C) was defined as the percentage of encapsulated amount of OVA or poly(I:C) compared to the amount of nanoparticles. anPLGA-OVA: OVA-loaded PLGA nanoparticles with negative surface charge. catPLGA-OVA: OVA-loaded PLGA nanoparticles with positive surface charge. anPLGA-OVA-PIC: OVA and poly(I:C) co-encapsulated anionic PLGA nanoparticles.

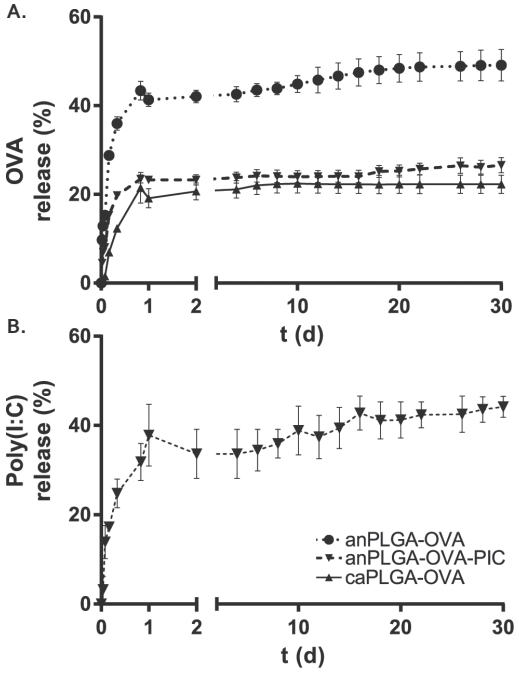

Figure 1: Release of OVA and poly(I:C) from PLGA nanoparticles *PLGA nanoparticles were dispersed into culture medium containing serum and incubated at 37 ºC. At different time points, the release sample was collected to determine the release amount of OVA (A) and poly(I:C) (B). Data is presented as mean ± SEM, n=3.*

3.2 Release of OVA and poly(I:C) from PLGA nanoparticles

Release of OVA and poly(I:C) from PLGA nanoparticles was measured *in vitro* in culture medium containing serum (**Figure 1**). The developed nanoparticles showed a burst release of OVA within the first day, followed by a slow release. At day 30 approximately 49%, 22% and 26% OVA was released from anPLGA-OVA, catPLGA-OVA and anPLGA-OVA-PIC, respectively. In case of poly(I:C), anPLGA-OVA-PIC followed the trend of OVA. At day 30, around 42% poly(I:C) was released. Thus, all of the PLGA nanoparticles released at most one half of their content within one month time.

3.3 OVA-loaded PLGA nanoparticles enhances antigen-induced activation of tg T helper cells and enables priming of tg Cytotoxic T cells after intradermal immunization using a hollow microneedle

To determine the induction of a cellular immune response towards a protein antigen that is delivered via hollow microneedles, we first examined the ability of a protein antigen to activate transgenic (tg) T cells that were adoptively transferred (**Figure 2A**). Naïve OVA specific $CD4^+$ and $CD8^+$ T cells were isolated from spleens of OT-II and OT-I mice, expressing a tg T Cell Receptor specific for the $CD4^+$ and $CD8^+$ T cell epitopes ($OVA_{323-339}$ and $OVA_{257-264}$) of the model antigen OVA, respectively[29, 30]. After staining with cell trace dyes, these cells were mixed and transferred into congenic recipient mice, allowing the distinction between host and donor T cells in flow cytometry, based on expression of the congenic marker (**Figure 2A**). One day later the recipient mice were immunized intradermally, using a hollow microneedle, with full length OVA protein or with the OVA epitopes (pOVA). These epitopes do not require any antigen processing in order to activate tg T cells and served as a positive control. We first determined if $CD4^+$ T helper cells were activated in the present study. Tg $CD4^+$ T cells were detected in flow cytometry as $CD4^+$ $CD45.2^+$ T cells within the lymphocyte gate in either draining inguinal lymph nodes (dLN) or in the spleens. In OVA protein-immunized mice, a small increase in numbers of tg $CD4^+$ T cells compared to PBS group was found in the dLN at day 5 after immunization, while in mice immunized with peptides numbers of tg $CD4^+$ T cells were higher in both dLN and spleen (**Figure 2B**). In mice immunized with OVA protein, minimal systemic responses were measured in the spleen at day 7 (**Figure 2C, F**), and furthermore, minimal numbers of transferred $CD4^+$ T cells activated by OVA protein were fully proliferated (**Figure 2D-F**; depicted by more than 6 dilutions of cell trace dye).

We then determined whether OVA encapsulation in PLGA nanoparticles could enhance OVA-specific tg $CD4^+$ T cell responses. When mice were immunized with OVA-loaded anionic and cationic PLGA nanoparticles (PLGA-OVA), we detected high numbers of OVA-specific tg $CD4^+$ T cells in dLN, both at day 5 and 7 post-immunization (**Figure 2B**). And in spleen these numbers were also significantly higher (**Figure 2C**) than in mice immunized with soluble OVA. Total numbers of tg $CD4^+$ T cells retrieved from PLGA nanoparticle

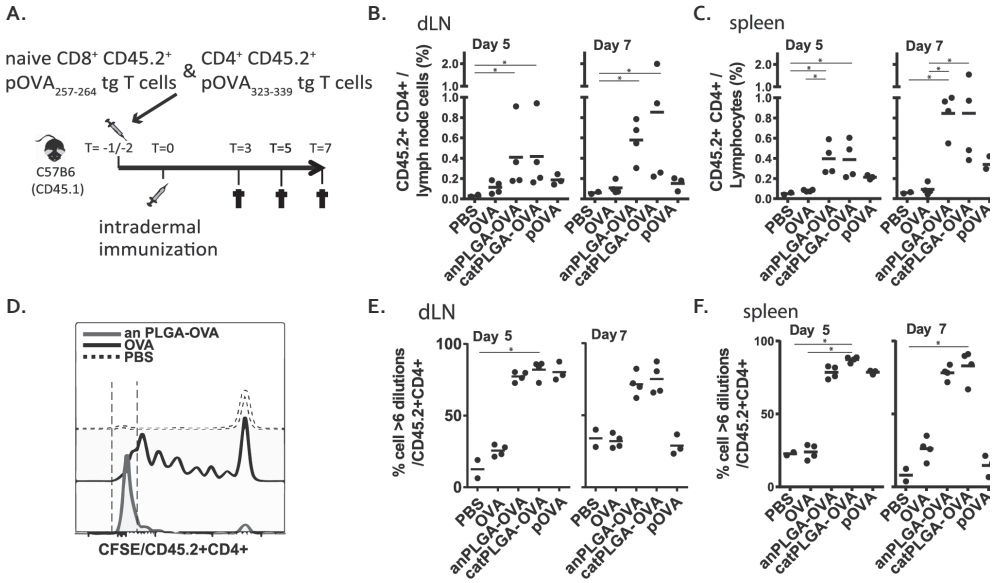

Figure 2: Encapsulation of OVA by PLGA nanoparticles enhances activation of tg $CD4^+$ T cells after intradermal immunization using hollow microneedle

*(A) Experimental design; naïve $CD8^+$ tg T cells specific for $OVA_{257-264}$ were isolated from spleens of OT-I mice and stained with Cell Trace Violet. $CD4^+$ tg T cells specific for $OVA_{323-339}$ were isolated from spleens of OT-II mice and stained with carboxyfluorescein succinimidyl ester (CFSE). From both cell types 1 × 10^6 cells were injected in tail vain of B6.SJL mice 1 or 2 days before intradermal immunization. T cell responses were analyzed on day 3, 5 and 7. (B-F) $CD4^+$ T cell response of tg transferred T cells. (B-C) Amount of transferred tg T cells as percentage of $CD45.2^+CD4^+$ cells in either dLN cells or lymphocyte gate of splenocytes. (D) Indication of fully proliferated (>6 dilutions) cells in the CFSE window of CTV^- / $CD45.2^+CD4^+$ / lymphocyte gate. (E-F) Percentage of cells that are $CD45.2^+CD4^+$ and divided more than 6 times as measured by CFSE intensity on day 5 or 7 in either dLN (E) or spleen (F) after intradermal immunization via hollow microneedles with the formulations indicated on x axes. Graphs are representative for 1 of total 2 independent experiments. Per experiment the number of mice used is n=4 for OVA, anPLGA-OVA and catPLGA immunization groups, n=3 for pOVA immunization groups, n=2 for PBS immunization group (as depicted by the number of symbols in the graph). Statistical significance was determined using Kruskal-Wallis, $p<0.05$ and multiple comparison/post hoc analysis was done comparing immunization strategies versus PBS or OVA immunization with Dunn's correction, *=$p<0.05$*

immunized mice were also much higher than in mice immunized with peptide (**Figure 2B, -C**). Over 95% of these cells were fully proliferated in anPLGA-OVA and catPLGA-OVA groups, while OVA induced only slightly more fully proliferated cells than PBS locally on day 5 and systemically on day 7. Immunizing with the OVA peptides showed a high proliferation rate at day 5 only, while at day 7 the numbers of fully proliferated cells dropped (**Figure 2E-F**). No differences were observed between responses detected against anPLGA-OVA and catPLGA-OVA. Taken together, we show that encapsulation in PLGA nanoparticles enhanced the activation of tg T helper cells by OVA after intradermal immunization using hollow microneedles.

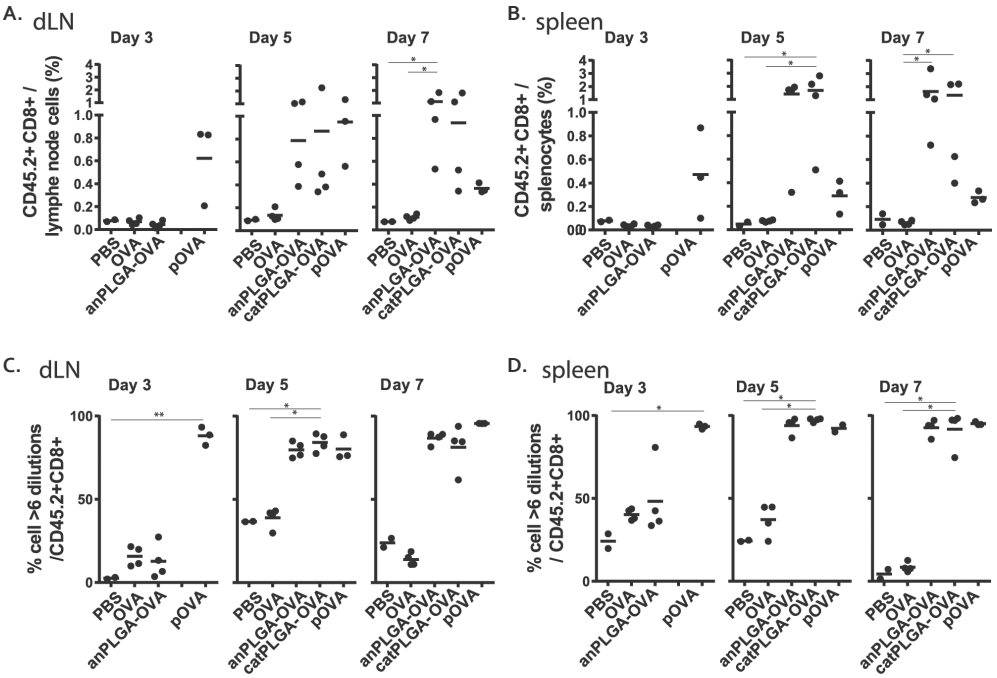

Figure 3: Encapsulation of OVA by PLGA nanoparticles enables activation of tg CD8⁺ T cells after intradermal immunization using hollow microneedle

*CD8⁺ T cell response of tg transferred T cells. (A, B) Amount of transferred tg T cells as percentage of CD45.2⁺CD8⁺ cells in either dLN cells or lymphocyte gate of splenocytes. (C, D) Percentage of cells that are CD45.2⁺CD8⁺ and divided more than 6 times as measured by Cell Trace Violet intensity on day 3, 5 or 7 in either dLN (C) or spleen (D) after intradermal immunization via hollow microneedles with the formulations indicated on X-axes. Graphs are representative for 1 of total 2 independent experiments. Per experiment the number of mice used is n=4 for OVA, anPLGA-OVA and catPLGA immunization groups, n=3 for pOVA immunization groups, n=2 for PBS immunization group (as depicted by the number of symbols in the graph). Statistical significance was determined using Kruskal-Wallis, p<0.05 and multiple comparison/post hoc analysis was done comparing immunization strategies versus PBS immunization with Dunn's correction, *=p<0.05*

Next, it was determined if the followed immunization strategy also induced a cytotoxic cellular immune response, to provide protection against intracellular pathogens or tumors. Activation and proliferation of $CD8^+$ tg T cells was measured in the same experimental setup as shown in **Figure 2A**. As expected, no increase in the numbers of tg $CD8^+$ T cells was detected in either dLN or spleen at day 3, 5 or 7 after immunization with soluble OVA protein (**Figure 3A, B**). On day 3, immunization with OVA induced some T cell proliferation, as shown by dilution of cell trace dye (**Figure 3C, D**), although this proliferation did not lead to a significant increase in tg $CD8^+$ T cell numbers (**Figure 3A, B**). In contrast, immunization with OVA-loaded PLGA nanoparticles, induced a marked increase in tg $CD8^+$ T cell numbers not only in dLN but also in spleen, as detected at both days 5 and 7 (**Figure 3A, B**). Most of these cells were fully proliferated and there was no difference observed between responses induced by anPLGA-OVA and catPLGA-OVA. Immunization with OVA peptides also induced a systemic tg $CD8^+$ T cell response, detected at day 5, but in contrast to nanoparticle-immunization, this response decreased significantly at day 7 in spleen as well as dLN. This was probably due to differing kinetics of T cell responses triggered by precise T cell epitopes, compared to full length OVA, which requires prior antigen processing. In conclusion, our data indicate that encapsulation in PLGA nanoparticles enables OVA to trigger $CD8^+$ tg T cell responses upon hollow microneedle-mediated intradermal delivery.

3.4 OVA primes both endogenous $CD4^+$ and $CD8^+$ T cell responses in immunized hosts when particulated in PLGA nanoparticles or adjuvanted with TLR3 agonist

Having shown that hollow microneedle-mediated immunization with OVA-loaded PLGA nanoparticles activates adoptively transferred tg T cells (**Figure 2 and 3**), we next examined whether this strategy also primes endogenous T cell responses in immunized hosts. To this end, wild type mice were immunized at day 0, 3 and 6 with either OVA, OVA adjuvanted with TLR3 agonist poly(I:C) (OVA+PIC), anPLGA-OVA, catPLGA-OVA or anPLGA-OVA-PIC (**Table 1; Figure 4A**).

At day 13, antigen-specific $CD8^+$ T cell responses were detected by intracellular IFNγ cytokine staining (**Supplement Figure 1A**). Background levels of IFNγ produced by $CD8^+$ T cells was low in all mice, as depicted by restimulation of cells with medium (**Figure 4B, C**). As expected, no $OVA_{257\text{-}264}$-specific $CD8^+$ T cell response was detected in mice immunized with soluble OVA (**Figure 4B, C).** In contrast, responses to this epitope were clearly detectable in dLN (**Figure 4B**) and the spleen (**Figure 4C**) of mice immunized with either OVA+PIC, as well as catPLGA-OVA or anPLGA-OVA. Responses in the anPLGA-OVA mouse group tended to be lower than in the catPLGA-OVA group. The addition of poly(I:C) enhanced the response induced by anPLGA-OVA immunization, although OVA-PIC only already showed some CD8 activation as well **(Figure 4B, -C).** Thus, following

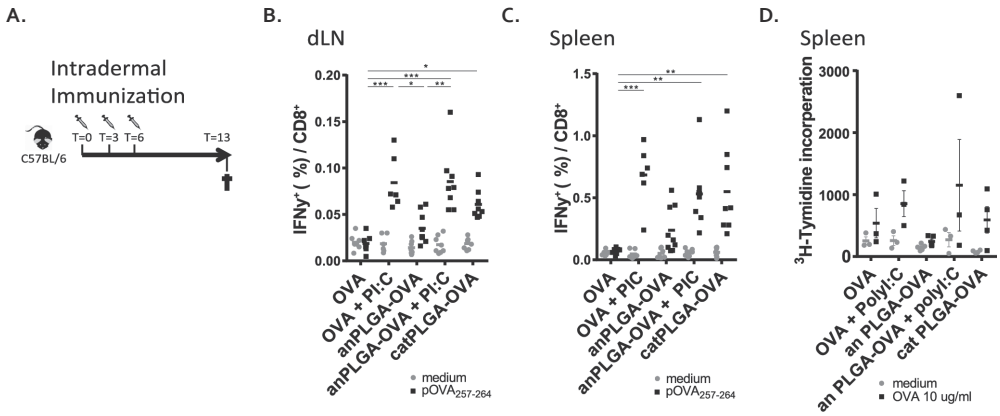

Figure 4: Specific endogenous T cell responses induced by OVA when particulated in anionic or cationic PLGA nanoparticles or when adjuvanted with TLR3 agonist

*(A) Schematic overview of immunization strategy of measuring wild type T cell responses. Intradermal immunization on day 0, 3 and 6 and responses measured 7 days after final immunization (day 13). (B, C) Percentage of IFNγ⁺ cells in CD8⁺ gate within the lymphocyte gate on FSC/SSC of dLN (B) or spleens (C) depicted in black symbols. IFNγ⁺ cells upon stimulation with medium is considered background and shown in gray. Results were pooled of 2 experiments with a total of 6-9 mice/group. (D) CD4⁺ T cell response was measured by proliferation of splenocytes upon stimulation of OVA protein. Incorporation of ³H-thymdine in DNA was measured liquid scintillation counting as CCTM. Statistical significance was determined using Kruskal-Wallis, p<0.05 and multiple comparison/post hoc analysis was done comparing all immunization groups with Dunn's correction, *=p<0.05, **=p<0.01, ***=p<0.001*

hollow microneedle-mediated delivery, a specific recipient CD8⁺ T cell response is induced by OVA when encapsulated in cationic PLGA nanoparticles or when adjuvanted with TLR3 agonist with or without anionic PLGA nanoparticles.

Furthermore, induction of OVA-specific CD4⁺ T cell responses in the immunized mice was determined by measuring ³H-thymidine incorporation in 72 h splenocyte cultures incubated with OVA protein. Some OVA-specific proliferation was detected in mice immunized with OVA+PIC, catPLGA-OVA, and anPLGA-OVA-PIC (**Figure 4D**), although no significant differences between groups were observed.

Thus, hollow microneedle-mediated, intradermal immunization with PLGA nanoparticle encapsulated OVA with or without poly(I:C) induces clearly detectable $OVA_{257-264}$-specific CD8⁺ T cell responses and minor OVA-specific CD4⁺ T cell responses in mice.

3.5 Protective immune response towards recombinant rLM-OVA after intradermal immunization using hollow microneedles

$CD8^+$ T cells play an essential role in clearance of the intracellular bacterium *Listeria monocytogenes*.[31] Next, we determined whether hollow microneedle-mediated vaccination with PLGA nanoparticles induces protective immunity against rLM-OVA. Mice were immunized with OVA, OVA-PIC, anPLGA-OVA, catPLGA-OVA or anPLGA-OVA-PIC at day 0, 3 and 6 and challenged with the bacterium, 21 days after final immunizations (**Figure 5A**). Unimmunized mice served as a negative control and mice immunized with rLM-OVA at day 6 served as positive control, as these mice are typically able to completely clear the bacterium within 3 days after challenge. Determination of CFU counts in the spleens at day 30 showed that mice immunized with rLM-OVA indeed completely cleared the challenge dose, while spleens of non-immunized mice contained on average approximately 100.000 bacteria (**Figure 5B**). While immunization with soluble OVA, anPLGA-OVA or OVA-PIC failed to protect **(Figure 5B)**, protection was observed in at least one mouse immunized with catPLGA-OVA. Moreover, anPLGA-OVA-PIC induced full protection, resulting in zero bacteria count in the spleen, similar to mice immunized with rLM-OVA. This indicates that immunization with anPLGA-OVA-PIC, and to some degree catPLGA-OVA, via the intradermal route using hollow microneedles, elicits a protective cellular immune response.

To study the possible relation between T cell response and the capacity to clear the pathogen, the T cell response in the spleen of the mice was measured. Quantification of T cell responses 5 days after challenge with rLM-OVA showed that all immunization regimens triggered OVA-specific $CD4^+$ T cell responses, and that poly(I:C) did not further increase these responses **(Figure 5C).** In all immunized groups except for OVA-immunized mice a particularly robust activation of antigen-specific $CD8^+$ T cells was detected (**Figure 5D**). Remarkably, the minor population of activated $CD8^+$ T cells in OVA-immunized mice consisted of 40% central memory T cells (Tcm; $CD62L^+CD44^+$) and 60% effector T cells and effector memory T cells (Teff/Tem ;$CD62L^-CD44^+$). In contrast, in the other immunization groups the Tcm populations were much smaller and the Teff/Tem cell population much larger (**sup Figure 1B-D; solid line**). While Tcm:Teff/Tem cell ratio failed to correlate with immune protection, cells within the $CD62L^-CD44^+$gate were further analyzed (**sup Figure 1B-D; dotted line**). We found higher $CD44^{int}$:$CD44^{hi}$ cell ratios in mice that had received anPLGA-OVA-PIC, catPLGA-OVA and rLM-OVA, i.e. the immunization regimens that led to reduced CFU counts following bacterial challenge (**Figure 5E**). Thus, the presence of antigen-specific $CD44^{int}$ $CD8^+$ T cells seems favorable for immune protection to rLM-OVA infection.

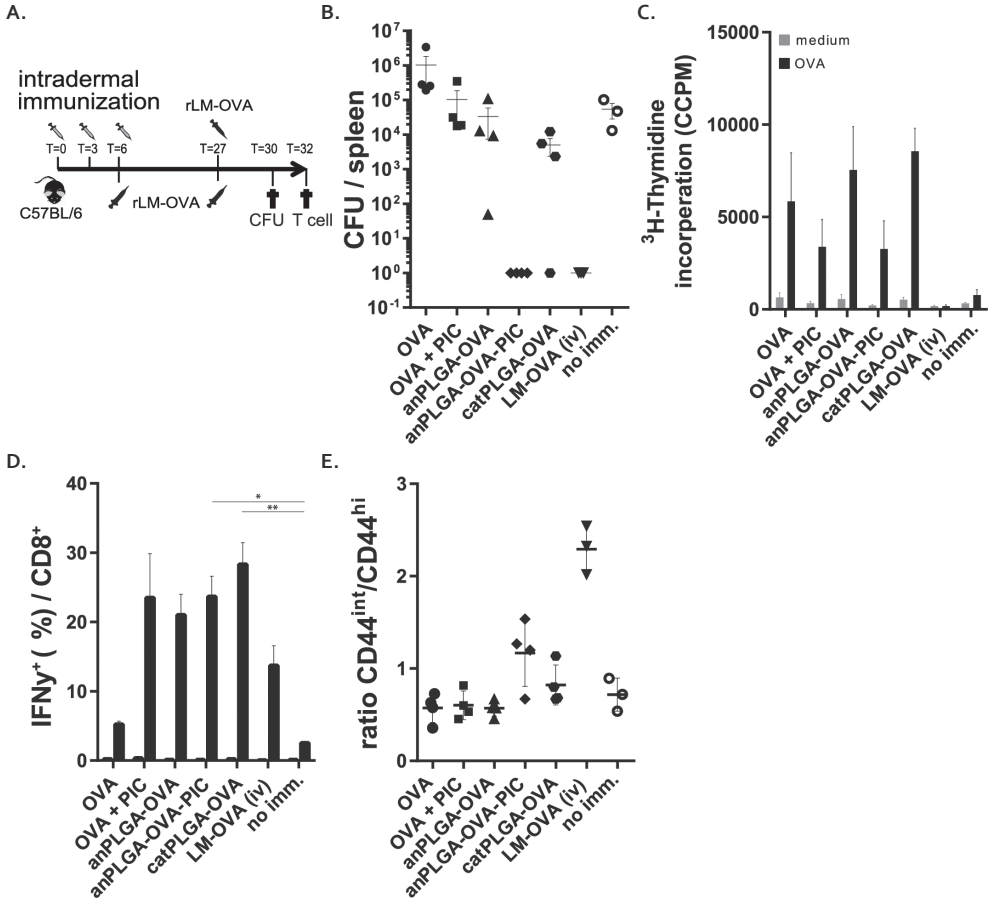

Figure 5: Protective immune response towards rLM-OVA after hollow microneedle mediated intradermal immunization *(A) Schematic overview of challenge study in which the mice received an i.v. challenge of 100.000 recombinant Listeria monocytogenes-OVA 21 days after 3 immunizations with OVA with or without negatively or positively charged PLGA NP or with or without poly(I:C). CFU count of rLM-OVA in spleen were determined 3 days after challenge and T cell activation was measured 5 days after challenge. (B) Spleens were isolated and serial dilutions were plated on BHI agar plates and CFU's were counted 36 hours after incubation at 37°C. (C) $CD4^+$ T cell and (D+E) $CD8^+$ T cell responses were measured identical to procedure figure 3B+D in spleens. Gentamycin was added to culture medium to prevent further growth of potential rLM-OVA. Per experiment n=4 for OVA, anPLGA-OVA and catPLGA immunization groups, n=3 for pOVA immunization groups, n=2 for PBS immunization group (as depicted by the number of symbols in the graph). Statistical significance was determined using Kruskal-Wallis, p<0.05 and multiple comparison/post hoc analysis was done with Dunn's correction, *=p<0.05*

4 Discussion

Nowadays, most of the vaccines under investigation are based on recombinant proteins or subunits of pathogens, because of improved safety and lower production cost compared to live or attenuated vaccines.[32] However, generally such vaccines are poorly immunogenic and fail to elicit robust cell-mediated immunity against intracellular pathogens. In this respect, nanoparticle-based delivery of antigens may be an attractive tool, because it can improve immune response induction to encapsulated antigens.[33] In this study, OVA was used as a model antigen and encapsulated into PLGA nanoparticles with or without the adjuvant poly(I:C). The capacity of the nanoparticle formulations to stimulate cell-mediated immunity was investigated by intradermal immunization using hollow microneedles. In this study, we show that intradermal delivery using hollow microneedles can elicit a protective cellular immune response when the antigen is encapsulated in cationic or adjuvanted anionic PLGA nanoparticles. These data expand on previous studies using hollow microneedles where humoral immune responses were detected,[7-9] which illustrated the attractiveness of the intradermal route for the delivery of vaccines. In our studies, we elaborated on the potential to induce $CD8^+$ T cells in the skin using microneedles, specifically using hollow microneedles.

Nanocarriers used for delivery of proteins or subunit vaccines enhance antigen uptake by antigen presenting cells and contribute to a prolonged presentation of the vaccine antigen at the cell surface.[34, 35] This leads to activation of a cellular immune response, which was exemplified in previous studies showing that PLGA nanoparticle-encapsulated antigens, with or without adjuvant, may induce strong T helper type 1 and cytotoxic T cell immune response (Th1/CTL) response when delivered systemically or subcutaneously.[15, 17, 36] However, relatively little is known about the immune responses elicited by nanoparticle vaccines when administered intradermally using microneedles. On the one hand, inducing conduits in the skin with microneedles and subsequent application of nanoparticles, loaded with either OVA or antigen-encoding cDNA, induced an immune response.[37, 38] Nevertheless, this method of delivery differs from intradermal administration by microneedles. On the other hand, some previous studies on model subunit vaccines using microneedles, such as nanopatches to deliver non-encapsulated TLR adjuvants or pH sensitive microneedles arrays loaded with high doses of protein induced $CD8^+$ T cell responses.[39-41] However, in these studies using microneedles none of the vaccine antigens were encapsulated in nanoparticles. In one study, dissolving microneedles loaded with PLGA nanoparticle encapsulated antigens were used for intradermal vaccination, and shown to induce a robust antigen-specific protective cellular immune response in mice.[24]

Our data show that hollow microneedle-delivered nanoencapsulated OVA not only activated transferred tg T cells, but also primed endogenous protective $CD8^+$ T cell responses in immunized mice. In mice adoptively transferred with tg T cells, an endogenous T cell response could not be detected (not shown). This may be explained by the single

injection immunization regimen in these studies, which may be sufficient to prime adoptively transferred tg CD8+ T cells, but not the naïve antigen-specific T cell repertoire. Alternatively, interference of the relatively easily activated tg T cells with priming of naïve T cells of recipient mice, for example by cytotoxicity towards antigen presenting pAPC as part of an immune homeostasis feedback loop, may also explain this observation. For this reason, to examine whether hollow microneedle-mediated immunization with PLGA nanoparticles encapsulated OVA may prime OVA-specific endogenous CD8+ T cells in mice, a priming procedure was used consisting of three immunizations delivered over a time period of 6 days. This protocol had been shown to induce cellular immune responses following dermal DNA tattoo immunization,[26, 42] but not yet when using hollow microneedles.[7] We report here that this prime boost protocol indeed elicits vigorous CD8+ T cell responses in mice immunized with PLGA encapsulated antigen, when using hollow microneedles as delivery method.

A variety of dendritic cells in the dermis and epidermis have been shown to contribute to immune activation following dermal immunization,[43, 44] and they all express diverse pathogen recognition receptors, such as Toll-like receptors (TLRs). In agreement with this observation, multiple intradermal immunization studies using different administration methods have shown added effects of different Toll-like receptor (TLR) agonists based adjuvants.[16, 45] In our study, co-delivery of OVA and the TLR3 agonist poly(I:C) in PLGA nanoparticles, led to protective cellular immune responses to rLM-OVA. Possibly, the nanoparticles act as a depot system and stimulate the immune system by controlling the release of OVA and poly(I:C), resulting in prolonged OVA presentation and enhanced immunogenicity.[23]

Positively charged cationic PLGA nanoparticles are considered to be more immunogenic than anionic PLGA nanoparticle, as their positive surface charge facilitate the interaction with anionic cell membranes, enhancing uptake of these nanoparticles by phagocytic cells[46]. However, this enhanced interaction can also lead to increased cell cytotoxicity,[10] contributing to the challenges faced for therapeutic use in humans. In our adoptive transfer studies anPLGA-OVA and catPLGA-OVA seemed to perform equally well. However, catPLGA-OVA primed the endogenous cellular immune responses efficiently, while anPLGA-OVA did not show significant increase of response compared to OVA. Although one mouse showed full protection from subsequent infection with rLM-OVA after immunization with catPLGA-OVA, no statistical difference in degree of immune protection induced by cationic compared to anionic PLGA-OVA was detected. Inclusion of poly(I:C) in the anionic nanoparticles was needed to fully protect immunized mice from infection.

Remarkably, although immune protection differed between mice immunized with OVA particulated in cationic or anionic PLGA without or with poly(I:C), vigorous OVA-specific CD8+ T cell responses were detected in all mouse groups except for mice

immunized with soluble OVA. Difference in antigen release can have a role in shaping the memory phenotype,[47] however we found similar release profiles. Further analysis of $CD8^+$ T cell phenotype showed that there was no difference within percentage of Tcm and Tem/Teff cells between the different PLGA NP immunized groups, but an enhanced ratio of $CD8^+$ T cells with $CD44^{int}$ phenotype was detected in mice immune to rLM-OVA challenge. Thus, although no clear definition of $CD44^{int}CD62L^{neg}$ is available,[48-50] we show a correlation between their presence and intradermal immunization-induced protective immunity to challenge with rLM-OVA.

Taken together, we show that hollow microneedles are an excellent tool for intradermal vaccination, leading to the induction of minor $CD4^+$ T cell and vigorous $CD8^+$ T cell responses to PLGA nanoparticle encapsulated antigens. Evoked CD8 T^+ cell responses provided protection against an intracellular bacterium if poly(I:C) was co-encapsulated with the OVA antigen. Future studies may show whether other adjuvants have similar effects or whether specific adjuvants may induce protection to specific categories of intracellular pathogens.

Acknowledgements

The research leading to these results has received support from the Innovative Medicines Initiative Joint Undertaking under grant agreement n° [115363], resources of which are composed of financial contribution from the European Union's Seventh Framework Programme (FP7/2007-2013) and EFPIA companies' in kind contribution. Furthermore, G. Du acknowledges for part support from Chinese Council Scholarship. Furthermore, we wish to thank I.S. Ludwig, P.J.S. van Kooten, and M.A.A. Jansen, Utrecht University, Utrecht, The Netherlands, for technical assistance. Graphical abstract has been made by adapting images from the Servier medical art bank by Servier on servier.com.

References

1. Levin C, Perrin H, Combadiere B. Tailored immunity by skin antigen-presenting cells. Hum Vaccin Immunother. 2015;11(1):27-36.
2. van der Maaden K, Jiskoot W, Bouwstra J. Microneedle technologies for (trans)dermal drug and vaccine delivery. J Control Release. 2012;161(2):645-55.
3. Kim Y, Park J, Prausnitz M. Microneedles for drug and vaccine delivery. Adv Drug Deliv Rev. 2012;64(14):1547-68.
4. Larraneta E, McCrudden MTC, Courtenay A, Donnelly R, Larrañeta E. Microneedles: A New Frontier in Nanomedicine Delivery. Pharm Res. 2016;33(5):1055-73.
5. Prausnitz M. Microneedles for transdermal drug delivery. Adv Drug Deliv Rev. 2004;56(5):581-7.
6. Quinn H, Kearney M, Courtenay A, McCrudden MTC, Donnelly R. The role of microneedles for drug and vaccine delivery. Expert Opin Drug Deliv. 2014;11(11):1769-80.
7. Van Der Maaden K, Trietsch SJ, Kraan H, Varypataki EM, Romeijn S, Zwier R, et al. Novel hollow microneedle technology for depth-controlled microinjection-mediated dermal vaccination: A study with polio vaccine in rats. Pharm Res. 2014;31(7):1846-54.
8. Schipper P, van der Maaden K, Romeijn S, Oomens C, Kersten G, Bouwstra J, et al. Determination of Depth-Dependent Intradermal Immunogenicity of Adjuvanted Inactivated Polio Vaccine Delivered by Microinjections via Hollow Microneedles. Pharm Res. 2016;33(9):2269-79.
9. Schipper P, van der Maaden K, Romeijn S, Oomens C, Kersten G, Jiskoot W, et al. Repeated fractional intradermal dosing of an inactivated polio vaccine by a single hollow microneedle leads to superior immune responses. J Control Release. 2016.
10. Zhao L, Seth A, Wibowo N, Zhao C, Mitter N, Yu C. Nanoparticle vaccines. Vaccine. 2014;32(3):327-37.
11. Kundig T, Storni T, Kündig T, Senti G, Johansen P. Immunity in response to particulate antigen-delivery systems. Adv Drug Deliv Rev. 2005;57(3):333-55.
12. Parveen S, Misra R, Sahoo S. Nanoparticles: a boon to drug delivery, therapeutics, diagnostics and imaging. Nanomedicine. 2012;8(2):147-66.
13. De Geest B, Willart M, Hammad H, Lambrecht B, Pollard C, Bogaert P, et al. Polymeric multilayer capsule-mediated vaccination induces protective immunity against cancer and viral infection. ACS Nano. 2012;6(3):2136-49.
14. Manolova V, Flace A, Bauer M, Schwarz K, Saudan P, Bachmann M. Nanoparticles target distinct dendritic cell populations according to their size. Eur J Immunol. 2008;38(5):1404-13.
15. Varypataki E, Silva A, Barnier Quer C, Collin N, Ossendorp F, Jiskoot W. Synthetic long peptide-based vaccine formulations for induction of cell mediated immunity: A comparative study of cationic liposomes and PLGA nanoparticles. J Control Release. 2016;226:98-106.
16. Varypataki E, van der Maaden K, Bouwstra J, Ossendorp F, Jiskoot W. Cationic liposomes loaded with a synthetic long peptide and poly(I:C): a defined adjuvanted vaccine for induction of antigen-specific T cell cytotoxicity. AAPS J. 2015;17(1):216-26.
17. Hamdy S, Molavi O, Ma Z, Haddadi A, Alshamsan A, Gobti Z, et al. Co-delivery of cancer-associated antigen and Toll-like receptor 4 ligand in PLGA nanoparticles induces potent CD8+ T cell-mediated anti-tumor immunity. Vaccine. 2008;26(39):5046-57.
18. Danhier F, Ansorena E, Silva J, Le Breton A, Coco R, Préat V. PLGA-based nanoparticles: an overview of biomedical applications. J Control Release. 2012;161(2):505-22.
19. Panyam J, Labhasetwar V. Biodegradable nanoparticles for drug and gene delivery to cells and tissue. Adv Drug Deliv Rev. 2003;55(3):329-47.
20. Panyam J, Labhasetwar V. Biodegradable nanoparticles for drug and gene delivery to cells and tissue. Adv Drug Deliv Rev. 2012;64(supplement):61-71.
21. Chong C. Enhancement of T helper type 1 immune responses against hepatitis B virus core antigen by PLGA nanoparticle vaccine delivery. J Controlled Release. 2005;102(1):85-99.

22. Schlosser E, Mueller M, Fischer S, Basta S, Busch D, Gander B, et al. TLR ligands and antigen need to be coencapsulated into the same biodegradable microsphere for the generation of potent cytotoxic T lymphocyte responses. Vaccine. 2008;26(13):1626-37.
23. Akagi T, Baba M, Akashi M, Kunugi S, Yamaoka T. Biodegradable Nanoparticles as Vaccine Adjuvants and Delivery Systems: Regulation of Immune Responses by Nanoparticle-Based Vaccine. In: BERLIN: Springer Berlin Heidelberg; 2012. p. 31-64.
24. Zaric M, Lyubomska O, Touzelet O, Poux C, Al Zahrani S, Fay F, et al. Skin dendritic cell targeting via microneedle arrays laden with antigen-encapsulated poly-D,L-lactide-co-glycolide nanoparticles induces efficient antitumor and antiviral immune responses. ACS Nano. 2013;7(3):2042-55.
25. Slutter B, Plapied L, Fievez V, Alonso Sande M, des Rieux A, Slütter B, et al. Mechanistic study of the adjuvant effect of biodegradable nanoparticles in mucosal vaccination. J Control Release. 2009;138(2):113-21.
26. Platteel AC, de Groot AM, Keller C, Andersen P, Ovaa H, Kloetzel P, et al. Strategies to enhance immunogenicity of cDNA vaccine encoded antigens by modulation of antigen processing. Vaccine. 2016;34(42):5132-40.
27. SHEN H, MATLOUBIAN M, AHMED R, Slifka MK, Jensen ER, Miller JF. Recombinant Listeria monocytogenes as a live vaccine vehicle for the induction of protective anti-viral cell-mediated immunity. Proc Natl Acad Sci U S A. 1995;92(9):3987-91.
28. Pope C, Kim SK, Marzo A, Masopust D, Williams K, Jiang J, et al. Organ-specific regulation of the CD8 T cell response to Listeria monocytogenes infection. J Immunol [Internet]. 2001;166(5):3402-9.
29. Kelly JM, Sterry SJ, Cose S, Turner SJ, Fecondo J, Rodda S, et al. Identification of conserved T cell receptor CDR3 residues contacting known exposed peptide side chains from a major histocompatibility complex class I-bound determinant. Eur J Immunol. 1993;23(12):3318-26.
30. Barnden MJ, Allison J, Heath WR, Carbone FR. Defective TCR expression in transgenic mice constructed using cDNA-based alpha- and beta-chain.... Immunol Cell Biol. 1998;76(1):34.
31. McGregor DD, Koster FT, Mackaness GB. Biological sciences: The short lived small lymphocyte as a mediator of cellular immunity. Nature. 1970;228:855-6.
32. Perrie Y, Mohammed A, Kirby D, McNeil S, Bramwell V. Vaccine adjuvant systems: enhancing the efficacy of sub-unit protein antigens. Int J Pharm. 2008;364(2):272-80.
33. Silva J, Videira M, Preat V, Florindo H, Gaspar R, Préat V. Immune system targeting by biodegradable nanoparticles for cancer vaccines. J Control Release. 2013;168(2):179-99.
34. Shen H, Ackerman A, Cody V, Giodini A, Hinson E, Cresswell P, et al. Enhanced and prolonged cross-presentation following endosomal escape of exogenous antigens encapsulated in biodegradable nanoparticles. Immunology. 2006;117(1):78-88.
35. Waeckerle Men Y, Allmen EU, Gander B, Scandella E, Schlosser E, Schmidtke G, et al. Encapsulation of proteins and peptides into biodegradable poly(D,L-lactide-co-glycolide) microspheres prolongs and enhances antigen presentation by human dendritic cells. Vaccine. 2006;24(11):1847-57.
36. Waeckerle Men Y, Groettrup M. PLGA microspheres for improved antigen delivery to dendritic cells as cellular vaccines. Adv Drug Deliv Rev. 2005;57(3):475-82.
37. Bal S, Slutter B, Jiskoot W, Bouwstra J, Slütter B. Small is beautiful: N-trimethyl chitosan-ovalbumin conjugates for microneedle-based transcutaneous immunisation. Vaccine. 2011;29(23):4025-32.
38. Kumar A, Wonganan P, Sandoval M, Li X, Zhu S, Cui Z. Microneedle-mediated transcutaneous immunization with plasmid DNA coated on cationic PLGA nanoparticles. J Control Release. 2012;163(2):230-9.
39. Ng H, Fernando GJP, Kendall MAF. Induction of potent $CD8^+$ T cell responses through the delivery of subunit protein vaccines to skin antigen-presenting cells using densely packed microprojection arrays. J Control Release. 2012;162(3):477-84.
40. Van Der Maaden K, Varypataki EM, Romeijn S, Ossendorp F, Jiskoot W, Bouwstra J. Ovalbumin-coated pH-sensitive microneedle arrays effectively induce ovalbumin-specific antibody and T-cell responses in mice. European Journal of Pharmaceutics and Biopharmaceutics. 2014;88(2):310-5.

41. Van Der Maaden K, Varypataki EM, Yu H, Romeijn S, Jiskoot W, Bouwstra J. Parameter optimization toward optimal microneedle-based dermal vaccination. European Journal of Pharmaceutical Sciences. 2014;64:18-25.
42. Bins AD, Jorritsma A, Wolkers MC, Hung CF, Wu TC, Schumacher TNM, et al. A rapid and potent DNA vaccination strategy defined by in vivo monitoring of antigen expression. Nat Med. 2005;11(8):899-904.
43. Fehres C, Garcia Vallejo J, Unger WWJ, van Kooyk Y. Skin-resident antigen-presenting cells: instruction manual for vaccine development. Front Immunol. 2013;4:157-.
44. Zaric M, Lyubomska O, Poux C, Hanna ML, McCrudden MT, Malissen B, et al. Dissolving microneedle delivery of nanoparticle-encapsulated antigen elicits efficient cross-priming and th1 immune responses by murine langerhans cells. J Invest Dermatol. 2015;135(2):425-34.
45. Weldon W, Zarnitsyn V, Esser ES, Taherbhai M, Koutsonanos D, Vassilieva E, et al. Effect of adjuvants on responses to skin immunization by microneedles coated with influenza subunit vaccine. PLoS ONE. 2012;7(7):e41501-.
46. Foged C, Brodin B, Frokjaer S, Sundblad A. Particle size and surface charge affect particle uptake by human dendritic cells in an in vitro model. Int J Pharm. 2005;298(2):315-22.
47. Demento S, Cui W, Criscione J, Stern E, Tulipan J, Kaech S, et al. Role of sustained antigen release from nanoparticle vaccines in shaping the T cell memory phenotype. Biomaterials. 2012;33(19):4957-64.
48. Pihlgren M, Arpin C, Walzer T, Tomkowiak M, Thomas A, Marvel J, et al. Memory CD44(int) CD8 T cells show increased proliferative responses and IFN-gamma production following antigenic challenge in vitro. Int Immunol. 1999;11(5):699-706.
49. Roberts A, Ely K, Woodland D. Differential contributions of central and effector memory T cells to recall responses. J Exp Med. 2005;202(1):123-33.
50. Opata MM, Stephens R. Early Decision: Effector and Effector Memory T Cell Differentiation in Chronic Infection. Curr Immunol Rev. 2013 Aug;9(3):190-206.

Supplementary Information

Supplement figure 1: Gating strategies and memory phenotype *(A) Gating strategy used for determination of $CD8^+$ T cell response. After live gate on forward/sideward scatter, double or adhering cells are excluded on FSC-A/FSC-H gate. IFNy+ cells were determined after gating on $CD8^{\pm}$ cells. (B) All CD8+ cells were used to determine different population on CD62L and CD44 surface markers. Memory phenotype was next determined on CD8+IFNy+ population only. (C+D) Percentage of Tcm (CD62L+ CD44int/hi) and Teff/Tem (CD62L-CD44int/hi) in the specific T cell population. Statistical significance was determined using Kruskal-Wallis, and multiple comparison/post hoc analysis was done with Dunn's correction, *=p<0.05.*


4

Strategies to enhance immunogenicity of cDNA vaccine encoded antigens by modulation of antigen processing

Vaccine. 2016 sept 30; 34 (42):5132-5140

Anouk C.M. Platteel [a]
Anne Marit de Groot [a]
Christin Keller [b,c]
Peter Andersen [d]
Huib Ovaa [e]
Peter M. Kloetzel [b,c]
Michele Mishto [b,c]
Alice J.A.M. Sijts [a]

a Department of Infectious Diseases and Immunology, Faculty of Veterinary Medicine, Utrecht University, Utrecht, The Netherlands
b Institut für Biochemie, Charité - Universitätsmedizin Berlin, Berlin, Germany
c Berlin Institute of Health, Berlin, Germany
d Department of Infectious Disease Immunology, Statens Serum Institut, Copenhagen, Denmark
e Department of Chemical Immunology, Leiden University Medical Center, Leiden, The Netherlands

Graphical abstract

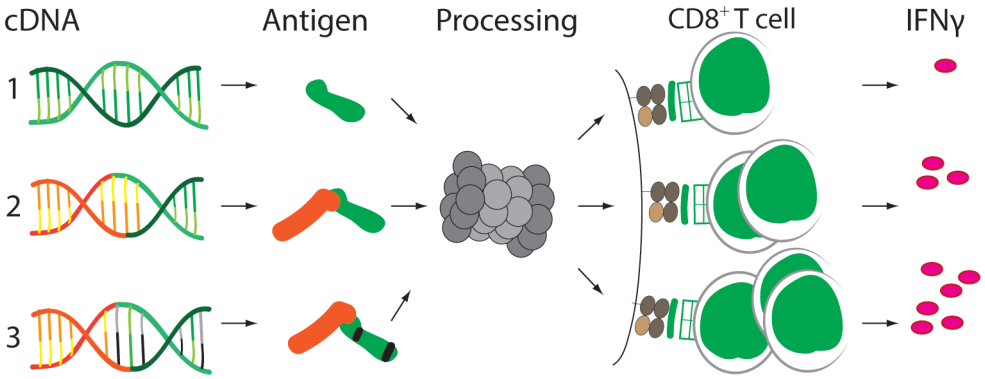

Vaccine H56 antigen cDNA (1), fused to TTFC (tetanus toxin fragment C) or UB (ubiquitin) cDNA (2) and modified to flank $CD8^+$ T cell epitope' C-termini with a glutamic acid residue (3) was administered by tattoo immunization. Linkage to either TTFC or UB enhanced $CD8^+$ T cell responses to all epitopes, while replacement of C-terminal epitope flanks for a Glu residue further increased the $CD8^+$ T cell response to 4 out of 6 epitopes. These strategies can be exploited for vaccine design.

Abstract

Most vaccines are based on protective humoral responses while for intracellular pathogens $CD8^+$ T cells are regularly needed to provide protection. However, poor processing efficiency of antigens is often a limiting factor in $CD8^+$ T cell priming, hampering vaccine efficacy. The multistage cDNA vaccine H56, encoding three secreted *Mycobacterium tuberculosis* antigens, was used to test a complete strategy to enhance vaccine' immunogenicity. Potential $CD8^+$ T cell epitopes in H56 were predicted using the NetMHC3.4/ANN program. Mice were immunized with H56 cDNA using dermal DNA tattoo immunization and epitope candidates were tested for recognition by responding $CD8^+$ T cells in *ex vivo* assays. Seven novel $CD8^+$ T cell epitopes were identified. H56 immunogenicity could be substantially enhanced by two strategies: (i) fusion of the H56 sequence to cDNA of proteins that modify intracellular antigen processing or provide $CD4^+$ T cell help, (ii) by substitution of the epitope's hydrophobic C-terminal flanking residues for polar glutamic acid, which facilitated their proteasome-mediated generation. We conclude that this whole strategy of *in silico* prediction of potential $CD8^+$ T cell epitopes in novel antigens, followed by fusion to sequences with immunogenicity-enhancing properties or modification of epitope flanking sequences to improve proteasome-mediated processing, may be exploited to design novel vaccines against emerging or 'hard to treat' intracellular pathogens.

Keywords

CD8 T cell
Flanking residue optimization
Proteasome
Antigen presentation
MHC class I-restricted epitopes
Dermal DNA tattoo immunization

1. Introduction

$CD8^+$ T cells recognize epitopes of pathogen-derived, intracellularly degraded proteins that are presented by MHC class I molecules. A major role in the generation of such epitopes is played by proteasomes. Proteasomes usually liberate the C-terminus of the epitope by cleaving after hydrophobic or basic residues.[1] The N-terminus may undergo further N-terminal trimming by cytosolic or ER-localized amino- and endopeptidases. The correctly sized ligands that contain a correct binding motif will bind to newly assembled MHC class I molecules and presented at the cell surface.[2,3]

Proteasomes consist of four rings composed of seven subunits each and are present in every cell of an organism. In standard proteasomes, the β1, β2 and β5 subunits, located in the inner rings, display catalytic activity. Upon exposure of cells to inflammatory cytokines, expression of three homologous subunits, β1i/LMP2, β2i/MECL1 and β5i/LMP7 is induced, which leads to the formation of intermediate- or immunoproteasomes.[4] The different pocket conformations and peptide transport dynamics alter the quantity of peptides produced by the proteasomes.[5–10]

Multiple strategies can be used to influence epitope generation and processing by the proteasome which can enhance immunogenicity of $CD8^+$ T cell epitopes and thus could aid in designing better vaccines against intracellular pathogens. Especially for DNA vaccines, which generally elicit cellular responses in animals but show limited immunogenicity in clinical studies,[11] those strategies can help to increase immunogenicity.

One strategy directly targets proteasome-mediated processing; since the proteasome usually creates the epitope' C-terminus, characteristics of the last amino acid of the epitope (at P1 position) and the C-terminally flanking residue (at P1′ position) in the protein sequence have been shown to greatly influence epitope processing.[12–17] Although the limited size of the datasets analyzed so far does not allow generalizations, proteasomes often favor hydrolyzing the peptide bond between hydrophobic large residues at P1 and polar large residues at P1′, whereas hydrophobic large residues at P1′ are disfavored.[8] By for example introducing a residue at P1′ that is favored by the proteasome, chances of effective processing may be increased.

A second strategy to influence epitope processing is fusion of the target cDNA to cDNA that codes for proteins with immunogenicity-enhancing properties. The underlying mechanisms differ with the characteristics of the fusion protein but both self-derived (*e.g.* HSP-70,[18] invariant chain[19]) as well as pathogen-derived proteins (*e.g. E. coli* β-glucoronidase[20]) have been reported to enhance immunogenicity.

We combined these strategies to study the effect of antigen processing modulation on the immunogenicity of a DNA-encoded antigen. The multistage DNA vaccine H56 was used as a model antigen, which expresses the full protein sequence of the *Mycobacterium tuberculosis (Mtb)* antigens Ag85B, ESAT-6 and Rv2660c.[21] This vaccine was delivered

using dermal DNA tattoo immunization, which is a proven method to induce an effective $CD8^+$ T cell response.[22] We report seven novel $CD8^+$ T cell epitopes in H56, identified using *in silico* prediction.[23] Immunogenicity of H56 was enhanced by fusion of the H56-encoding cDNA sequences to cDNA encoding ubiquitin or TTFC, and by substitution of C-terminal flanking residues of epitopes. The two proposed approaches increased the immunogenicity and such a combined strategy may be applied in vaccine design.

2. Material and methods

2.1. Peptide synthesis and 20S proteasome purification

All peptides were synthesized using Fmoc solid phase chemistry. The sequence enumeration of the synthetic peptides referred to the vaccine H56.[21] In particular, for the polypeptides $H56_{53–79}$ (WDINTPAFEWYYQSGLSIVMPVGGQSS) the residue V_{71} was substituted to E, for $H56_{137–160}$ (LAAYHPQQFIYAGSLSALLDPSQG) L_{155} to E and for $H56_{64–86}$ (YQSGLSIVMPVGGQSSFYSDWYS) Y_{81} to E. 20S proteasomes were purified from 5 pooled spleens of C57BL/6 mice[7] and purity was verified.[8]

2.2. *In vitro* digestion of synthetic polypeptide and peptide quantification

The synthetic polypeptides (20 μM) were digested by 2 μg 20S proteasomes in 100 μl TEAD buffer (Tris 20 mM, EDTA 1 mM, NaN_3 1 mM, DTT 1 mM, pH 7.2) for a period of 1–4 h at 37 °C. Liquid-chromatography mass spectrometry (LC-MS) analyses of polypeptide digestion products was performed with the ESI-ion trap instrument DECA XP MAX and the LTQ Orbitrap XL MS (ThermoFisher Scientific) coupled with nanoUPLC Ultimate 3000 (Thermo Scientific Dionex).[24] The database used for the LC-MS/MS analyses was generated by applying the SpliceMet algorithm to allow the identification of linear and spliced peptides.[25] Quantification of peptides was carried out by applying QME to the LC-MS analyses by DECA XP MAX of the *in vitro* digestion kinetics.[24] QME estimates the absolute content of peptide products based on their MS ion peak area measured in the digestion probe. It makes use of the law of mass conservation and MS instrument features. The QME algorithm parameters were empirically computed in a previous study.[24] QME also estimates the site-specific cleavage strength (SCS), which describes the relative frequencies of proteasome cleavage after residues of the synthetic polypeptide.[24] The values showed in this study are the averages of SCS measured over time.[24] For the comparison of the SCS and the investigated peptides of wild type and E-substituted synthetic substrates we ran QME by including only the peptide products common to the wild type and corresponding substituted substrates.[26]

2.3. Mice, DNA and dermal tattoo immunization

Six week old CB6F1 mice from Charles River were immunized at day 0, 3 and 6 with 15 µl cDNA (2 µg/µl) in TE buffer with a 9-needle bar mounted on a tattoo rotary device (Cheyenne) on 100 Hz, at 1 mm depth for 1 min.[22] The full length H56 cDNA[21] was codon optimized and inserted 3′ of tetanus toxin fragment C domain 1 (TTFC),[27,28] ubiquitin (UB) with UB_{75} mutated to A and UB_{76} mutated to V,[29] HLA-F-adjacent transcript 10 (FAT10)[29] or mouse invariant chain (mLi)[30] in pVAX1 vector (Invitrogen). In the H56_E construct (ThermoFisher Scientific), H56-V_{71}, H56-Y_{81}, H56-T_{104}, H56-L_{155}, H56-M_{170} and H56-S_{364} were changed into E (GAA). All animal experiments were approved by the Animal Ethics Committee from Utrecht University (DEC.2014.II.01.001, DEC.2014.II.08.069).

2.4. Analysis of specific $CD8^+$ T cell or $CD4^+$ T cell responses

2.4.1. Intracellular cytokine staining (ICS)

T cell responses were quantified as reported.[7] Briefly, 2.5×10^6 erythrocyte depleted splenocytes were incubated in RPMI 1640 supplemented with 10% FCS (Lonza), 2 mM l-glutamine, 30 µM 2-mercaptoethanol, and penicillin/streptomycin (RPMI medium) with or without 1 (CD8) or 10 µg/ml synthetic peptide (CD4) and 10 µM monensin (eBioscience), for 6 h at 37 °C. Cells were stained with an APC-conjugated anti-mouse CD8 antibody (53–6.7; eBioscience) or APC-conjugated anti-mouse CD4 (L3T4; eBioscience) in the presence of anti-mouse CD16/CD32 (2.4G2; made in house), fixed and stained with PE-conjugated anti-mouse IFNγ antibody (XMG1.2; eBioscience) and analyzed on a FACS Canto II (BD Biosciences) using FlowJo software (Tree Star).

2.4.2. IFNγ ELISpot

MAIP ELISPOT plates (Millipore) were coated overnight with 2 µg/ml AN18 in PBS at 4 °C. Wells were washed and blocked with RPMI medium (Life Technologies). 5×10^5 erythrocyte depleted splenocytes were plated with or without 2 µg/ml synthetic peptide for 6 h in RPMI medium at 37 °C. Plates were washed with PBS plus 0.01% tween 20 (PBST), and IFNγ was detected with biotinylated IFNγ antibody (XMG1.2; BD), followed by alkaline phosphatase-conjugated streptavidin (Jackson Immuno Research Laboratories), in PBST supplemented with 2% BSA. The assay was developed with the Vector blue substrate kit (Vector Laboratories) and analyzed using an ELISpot plate reader and scanner (AELVIS).

2.4.3. *In vivo* killing assay

CB6F1 splenocytes were divided into two populations and labeled with either 0.4 µM or 4 µM CFSE (Invitrogen) in PBS at room temperature for 10 min and quenched with FCS HI. CFSE high cells were subsequently pulsed with 1 µM of $H56_{146–154}$ IYAGLSAL, $H56_{161–169}$ MGPSLIGLA, $H56_{62–70}$ WYYQSGLSI, $H56_{72–80}$ MPVGGQSSF, $H56_{95–103}$

QTYKWETFL and $H56_{354–363}$ NALQNLARTI in PBS containing 2% FCS, for 1 h at 37 °C, and washed with PBS before i.v. injection.

2.5. Statistical analysis

To compare functionality of responses or responses to individual epitopes, both between the H56 immunized group compared to the control group, epitope specific responses of every mouse were corrected for background IFNγ level as measured in samples incubated without peptide, in both IFNγ ELISpot and IFNγ ICS. The variance homogeneity was tested using Levene's test. A two-tailed independent sample T test was used, combined with a Holm-Sidak correction for multiple comparisons. P values < 0.05 were considered significant.

3. Results

3.1. Identification of novel CD8$^+$ T cell epitopes in H56

Rational vaccine design aimed at inducing protective CD8$^+$ T cell responses would start with predicting the pathogen-derived potential epitopes. To test this approach we used the Mtb vaccine candidate H56 in which we predicted potential CD8$^+$ T cell epitopes for H-2b and H-2d MHC class I molecules using the NetMHC3.4/ANN prediction algorithm.[23] As expected, the known epitopes e.g. $H56_{72–80}$ MPVGGQSSF and $H56_{146–154}$ IYAGLSAL,[31–33] as well as 14 novel epitope candidates, were predicted to bind the H-2b, d MHC class I molecules with IC_{50} < 500 nM (Table 1). To determine which of these were epitopes, peptide-specific CD8$^+$ T cell responses were determined *ex vivo* in spleens of mice immunized with H56 cDNA, using dermal DNA tattoo immunization.[22] Intracellular IFNγ staining (ICS) (Figure 1A) showed that four peptides ($H56_{62–70}$ WYYQSGLSI, $H56_{72–80}$ MPVGGQSSF, $H56_{146–154}$ IYAGLSAL, $H56_{161–169}$ MGPSLIGLA), out of 16 potential epitopes, were recognized by CD8$^+$ T cells of mice immunized with a H56 containing construct when compared to mice immunized with a control construct (Figure 1C). For five other peptides ($H56_{95–103}$ QTYKWETFL, $H56_{309–316}$ VTSIHSLL, $H56_{354–363}$ NALQNLARTI, $H56_{427–434}$ SQFTFSSR, $H56_{443–451}$ AGQSWCAIL) a trend towards recognition was visible (Figure 1C). Of these epitopes, $H56_{309–316}$ VTSIHSLL and $H56_{354–363}$ NALQNLARTI derive from ESAT-6, $H56_{427–434}$ SQFTFSSR and $H56_{443–451}$ AGQSWCAIL from Rv2660c, and all other peptides from Ag85B. CD8$^+$ T cell responses to the identified epitopes persisted until 50 days after immunization (Figure 1D) and dominance hierarchy of responding CD8$^+$ T cells was maintained over time, with the already known epitope $H56_{72–80}$ MPVGGQSSF[31–33] being responsible for the activation of the largest percentage of specific CD8$^+$ T cells.

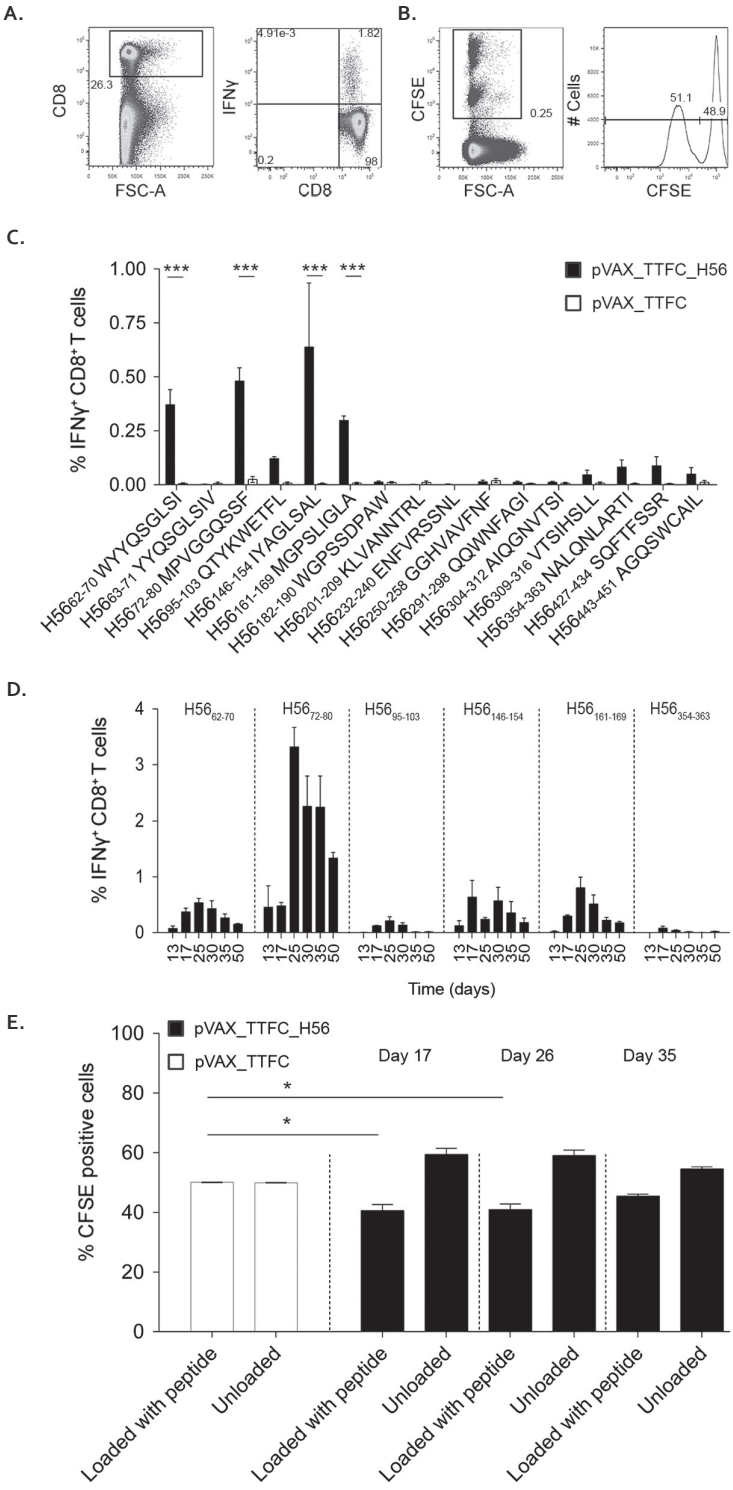
A.
CD8
26.3
FSC-A
IFNγ
4.91e-3
1.82
0.2
98
CD8
B.
CFSE
0.25
FSC-A
Cells
51.1
48.9
CFSE
C.
% IFNγ+ CD8+ T cells
1.00
0.75
0.50
0.25
0.00
***
pVAX_TTFC_H56
pVAX_TTFC
H56 62-70 WYYQSGLSI
H56 63-71 YYQSGLSIV
H56 72-80 MPVGGQSSF
H56 95-103 QTYKWETFL
H56 146-154 IYAGLSAL
H56 161-169 MGPSLIGLA
H56 182-190 WGPSSDPAW
H56 201-209 KLVANNTRL
H56 232-240 ENFVRSSNL
H56 250-258 GGHVAVFNF
H56 291-298 QQWNFAGI
H56 304-312 AIQGNVTSI
H56 309-316 VTSIHSLL
H56 354-363 NALQNLARTI
H56 427-434 SQFTFSSR
H56 443-451 AGQSWCAIL
D.
% IFNγ+ CD8+ T cells
H56 62-70
H56 72-80
H56 95-103
H56 146-154
H56 161-169
H56 354-363
Time (days)
E.
% CFSE positive cells
pVAX_TTFC_H56
pVAX_TTFC
Day 17
Day 26
Day 35
*
*
Loaded with peptide
Unloaded

Figure. 1. CD8 T⁺ cell responses specific for novel epitopes in H56 are functional and persist 50 days after immunization. *(A, B) CB6F1 mice were immunized with H56 cDNA using dermal DNA tattooing and percentages or killing capacity of IFNγ- producing, H56 epitope-specific CD8⁺ T cells in the spleen were determined using (A) intracellular cytokine staining or (B) in vivo killing assays. (C, D) At day 17 (C) or indicated time intervals (D), percentages of CD8⁺ T cells, specific for indicated H56 peptides, were measured ex vivo. Data are shown as mean of 5–8 mice per group ± SEM per peptide corrected for IFNγ background level as measured in control samples that were incubated without peptide, and are representative of 2 independent experiments. (E) At indicated days, pVAX_TTFC_H56- (black bars) or pVAX_TTFC (white bars) immunized animals were injected with splenocytes labeled with CFSE and synthetic $H56_{62-70}$ WYYQSGLSI, $H56_{72-80}$ MPVGGQSSF, $H56_{95-103}$ QTYKWETFL, $H56_{146-154}$ IYAGLSAL, $H56_{161-169}$ MGPSLIGLA and $H56_{354-363}$ NALQNLARTI. Bars indicate percentages of CFSE labeled cells in the spleen after 2 h of 5 mice per group ± SEM. (C, E) All data were analyzed using a two tailed independent sample T test comparing pVAX_TTFC_H56 immunized animals with pVAX_TTFC immunized control animals per peptide, combined with a Sidak-Holm correction for multiple comparisons. P values < 0.05 are depicted with * and P < 0.001 with ***.*

Table 1. Predicted CD8⁺ T cell epitopes in H56.

Allele	Start	End	Sequence	IC_{50} (nM)[a]
H-2Ld	62	70	WYYQSGLSI	47.38
H-2Kd	63	71	YYQSGLSIV	13.27
H-2Kd	72	80	MPVGGQSSF	11.81
H-2Kb	95	103	QTYKWETFL	128.41
H-2Kd	146	154	IYAGSLSAL	3.88
H-2Kd	161	169	MGPSLIGLA	676.78
H-2Dd	182	190	WGPSSDPAW	47.13
H-2Dd	201	209	KLVANNTRL	303.29
H-2Kb	232	240	ENFVRSSNL	264
H-2Kd	250	258	GGHNAVFNF	63.73
H-2Kb	291	298	QQWNFAGI	180.79
H-2Ld	304	312	AIQGNVTSI	558.05
H-2Kb	309	316	VTSIHSLL	477.84
H-2Db	354	363	NALQNLARTI	280.87
H-2Kb	427	434	SQFTFSSR	395.10
H-2Dd	443	451	AGQSWCAIL	392.12

[a] *NetMHC 3.4/ANN[23] predicted H-2b and H-2d binding affinities (IC_{50}). All peptides were included in this study[57].*

To check whether the H56 cDNA vaccine-induced $CD8^+$ T cells displayed killing capacity, in vivo killing assays were performed at different days (Figure 1B). At day 17 and 25, from the 1: 1 ratio of cells that were labeled in high carbofluorescein succinimidyl ester (CFSE) concentration and loaded with epitopes ($H56_{62–70}$ WYYQSGLSI, $H56_{72–80}$ MPVGGQSSF, $H56_{95–103}$ QTYKWETFL, $H56_{146–154}$ IYAGLSAL, $H56_{161–169}$ MGPSLIGLA and $H56_{354–363}$ NALQNLARTI) versus unloaded cells that were labeled in low CFSE concentration, we found less CFSE high cells back in the H56 immunized mice, implying specific killing of peptide loaded splenocytes by H56 specific $CD8^+$ T cells (Figure 1E). In the mice that were immunized with a control construct, this balance was still 1: 1.

Thus, by applying the NetMHC3.4/ANN prediction algorithm, we identified 16 potential epitopes of which four ($H56_{62–70}$ WYYQSGLSI, $H56_{72–80}$ MPVGGQSSF, $H56_{146–154}$ IYAGLSAL, $H56_{161–169}$ MGPSLIGLA) were recognized by $CD8^+$ T cells of H56 immunized mice. These responses could be measured up to day 50 after immunization and $CD8^+$ T cells showed measurable killing capacity until day 26.

3.2. Fusion of H56 cDNA to cDNA of UB or TTFC in antigen construct increases immunogenicity

Fusion of antigen-encoding cDNA to cDNA, encoding specific pathogen-derived proteins or self-proteins involved in antigen processing, is known to increase immunogenicity.[18,27–30,34–36] To determine whether the immunogenicity of H56 could be improved likewise, different cDNA fusion constructs encoding H56 preceded by self- and non-self-derived proteins were tested. ICS for identification of specific $CD8^+$ T cells (Figure 2A) or $CD4^+$ T cells[37,38] (Figure 2B) at day 17 showed that constructs with ubiquitin (UB)[29,36] or tetanus toxin fragment C (TTFC)[27,28] fused to the N-terminal end of H56, were capable of enhancing $CD8^+$ T cell responses to the H56 epitopes, as compared to responses elicited by immunization with H56 alone, which is poorly immunogenic in this experimental setting (Figure 2C). The dominance hierarchy of the responses to different epitopes seemed similar for the two H56 fusion constructs, with $H56_{72–80}$ MPVGGQSSF being responsible for activation of the largest percentage of $CD8^+$ T cells. The control peptide $OVA_{257–264}$ was not recognized, illustrating specificity of the responses. Fusion of H56 to TTFC and UB also enhanced H56 specific $CD4^+$ T cell responses (Figure 2D, E). HLA-F-adjacent transcript 10 (FAT10)[29,39] and mouse invariant chain (mLi)[19,30] did not increase H56 specific $CD8^+$ or $CD4^+$ T cell responses (Supplementary Figure 1). We conclude that TTFC and UB are able to increase immunogenicity of the H56 encoding construct.

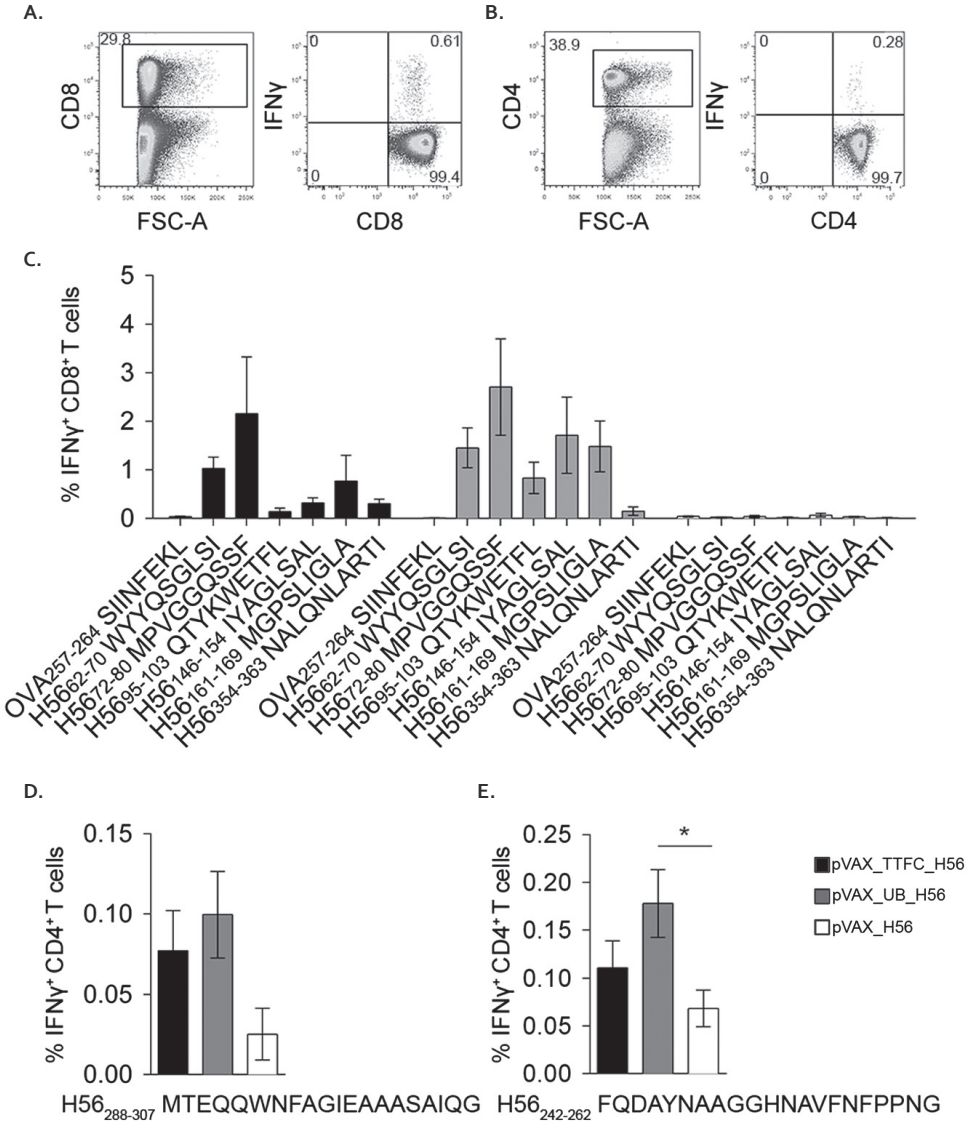

Figure 2. Fusion of H56 cDNA to cDNA of UB and TTFC enhances immunogenicity. *(A, B) CB6F1 mice were immunized with H56 cDNA using dermal DNA tattooing and percentages of (A) specific $CD8^+$ T cells and (B) CD_4^+ T cells were determined using intracellular cytokine staining at day 17. (C) Data of $CD8^+$ T cells are shown as mean of 4–5 mice per group ± SEM per peptide corrected for IFNγ background level as measured in control samples that were incubated without peptide. (D, E) Data of CD_4^+ T cells are shown as mean of 4–5 mice per group ± SEM per peptide corrected for IFNγ background level as measured in control samples that were incubated without peptide. P values < 0.05 are depicted with *.*

3.3. Substitution of the C-terminal flanking residues of identified H56 epitopes generally increases immunogenicity

The substitution of C-terminal flanking residues of epitopes in the parental antigen sequence can affect proteasome-mediated cleavage and therefore have major consequences for epitope generation.[12–17] In 5 out of 6 epitopes used in the current study, P1 contains a hydrophobic large residue with the exception of $H56_{161–169}$ MGPSLIGLA (Table 2). Of those 6 epitopes, 3 have a hydrophobic large residue at P1′ as well, thereby creating a peptide bond that has been shown to be infrequently hydrolyzed by proteasomes.[8] In order to further enhance immunogenicity of the vaccination, we adopted a second strategy in which the flanking residues of the H56 peptides $H56_{62–70}$ WYYQSGLSI, $H56_{72–80}$ MPVGGQSSF, $H56_{95–103}$ QTYKWETFL, $H56_{146–154}$ IYAGLSAL, $H56_{161–169}$ MGPSLIGLA, and $H56_{354–363}$ NALQNLARTI were changed to glutamic acid (E).[8] As proof of principle we also included the weakly immunogenic epitopes in our experimental set up, since especially their immunogenicity may be enhanced by introduction of novel COOH-terminal flanking residues that facilitate proteasome-mediated epitope generation. Reponses of mice immunized with the modified H56 construct were compared to those triggered by the wildtype H56 version using IFNγ ELISpot (Figure 3A) and IFNγ ICS (Figure 3B). Both assays showed the same pattern of $CD8^+$ T cell responses that were enhanced to E-flanked epitopes. IFNγ ELISpot showed 3 out of 6 E-flanked epitopes to be enhanced (Figure 3C) and ICS 2 out of 6 (Figure 3D). The overall results of these two assays, despite inter-experimental differences, were similar and combining these two assays, we found that 4 epitopes ($H56_{62–70}$ WYYQSGLSI, $H56_{72–80}$ MPVGGQSSF, $H56_{161–169}$ MGPSLIGLA, $H56_{354–363}$ NALQNLARTI) showed an enhanced immunogenicity following substitution of their C-terminal flanking residue for E, whereas immunogenicity of $H56_{146–154}$ IYAGLSAL seemed mildly diminished. The control peptide $OVA_{257–264}$ was not recognized, illustrating specificity of the responses. The substitutions at the P1′ site were not in the regions encoding the H56 $CD4^+$ T cell epitopes $H56_{242–262}$ FQDAYNAAGGHNAVFNFPPNG and $H56_{288–307}$ MTEQQWNFAGIEAAASAIQG[37,38] and they did not influence the $CD4^+$ T cell response to these epitopes (Figure 3E, F). Thus, C-terminal flanking residue substitution to E, where the hydrophobic epitope C-terminus is followed by a hydrophobic large or small residue in the wildtype sequence, can increase the $CD8^+$ T cell response independent of the $CD4^+$ T cell response.

3.4. The substitution of the C-terminal flanking residue of H56 derived epitopes alters their generation dynamics by the proteasome

To investigate the biochemical effects of substitution of the C-terminal flanking residues of the H56-derived epitopes into E, we performed *in vitro* digestions of the synthetic substrates $H56_{137–160}$, $H56_{64–86}$, and $H56_{53–79}$ with mouse spleen 20S proteasomes. In the digestions of the first two substrates we identified the epitopes $H56_{146–154}$ IYAGLSAL and $H56_{72–80}$

MPVGGQSSF and their potential N-extended precursors, for the latter substrate we neither identified the epitope $H56_{62–70}$ WYYQSGLSI nor its potential precursors (data not shown). The inability of MS to identify epitopes in *in vitro* proteasome-mediated digestions, which are generated *in vivo* in a proteasome-dependent fashion, has been reported[24,40,41] and is likely due to the limited sensitivity of the MS methods used.

By using the quantitative analytical approach based on QME method,[24] for comparison of $H56_{137–160}$ and $H56_{64–86}$ wild type and mutated substrates, we observed that the H56 $L_{155}E$ and the $Y_{81}E$ substitutions did not improve the relative frequency of cleavage after the preceding residues L_{154} and F_{80}, respectively (Supplementary Figure 2). The substitutions however modified the peptide pool produced by the proteasome (data not shown) and altered the overall substrate degradation rate and the proteasome preference of hydrolysis of peptide bonds distant from the H56 $L_{155}E$ or the $Y_{81}E$ substitutions (Figure 4 and Supplementary Figure 2).

The H56 $L_{155}E$ substitution decelerated the degradation of the synthetic substrate (Figure 4A), which partially hampered the amount of the epitope $H56_{146–154}$ IYAGLSAL (Figure 4B) and its potential precursor $H56_{140–154}$ (Figure 4C), which was also produced in vitro. The altered substrate degradation was likely to be the only factor influencing the epitope and precursor generation since the epitope generation efficiency was unaffected (Figure 4D). On the contrary, the $Y_{81}E$ substitution enhanced the substrate degradation rate (Figure 4E), the amount of the epitope $H56_{72–80}$ MPVGGQSSF (identified only in the mutated substrate $H56_{64–86}$ digestion; Figure 4F) and of its N-extended potential precursors $H56_{69–80}$ and $H56_{71–80}$ (Figure 4G). In contrast to the other epitopes the substitution in this case directly improved not only the absolute amount of the N-extended potential precursor but also its generation efficiency (Figure 4H). Of note, N-extended versions of other self and virus epitopes have been demonstrated to be able to trigger a $CD8^+$ T cell response even in absence of N-terminal trimming.[26,42] This *in vitro* quantitative analysis could thus explain the enhanced in vivo responses to E-flanked $H56_{72–80}$ MPVGGQSSF.

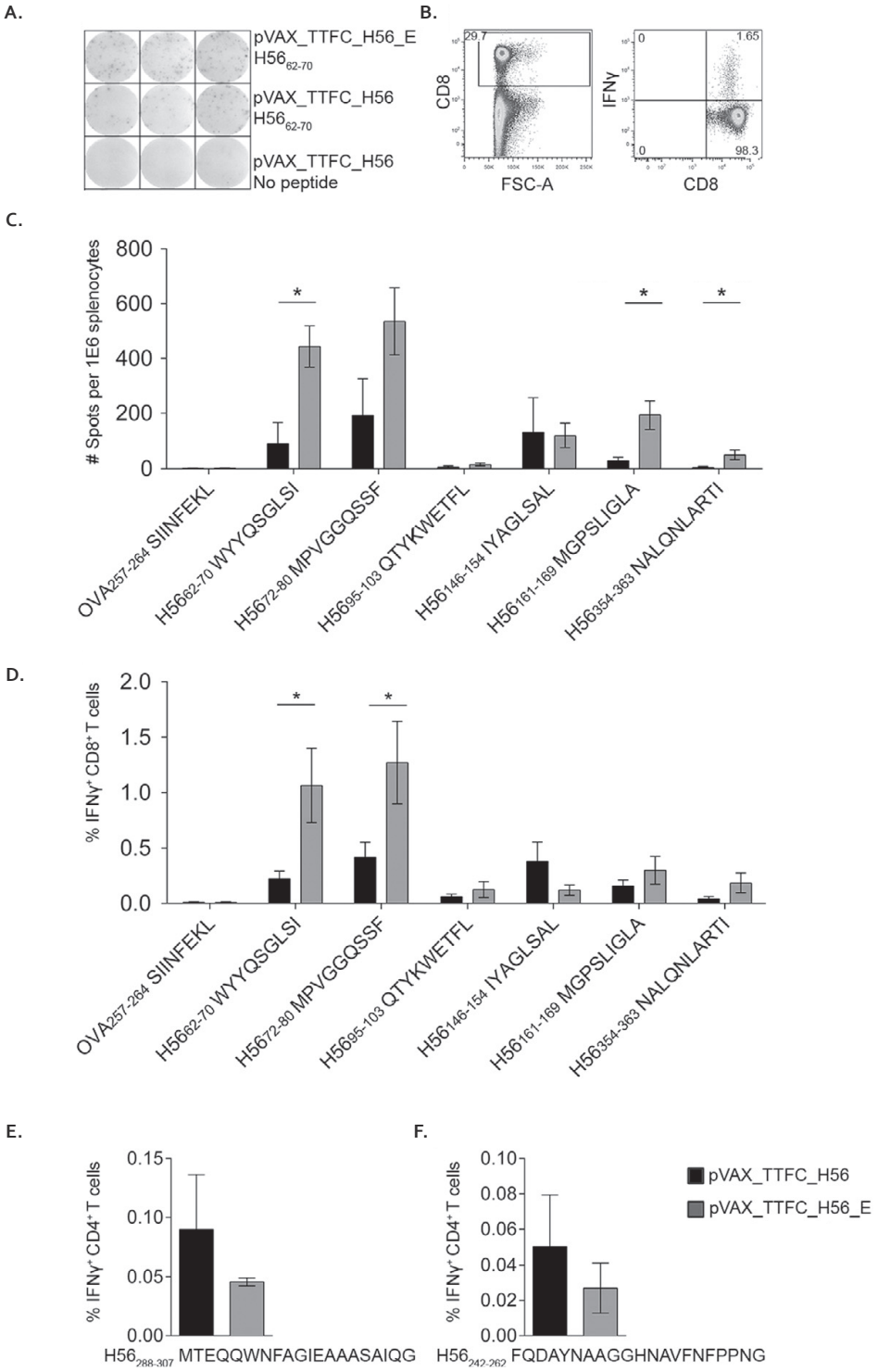
A.
pVAX_TTFC_H56_E
H56 62-70
pVAX_TTFC_H56
H56 62-70
pVAX_TTFC_H56
No peptide
B.
29.7
CD8
FSC-A
0
1.65
0
98.3
IFNγ
CD8
C.
Spots per 1E6 splenocytes
800
600
400
200
0
*
*
*
OVA257-264 SIINFEKL
H5662-70 WYYQSGLSI
H5672-80 MPVGGQSSF
H5695-103 QTYKWETFL
H56146-154 IYAGLSAL
H56161-169 MGPSLIGLA
H56354-363 NALQNLARTI
D.
% IFNγ+ CD8+ T cells
2.0
1.5
1.0
0.5
0.0
*
*
OVA257-264 SIINFEKL
H5662-70 WYYQSGLSI
H5672-80 MPVGGQSSF
H5695-103 QTYKWETFL
H56146-154 IYAGLSAL
H56161-169 MGPSLIGLA
H56354-363 NALQNLARTI
E.
% IFNγ+ CD4+ T cells
0.15
0.10
0.05
0.00
H56288-307 MTEQQWNFAGIEAAASAIQG
F.
% IFNγ+ CD4+ T cells
0.10
0.08
0.06
0.04
0.02
0.00
H56242-262 FQDAYNAAGGHNAVFNFPPNG
pVAX_TTFC_H56
pVAX_TTFC_H56_E

Figure 3. C-terminal flanking residue modulation of epitopes from hydrophobic- to polar residues enhances immunogenicity. *(A–D) CB6F1 mice were immunized with H56 cDNA using dermal DNA tattooing. (A, C) At day 17 IFNγ ELISpot was used to measure IFNγ secreting T cells in spleen. Data are shown as mean ± SEM of 5 mice per group per peptide corrected for IFNγ background level as measured in control samples that were incubated without peptide, and are representative of pooled data of 2 independent experiments out of 4 independent experiments. (B, D) Additionally at day 17 using, intracellular cytokine staining, percentages of epitope specific $CD8^+$ T cells in the spleen were measured ex vivo. Data are shown as mean ± SEM of 5 mice per group measured in triplicate per corrected for IFNγ background level as measured in control samples that were incubated without peptide, and are representative of 3 independent experiments. (E, F) Data of $CD4^+$ T cells are shown as mean of 4 mice per group ± SEM per peptide corrected for IFNγ background level as measured in control samples that were incubated without peptide. (A–D) All data were analyzed using a two tailed independent sample T test comparing pVAX_TTFC_H56 immunized animals with pVAX_TTFC_H56_E immunized animals per peptide, combined with a Sidak-Holm correction for multiple comparisons. P values < 0.05 were considered significant and marked by *.*

Table 2. Characteristics of last amino acid of epitope or first C-terminal flanking residue of different $CD8^+$ T cell epitopes in H56.

Epitope	Characteristics P1 [a]	Residue at P1′	Characteristics P1′ [a]
$H56_{62–70}$ WYYQSGLSI	HL	V	HS
$H56_{72–80}$ MPVGGQSSF	HL	Y	HL
$H56_{95–103}$ QTYKWETFL	HL	T	PS
$H56_{146–154}$ IYAGLSAL	HL	L	HL
$H56_{161–169}$ MGPSLIGLA	HS	M	HL
$H56_{354–363}$ NALQNLARTI	HL	S	PS

[a] *Amino acid characteristics of last residue of epitope (P1) and C-terminal flanking residue (P1'). Amino acid characteristic acronyms are the following: HS, hydrophobic small; HL, hydrophobic large; PS, polar small.*

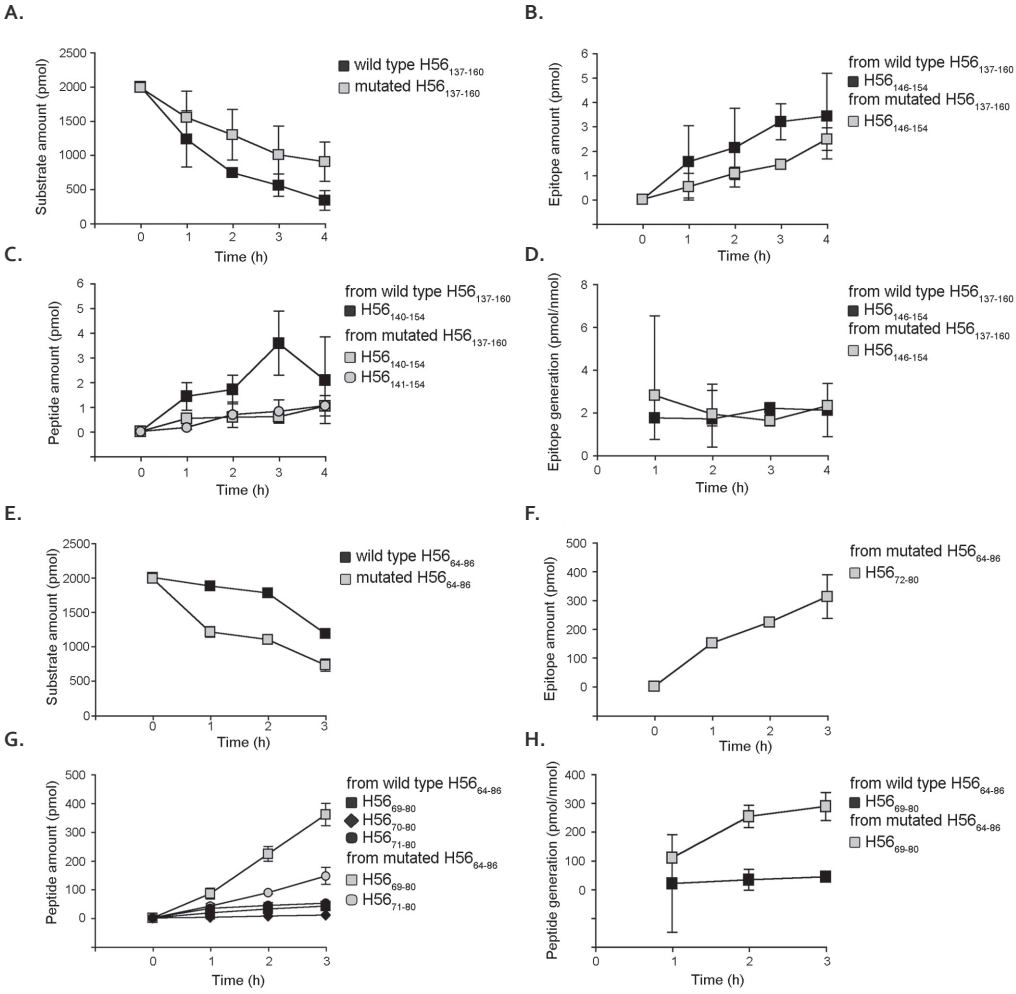

Figure 4. Substitution at the C-terminal flanking epitope residue affects the epitope production by 20S proteasomes. *(A, E) Quantitative kinetics of substrate degradation and (B–D, F–H) generation of the immuno-relevant peptides of the synthetic wild type and mutated (A–D) $H56_{137–160}$ and (E–H) $H56_{64–86}$ substrates by mouse spleen 20S proteasomes. Peptide quantification was carried out by applying QME to the LC-MS analyses. Data are the mean and bars the SD of repeated measurements of a representative kinetics of two independent experiments. (D, H) The generation efficiency for the epitopes $H56_{146–154}$ and the potential precursor $H56_{69–80}$, measured as pmol peptide per nmol of substrate consumed over time, was compared between wild type and mutated substrates.*

4. Discussion

Most vaccines aim to induce humoral responses, with immune protection mediated by neutralizing antibodies. In a number of diseases caused by intracellular pathogens, such vaccines provide insufficient protection. Because $CD8^+$ T cells can provide protection in these cases, novel vaccination strategies are developed allowing the induction of effective $CD8^+$ T cell responses. Modulation of antigen processing represents a strategy to enhance vaccine efficacy and here we report its applicability. In the model antigen H56 seven epitopes ($H56_{62–70}$ WYYQSGLSI, $H56_{95–103}$ QTYKWETFL, $H56_{161–169}$ MGPSLIGLA, $H56_{309–316}$ VTSIHSLL, $H56_{354–363}$ NALQNLARTI, $H56_{427–434}$ SQFTFSSR, $H56_{443–451}$ AGQSWCAIL) were discovered. Among them one – *i.e.* the epitope $H56_{62–70}$ WYYQSGLSI - was found as an epitope presented by HLA-A* 24:02 MHC class I molecules.[43] The processing of H56 was altered in order to increase immunogenicity. We report that fusion of H56 cDNA to cDNA encoding TTFC or UB (Figure 2) alone or in combination with a change of the (hydrophobic) C-terminal epitope flanking residues to polar residues, improves the vaccine-induced epitope specific $CD8^+$ T cell response (Figs. 3 and 4).

Numerous methods to enhance DNA vaccine potency have been reported in recent years, either by co-delivery of chemokines,[44] TLR agonists[45] or co-stimulatory genes.[46] In the current study we report fusion to UB or TTFC to enhance immunogenicity. TTFC domain 1 has been shown to increase immunogenicity[27,28,47] and was therefore used in the current study to discover novel epitopes since H56 in itself is poorly immunogenic in cDNA tattoo immunization (Figure 2C). We have no indications that TTFC affects the specificity of induced $CD8^+$ T cell responses, since (i) the known epitopes $H56_{146–154}$ IYAGLSAL and $H56_{72–80}$ MPVGGQSSF [31–33] were confirmed in our study, and (ii) immunization with the pVAX_H56 construct induced similar responses as immunization with the pVAX_TTFC_H56 fusion construct, but percentages of epitope specific $CD8^+$ T cells were very low. The immunogenicity enhancing properties of TTFC is likely due to peptide P30 ($TTFC_{91–111}$) which contains multiple HLA-DR- and -DP-presented $CD4^+$ T cell epitopes[34,48] as well as mouse MHC class II presented epitopes.[28] $CD4^+$ T cell help is crucial for $CD8^+$ T cell responses in DNA vaccination.[27,28,49] In our study, we even found TTFC to be able to enhance the H56 specific $CD4^+$ T cell response. UB naturally does not contain $CD4^+$ T cell epitopes but was able to enhance H56 specific $CD4^+$ T cells in the current study, as shown before for viral antigens.[36] This immunogenicity enhancement might be due to modified degradation kinetics when an antigen is fused to UB[29] but also to a different antigen routing in cross-presenting professional antigen presentation cells, thereby leading to improved $CD4^+$ and $CD8^+$ T cell priming.

Besides by linkage to immunogenicity-enhancing sequences, a more immediate way of modulating antigen processing is directly influencing the cleavage by the proteasome by alteration of C-terminal flanking residues of epitopes. This can be tested accurately *in vitro*.

Correlations between quantitative analysis of *in vitro* proteasome-mediated digestions and *in vivo* data have been shown[7,41,50] and are confirmed in this study. Noteworthy however, the E-substitutions in the mutated version had unpredictable effects on the usage of substrate cleavage-sites distant to the substitution and the substrate turnover as demonstrated in other examples.[26,42] This can be caused by substitution-dependent alterations of the substrate transport in the proteasome cavity or the regulation of non-catalytic modifier sites, which have been described as driving factors of proteasomal dynamics.[5]

In the current study an *Mtb* antigen was used as a model vaccine antigen but the proven strategies could be of help in vaccination against actual *Mtb* infection as well. Super immunogenic epitopes derived from conserved antigens, that induce vigorous responses associated with inflammation, immunopathology, and lung cavitation can be crucial for existence and transmission of *Mtb*.[51–53] It was therefore suggested to focus on variable antigens and target cryptic- or subdominant epitopes.[53] In mice a reduction in *Mtb* bacterial load has already been shown following vaccination with different subdominant antigens in glucopyranosyl lipid adjuvant in stable emulsion.[54] $CD8^+$ T cells specific for a selection of the novel (subdominant) epitopes showed killing capacity until day 26 in this study. Whether these $CD8^+$ T cell populations are effectively reactivated upon exposure with the pathogen remains to be determined. It should be noted however that, contrary to mice in which, depending on the strain, $CD4^+$ or $CD8^+$ T cells control infection,[31] in humans multifunctional $CD4^+$ T cells seem to be more important than $CD8^+$ T cells, as illustrated by findings that *Mtb*-infected HIV patients that lack $CD4^+$ but still possess $CD8^+$ T cells rapidly succumb to infection.[55,56] When, as is the case in the current study, sufficient $CD4^+$ T cell help is provided to the $CD8^+$ T cells by successful vaccine design, vaccine improvement by eliciting $CD8^+$ T cell responses also to subdominant epitopes could increase *Mtb* vaccine efficacy.

Competiting financial interest

The authors declare that they have no conflict of interest.

Acknowledgment

Support was by European Union's Seventh Framework Program [FP7/2007-2013] - Grant No. 280873 ADITEC to A.S., BIH CRG1-TP1 and Einstein Stiftung Berlin (A2013-174) to P.-M.K. We thank dr. I. Ludwig, D. Janssen, and K. Textoris-Taube for technical assistance. The codon optimized version of H56 and mouse invariant chain were kindly provided by Dr. A. Cara, UB and FAT10 by Dr. F. Ebstein, TTFC by Prof. T.N.M. Schumacher and the peptides by Dr. P. Henklein, P. Kunert and B. Brecht-Jachan.

References

1 P. KloetzelAntigen processing by the proteasome. Nat Rev Mol Cell Biol, 2 (3) (2001), pp. 179-187

2 K.L. Rock, I.A. York, T. Saric, A.L. GoldbergProtein degradation and the generation of MHC class I-presented peptides Adv Immunol, 80 (2002), pp. 1-70

3 E.J.A.M. Sijts, P. KloetzelThe role of the proteasome in the generation of MHC class I ligands and immune responses Cell Mol Life Sci, 68 (9) (2011), pp. 1491-1502

4 M. Aki, N. Shimbara, M. Takashina, K. Akiyama, S. Kagawa, T. Tamura, et al.Interferon-γ induces different subunit organizations and functional diversity of proteasomes J Biochem, 115 (2) (1994), pp. 257-269

5 J. Liepe, H.G. Holzhütter, E. Bellavista, P.M. Kloetzel, M.P.H. Stumpf, M. MishtoQuantitative time-resolved analysis reveals intricate, differential regulation of standard- and immuno-proteasomes eLife, 4 (2015), p. e07545 2015

6 M. Mishto, E. Bellavista, C. Ligorio, K. Textoris-Taube, A. Santoro, M. Giordano, et al.Immunoproteasome LMP2 60HH variant alters MBP epitope generation and reduces the risk to develop multiple sclerosis in Italian female population PLoS ONE, 5 (2) (2010)

7 A.C.M. Platteel, M. Mishto, K. Textoris-Taube, C. Keller, J. Liepe, D.H. Busch, et al.CD8+ T cells of Listeria monocytogenes-infected mice recognize both linear and spliced proteasome products Eur J Immunol, 46 (5) (2016), pp. 1109-1118

8 M. Mishto, J. Liepe, K. Textoris-Taube, C. Keller, P. Henklein, M. Weberruß, et al.Proteasome isoforms exhibit only quantitative differences in cleavage and epitope generation Eur J Immunol, 44 (12) (2014), pp. 3508-3521

9 M. Arciniega, P. Beck, O.F. Lange, M. Groll, R. HuberDifferential global structural changes in the core particle of yeast and mouse proteasome induced by ligand binding Proc Natl Acad Sci USA, 111 (26) (2014), pp. 9479-9484

10 A.M. Ruschak, L.E. KayProteasome allostery as a population shift between interchanging conformers Proc Natl Acad Sci USA, 109 (50) (2012)

11 J.S. Tregoning, E. KinnearUsing plasmids as DNA vaccines for infectious diseases Microbiol Spectr, 2 (6) (2014)

12 S. Le Gall, P. Stamegna, B.D. WalkerPortable flanking sequences modulate CTL epitope processing J Clin Invest, 117 (11) (2007), pp. 3563-3575

13 A.X.Y. Mo, S.F.L. Van Lelyveld, A. Craiu, K.L. RockSequences that flank subdominant and cryptic epitopes influence the proteolytic generation of MHC class I-presented peptides J Immunol, 164 (8) (2000), pp. 4003-4010

14 N.J. Beekman, P.A. Van Veelen, T. Van Hall, A. Neisig, A. Sijts, M. Camps, et al.Abrogation of CTL epitope processing by single amino acid substitution flanking the C-terminal proteasome cleavage site J Immunol, 164 (4) (2000), pp. 1898-1905

15 F. Ossendorp, M. Eggers, A. Neisig, T. Ruppert, M. Groettrup, A. Sijts, et al.A single residue exchange within a viral CTL epitope alters proteasome-mediated degradation resulting in lack of antigen presentation Immunity, 5 (2) (1996), pp. 115-124

16 M. Del Val, H. Schlicht, T. Ruppert, M.J. Reddehase, U.H. KoszinowskiEfficient processing of an antigenic sequence for presentation by MHC class I molecules depends on its neighboring residues in the protein Cell, 66 (6) (1991), pp. 1145-1153

17 U. Seifert, H. Liermann, V. Racanelli, A. Halenius, M. Wiese, H. Wedemeyer, et al.Hepatitis C virus mutation affects proteasomal epitope processing J Clin Invest, 114 (2) (2004), pp. 250-259

18 K.R. Qazi, M. Wikman, N. Vasconcelos, K. Berzins, S. Ståhl, C. FernándezEnhancement of DNA vaccine potency by linkage of Plasmodium falciparum malarial antigen gene fused with a fragment of HSP70 gene Vaccine, 23 (9) (2005), pp. 1114-1125

19 K. Karwacz, S. Mukherjee, L. Apolonia, M.P. Blundell, G. Bouma, D. Escors, et al.Nonintegrating lentivector vaccines stimulate prolonged T-cell and antibody responses and are effective in tumor therapy J Virol, 83 (7) (2009), pp. 3094-3103

[20] M. Šmahel, D. Pokorná, J. Macková, J. VlasákEnhancement of immunogenicity of HPV16 E7 oncogene by fusion with E. coli ß-glucuronidase J Gene Med, 6 (10) (2004), pp. 1092-1101

[21] C. Aagaard, T. Hoang, J. Dietrich, P.-J. Cardona, A. Izzo, G. Dolganov, et al.A multistage tuberculosis vaccine that confers efficient protection before and after exposure Nat Med, 17 (2) (2011), pp. 189-195

[22] A.D. Bins, A. Jorritsma, M.C. Wolkers, C. Hung, T. Wu, T.N.M. Schumacher, et al.A rapid and potent DNA vaccination strategy defined by in vivo monitoring of antigen expression Nat Med, 11 (8) (2005), pp. 899-904

[23] C. Lundegaard, K. Lamberth, M. Harndahl, S. Buus, O. Lund, M. NielsenNetMHC-3.0: accurate web accessible predictions of human, mouse and monkey MHC class I affinities for peptides of length 8–11 Nucleic Acids Res, 36 (Web Server issue) (2008), pp. W509-W512

[24] M. Mishto, A. Goede, K.T. Taube, C. Keller, K. Janek, P. Henklein, et al.Driving forces of proteasome-catalyzed peptide splicing in yeast and humans Mol Cell Proteomics, 11 (10) (2012), pp. 1008-1023

[25] J. Liepe, M. Mishto, K. Textoris-Taube, K. Janek, C. Keller, P. Henklein, et al.The 20S proteasome splicing activity discovered by SpliceMet PLoS Comput Biol, 6 (6) (2010)

[26] K. Textoris-Taube, C. Keller, J. Liepe, P. Henklein, J. Sidney, A. Sette, et al.The T210M substitution in the HLA-A*02:01 gp100 epitope strongly affects overall proteasomal cleavage site usage and antigen processing J Biol Chem, 290 (51) (2015), pp. 30417-30428

[27] K. Oosterhuis, P. Hlschläger, J.H. Van Den Berg, M. Toebes, R. Gomez, T.N. Schumacher, et al.Preclinical development of highly effective and safe DNA vaccines directed against HPV 16 E6 and E7 Int J Cancer, 129 (2) (2011), pp. 397-406

[28] K. Oosterhuis, E. Aleyd, K. Vrijland, T.N. Schumacher, J.B. HaanenRational design of DNA vaccines for the induction of human papillomavirus type 16 E6- and E7-specific cytotoxic T-cell responses Hum Gene Ther, 23 (12) (2012), pp. 1301-1312

[29] F. Ebstein, A. Lehmann, P. KloetzelThe FAT10- and ubiquitin-dependent degradation machineries exhibit common and distinct requirements for MHC class I antigen presentation Cell Mol Life Sci, 69 (14) (2012), pp. 2443-2454

[30] H.M. Rowe, L. Lopes, Y. Ikeda, R. Bailey, I. Barde, M. Zenke, et al.Immunization with a lentiviral vector stimulates both CD4 and CD8 T cell responses to an ovalbumin transgene Mol Ther, 13 (2) (2006), pp. 310-319

[31] K. Radoševic, C.W. Wieland, A. Rodriguez, G.J. Weverling, R. Mintardjo, G. Gillissen, et al.Protective immune responses to a recombinant adenovirus type 35 tuberculosis vaccine in two mouse strains: CD4 and CD8 T-cell epitope mapping and role of gamma interferon Infect Immun, 75 (8) (2007), pp. 4105-4115

[32] O. Denis, A. Tanghe, K. Palfliet, F. Jurion, T.-P. Van Den Berg, A. Vanonckelen, et al.Vaccination with plasmid DNA encoding mycobacterial antigen 85A stimulates a CD4+ and CD8+ T-cell epitopic repertoire broader than that stimulated by mycobacterium tuberculosis H37Rv infection Infect Immun, 66 (4) (1998), pp. 1527-1533

[33] S. D'Souza, O. Denis, T. Scorza, F. Nzabintwali, H. Verschueren, K. HuygenCD4+ T cells contain mycobacterium tuberculosis infection in the absence of CD8+ T cells in mice vaccinated with DNA encoding Ag85A Eur J Immunol, 30 (9) (2000), pp. 2455-2459

[34] F.K. Stevenson, J. Rice, C.H. Ottensmeier, S.M. Thirdborough, D. ZhuDNA fusion gene vaccines against cancer: From the laboratory to the clinic Immunol Rev, 199 (2004), pp. 156-180

[35] J. Brulet, F. Maudoux, S. Thomas, K. Thielemans, A. Burny, O. Leo, et al.DNA vaccine encoding endosome-targeted human papillomavirus type 16 E7 protein generates CD4+ T cell-dependent protection Eur J Immunol, 37 (2) (2007), pp. 376-384

[36] F. Rodriguez, J. Zhang, J.L. WhittonDNA immunization: ubiquitination of a viral protein enhances cytotoxic T-lymphocyte induction and antiviral protection but abrogates antibody induction J Virol, 71 (11) (1997), pp. 8497-8503

[37] L. Brandt, T. Oettinger, A. Holm, Å.B. Andersen, P. AndersenKey epitopes on the ESAT-6 antigen recognized in mice during the recall of protective immunity to mycobacterium tuberculosis J Immunol, 157 (8) (1996), pp. 3527-3533

[38] K. Huygen, E. Lozes, B. Gilles, A. Drowart, K. Palfliet, F. Jurion, et al.Mapping of TH1 helper T-cell epitopes on major secreted mycobacterial antigen 85A in mice infected with live mycobacterium bovis BCG Infect Immun, 62 (2) (1994), pp. 363-370

[39] M. Basler, S. Buerger, M. GroettrupThe ubiquitin-like modifier FAT10 in antigen processing and antimicrobial defense Mol Immunol, 68 (2015), pp. 129-132

[40] J. Chapiro, S. Claverol, F. Piette, W. Ma, V. Stroobant, B. Guillaume, et al.Destructive cleavage of antigenic peptides either by the immunoproteasome or by the standard proteasome results in differential antigen presentation J Immunol, 176 (2) (2006), pp. 1053-1061

[41] F. Ebstein, K. Textoris-Taube, C. Keller, R. Golnik, N. Vigneron, B.J. Van den Eynde, et al.Proteasomes generate spliced epitopes by two different mechanisms and as efficiently as non-spliced epitopes Sci Rep, 6 (2016), p. 24032

[42] S. Tenzer, E. Wee, A. Burgevin, G. Stewart-Jones, L. Friis, K. Lamberth, et al.Antigen processing influences HIV-specific cytotoxic T lymphocyte immunodominance Nat Immunol, 10 (6) (2009), pp. 636-646

[43] F.F. Weichold, S. Mueller, C. Kortsik, W.E. Hitzler, M.J. Wulf, D.M. Hone, et al.Impact of MHC class I alleles on the M. tuberculosis antigen-specific CD8+ T-cell response in patients with pulmonary tuberculosis Genes Immun, 8 (4) (2007), pp. 334-343

[44] M.A. Kutzler, K.A. Kraynyak, S.J. Nagle, R.M. Parkinson, D. Zharikova, M. Chattergoon, et al.Plasmids encoding the mucosal chemokines CCL27 and CCL28 are effective adjuvants in eliciting antigen-specific immunity in vivo Gene Ther, 17 (1) (2010), pp. 72-82

[45] A. Schneeberger, C. Wagner, A. Zemann, P. Lührs, R. Kutil, M. Goos, et al.CpG motifs are efficient adjuvants for DNA cancer vaccines J Invest Dermatol, 123 (2) (2004), pp. 371-379

[46] A. Iwasaki, B.J.N. Stiernholm, A.K. Chan, N.L. Berinstein, B.H. BarberEnhanced CTL responses mediated by plasmid DNA immunogens encoding costimulatory molecules and cytokines J Immunol, 158 (10) (1997), pp. 4591-4601

[47] K. Oosterhuis, J.H. Van Den Berg, T.N. Schumacher, J.B.A.G. HaanenDNA vaccines and intradermal vaccination by DNA tattooing Curr Top Microbiol Immunol, 351 (1) (2012), pp. 221-250

[48] P. Panina-Bordignon, A. Tan, A. Termijtelen, S. Demotz, G. Corradin, A. LanzavecchiaUniversally immunogenic T cell epitopes: promiscuous binding to human MHC class II and promiscuous recognition by T cells Eur J Immunol, 19 (12) (1989), pp. 2237-2242

[49] M.C. Wolkers, M. Toebes, M. Okabe, J.B.A.G. Haanen, T.N.M. SchumacherOptimizing the efficacy of epitope-directed DNA vaccination J Immunol, 168 (10) (2002), pp. 4998-5004

[50] P. Deol, D.M.W. Zaiss, J.J. Monaco, A.J.A.M. SijtsRates of processing determine the immunogenicity of immunoproteasome- generated epitopes J Immunol, 178 (12) (2007), pp. 7557-7562

[51] M. Coscolla, R. Copin, J. Sutherland, F. Gehre, B. De Jong, O. Owolabi, et al.M. tuberculosis T cell epitope analysis reveals paucity of antigenic variation and identifies rare variable TB antigens Cell Host Microbe,
18 (5) (2015), pp. 538-548

[52] A. Dorhoi, S.H.E. KaufmannPathology and immune reactivity: understanding multidimensionality in pulmonary tuberculosis Semin Immunopathol, 38 (2) (2016), pp. 153-166

[53] J.S. Woodworth, P. AndersenReprogramming the T cell response to tuberculosis Trends Immunol, 37 (2) (2016), pp. 81-83

[54] M.T. Orr, G.C. Ireton, E.A. Beebe, P.-D. Huang, V.A. Reese, D. Argilla, et al.Immune subdominant antigens as vaccine candidates against Mycobacterium tuberculosis J Immunol, 193 (6) (2014), pp. 2911-2918

[55] W.J. Burman, B.E. JonesClinical and radiographic features of HIV-related tuberculosis Semin Respir Infect, 18 (4) (2003), pp. 263-271

[56] C. Geldmacher, N. Ngwenyama, A. Schuetz, C. Petrovas, K. Reither, E.J. Heeregrave, et al.Preferential infection and depletion of Mycobacterium tuberculosis-specific CD4 T cells after HIV-1 infection J Exp Med, 207 (13) (2010), pp. 2869-2881

[57] B. Peters, A. SetteIntegrating epitope data into the emerging web of biomedical knowledge resources Nat Rev Immunol, 7 (6) (2007), pp. 485-490

Supporting Information

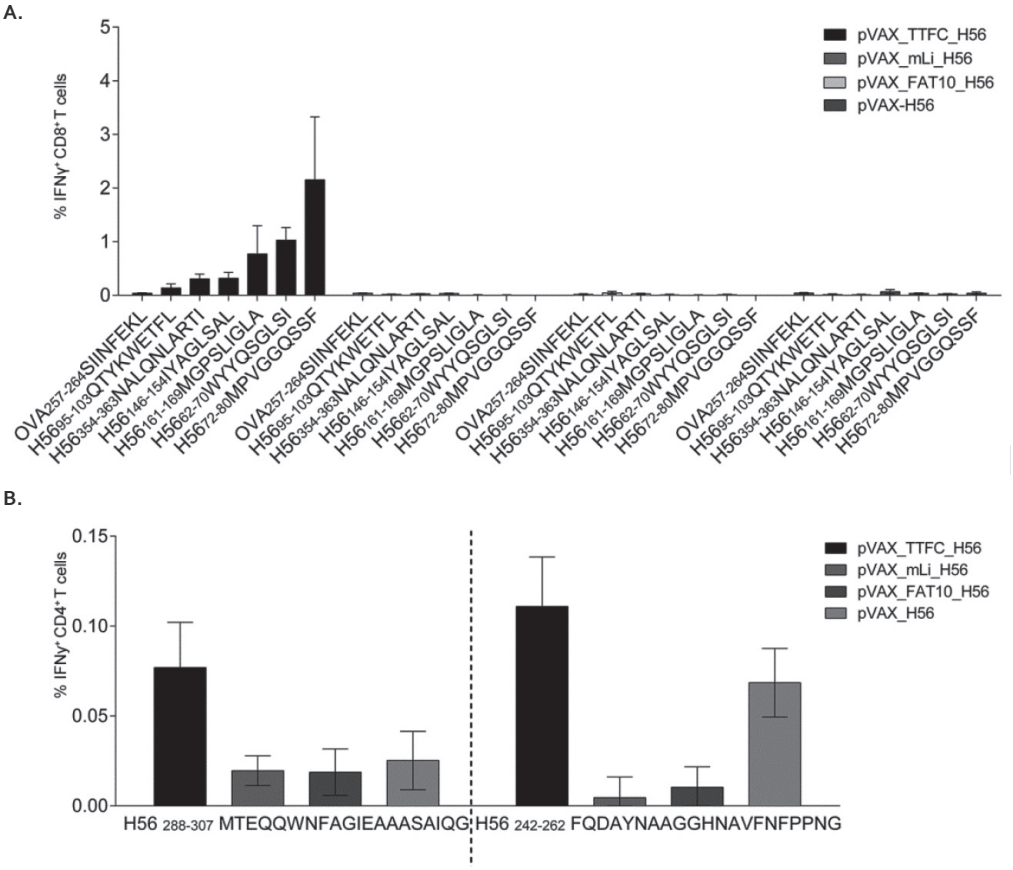

Supplementary figure 1. H56-specific CD8⁺ and CD4⁺ T cell responses in tattoo- immunized mice (A, B) *Groups of 5 female CB6F1 mice were immunized with the indicated constructs using dermal DNA tattoo immunization and at day 17 splenocytes were harvested and re-stimulated ex vivo with (***A***) $H56_{98-103}$ QTYKWETFL, $H56_{354-363}$ NALQNLARTI, $H56_{146-154}$ IYAGLSAL, $H56_{161-169}$ MGPSLIGLA, $H56_{62-70}$ WYYQSGLSI, $H56_{72-80}$ MPVGGQSSF or without peptide or (***B***) $H56_{288-307}$ MTEQQWNFAGIEAAASAIQG or $H56_{242-262}$ FQDAYNAAGGHNAVFNFPPNG and then stained with fluorochrome- conjugated mAbs to detect CD8 and CD4 cell surface expression and intracellular IFNγ. Representative FACS plots, analyzed with FlowJo software, including percentages of IFNγ⁺ CD8⁺ and IFNγ⁺ CD4⁺ T cells are shown in Figure 2A and Figure 2B, respectively.*

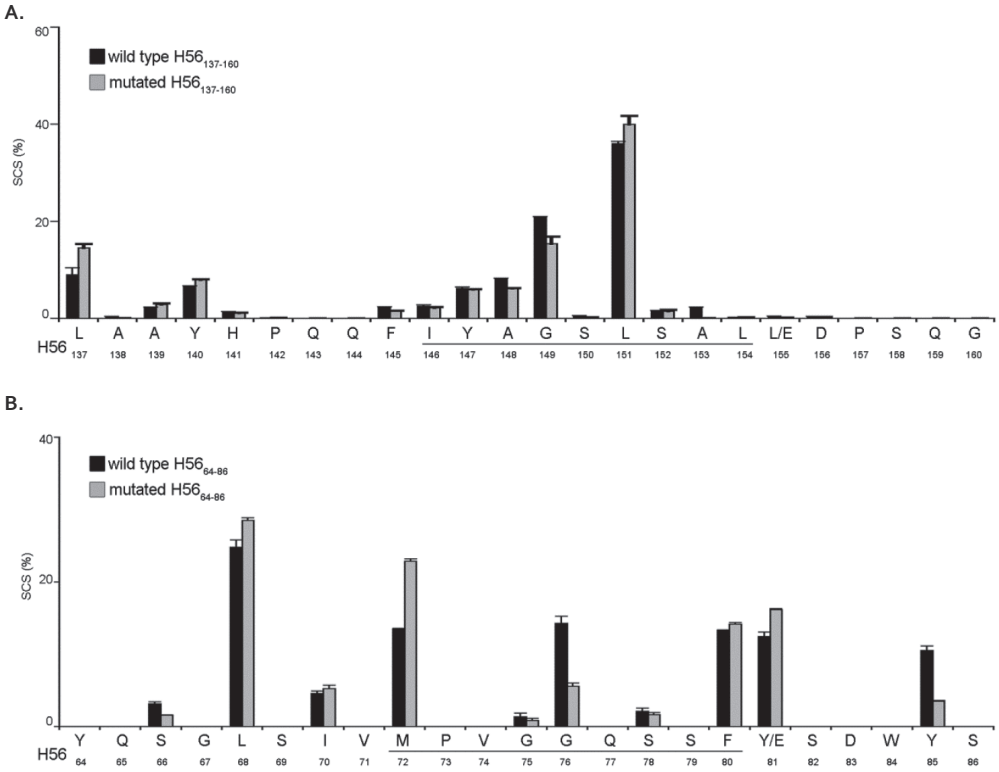

Supplementary figure 2. Relative frequency of proteasome-mediated cleavages in wild type and mutated $H56_{137\text{-}160}$ and $H56_{64\text{-}86}$ substrates. (A, B) *The site-specific cleavage strength (SCS), which describes the relative frequency of proteasome-mediated cleavage after any given residue of the synthetic polypeptide substrate,[1] in wild type and mutated (**A**) $H56_{137\text{-}160}$ and (**B**) $H56_{64\text{-}86}$ substrates detected following in vitro digestion with purified mouse 20S proteasomes is shown. For the SCS computation we applied the QME method to the pool of peptides common to the wild type and mutated substrates as explained elsewhere.[2] The values are the average and bars the SD of 2 measurements and of 4 time points of a representative assay. The epitopes $H56_{146\text{-}154}$ and $H56_{72\text{-}80}$ are marked by a line.*

References

1 Mishto M, Goede A, Taube KT, Keller C, Janek K, Henklein P et al. Driving forces of proteasome-catalyzed peptide splicing in yeast and humans. Molecular and Cellular Proteomics 2012;11(10):1008-23.

2 Textoris-Taube K, Keller C, Liepe J, Henklein P, Sidney J, Sette A et al. The T210M substitution in the HLA-A*02:01 gp100 epitope strongly affects overall proteasomal cleavage site usage and antigen processing. J Biol Chem 2015.

Part II

Delivery and Immunogenicity of Biopharmaceuticals for Therapy


5

Overcoming lipidoid-mediated TLR4 activation with lipidoid-polymer nanoparticles: *In silico* modelling and *in vitro* testing

In review

Anne Marit de Groot[a]*
Kaushik Thanki[b]*
Monique Gangloff[c]
Emily Falkenberg[b]
Xianghui Zeng[b]
Djai C.J. van Bijnen[a]
Willem van Eden[a]
Henrik Franzyk[d]
Hanne M. Nielsen[b]
Femke Broere[a]
Nick J. Gay[c]
Camilla Foged[b]
Alice J.A.M. Sijts[a]

[a] Department of Infectious Diseases and Immunology, Utrecht University, Utrecht, The Netherlands
[b] Department of Pharmacy, Faculty of Health and Medical Sciences, University of Copenhagen, DK-2100 Copenhagen, Denmark
[c] Department of Biochemistry, University of Cambridge, Cambridge, United Kingdom
[d] Department of Drug Design and Pharmacology, Faculty of Health and Medical Sciences, University of Copenhagen, DK-2100 Copenhagen, Denmark

* equal contribution

Graphical abstract

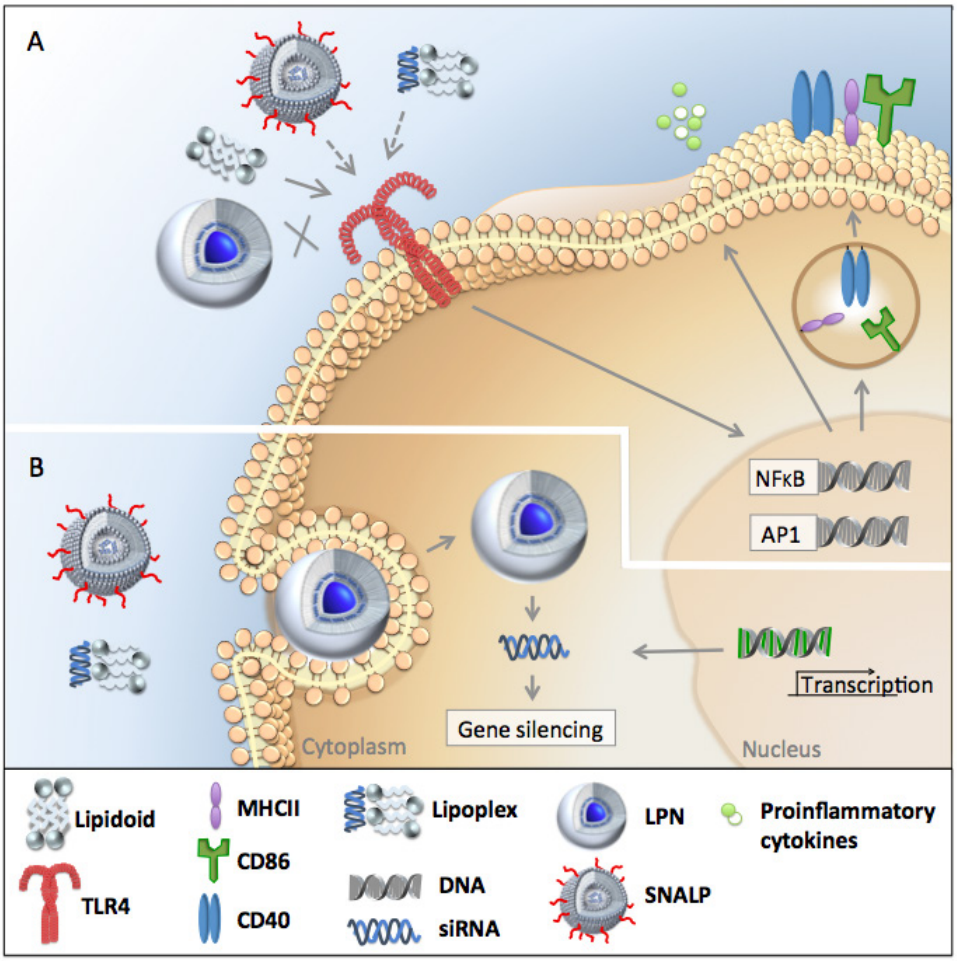

Abstract

Therapeutics based on small interfering RNA (siRNA) have promising potential as antiviral and anti-inflammatory reagents. To deliver siRNA across cell membranes to the RNA interference pathway in the cytosol of target cells, non-viral nanoparticulate delivery approaches are explored. We recently showed that encapsulation of siRNA in lipid-polymer hybrid nanoparticles (LPNs) based on poly(DL-lactic-co-glycolic acid) (PLGA) and cationic lipid-like materials (lipidoids) remarkably enhances intracellular delivery of siRNA as compared to siRNA delivery with LPNs modified with dioleoyltrimethylammoniumpropane (DOTAP) as the lipid component. However, potential lipid-mediated immune modulation remains unexplored. Testing lipidoids and DOTAP for innate immune receptor activating properties, we found that lipidoids, but not DOTAP are agonists for human toll-like receptor 4 (TLR4) and activate murine antigen-presenting cells *in vitro*. This agonistic effect was further confirmed *in silico* using a prediction model based on crystal structures. However, by combining lipidoids with PLGA into LPNs, TLR4 activation was abrogated, demonstrating that particle engineering is essential for preventing lipidoid-induced TLR4 activation. TLR4 activation was also measured for lipidoids formulated as stable nucleic acid lipid particles, which is the reference formulation for siRNA delivery. In conclusion, lipidoid-mediated TLR4 activation during siRNA delivery can be overcome via optimization of formulation design.

Keywords

lipidoids
lipid-polymer hybrid nanoparticles
TLR4
immune modulation
stable nucleic acid lipid particles (SNALPs)
lipoplexes
molecular modelling

1. Introduction

Small interfering RNA (siRNA) holds a highly promising therapeutic potential for the treatment of a variety of diseases via gene silencing.[1-3] However, the physicochemical properties of siRNA often limit its therapeutic efficacy rendering it unfavorable for efficient intracellular delivery to the RNA interference (RNAi) pathway mediating gene silencing in the cytosol of the target cells. These properties include a relatively large molecular weight and high hydrophilicity as a result of the polyanionic phosphate backbone, leading to negligible cellular membrane permeation. Therefore, realization of the therapeutic potential of siRNA is fully dependent on the design and development of efficacious and safe siRNA delivery technologies.

Intracellular delivery of siRNA can be enhanced by employing nanoparticle-based delivery approaches.[4-7] Lipid-based delivery systems, in particular cationic lipids, have been shown to facilitate overcoming critical barriers to efficient siRNA delivery, which include pharmacokinetic barriers (a short circulation half-life due to susceptibility for nuclease degradation) and barriers at the cellular level (cellular uptake, intracellular trafficking and endosomal escape to reach the cytosol).[5] However, major drawbacks of commonly applied cationic lipids for siRNA delivery, *e.g.,* 1,2-dioleoyl-3-trimethylammonium-propane (DOTAP), 1,2-di-O-octadecenyl-3-trimethylammonium propane (DOTMA) and dimethyldioctadecyl-ammonium bromide (DDAB), include: (*i*) limited electrostatic interaction with siRNA as a result of the single quaternary ammonium headgroup, (*ii*) activation of the innate immune system leading to undesired side effects, and (*iii*) unfavorable biodistribution because of nonspecific tissue distribution and protein binding, eventually resulting in a relatively narrow therapeutic window.[8, 9]

Recent advances in the field of RNAi therapeutics have led to the identification of a novel class of synthetic cationic lipids, the so-called lipidoids, which are capable of mediating highly efficient intracellular delivery of siRNA.[10-14] Lipidoids are lipid-like structures containing multiple secondary and tertiary amino groups, which confer highly efficient interaction with anionic siRNA molecules.[10] Lipidoids have been formulated as long-circulating stable nucleic acid lipid particles (SNALPs), comprised also of cholesterol and PEGylated phospholipids, for intravenous administration.[10, 15] The therapeutic efficacy of lipidoid-based SNALPs has been demonstrated in a number of *in vivo* models, but data from these studies also indicates potential symptoms of splenomegaly at higher doses.[10] In addition, lipidoids, even in combination with control siRNA, can induce immunostimulatory effects[16] Several clinical trials involving SNALPs have been terminated owing to the occurrence of an influenza-like syndrome in the dosed patients[17-19] Premedication with corticosteroids is often necessary to circumvent infusion-related problems[20, 21] Hence, there is an urgent need for the design and development of novel and safe drug delivery systems that can be applied to overcome the hurdles involved in intracellular delivery of siRNA. Recently, we recognized the potential of

one specific type of nanocarriers, *i.e.,* lipid-polymer hybrid nanoparticles (LPNs), and highly promising results were demonstrated for safe and efficient intracellular delivery of siRNA.[22]

While gene silencing efficiency and effect on cell viability are often reported in the literature, the immune modulatory effects of siRNA and delivery systems remains poorly described. Nucleic acids generally activate the innate immune system *via* binding to pattern-recognition receptors (PRRs), among them the Toll-like receptors (TLRs).[23] Chemical modifications of siRNA are commonly used to reduce undesired immune effects.[24] However, excipients used for siRNA delivery systems may also be recognized by the immune system because they adopt a structure similar to components of pathogens and hence stimulate a cascade of deleterious immune effects, which may lead to failure of therapy.[25] So far, immunogenicity assessment of lipidoids has not been reported, albeit a thorough evaluation is warranted, considering their promising therapeutic potential.

The purpose of the present study was to assess the immune modulatory effects of an array of compounds comprising different degree of alkylation, *i.e.,* lipidoid 4 (L_4), lipidoid 5 (L_5), lipidoid 6 (L_6), and lipidoid mix (L_{mix}) (Supplementary data, Figure S1)[10] by using human TLR reporter cell line-based assays and *in silico* modelling. Furthermore, the immune modulatory effects of lipidoid-containing LPNs were compared to those of lipoplexes, SNALPs and DOTAP-modified LPNs.

2. Materials and methods

2.1 Materials

2'-O-methyl modified dicer substrate asymmetric siRNA duplexes directed against enhanced green fluorescent protein (EGFP-siRNA) and scrambled negative control siRNA were synthesized by GlaxoSmithKline (Stevenage, UK) and provided generously as dried, purified and desalted duplexes (Supplementary data, Table S1). The siRNA stock solutions were prepared in 4-(2-hydroxyethyl)-1-piperazineethanesulfonic acid) (HEPES) buffer (5 mM, pH 7.4) and re-annealed employing a standard protocol recommended by IDT (Coralville, IA, USA). PLGA with a lactide-to-glycolide molar ratio of 75:25 and a molecular weight of 20 kDa was procured from Wako Pure Chemical Industries (Osaka, JP). Polyvinylalcohol (PVA) 403 with an 80.0% degree of hydrolysis was purchased from Kuraray (Osaka, JP). Cholesterol, DOTAP and N-palmitoyl-sphingosine-1-succinyl[methoxy(polyethylene glycol)2000] (C_{16} PEG_{2000} ceramide) were obtained from Avanti Polar Lipids (Alabaster, AL, USA). Heparin, octyl-β-d-glucopyranoside (OG) and Tris–EDTA buffer (10 mM Tris, 1 mM EDTA, pH 7.5) (TE buffer) were purchased from Sigma-Aldrich (St. Louis, MO, USA). RNase-free diethyl pyrocarbonate (DEPC)-treated Milli-Q water was used for all buffers and dilutions. All other chemicals unless stated were of analytical grade and obtained from local suppliers.

2.2 Preparation of lipoplexes

The array of lipidoids was synthesized, purified and characterized as previously described.[22] Lipoplexes were prepared by co-incubation of the lipidoids (L_4, L_5, L_6 and L_{mix}) and EGFP-siRNA. A stock solution (40 mg/ml) of the respective lipidoid was prepared by dissolving it in dimethyl sulfoxide (DMSO) containing 1% (v/v) trifluoroacetic acid. Lipoplexes were prepared by addition of the stock solution to an siRNA solution in TE-buffer at a lipidoid:siRNA ratio of 1:20 (w/w). The lipoplexes were vigorously vortexed before use. For L_{mix}, the molecular weight of L_5 was assumed for molarity calculations.

2.3 Preparation of SNALPs

Lipidoid-based SNALPs were prepared as reference formulation for comparative purpose. A previously reported ethanol destabilization method[10] was adopted[22] and employed for preparation of L_5-modified SNALPs and L_{mix}-modified SNALPs. Briefly, an *in situ* buffer formation technique was used to formulate lipidoid-based SNALPs considering its low solubility in EtOH. The lipidoid, cholesterol and C_{16} PEG_{2000} ceramide were dissolved in EtOH at molar ratio of 42:48:10 using glacial acetic acid, and the mixture was added to an aqueous solution of NaOAc, resulting into formation of non-loaded SNALPs. The SNALPs were prepared at a lipid concentration of 10 mg/ml and loaded with EGFP-siRNA at an siRNA:lipid loading ratio of 1:7.5 (w/w) at 37°C for 30 min. The siRNA-loaded SNALPs were dialyzed against 1000x volume phosphate-buffered saline (pH 7.4) using a 100 kDa molecular weight cut off dialysis membrane cassette (Float-A-Lyzer®, G2, Spectrum Laboratories, Rancho Dominguez, CA, US) for 2 h at room temperature to remove excess EtOH and un-entrapped siRNA. The detailed protocol for the preparation of SNALPs has been reported elsewhere.[22]

2.4 Preparation of LPNs

Lipidoid- and DOTAP-modified LPNs were prepared by using the double emulsion solvent evaporation method, as reported previously,[26] but with a slight modification.[22] Briefly, an aqueous phase (w_1) comprising the required amount of EGFP-siRNA in 125 µl HEPES buffer (5 mM, pH 7.4) was added to an organic phase (o, 250 µl CH_2Cl_2) containing PLGA and lipidoid or DOTAP. The formed primary emulsion was subjected to probe-sonication at an amplitude of 50 (Misonix, Qsonica, LLC. CT, USA) in an ice bath. The primary w_1/o emulsion was phase inversed by addition of 1 ml of 2% (w/v) PVA solution and vigorous vortexing for 1 min. The formed secondary w_1/o/w_2 double emulsion was subsequently subjected to probe-sonication at an amplitude of 50 for additional 60 s. The size-reduced emulsion was transferred to a 25 ml beaker, and 5 ml of 2% (w/v) PVA solution was added under stirring. The stirring was continued for 45 min to facilitate the evaporation of the organic solvent. The prepared LPNs were then washed, purified and lyophilized as reported previously.[22] The lipidoid-modified LPNs were prepared at

a lipidoid content of 15% (w/w) of the total solid content, whereas DOTAP-modified LPNs were prepared at 10% (w/w). Furthermore, the siRNA:lipidoid weight ratio was kept constant at 1:20 in case of lipidoid-modified LPNs, whereas it was 1:10 (w/w) for the DOTAP-modified LPNs.

2.5 Physicochemical characterization

The formulations were characterized with respect to hydrodynamic diameter, polydispersity index (PDI), zeta potential, and siRNA entrapment efficiency as previously described.[22] In brief, a dynamic light scattering technique employing photon correlation spectroscopy (Zetasizer Nano ZS, Malvern Instruments, Worcestershire, UK)) was used to measure the particle size and PDI of the formulations. Furthermore, the same samples were also used to measure the zeta potential employing the principles of laser-Doppler micro-electrophoresis. The data for three independent batches was recorded and analyzed using the Zetasizer Software version 7.11 (Malvern Instruments Ltd).

The siRNA entrapment efficiency of LPNs and SNALPs was evaluated using a previously reported procedure.[22, 26] Briefly, siRNA was extracted from the formulations and subsequently quantified using the Quant-iT™ RiboGreen® RNA Assay Kit (Molecular Probes, Invitrogen Inc, Paisley, UK) according to the manufacturer's protocol. The encapsulation efficiency and practical loading were calculated using the following equations:

$$\textit{Encapsulation efficiency} = \frac{\textit{Amount of entrapped siRNA}}{\textit{Total amount of added siRNA}} \times 100 \qquad \text{Equation 1}$$

$$\textit{Practical loading} = \frac{\textit{Amount of entrapped siRNA}}{\textit{Total weight of nanoparticles}} \times 100 \qquad \text{Equation 2}$$

2.6 Toll-like receptor activation assays

The human TLR reporter cell lines (HEK-Blue™ hTLR2, -hTLR3, -hTLR4, -hTLR7 and –hTLR9 reporter cells) were cultured according to the manufacturer´s instructions (Invivogen, Toulouse, FR). Activation of hTLRs was measured according to the previously reported protocol.[27] In brief, cells were seeded in flat 96-well plates and stimulated with different dilutions of fully dispersed lipids, lipoplexes, LPNs and SNALPs, respectively, for 16 h at 37 °C, after which the cell culture supernatants were incubated with protein substrate QUANTIBlue™ (Invivogen) for 1 h. Absorption was measured using a microplate reader (Bio-Rad 550, Bio-Rad Laboratories, Inc., CA, USA) at OD_{650} nm. The control value (solvent incubated) was subtracted from sample value. The relative alkaline phosphatase levels were then defined relative to the maximum TLR activation by the corresponding agonist.

2.7 BM-APC differentiation and APC maturation assays

Murine BM-APCs were differentiated with GM-CSF and cultured according to a reported protocol.[27] Briefly, BM-APCs were stimulated with PBS (1:100 or 1:25, v/v), LPS (O127:B8, 10 ng/ml, Sigma-Aldrich, MO, USA) or with a concentration series of fully dispersed lipids, lipoplexes, LPNs or SNALPs, respectively, for 16 h at 37°C. Maturation was measured by antibody staining of the maturation markers CD40 and CD86, and the samples were analyzed using flow cytometry. Ethical approval for the mouse experiment was obtained from the Animal Experiment Committee of Utrecht University, The Netherlands, #DEC.2013.II.09.102.

2.8 Molecular modelling studies

The atomic coordinates of DOTAP and L_4, L_5 and L_6 lipidoids were generated using the Sybyl software, a general molecular modelling program from Tripos, for which a partial license was donated to the Department of Biochemistry, University of Cambridge, UK.[28] Briefly, Sybyl's sketching tool was used to build the molecules, followed by a clean-up, which performs rough dynamics. Constraints were applied to bond lengths, angles, and torsions. The geometry of the molecules was optimized using the Powell minimization method with initial optimization based on the Simplex method, with a gradient of 0.05 kcal/mol and a maximum of 100 cycles of iteration. Partial charges were computed based on the Gasteiger-Hückel charge method using calculator plugin of Marvin Suite (Version 17.2.20, ChemAxon, Budapest, Hungary).[29] AutoDockTools4.[30] was used to convert the atomic coordinate files into a Protein Data Bank (PDB) – partial charge, Q and atom type, T (PDBQT) format that contains the partial charges and atom types of the molecules, in addition to the atomic coordinates.[30]

For docking studies, the human crystal structures of lymphocyte antigen 96 (also known as MD-2) in the absence and presence of TLR4 (PDB codes 2E59 and 3FXI, respectively) were used for docking upon removal of the ligands bound to the protein complexes. The potential ligands (DOTAP and L_5) were docked into MD-2 using Autodock Vina.[31] The protein component was kept rigid, whereas the ligand was allowed full flexibility. The Autogrid parameters were computed on an initial grid size of 32 x 32 x 32 $Å^3$, with a spacing of 1 Å. The grid was centered on MD-2 at x = + 22.626; y = - 9.61; z = + 15.271. The default optimization parameters were used for the iterated search in Vina, with a value of 32 for exhaustiveness. Flexible docking performed with DOTAP and lipidoid ligands generated a number of poses, ranked according to their binding energies. The highest energy poses predicting to the best binding mode according to the Vina algorithm were then subjected to rigid docking in order to compare the binding affinity of molecules of different sizes. The conformation of the docked ligands and their contacts with MD-2 and TLR4, where appropriate, were analyzed using PISA.[32] Structural images were generated in PyMol (http://www.pymol.org) and Chimera.[33] Detailed interactions were also analyzed

using LigPlot+.[34] Control docking experiments were performed on ligands with known crystal structures to compare their binding energies to lipidoids and DOTAP molecules. Controls included a potent TLR4/MD-2 agonist: the lipid A moiety of *Escherichia coli* LPS[35]; a species-specific antagonist: lipid Iva[36]; and a potent antagonist: eritoran.[37] Rigid docking of these control ligands provided the binding energies that directly related to the experimental conformations adopted by these molecules.

2.9 Statistics

Results are expressed as mean values ± standard deviation (SD). Statistical analysis was performed using GraphPad Prism (GraphPad, La Jolla, CA, USA). Statistically significant differences were assessed by analysis of variance (ANOVA), followed by a Dunnett's multiple comparison test, *p*-value below 0.05 was considered statistically significant. Significance of the results is indicated according to *p* values (*, $p < 0.05$; **, $p < 0.01$; and ***, $p < 0.001$). A *p* value below 0.05 was considered statistically significant.

3. Results

3.1 Bulk lipidoids activate TLR4 responses

The potential immunogenicity of lipidoids reported previously[10] was evaluated by assessing the ability of the bulk compounds to activate the innate immune system via TLRs by using human TLR reporter cell lines. A concentration-dependent increase in the activation of TLR4 was noted for all lipidoids, *i.e.* L_4, L_5, L_6 and L_{mix} up to 1 μM concentrations (**Figure 1A**). The discrepancies in TLR4 activation above 1 μM could be attributed to the differential interference of the compounds with the assay: The strongest TLR4 activation was noted for L_6, which could be attributed to multiple factors, including interference with cell viability and the physicochemical properties of the lipidoids. No significant difference in the activation of TLR4 was noted between L_4 and L_5 at the highest tested concentration (*p*-value > 0.05). Overall, a statistically significant higher TLR4 activation was noted for L_6 (*p*-value < 0.001) and L_{mix} (*p*-value < 0.01) as compared to L_5, for which reason L_5 was selected for further testing (Figure 1C-F). In contrast to L_4-L_6, DOTAP did not activate TLR4 in the tested concentration range up to 28.6 μM, although, TLR4 activation was noted at the highest concentration DOTAP tested (0.29 mM, *p*-value < 0.01) (**Figure 1B**). In order to assess further potential assay interference due to changes in cell viability, the experiments were performed in the presence of the TLR4 agonist lipopolysaccharide (LPS). Both for L_5 and DOTAP, interference with the measurement of TLR4 activity was found at higher concentrations (**Figure 1C**). The lipidoids were also tested for their ability to activate TLR2, however, no activation was noted for L_5 even at the highest tested concentration (10 μg/ml), whereas the positive control Pam_3CSK_4

activated TLR2 (**Figure 1D**). However, all lipidoids at concentrations above 1 μM did interfere with the TLR2 activation, as demonstrated in the presence of the activator Pam_3CSK_4 (**Figure 1E**). To validate the observed results, the activity of L_5 was also tested against TLR3, and no activation was noted (**Figure 1F**). The activity of L_5 was also tested against TLR7 and TLR9, but no activation was measured either (data not shown). Thus, L_4, L_5, and L_6, but not DOTAP activates TLR4 and interference with activation occurs at higher concentrations for all.

3.2 *In silico* prediction of docking to TLR4/MD-2 suggests that lipidoids are potent agonists

Lipidoids have been designed for optimal RNA interference experiments. Their cationic headgroups neutralize the anionic charges of the nucleic acids they transport, while their lipid moieties provide a hydrophobic scaffold ideally suited to cross membranes. These features seem to also target the innate immune LPS sensor TLR4/MD-2. TLR4 is associated with myeloid differentiation factor 2 (MD-2) on the cell surface, and MD-2 is required for signaling.[38] While the number of acyl chains and the presence of phosphate groups are key features for LPS recognition, here we explore the potential binding mode of positively charged lipidoids containing tetra amine backbones. We will refer to the headgroup amines as N1, N2, N3 and N4 in the following section. The tetra-acylated lipidoid (L_4) is made up of an acylated backbone with two acyl chains bound to terminal headgroup amines (N1 and N4) while penta-acylated lipidoid (L_5) has an extra acyl chain at N3 and hexa-acylated lipidoid (L_6) has two extra acyl chains at N2 and N3 (**Figure S1**). At pH 7.0, L_4 lipidoid is predicted to possess protonated headgroup amines in positions N1 and N3. Upon acidification, an additional protonation may arise on N4. The protonation state differs slightly in L_5, wherein an extra acyl chains shifts protonations to positions N2 and N4 at pH 7.0, and N1, N2 and N4 in more acidic conditions (pH 6.0). In contrast, the protonation is predicted on N1 and N4 amines at both pH 7.0 and pH 6.0 in case of L_6. More acidic environments of pH 5.0 and below may trigger a third protonation at N2. The experimentally observed interaction of lipidoids with TLR4 cell lines is further investigated by *in silico* docking studies. We have performed docking at pH 7.0 to compare binding affinities to MD-2 and TLR4 (**Table 1**) and identified the binding modes for lipidoids (**Supplementary information**, Tables S3-S6) using Autodock Vina software (31). DOTAP and other ligand complexes with known crystal structures are included as controls. These comprise of species-specific antagonist lipid IVa,[36] the potent agonist lipid A of LPS from *Escherichia coli*,[35] and the potent antagonist eritoran.[37]

The predicted binding energies suggest that lipidoids are notably more potent than other known TLR4 agonists with a predicted binding energy of -32.7 kcal/mol for L_4, -39.2 kcal/mol for L_5 and -41.4 kcal/mol for L_6, whereas a much lower binding energy was predicted for DOTAP (-22.6 kcal/mol, **Table 1**). The binding to MD-2 in inactive[36] and

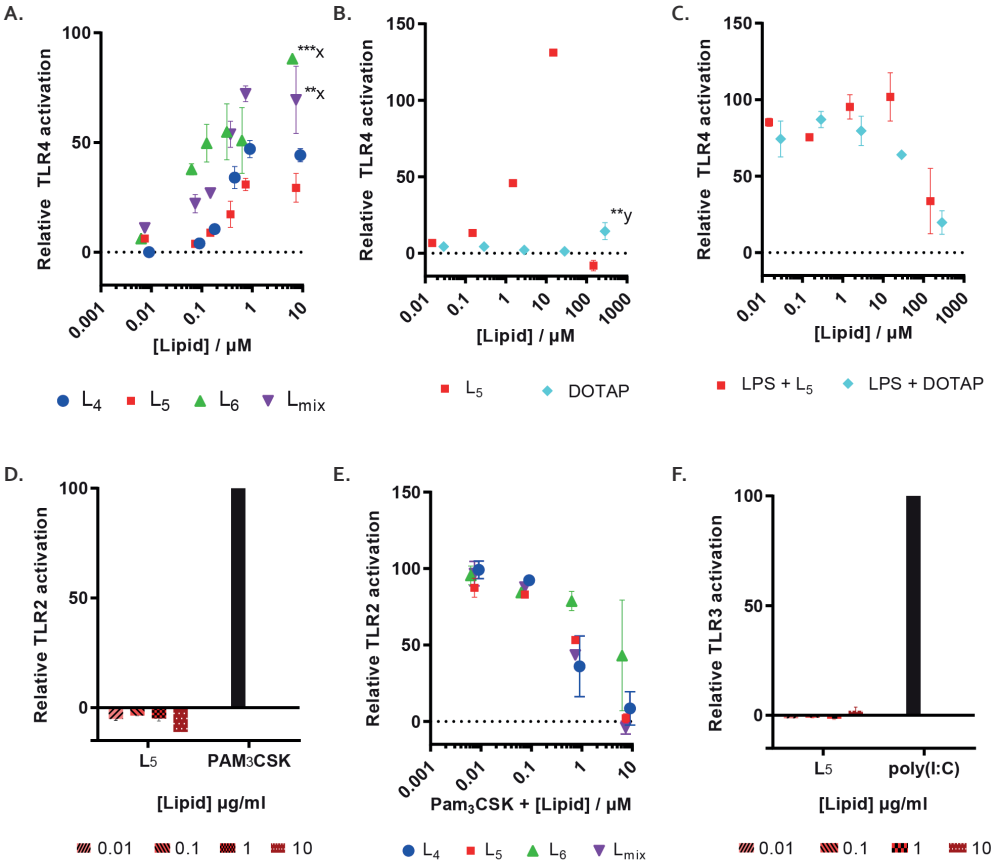

Figure 1: Lipidoid-induced Toll-like receptor activation was assessed using HEKblue human TLR reporter cell lines. *TLR4-expressing cells were stimulated with L_4, L_5, L_6, and L_{mix} concentrations ranging from 0.001-10 µM, for 16 h at 37 °C (A) as well as with L_5 or DOTAP in the concentration range from 0.01-300 µM (B). Activation of the TLR4-expressing cell line by L_5 or DOTAP in the presence of LPS, 10 ng/ml (C). Incubation of the TLR2-expressing cell line with L_5 and the positive control PAM_3CSK_4 (D). Incubation of the TLR2-expressing cell line with lipidoids in the presence of PAM_3CSK_4, 100 ng/ml (E). Incubation of the TLR3-expressing cell line with L_5 and positive control poly(I:C) (F). Data have been corrected for background measured for medium-stimulated cells and are shown relative to the maximal response (100%) with the respective selective agonists: LPS (10 ng/ml for TLR4) (A-C), PAM_3CSK_4 (100 ng/ml for TLR2) (D-E) and poly(I:C) (5 µg/ml for TLR3) (F). Data represent mean values ± SD (n=3) and represent results of one of two independent experiments. Statistically significant differences from L_5 are indicated with x and from PBS is indicated with y: *p < 0.05, **p < 0.01 and ***p < 0.001.*

active conformations,[35] respectively, was also compared. For all crystal structures published to date, agonists seem to interact with the F126 loop of MD-2 that subsequently adopts a more compact conformation enabling TLR4 dimerization.[35] In contrast, in the absence of ligand or in the presence of an antagonist, this loop protrudes into the solvent, which prevents receptor dimerization, either directly by causing steric hindrance, or indirectly by not contributing to the dimerization interface.[37] Hence, the predicted binding of L_5 to active and inactive MD-2, respectively, was compared: The affinity was highest for the active MD-2 (-36.5 kcal/mol, as compared to -33.2 kcal/mol for inactive MD-2). The opposite is the case of known antagonist in humans, lipid IVa: The affinity for the inactive conformation of MD-2 was -25.1 kcal/mol, as compared to -18.5 kcal/mol for the active MD-2. The affinity of DOTAP for inactive MD-2 was remarkably low (-11.1 kcal/mol), which suggests that its binding is probably not specific. Hence, data support that L_5 is likely to bind and activate TLR4/MD-2, while DOTAP binding remains questionable. Interestingly, other tested lipidoids (L_4 and L_6) also exhibited similar profiles for binding energies to active and inactive TLR4/MD-2 (**Table 1**). Although, the difference in the predicted binding energies was relatively higher in case of L_4 and L_6, primary emphasis was given to L_5 because of its relatively higher transfection potential.

Further, although *E.coli* LPS is the most potent TLR4/MD-2 agonist, its lipid A moiety is predicted to bind with affinities comparable but lower that L_5, which range from -27.7 kcal/mol for active MD-2 to -34.7 kcal/mol to the TLR4/MD-2 dimeric complex. This suggests that core sugars contribute to the activity of LPS. Tetra-acylated eritoran in contrast lacks sugars and resembles lipid IVa in terms of binding energies (-23.3 and -25.1 kcal/mol, respectively, **Table 1**). As for LPS, L_5 binds in the hydrophobic cleft of MD-2, where it makes extensive contacts both with MD-2 and the TLR4 dimer (referred to as TLR4', **Figure 2A**). The lack of direct interaction with TLR4 at the primary binding site is not uncommon and has also been described for another unconventional ligand, neoseptin.[39] L_5 is buried deeply in the MD-2 pocket (**Figure 2B**) where it is located much deeper than lipid IVa (**Figure 2C**), which is an antagonist in humans.[36] Its positioning is partially overlapping the binding region described for a neoseptin dimer bound to mouse TLR4/MD-2.[39] L_5 is much larger than the neoseptin dimer and makes additional contacts throughout the hydrophobic cavity involving in particular the MD-2 residues I32, L78, Y102, F119, F121, K122, F126 and F151, which surround the ligand and mediate the strongest van der Waals interactions within the complex. In contrast to neoseptin, that is only able to activate mouse TLR4/MD-2, cell-based assays show that L_5 is active on both human and mouse proteins, probably as a result of the extensive hydrophobic network, which is conserved across species.

However, no strong hydrogen bonds or ionic interactions could be predicted between L_5 and TLR4/MD-2, implying a lack of specificity in binding. This is unusual for protein-ligand interactions and has to date only been described for DNA-ligand stacking interactions.[40] The high flexibility of the L_5 molecule may allow it to fit well into the

Table 1: Predicted binding energies for compounds to human TLR4/MD-2 (at pH 7.0).

Ligand	Active hTLR4/MD-2 (3FXI)	Active hMD-2 (3FXI)	Inactive hMD-2 (2E59)
L_4	-32.7	-31.1	-23.6
L_5	-39.2	-36.5	-33.2
L_6	-41.4	-38.3	-25.7
DOTAP	-22.6	-22.3	-11.1
Lipid IVa[a]	n.d.	-18.5[b]	-25.1
E.coli lipid A[a]	-34.7	-27.7	n.d.
Eritoran[a]	n.d.	-15.6[b]	-23.3

Values are given in kcal/mol; n.d.: not determined; [a]: binding energies are given for rigid docking to match the ligand conformations observed in the crystal structures; [b]: lipid IVA and eritoran are antagonists. The binding energies to active hMD-2 are extrapolated from rigid docking of the ligand conformation observed in the crystal structures, 2E59 and 1Z65, respectively.

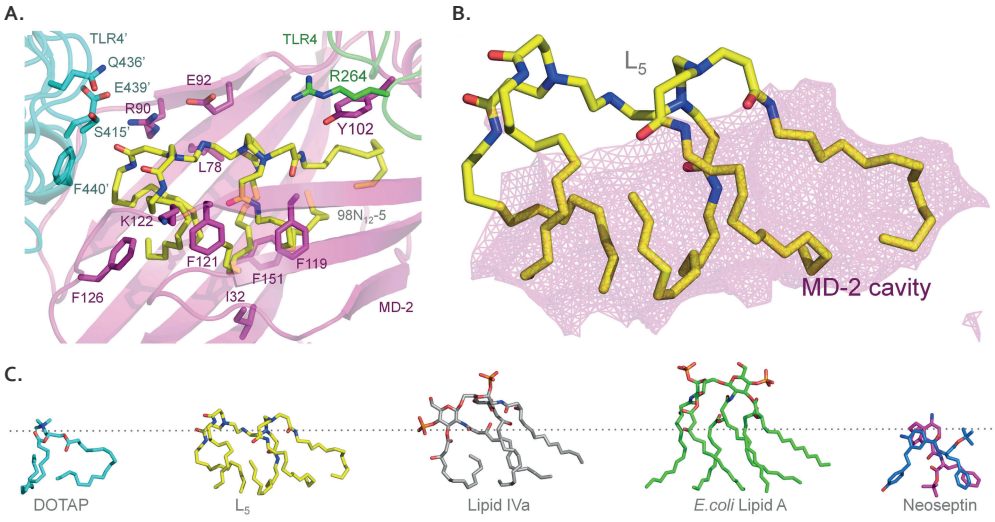

***Figure 2: Binding mode of L_5. (A)**: Graphical representation of L_5 (yellow) binding to TLR4/MD-2 with primary TLR4 (green), secondary TLR4 at the dimer interface noted TLR4' (cyan), and MD-2 (magenta). L_5 and its closest protein contacts are shown as sticks with oxygen (red) and nitrogen (blue) atoms. Close-up of L_5 filling up the hydrophobic cavity of MD-2 (B): The solvent-accessible pocket of MD-2 is represented as a semi-transparent pink mesh. Different ligand conformations predicted for TLR4/MD-2 binding (C): DOTAP, L_5, the species-specific antagonist lipid IVa as observed in complex with human MD-2 (PDB code 2E59); the potent agonist E. coli lipid A (PDB code 3FXI), and the species-specific agonist neoseptin, as observed in complex with mouse TLR4/MD-2 (PDB code 5HG4). The dotted line represents the same position of the ligand in the MD-2 cavity. See also Figure S3.*

hydrophobic binding pocket, mediating extensive hydrophobic contacts within the complex. While hydrogen bond formation provides binding specificity and rigidity in molecular interactions, we cannot rule out that water molecules and counter ions may associate with the cationic headgroup.[41] Potential hydrogen bonds and polar interactions are foreseen with neighboring residues from MD-2 (residues R90 and E92), TLR4 (R264) and at the dimer interface with TLR4' at S415', Q436' and E439' (**Figure 2** and **Table S3**). While DOTAP binding to inactive MD-2 is non-specific, binding to the active form of MD-2 nevertheless seems to be possible according to our docking predictions. However, DOTAP docks more than 10 Å from residue F126 and more than 15 Å from the dimerization interface when artificially associated to the active conformation of MD-2. Together with the lack of affinity of DOTAP for inactive MD-2, these data suggest that DOTAP does not possess any of the features essential for TLR4 activity, which is in sharp contrast to L_5.

Docking further suggests that the hydrophobic moiety of L_4 is sufficient to bind within the MD-2 cavity and perform stabilizing contacts with F126 loop required for receptor activation.[42] Additional acyl chains promote a more surface exposed conformation of the lipidoids with additional hydrophobic and hydrophilic contacts (Supplementary information, **Table S4**). In particular, L_6 is the only lipidoid able to interact with TLR4 at the primary site as well as the dimer interface (Supplementary information, **Table S5**). Indeed TLR4 R264 is a hydrogen bond donor to the carbonyl group of the acyl chain linked to N3. The additional contacts made by L_6 contribute to its enhanced TLR4 activity compared to less-acylated lipidoids. All lipidoids studied here share conserved interactions with E439' at the TLR4 dimer interface. The docking poses and binding affinities are in accordance with the observed TLR4 activity in cell-based assays.

3.3 Lipidoids induce maturation of professional antigen-presenting cells

Besides induction of an inflammatory response, activation of the adaptive immune system by the developed siRNA delivery systems should also be avoided. Professional antigen-presenting cells (pAPCs) are initiators of adaptive responses, and upon encounter with drug delivery systems, they may prime the cells of the adaptive immune system by inducing differentiation from an immature to a mature cell type.[43] First, to test whether lipidoids affect viability and induce maturation of pAPCs, murine bone marrow (BM)-derived APCs were incubated with L_5. A noticeable decrease in the viability of BM-APCs occurred upon treatment with L_5 at concentrations above 10 μg/ml, as compared to BM-APCs incubated with solvent or LPS alone (**Figure 3A)**. But, within the live cell population, no difference was observed in the percentage of cells with a dendritic-like phenotype measured as CD11c and major histocompatibility complex (MHC) class II double-positive cells. However, a concentration-dependent increase in maturation was

noted in case of L_5 up to 10 µg/ml, which was measured as an increase in the percentage of $CD40^+$ cells (**Figure 3B**). Reduced maturation at higher concentrations could be attributed to cytotoxicity **(Figure 3A)**. Thus, lipidoids not only activate TLR4 pathway, but also induce maturation of BM-APCs.

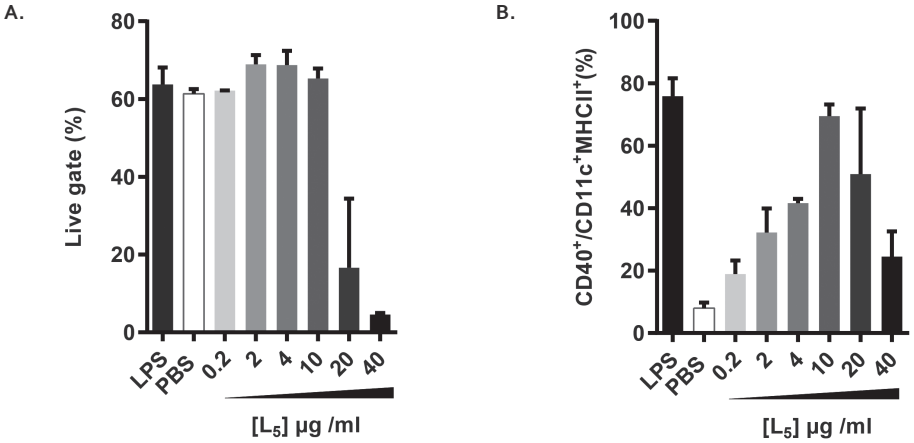

Figure 3: Lipidoid mediated cell maturation was tested by stimulating murine bone marrow-derived pAPCs differentiated with granulocyte macrophage colony-stimulating factor (GM-CSF). (A) *Cell viability is shown as the percentage of cells in the live gate quantified by flow cytometry upon stimulation with indicated concentrations of L_5, and compared to viability of BM-APCs incubated with LPS and PBS. (B) Maturation, measured as the upregulation of the activation marker CD40 in $CD11c^+MHCII^+$ cells, and compared to CD40 levels on LPS (10 ng/mL) and PBS (1:25) incubated BM-APCs (B). Data represent mean values ± Standard error (n=2) and represent results of one of a total of two independent experiments.*

3.4 TLR4 activation and pAPC maturation are influenced by the type of formulation

The influence of formulation type on the immune modulating properties of lipidoids was then assessed systematically by measuring TLR4 activation upon incubation with three different types of formulations of lipidoids, *viz.* lipoplexes, SNALPs and LPNs. Lipoplexes is the simplest type of formulation, which were prepared by simple co-incubation of siRNA and lipidoids at a fixed ratio of 1:20 (w/w). A concentration-dependent increase in the relative TLR4 activation was measured for all types of lipoplexes, composed of L_4, L_5, or L_6 lipidoids (**Figure 4A**). In case of lipoplexes containing L_{mix} a decrease in TLR4 activation was noted at the highest concentration of 27 nM, as compared to that measured at 2.7 nM, which could be attributed to the interference with the measurement of TLR4 activation associated with toxicity (data not shown). Furthermore, the pAPC maturation assay revealed that all tested lipoplexes were well-tolerated till 2.7 nM,

albeit significant maturation was noted in all cases at the highest concentration of 27 nM (**Figure 4B**). Interestingly, remarkably higher pAPC maturation was observed after incubation with bulk lipidoids (Figure 3A), compared to incubation with lipoplexes, suggesting an influence of siRNA complexation on the immune-stimulating properties of lipidoids.

In addition, SNALPs formulated with either L_5 or L_{mix} were prepared as described previously (Supplementary data, **Table S2**).[10] Both L_5 SNALPs and L_{mix} SNALPs induced concentration-dependent TLR4 activation from 2.5 nM till 27 nM, beyond which a decrease in TLR4 activation was noted for both formulations (**Figure 4C**). This decrease was attributed to the interference with the measurement of TLR4 activation (data not shown). Like lipoplexes, both types of SNALPs induced significantly higher pAPC maturation at concentrations above 2.7 nM, measured as the upregulation of the maturation marker CD86 on BM-APCs (**Figure 4D**).

Finally, siRNA-loaded LPNs were prepared with lipidoids as described previously (22). A series of LPNs were prepared with the different subtypes of lipidoids and DOTAP (Supplementary data, **Table S2**). No TLR4 activation could be detected for LPNs modified with the lipidoids up to 100 nM siRNA (**Figure 4E**), independently of the lipidoid used. Furthermore, these LPNs, modified with either lipidoid or DOTAP, did not induce any upregulation of maturation markers, indicating that they do not induce pAPC maturation (**Figure 4F)**. Interestingly, these LPNs did not influence the viability of BM-APCs (Supplementary data, **Figure S2**). Thus, as LPNs do not have detectable immune-activating properties, the LPN-based formulation approach is a promising delivery technology for further development of siRNA-based therapies.

4. Discussion

In previous studies we showed that both DOTAP- (44) and in particular lipidoid-modified LPNs are promising delivery systems for siRNA, with an effective silencing of gene expression in cellular systems.[22] However, to date very few studies have addressed the potential undesired immune activation mediated by siRNA delivery systems. In the present study, the immune-modulatory effects of newer generation cationic lipids, *i.e.* lipidoids and various formulations composed of lipidoids, were tested. The results clearly demonstrate that bulk lipidoids are able to specifically activate TLR4, in contrast to the commonly used cationic lipid DOTAP. However, formulation as lipidoid-modified LPNs overcomes the lipidoid-mediated TLR4 activation, making them a promising tool for siRNA delivery.

In agreement with the observed TLR4 activation by the lipidoids *in vitro*, when analyzing possible binding to TLR4/MD-2 *in silico*, we found that lipidoids ranging from L_4 to L_6

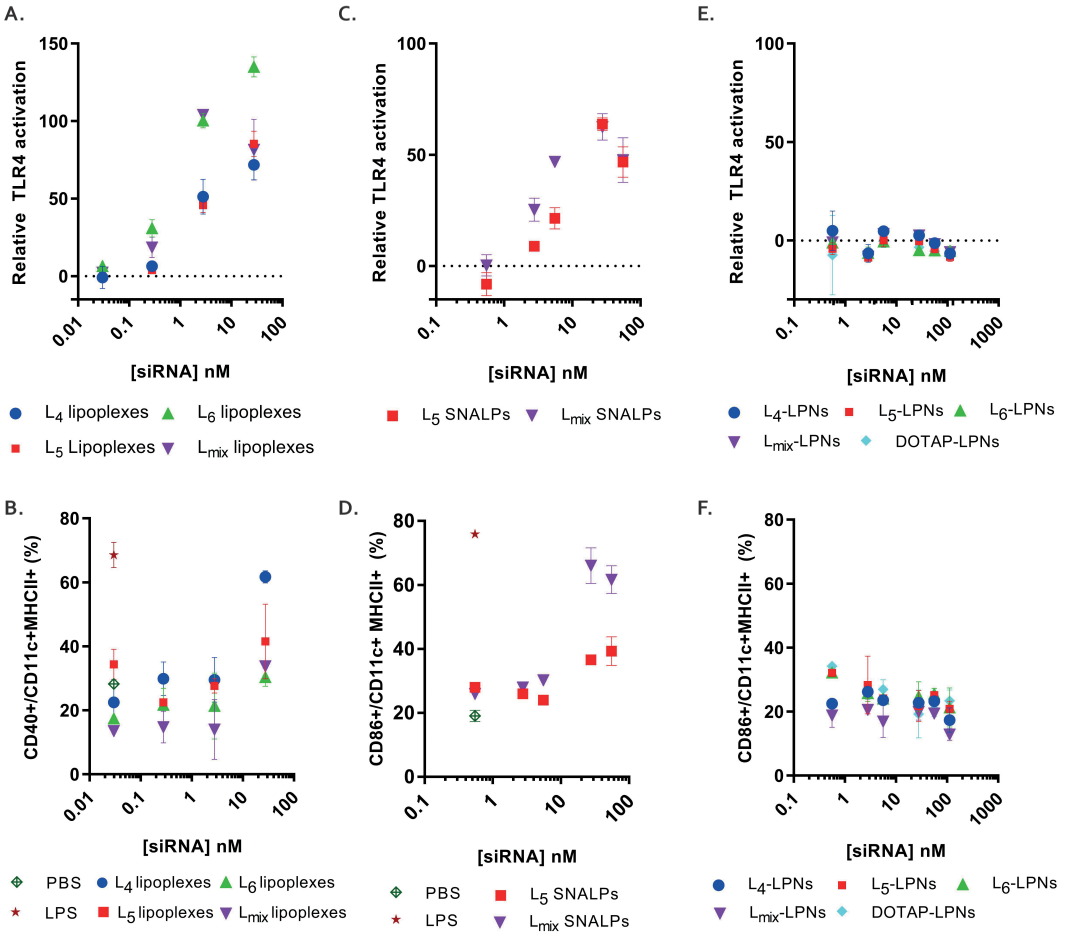

Figure 4: Immune activation by lipidoid-based SNALPs and lipoplex and not by lipidoid-modified LPN. *Activation of the hTLR4 receptor cell line (A) and pAPC maturation (B) by lipoplexes composed of L_4, L_5, L_6, or L_{mix} with siRNA-EGFP. Activation of the hTLR4 receptor cell line (C) and pAPC maturation (D) by SNALPs prepared with L_5, or L_{mix}. Activation of the hTLR4 receptor cell line (E) and pAPC maturation (F) induced by LPNs prepared with L_4, L_5, L_6, L_{mix}, or DOTAP. Sample OD were corrected for OD value measured for the negative control (solvent 1:10) and divided by the maximum OD (LPS 10 ng/ml). Professional APC maturation was tested by stimulating murine bone marrow-derived, GM-CSF-differentiated pAPCs. Maturation was measured as the upregulation of activation marker (either CD40 or CD86) in $CD11c^+MHCII^+$ cells and compared to the levels on BM-APCs stimulated with LPS (10 ng/mL) and PBS, as quantified by flow cytometry. See also Figure S2. Data represent mean values ± SD (n=3 For A, C, E and n=2 for B, D, F)*

fitted into the MD-2 groove. While L_5 may be the most potent siRNA transfection reagent, L_6 was the most immune-reactive. This is not surprising as the best TLR4 activators known to date are bacterial hexa-acylated LPS molecules. Penta-acylated lipids such as LPS from *Rhodobacter sphaeroides*[45] and tetra-acylated ones such as lipid IVa and eritoran are either species-specific partial agonists or antagonists.[46] Thus, lipidoids including L_4-L_6 may adopt a conformation suitable for binding to MD2, which is a prerequisite for dimerization and activation of TLR4.[35, 36] In contrast, DOTAP was not predicted to bind with high specificity to MD-2 and does therefore not qualify neither as a TLR4 agonist nor as an antagonist, based on the *in silico* modelling. Taken together, the *in silico* predictions correlate well with the measured TLR4-activating abilities of the different test substances. Thus, *in silico* modelling of structures seems to be an excellent method to investigate potential for TLR4 binding and could be applied in further development of therapeutic drug delivery systems.

When comparing the different L_5-containing delivery systems, *i.e.* LPNs, SNALPs and lipoplexes, for their ability to activate TLR4, the main difference observed is that the lipoplexes and SNALPs do activate TLR4, while formulation as LPN overcomes the lipidoid mediated TLR4 activation. Thus, the *in vitro* data suggest that LPNs provide a non-immunogenic modality for intracellular siRNA delivery. In contrast to LPNs, SNALPs containing L_5 activate TLR4 and those SNALPs are currently being developed for antiviral activity.[15, 47, 48] This differential activation of TLR4 by differently formulated lipidoids might be explained by a difference in two physicochemical characteristics; (*i*) the way the lipidoid molecules are exposed on the nanoparticle surface, and (*ii*) the presentation of the lipidoid-particle combination to the receptor.[49] Because SNALPs and LPNs consist of different materials, the structure of the particles and, most likely therefore the exposure of L_5 on the particle surface, differs for the two particle types. We suggest that the LPS-binding protein (LBP) that is normally able to extract LPS from the membrane structure of bacteria,[50, 51] is able to access the lipidoids in the SNALPs but not LPNs. As a consequence, the particles have different abilities to interact with the MD-2/TLR4 molecules. However, direct LBP binding was not examined, which could be included into further studies of particle engineering.[52]

The differences in innate immune activation that we observe provide different opportunities for the field of advanced drug delivery formulations. If aiming for delivery of an antiviral or an antitumor drug, immune activation (within the safe range) is a desired outcome. The immune stimulating effects of unmodified RNA in combination with SNALPs have already been described and are likely to contribute to effective antiviral therapy[47, 38]; lipidoid-mediated TLR4 activation of SNALPs could contribute to that. Taken together, the different possibilities for the design of drug delivery systems provide a range of opportunities to modify the design to promote a specific, desirable outcome.

Acknowledgements

We gratefully acknowledge the support from the Innovative Medicines Initiative Joint Undertaking under grant agreement NO.115363 resources of which are composed of financial contribution from the European Union's Seventh Framework Programme (FP7/2007-2013) and EFPIA companies' in kind contribution. This project has received funding from the European Union's Seventh Framework Programme for research, technological development and demonstration under grant agreement No. 600207. We are also grateful to the Danish Council for Independent Research and FP7 Marie Curie Actions – COFUND (Grant No. DFF-4093-00292), the Lundbeck Foundation, Denmark (Grant No. R181-2014-3793), Hørslev-Fonden, Denmark, and the Carlsberg Foundation, Denmark, for financial support. We also acknowledge ChemAxon for generously providing the academic license of Marvin Suite including calculator plugins. MG and NJG would like to thank the Wellcome Trust for funding (RG68325) as well as the Medical Research Council for MG's Career Development Funding (RG87390).

Notes

KT, XZ, HF, HMN and CF are co-inventors of a patent application relating to the cationic lipid structure (European patent application no 16160931.8). All rights have been assigned to University of Copenhagen. All other authors report no potential conflicts.

Author Contributions

Conceptualization, A.M.G., K.T., C.F., and A.J.A.M.S.; **Methodology**, A.M.G., K.T., M.G., H.F., C.F., N.J.G., H.M.N., and A.J.A.M.S.; **Investigation**, A.M.G., K.T., D.C.J.B., M.G., E.F., and X.Z.; **Writing – Original Draft**, A.M.G., K.T., and M.G.; **Writing – Review & Editing,** A.M.G., K.T., C.F., A.J.A.M.S., W.E., M.G., H.M.N., and H.F.; **Funding Acquisition**, A.J.A.M.S., W.E., C.F., H.M.N., M.G., and N.J.G; **Supervision**, A.J.A.M.S., F.B., N.J.G., H.F., H.M.N., and C.F..

References

1. Fire A, Xu S, Montgomery MK, Kostas SA, Driver SE, Mello CC. Potent and specific genetic interference by double-stranded RNA in Caenorhabditis elegans. Nature. 1998;391(6669):806-11.
2. Hannon G. RNA interference. Nature. 2002;418(6894):244-51.
3. Wilkins C, Dishongh R, Moore S, Whitt M, Chow M, Machaca K. RNA interference is an antiviral defence mechanism in Caenorhabditis elegans. Nature. 2005;436(7053):1044-7.
4. Oh Y, Park T. siRNA delivery systems for cancer treatment. Adv Drug Deliv Rev. 2009;61(10):850-62.
5. Tseng Y, Mozumdar S, Huang L. Lipid-based systemic delivery of siRNA. Adv Drug Deliv Rev. 2009;61(9):721-31.
6. Asami Y, Yoshioka K, Nishina K, Nagata T, Yokota T. Drug delivery system of therapeutic oligonucleotides. Drug Discov Ther. 2016;10(5):256-62.
7. Juliano R. The delivery of therapeutic oligonucleotides. Nucleic Acids Res. 2016;44(14):6518-48.
8. Lv H, Zhang S, Wang B, Cui S, Yan J. Toxicity of cationic lipids and cationic polymers in gene delivery. J Controlled Release. 2006 8/10;114(1):100-9.
9. Senior JH, Maskiewicz R, Trimble KR. Interaction of positively-charged liposomes with blood: implications for their application in vivo. Biochim Biophys Acta. 1991;1070(1):173-9.
10. Akinc A, Zumbuehl A, Goldberg M, Leshchiner E, Busini V, Hossain N, et al. A combinatorial library of lipid-like materials for delivery of RNAi therapeutics. Nat Biotechnol. 2008;26(5):561-9.
11. Sun S, Wang M, Knupp S, Soto Feliciano Y, Hu X, Kaplan D, et al. Combinatorial library of lipidoids for in vitro DNA delivery. Bioconjug Chem. 2012;23(1):135-40.
12. Wang M, Sun S, Alberti K, Xu Q. A combinatorial library of unsaturated lipidoids for efficient intracellular gene delivery. ACS Synth Biol. 2012;1(9):403-7.
13. Wu Y, Li L, Levkin P, Davidson G. Combinatorial synthesis and high throughput screening of lipidoids for gene delivery. J Control Release. 2015;213:e134-.
14. Mahon K, Love K, Whitehead K, Qin J, Akinc A, Leshchiner E, et al. Combinatorial approach to determine functional group effects on lipidoid-mediated siRNA delivery. Bioconjug Chem. 2010;21(8):1448-54.
15. Love K, Mahon K, Levins C, Whitehead K, Querbes W. Lipid-like materials for low-dose, in vivo gene silencing (vol 107, pg 1864, 2010). Proc Natl Acad Sci U S A. 2010;107(21):9915-.
16. Nguyen D, Mahon K, Chikh G, Kim P, Chung H, Vicari A, et al. Lipid-derived nanoparticles for immunostimulatory RNA adjuvant delivery. Proc Natl Acad Sci U S A. 2012;109(14):E797-803.
17. Kanasty R, Dorkin J, Vegas A, Anderson D. Delivery materials for siRNA therapeutics. Nat Mater. 2013;12(11):967-77.
18. Ho W, Zhang X, Xu X. Biomaterials in siRNA Delivery: A Comprehensive Review. Adv Healthc Mater. 2016;5(21):2715-31.
19. Wittrup A, Lieberman J. Knocking down disease: a progress report on siRNA therapeutics. Nat Rev Genet. 2015;16(9):543-52.
20. Coelho T, Adams D, Silva A, Lozeron P, Hawkins P, Mant T, et al. Safety and efficacy of RNAi therapy for transthyretin amyloidosis. N Engl J Med. 2013;369(9):819-29.
21. Fitzgerald K, Frank Kamenetsky M, Shulga Morskaya S, Liebow A, Bettencourt B, Sutherland J, et al. Effect of an RNA interference drug on the synthesis of proprotein convertase subtilisin/kexin type 9 (PCSK9) and the concentration of serum LDL cholesterol in healthy volunteers: a randomised, single-blind, placebo-controlled, phase 1 trial. Lancet. 2014;383(9911):60-8.
22. Thanki K, Zeng X, Justesen S, Tejlmann S, Falkenberg E, Van Driessche E, et al. Engineering of small interfering RNA-loaded lipidoid-poly(DL-Lactic-Co-Glycolic Acid) hybrid nanoparticles for highly efficient and safe gene silencing: A quality by design-based approach. Eur J Pharm Biopharm. 2017 nov;120:22-33.
23. Whitehead K, Dahlman J, Langer R, Anderson D. Silencing or stimulation? siRNA delivery and the immune system. In: UNITED STATES: Annual Reviews; 2011. p. 77-96.

24. Judge A, Lee A, Bola G, MacLachlan I. Design of noninflammatory synthetic siRNA mediating potent gene silencing in vivo. Mol Ther. 2006;13(3):494-505.
25. Lonez C, Vandenbranden M, Ruysschaert J. Cationic lipids activate intracellular signaling pathways. Adv Drug Deliv Rev. 2012;64(15):1749-58.
26. Ragelle H, Colombo S, Pourcelle V, Vanvarenberg K, Vandermeulen G, Bouzin C, et al. Intracellular siRNA delivery dynamics of integrin-targeted, PEGylated chitosan-poly(ethylene imine) hybrid nanoparticles: A mechanistic insight. J Control Release. 2015;211:1-9.
27. Zeng X, de Groot A, Sijts, Alice J A M, Broere F, Blenke E, Franzyk H, et al. Surface coating of siRNA-peptidomimetic nano-self-assemblies with anionic lipid bilayers: enhanced gene silencing and reduced adverse effects in vitro. Nanoscale. 2015;7(46):19687-98.
28. CLARK M, CRAMER R, VANOPDENBOSCH N. VALIDATION OF THE GENERAL-PURPOSE TRIPOS 5.2 FORCE-FIELD. Journal of computational chemistry. 1989;10(8):982-1012.
29. GASTEIGER J, MARSILI M. ITERATIVE PARTIAL EQUALIZATION OF ORBITAL ELECTRONEGATIVITY - A RAPID ACCESS TO ATOMIC CHARGES. Tetrahedron. 1980;36(22):3219-28.
30. Morris G, Huey R, Lindstrom W, Sanner M, Belew R, Goodsell D, et al. AutoDock4 and AutoDockTools4: Automated docking with selective receptor flexibility. J Comput Chem. 2009;30(16):2785-91.
31. Trott O, Olson A. AutoDock Vina: improving the speed and accuracy of docking with a new scoring function, efficient optimization, and multithreading. J Comput Chem. 2010;31(2):455-61.
32. Krissinel E, Henrick K. Inference of macromolecular assemblies from crystalline state. J Mol Biol. 2007;372(3):774-97.
33. Pettersen E, Goddard T, Huang C, Couch G, Greenblatt D, Meng E, et al. UCSF Chimera--a visualization system for exploratory research and analysis. J Comput Chem. 2004;25(13):1605-12.
34. Laskowski R, Swindells M. LigPlot+: multiple ligand-protein interaction diagrams for drug discovery. J Chem Inf Model. 2011;51(10):2778-86.
35. Park B, Song D, Kim H, Choi B, Lee H, Lee J. The structural basis of lipopolysaccharide recognition by the TLR4-MD-2 complex. Nature. 2009;458(7242):1191-5.
36. Ohto U, Fukase K, Miyake K, Satow Y. Crystal structures of human MD-2 and its complex with antiendotoxic lipid IVa. Science. 2007;316(5831):1632-4.
37. Kim H, Park B, Kim J, Kim S, Lee J, Oh S, et al. Crystal structure of the TLR4-MD-2 complex with bound endotoxin antagonist Eritoran. Cell. 2007;130(5):906-17.
38. Di Lorenzo F, Kubik L, Oblak A, Lore N, Kubik L, Hamad MA, et al. Activation of Human Toll-like Receptor 4 (TLR4)·Myeloid Differentiation Factor 2 (MD-2) by Hypoacylated Lipopolysaccharide from a Clinical Isolate of Burkholderia cenocepacia. J Biol Chem. 2015;290(35):21305-19.
39. Wang Y, Su L, Morin M, Jones B, Whitby L, Moresco EMY, et al. TLR4/MD-2 activation by a synthetic agonist with no similarity to LPS. Proc Natl Acad Sci U S A. 2016;113(7):E884-93.
40. Smirnov S, Matray T, Kool E, de los Santos C. Integrity of duplex structures without hydrogen bonding: DNA with pyrene paired at abasic sites. Nucleic Acids Res. 2002;30(24):5561-9.
41. Uster PS, Deamer DW. pH-dependent fusion of liposomes using titratable polycations. Biochemistry. 1985;24(1):1-8.
42. Gioannini T, Teghanemt A, Zhang D, Esparza G, Yu L, Weiss J. Purified monomeric ligand.MD-2 complexes reveal molecular and structural requirements for activation and antagonism of TLR4 by Gram-negative bacterial endotoxins. Immunol Res. 2014;59(1-3):3-11.
43. SALLUSTO F, LANZAVECCHIA A. Efficient presentation of soluble antigen by cultured human dendritic cells is maintained by granulocyte/macrophage colony-stimulating factor plus interleukin 4 and downregulated by tumor necrosis factor alpha. J Exp Med. 1994;179(4):1109-18.
44. Jensen D, Jensen L, Koocheki S, Bengtson L, Cun D, Nielsen H, et al. Design of an inhalable dry powder formulation of DOTAP-modified PLGA nanoparticles loaded with siRNA. J Control Release. 2012;157(1):141-8.

45. Irvine K, Gangloff M, Walsh C, Spring D, Gay N, Bryant C. Identification of key residues that confer Rhodobacter sphaeroides LPS activity at horse TLR4/MD-2. PLoS ONE. 2014;9(5):e98776-.
46. Ohto U, Fukase K, Miyake K, Shimizu T. Structural basis of species-specific endotoxin sensing by innate immune receptor TLR4/MD-2. Proc Natl Acad Sci U S A. 2012;109(19):7421-6.
47. Nguyen D, Chen SC, Lu J, Goldberg M, Kim P, Novobrantseva T, et al. Drug delivery-mediated control of RNA immunostimulation. Mol Ther. 2009;17(9):1555-62.
48. Akinc A, Goldberg M, Qin J, Dorkin JR, Gamba Vitalo C, Maier M, et al. Development of lipidoid-siRNA formulations for systemic delivery to the liver. Mol Ther. 2009;17(5):872-9.
49. Koraha J, Tsuneyoshi N, Kimoto M, Gauchat J, Nakatake H, Fukudome K. Comparison of lipopolysaccharide-binding functions of CD14 and MD-2. Clin Diagn Lab Immunol. 2005;12(11):1292-7.
50. Schumann RR, Leong SR, Flaggs GW, Gray PW, Wright SD, Mathison JC, et al. Structure and function of lipopolysaccharide binding protein. Science. 1990;249(4975):1429-31.
51. Vesy CJ, Kitchens RL, Wolfbauer G, Albers JJ, Munford RS. Lipopolysaccharide-binding protein and phospholipid transfer protein release lipopolysaccharides from gram-negative bacterial membranes. Infect Immun. 2000;68(5):2410-7.
52. Dentener MA, Vreugdenhil ACE, Hoet PHM, Vernooy JHJ, Nieman FHM, Heumann D, et al. Production of the acute-phase protein lipopolysaccharide-binding protein by respiratory type II epithelial cells: implications for local defense to bacterial endotoxins. Am J Respir Cell Mol Biol. 2000;23(2):146-53.

Supplementary information

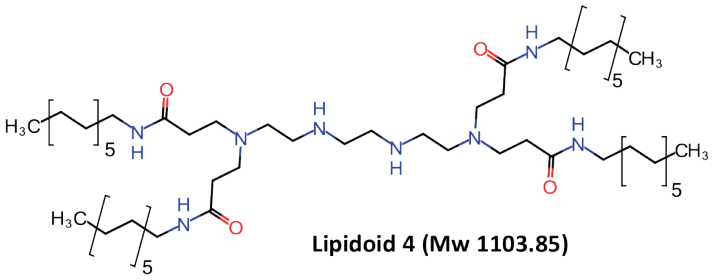

Lipidoid 4 (Mw 1103.85)

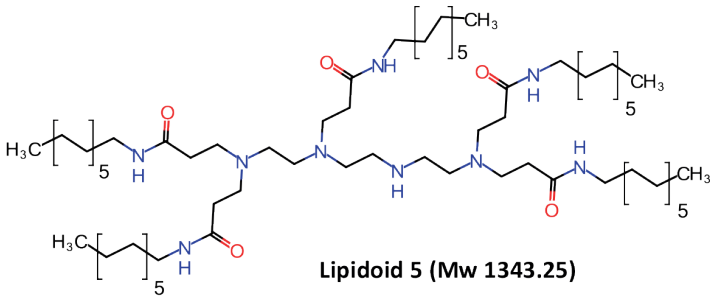

Lipidoid 5 (Mw 1343.25)

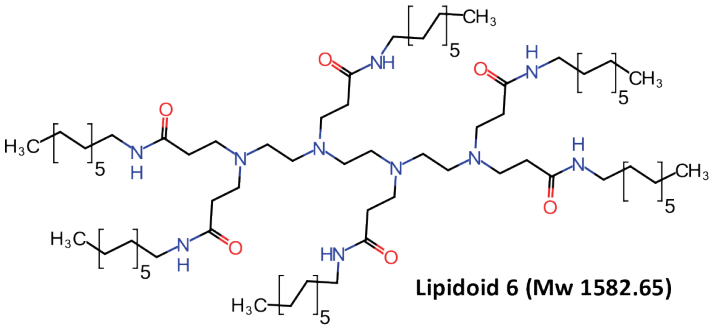

Lipidoid 6 (Mw 1582.65)

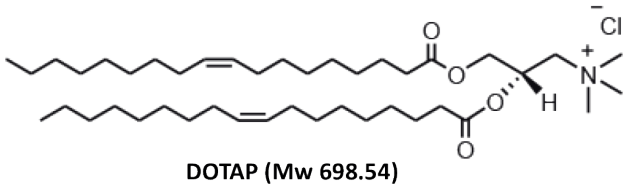

DOTAP (Mw 698.54)

Figure S1: Chemical structures of L_4, L_5, L_6 and DOTAP.

Table S1: siRNA sequences and modification patterns. *Lower case letters represent deoxyribonucleotides, underlined capital letters represent 2´-O-methylribonucleotides, while p denotes phosphate residues.*

Name	Target GenBank	Sense sequence	Antisense sequence
siRNA-EGFP	JQ064510.1	5′-pACCCUGAAGUUCAUCUGCACCACcg-3′	5′-CGGUGGUGCAGAUGAACUUCAGGGUCA-3′
Neg control		5′-AUCGUACGUACCGUCGUAUtt-3′	5′-AUACGACGGUACGUACGAUtt-3′

Table S2: Physicochemical characteristics of dispersions prepared in HEPES buffer (5 mM, pH 7.4). *Results denote mean values ± SD (n=3).*

Formulation	z-average (nm)	PDI	Zeta potential (mV)	Entrapment efficiency (%)	siRNA loading (µg siRNA/mg NPs)
L_5 SNALPs[a]	79.4 ± 1.2***	0.086 ± 0.020	-15.4 ± 1.1***	95.3 ± 4.2***	128.7 ± 5.6***
L_{mix} SNALPs[a]	85.9 ± 5.5***	0.074 ± 0.038	-10.0 ± 1.5***	81.9 ± 2.1*	110.6 ± 2.8***
L_4 LPNs[b]	204.3 ± 14.1	0.135 ± 0.024	26.8 ± 8.9	61.4 ± 2.8**	4.6 ± 0.2**
L_5 LPNs[b]	212.5 ± 11.5	0.121 ± 0.027	23.2 ± 5.1	72.5 ± 3.8	5.4 ± 0.3
L_6 LPNs[b, d]	286.7 ± 23.0***	0.375 ± 0.027***	3.6 ± 2.9**	75.5 ± 3.6	5.7 ± 0.3
L_{mix} LPNs[b]	201.0 ± 8.5	0.129 ± 0.019	32.8 ± 5.7	52.5 ± 2.9***	3.9 ± 0.2***
DOTAP LPNs[c]	192.7 ± 16.4	0.110 ± 0.013	26.5 ± 4.1	28.3 ± 2.3***	2.1 ± 0.2***

*[a] Prepared at an siRNA:lipid weight ratio of 1:7.5. [b] Prepared at 15% (w/w) lipidoid content at an siRNA:lipidoid weight ratio of 1:20; [c] Prepared at 10% (w/w) lipid content an siRNA:lipid weight ratio of 1:10; [d] A bimodal particle size distribution was noted. Statistically significant differences from L_5-modified LPNs are indicated: *p < 0.05, **p < 0.01 and ***p < 0.001.*

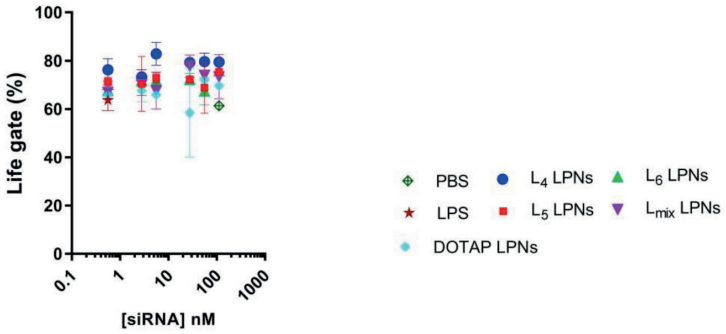

Figure S2: Lipidoid-polymer hybrid NP has no effect on cell viability of pAPC. *Cell viability is shown as the percentage of cells in the live gate quantified by flow cytometry upon stimulation with a concentration range of L_5 compared to BM-APCs incubated with LPS and PBS.*

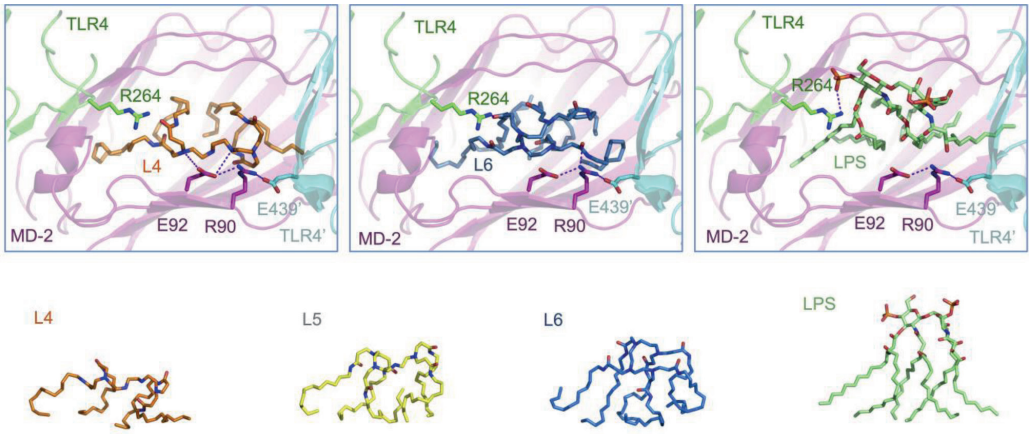

Figure S3: Proposed binding mode of lipidoids compared to lipid A moiety of LPS to TLR4-MD-2. *Top panels from left to right: L_4, L_6 and lipid A from LPS form hydrophilic contacts with TLR4 R264 at the primary binding site, MD-2 R90 and E92, which also form a ionic interaction with TLR4' E439' at the dimeric interface. TLR4 is represented in green cartoon, TLR4' in cyan and MD-2 in magenta. Bottom series from left to right: side views of L_4, L_5, L_6 and lipid A from LPS. TLR4-MD-2 are not shown. The lipidoids of increasing acyl chain number spread their acyl chains to mimic lipid A conformation adopted in contact of TLR4-MD-2 (35)[28].*

Table S3: TLR4-MD-2 contacts to L4

List of residues from TLR4-MD-2 at given distances from L_4 lipidoid according to best vina docking model. MD-2 R90 is neutralized by E92 on one side and TLR4 E439' at the dimer interface (both are at 3.2A). The same residues are in close proximity to the protonated amines of L_4 at position 1 and 3. L_4 is more distant to MD-2 residue F126, which undergoes conformational change upon activation compared to larger lipidoids. In contrast, L_4 is closer to the dimeric interface than L_5. This proximity is illustrated below by the presence of TLR4 dimer residues (labelled TLR4').

3.5 Å	4.0 Å	4.5 Å	5.0 Å
	TLR4' E439	TLR4' E439	TLR4' E439
	TLR4' F440	TLR4' F440	TLR4' F440
	TLR4' S441	TLR4' S441	TLR4' S441
		TLR4' F463	TLR4' F463
MD-2 I32	MD-2 I32	MD-2 I32	MD-2 I32
MD-2 L61	MD-2 I46	MD-2 I44	MD-2 I44
MD-2 I63	MD-2 V48	MD-2 I46	MD-2 I46
MD-2 L78	MD-2 I52	MD-2 V48	MD-2 V48
MD-2 I80	MD-2 L54	MD-2 I52	MD-2 I52
MD-2 R90	MD-2 L61	MD-2 L54	MD-2 L54
MD-2 I94	MD-2 I63	MD-2 L61	MD-2 L61
MD-2 F104	MD-2 Y65	MD-2 I63	MD-2 I63
MD-2 F119	MD-2 L71	MD-2 Y65	MD-2 Y65
MD-2 I124	MD-2 F76	MD-2 L71	MD-2 L71
MD-2 Y131	MD-2 L78	MD-2 L74	MD-2 L74
MD-2 I153	MD-2 I80	MD-2 F76	MD-2 F76
	MD-2 V82	MD-2 L78	MD-2 L78
	MD-2 L87	MD-2 I80	MD-2 I80
	MD-2 R90	MD-2 V82	MD-2 V82
	MD-2 E92	MD-2 L87	MD-2 L87
	MD-2 I94	MD-2 R90	MD-2 R90
	MD-2 F104	MD-2 E92	MD-2 E92
	MD-2 I117	MD-2 I94	MD-2 I94
	MD-2 F119	MD-2 Y102	MD-2 Y102
	MD-2 F121	MD-2 F104	MD-2 F104
	MD-2 I124	MD-2 V113	MD-2 V113
	MD-2 F126	MD-2 T115	MD-2 T115
	MD-2 Y131	MD-2 I117	MD-2 I117
	MD-2 C133	MD-2 S118	MD-2 S118
	MD-2 F147	MD-2 F119	MD-2 F119
	MD-2 F151	MD-2 F121	MD-2 S120
	MD-2 I153	MD-2 I124	MD-2 F121
		MD-2 F126	MD-2 K122
		MD-2 Y131	MD-2 I124
		MD-2 C133	MD-2 F126
		MD-2 F147	MD-2 Y131
		MD-2 F151	MD-2 C133
		MD-2 I153	MD-2 L146
			MD-2 F147
			MD-2 F151
			MD-2 I153

Table S4: L_5 binding mode to TLR4-MD-2

List of residues from TLR4-MD-2 at given distances from L_5 lipidoid according to best vina docking model.

3.5 Å	4.0 Å	4.5 Å	5.0 Å
	TLR4′ E439	TLR4′ S415	TLR4′ S415
	TLR4′ F440	TLR4′ E439	TLR4′ E439
		TLR4′ F440	TLR4′ F440
MD-2 I32	MD-2 I32	MD-2 I32	MD-2 I32
MD-2 L78	MD-2 I44	MD-2 I44	MD-2 I44
MD-2 Y102	MD-2 I46	MD-2 I46	MD-2 I46
MD-2 F119	MD-2 V48	MD-2 V48	MD-2 V48
MD-2 F121	MD-2 I52	MD-2 I52	MD-2 I52
MD-2 K122	MD-2 L54	MD-2 L54	MD-2 L54
MD-2 F126	MD-2 L61	MD-2 L61	MD-2 L61
MD-2 F151	MD-2 I63	MD-2 I63	MD-2 I63
	MD-2 Y65	MD-2 Y65	MD-2 Y65
	MD-2 L71	MD-2 L71	MD-2 L71
	MD-2 L74	MD-2 L74	MD-2 L74
	MD-2 F76	MD-2 F76	MD-2 F76
	MD-2 L78	MD-2 L78	MD-2 L78
	MD-2 I80	MD-2 I80	MD-2 I80
	MD-2 R90	MD-2 L87	MD-2 L87
	MD-2 E92	MD-2 R90	MD-2 R90
	MD-2 Y102	MD-2 E92	MD-2 E92
	MD-2 F104	MD-2 I94	MD-2 I94
	MD-2 I117	MD-2 Y102	MD-2 Y102
	MD-2 F119	MD-2 F104	MD-2 F104
	MD-2 S120	MD-2 I117	MD-2 V113
	MD-2 F121	MD-2 S118	MD-2 I117
	MD-2 K122	MD-2 F119	MD-2 S118
	MD-2 I124	MD-2 S120	MD-2 F119
	MD-2 F126	MD-2 F121	MD-2 S120
	MD-2 Y131	MD-2 K122	MD-2 F121
	MD-2 C133	MD-2 G123	MD-2 K122
	MD-2 V135	MD-2 I124	MD-2 G123
	MD-2 F147	MD-2 F126	MD-2 I124
	MD-2 L149	MD-2 Y131	MD-2 F126
	MD-2 F151	MD-2 C133	MD-2 Y131
	MD-2 I153	MD-2 V135	MD-2 C133
		MD-2 L146	MD-2 V135
		MD-2 F147	MD-2 L146
		MD-2 L149	MD-2 F147
		MD-2 F151	MD-2 L149
		MD-2 I153	MD-2 F151
			MD-2 I153

Table S5: L_6 binding mode to TLR4-MD-2

TLR4 R264 is a hydrogen bond donor to the carbonyl group of the acyl chain linked to N3. L6 is the only lipidoid making a hydrophilic contact at the primary TLR4 site as well as the dimer interface. Hydrophobic interactions are more extensive the bigger the lipidoid, but otherwise overlapping.

3.5 Å	4.0 Å	4.5 Å	5.0 Å
TLR4 R264	TLR4 R264	TLR4 R264	TLR4 R264
TLR4′ E439	TLR4′ E439	TLR4′ E439	TLR4′ Q436
TLR4′ F440	TLR4′ F440	TLR4′ F440	TLR4′ E439
			TLR4′ F440
			TLR4′ S441
MD-2 I32	MD-2 V24	MD-2 V24	MD-2 V24
MD-2 I46	MD-2 I32	MD-2 I32	MD-2 I32
MD-2 V48	MD-2 I44	MD-2 I44	MD-2 I44
MD-2 L61	MD-2 I46	MD-2 I46	MD-2 I46
MD-2 F76	MD-2 V48	MD-2 V48	MD-2 V48
MD-2 R90	MD-2 I52	MD-2 I52	MD-2 I52
MD-2 E92	MD-2 L54	MD-2 L54	MD-2 L54
MD-2 I94	MD-2 L61	MD-2 L61	MD-2 L61
MD-2 Y102	MD-2 I63	MD-2 I63	MD-2 I63
MD-2 I117	MD-2 Y65	MD-2 Y65	MD-2 Y65
MD-2 F119	MD-2 L71	MD-2 L71	MD-2 L71
MD-2 S120	MD-2 L74	MD-2 L74	MD-2 L74
MD-2 F121	MD-2 F76	MD-2 F76	MD-2 F76
MD-2 K122	MD-2 L78	MD-2 L78	MD-2 L78
MD-2 I124	MD-2 I80	MD-2 I80	MD-2 I80
MD-2 F126	MD-2 L87	MD-2 L87	MD-2 L87
	MD-2 R90	MD-2 R90	MD-2 R90
	MD-2 E92	MD-2 E92	MD-2 E92
	MD-2 I94	MD-2 I94	MD-2 V93
	MD-2 Y102	MD-2 Y102	MD-2 I94
	MD-2 F104	MD-2 F104	MD-2 Y102
	MD-2 V113	MD-2 V113	MD-2 F104
	MD-2 T115	MD-2 T115	MD-2 V113
	MD-2 I117	MD-2 I117	MD-2 T115
	MD-2 S118	MD-2 S118	MD-2 I117
	MD-2 F119	MD-2 F119	MD-2 S118
	MD-2 S120	MD-2 S120	MD-2 F119
	MD-2 F121	MD-2 F121	MD-2 S120
	MD-2 K122	MD-2 K122	MD-2 F121
	MD-2 G123	MD-2 G123	MD-2 K122
	MD-2 I124	MD-2 I124	MD-2 G123
	MD-2 F126	MD-2 F126	MD-2 I124
	MD-2 C133	MD-2 C133	MD-2 F126
	MD-2 V135	MD-2 V135	MD-2 C133
	MD-2 F147	MD-2 F147	MD-2 V135
	MD-2 L149	MD-2 L149	MD-2 L146
	MD-2 F151	MD-2 F151	MD-2 F147
	MD-2 I153	MD-2 I153	MD-2 L149
			MD-2 F151
			MD-2 I153

6

Surface coating of siRNA–peptidomimetic nano-self-assemblies with anionic lipid bilayers: enhanced gene silencing and reduced adverse effects *in vitro*

Nanoscale, 2015, 7, 19687-19698

Xianghui Zeng [a]
Anne Marit de Groot [b]
Alice J. A. M. Sijts [b]
Femke Broere [b]
Erik Oude Blenke [ac]
Stefano Colombo [a]
Willem van Eden [b]
Henrik Franzyk [d]
Hanne Mørck Nielsen [a]
Camilla Foged *[a]

[a] Department of Pharmacy, Faculty of Health and Medical Sciences, University of Copenhagen, Universitetsparken 2, DK-2100 Copenhagen Ø, Denmark.
[b] Division of Immunology, Department of Infectious Diseases and Immunology, Faculty of Veterinary Medicine, Utrecht University, Yalelaan 1, 3584 CL Utrecht, The Netherlands
[c] Department of Pharmaceutics, Utrecht Institute of Pharmaceutical Sciences, Faculty of Science, Utrecht University, Universiteitsweg 99, 3584 CG Utrecht, The Netherlands
[d] Department of Drug Design and Pharmacology, Faculty of Health and Medical Sciences, University of Copenhagen, Universitetsparken 2, DK-2100 Copenhagen Ø, Denmark

Abstract

Cationic vectors have demonstrated the potential to facilitate intracellular delivery of therapeutic oligonucleotides. However, enhanced transfection efficiency is usually associated with adverse effects, which also proves to be a challenge for vectors based on cationic peptides. In this study a series of proteolytically stable palmitoylated α-peptide/β-peptoid peptidomimetics with a systematically varied number of repeating lysine and homoarginine residues was shown to self-assemble with small interfering RNA (siRNA). The resulting well-defined nanocomplexes were coated with anionic lipids giving rise to net anionic liposomes. These complexes and the corresponding liposomes were optimized towards efficient gene silencing and low adverse effects. The optimal anionic liposomes mediated a high silencing effect, which was comparable to that of the control (cationic Lipofectamine 2000), and did not display any noticeable cytotoxicity and immunogenicity in vitro. In contrast, the corresponding nanocomplexes mediated a reduced silencing effect with a more narrow safety window. The surface coating with anionic lipid bilayers led to partial decomplexation of the siRNA–peptidomimetic nanocomplex core of the liposomes, which facilitated siRNA release. Additionally, the optimal anionic liposomes showed efficient intracellular uptake and endosomal escape. Therefore, these findings suggest that a more efficacious and safe formulation can be achieved by surface coating of the siRNA–peptidomimetic nano-self-assemblies with anionic lipid bilayers.

1 Introduction

In the ongoing search for effective vectors for siRNA delivery, many synthetic cationic carriers including polymers, lipids and peptides show a high transfection efficiency, but the implementation of these vectors has been hampered by potential toxicity.[1] Various reports demonstrate that polycations such as polylysine, polyethyleneimine and polyamidoamine display direct cellular toxicity, and they may also trigger complement activation.[2] In addition, interactions between cationic nanoparticles and the *in vivo* environment may potentially induce aggregation, suboptimal biodistribution and immunological reactions at the systemic level.[3] Compared to cationic carriers, anionic siRNA nanoparticles have offered promising evidence of efficacy without significant toxicity.[4] Therefore, it is desirable to engineer and further improve the design of siRNA carriers by exploring promising anionic delivery agents.

Previously, we have synthesized and characterized a library of proteolytically stable α-peptide/β-peptoid peptidomimetics with promising membrane-destabilizing and cell-penetrating properties that we envisage can be exploited for siRNA delivery.[5–7] The molecular structure of these peptidomimetics is based on an alternating hydrophobic/cationic design consisting of N-alkylated β-alanine (β-peptoid) units and α-amino acid units (homoarginine and lysine). This design is believed to benefit from the hydrophobicity of the benzyl side chains of the β-peptoid residues and the cationic charge and hydrogen bond-forming capability of the cationic α-amino acid residues. Such sequences show superior membrane-destabilizing properties and cellular uptake over that of octa-arginine (R8), and the altered peptoid backbone design confers proteolytic stability.[6] Hence, it is hypothesized that these peptidomimetics may facilitate delivery of siRNA across cell membranes. However, their high positive charge density potentially constitutes a toxicity risk for in vivo applications, and thus there is a need for formulating efficient siRNA vectors with lower adverse effects. To address this challenge we complexed palmitoylated versions of the peptidomimetics displaying a varied number of cationic charges, with siRNA into well-defined nano-self-assemblies. The resulting complexes were subsequently coated with a net anionic binary lipid mixture to mask the cationic charge resulting in the formation of net anionic liposomes. The palmitoylation was introduced to increase the colloidal stability of the complexes in physiologically relevant media via hydrophobic interactions.

Although comprehensive research efforts towards development of cationic lipid formulations for siRNA delivery have resulted in an improvement of protein knockdown, an increasing number of reports have demonstrated that many cationic lipid formulations elicit undesired immune responses.[8] Alternative liposomal delivery vectors with reduced immunogenicity and toxicity are therefore needed. In some reports, anionic lipid-based formulations have been utilized for effective DNA and siRNA transfection.[9–13] The group

of H. Harashima introduced an anionic lipid envelope structure, and multifunctional nanodevices were engineered based on this delivery approach.[14] However, the application of this lipid vector, in combination with new cationic peptides, and its impact on the efficiency and safety of siRNA delivery remain to be defined. We hypothesize that we may improve the delivery of siRNA and reduce adverse effects via three different means: (i) by the use of peptidomimetics with an appropriate cationic charge density for siRNA complexation; (ii) by stabilizing these complexes via addition of a hydrophobic acyl moiety to the peptidomimetics; and (iii) by subsequent coating of the complexes with anionic lipid membrane bilayers.

In the present work, novel formulations were designed for siRNA delivery using the peptidomimetics as complexing agents in anionic liposomes composed of 1,2-dioleoyl-sn-glycero-3-phosphoethanolamine (DOPE) and cholesteryl hemisuccinate (CHEMS). Thus, siRNA directed against enhanced green fluorescent protein (EGFP) was complexed with a library of palmitoylated α-peptide/β-peptoid oligomers with systematically varied charge density, and subsequently the complexes were coated with anionic membrane bilayers for safe and efficient siRNA delivery. The physicochemical properties of both the complexes and the liposomes were characterized with respect to size, charge and encapsulation efficiency. The gene silencing efficiency, toxicity and immunogenicity were evaluated in vitro. Furthermore, we examined the cellular association, intracellular uptake, subcellular localization and endosomal escape of the EGFP siRNA.

2 Materials and methods

2.1. Materials

Palmitoylated α-peptide/β-peptoid peptidomimetics (Figure 1A) were synthesized as previously described.[4] DOPE and CHEMS were purchased from Avanti Polar Lipids (Alabaster, AL, USA). 2′-O-Methyl modified dicer substrate asymmetric duplex siRNAs directed against EGFP and negative control firefly luciferase (FLuc) were supplied by Integrated DNA Technologies (IDT, Coralville, IA, USA). The siRNAs had the following sequences and modifications: EGFP, sense 5′-pACCCUGAAGUUCAUCUGCACCACcg-3′; antisense 5′-CGGUGGUGCAGAUGAACUUCAGGGUCA-3′; FLuc sense 5′-pGGUUCCUGGA ACAAUUGCUUUUAca-3′ and antisense 5′-UGUAAAAGCAAUUGUUCCAGGAA CCAG-3′, where lower-case letters represent deoxyribonucleotides, underlined capital letters represent 2′-O-methylribonucleotides, and p represents a phosphate residue.[15] EGFP siRNA labelled with Alexa488 was obtained from IDT. 3-(4,5-Dimethylthiazol-2-yl)-5-(3-carboxymethoxyphenyl)-2-(4-sulfophenyl)-2H-tetrazolium (MTS) was provided by Promega (Madison, WI, USA). Phenazine methosulfate (PMS), heparin (MW 14000 Da) and octyl β-D-glucopyranoside were purchased from Sigma-Aldrich (St. Louis, MO,

USA). Quant-iT™ RiboGreen RNA Reagent and Lipofectamine 2000 (Lip2k) were purchased from Invitrogen (Paisley, UK). Throughout the experiments, RNase-free materials and conditions were carefully applied.

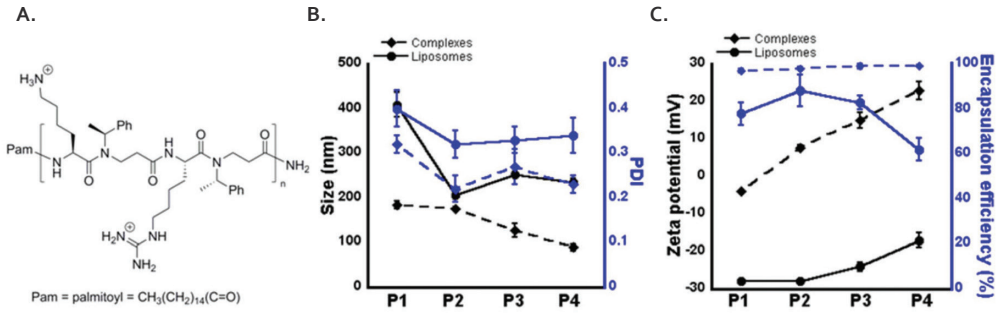

Figure 1 *(A) The sequence of α-peptide/β-peptoid oligomers with alternating hydrophobic and lysine and homoarginine motifs containing a variable number (n) of repeats (n = 1, 2, 3 or 4, P1–4), coupled to a palmitoyl lipid chain. (B) Particle size (black) and polydispersity index (PDI, blue) of complexes (prisms) and liposomes (circles), respectively, prepared using P1–4. (C) Zeta potential (black) and encapsulation efficiency (blue) of complexes and liposomes, respectively, prepared using P1–4. Values represent means ± SD (n = 3).*

2.2. Formulation of siRNA-loaded nanoparticles and characterization

Complexes of siRNA and the palmitoylated peptidomimetics (1–4 repeating units, Figure 1A) were prepared at an N/P ratio of 2: Solutions containing the required amount of the different peptidomimetics were made in 5 mM HEPES buffer, pH = 7.4. An siRNA solution (1.5 μM/27 μg mL^{-1} final concentration) was added dropwise to the peptidomimetic solutions while vortexing to facilitate the self-assembly process, and the complexes were then incubated for 30 min at room temperature (rt). The complexes were subsequently coated with lipids by using the lipid film hydration method.[16] In brief, a total amount of 137.5 nmol of DOPE and CHEMS at a molar ratio of 9:2 was dissolved in 250 μL of chloroform, which was then evaporated, resulting in the formation of a thin lipid film. A volume of 250 μL of the siRNA–peptidomimetic complex suspension was used to hydrate the film for 10 min while vortexing every minute, and the mixture was subsequently sonicated for 1 min using a Branson 2510 bath sonicator (Danbury, CT, USA). The final lipid concentration was 0.55 mM. The liposome mixture was passed through an Econo column (Bio-Rad, Hercules, CA, USA) filled with a Sepharose CL-4B matrix (GE Healthcare) to separate non-encapsulated siRNA from the liposomes. The particle size (diameter) and the polydispersity index (PDI) of the complexes and the liposomes were determined by dynamic light scattering (DLS),

and the surface charge of the particles was measured by analysis of the zeta potential using a Nanosizer NanoZS (Malvern Instruments, Worcestershire, UK) as previously described.[17] A volume of 30 μL siRNA-loaded formulation, diluted 30 times in MilliQ water, was used for the measurements, and all samples were measured in triplicate. For the measurement of the encapsulation efficiency, complexes and liposomes were dissociated by adding a heparin/detergent solution (1 mg mL^{-1} heparin and 1 mM octyl β-D-glucopyranoside in TE buffer). The samples were subsequently diluted and the siRNA was quantified by using the RiboGreen® RNA reagent according to the manufacturer's instructions. The encapsulation efficiency was calculated using the following equation:[17]

$$\text{Encapsulation efficiency} = \frac{\text{Actual siRNA loading}}{\text{Theoretical siRNA loading}} \times 100\%$$

As positive control, Lip2k, was complexed with siRNA according to the manufacturer's instructions.

2.3. Cell culture

The human non-small cell lung carcinoma cell line H1299 (ATCC, Manassas, VA, USA) was maintained in RPMI 1640 medium (Fisher Scientific, Waltham, MA, USA) supplemented with 100 U ml^{-1} penicillin, 100 μg ml^{-1} streptomycin, 2 mM L-glutamine (all from Sigma-Aldrich), and 10% (v/v) fetal bovine serum (FBS). H1299 cells stably expressing EGFP (H1299 EGFP) were used as reported previously,[15] and the cells were cultured in the same medium supplemented with 0.2 mg mL^{-1} geneticin (Invitrogen, Carlsbad, CA, USA). The cells were grown under an atmosphere of 5% CO_2/95% O_2 at 37 °C changing the growth medium three times a week and sub-cultured twice a week.

2.4. Determination of silencing efficiency *in vitro*

The H1299 EGFP cells were seeded in 12-well plates at a density of 100000 cells per well 24 h prior to the experiment. On the following day, the cells were transfected with the nanoparticles loaded with EGFP siRNA or FLuc siRNA, respectively, in serum-free RPMI medium.[15] After 48 h, the cells were washed with phosphate-buffered saline (PBS), trypsinised and resuspended in 300 μL PBS prior to analysis by flow cytometry. A total number of 10000 cells were measured per sample using a Gallios flow cytometer (Beckman Coulter, Fullerton, CA, USA), and the data were analyzed using the FlowJo software (Tree Star Inc., Ashland, OR, USA). For each condition, three separate samples were analysed. The percentage of gene silencing was calculated by using the FL-1 mean (mean of the EGFP fluorescence histogram). Cells transfected with nanoparticles loaded with FLuc siRNA were used as negative control.

2.5. Viability assay

The effect of the peptidomimetics, the complexes and the liposomes, respectively, on the viability of H1299 cells was determined using the MTS/PMS assay as previously described.[18] H1299 cells were seeded at a density of 9000 cells per well in 96-well plates and cultured for 24 h. The cells were then exposed to solutions of peptidomimetics or dispersions of particles in medium at different concentrations for 24 h at 37 °C. Cells incubated with sodium dodecyl sulfate (SDS), 0.2% (w/v), were used as a positive control, while untreated cells were used as a negative control. After incubation, the cells were washed with PBS, and 100 μL of freshly prepared MTS/PMS reagent in HBSS was added to each well followed by incubation at 37 °C for 1 h. The cell viability was determined by measuring the absorbance of the enzymatically formed formazan at 492 nm.

2.6. Toll-like receptor activation assay

Toll-like receptor (TLR) reporter cell lines (HEK-BlueTM-hTLR2, -hTLR3, -hTLR4, -hTLR7, and -hTLR9 reporter cells) were cultured as instructed by the manufacturer (Invivogen, Toulouse, France). The TLR reporter cell lines were stimulated with the peptidomimetics at concentrations of 0.5 μM or 5 μM, with the complexes and the liposomes at siRNA concentrations of 50 nM, or with the solvent alone, in a total volume of 100 μL for 20 h at 37 °C. As positive controls, the following agonists were used: PAM_3SCK (100 ng mL^{-1}) for TLR2, polyinosinic–polycytidylic acid [poly(I:C)] (5 μg mL^{-1}) for TLR3, lipopolysaccharide (LPS)-EK (10 ng mL^{-1}) for TLR4, CL264 (5 μg mL^{-1}) for TLR7 and ODN2006 (10 μg mL^{-1}) for TLR9 (all from Invivogen). To detect the reporter protein secreted alkaline phosphatase (SEAP), 20 μL of the supernatant was added to 180 μL of QUANTI-Blue™ substrate (Invivogen) and incubated for 1 h at 37 °C. Levels of SEAP were determined by measuring the absorbance using a microplate reader at 650 nm. Relative SEAP levels were defined as the sample level divided by the solvent control level.

2.7. Dendritic cell maturation assay

Femurs and tibia of adult CB6F1/CrL mice (6–8 weeks) were flushed with culture medium (Iscove's modified Dulbecco's medium) supplemented with 5% (v/v) fetal bovine serum (Lonza, Verviers, Belgium), 50 μM 2-mercaptoethanol (Sigma-Aldrich), penicillin and streptomycin and the cells were seeded in 12-well plates, at a concentration of 450000 cells in 1 mL culture medium (adapted from Lutz et al. 1999).[19] Dendritic cells were expanded with 20 ng nL^{-1} murine recombinant granulocyte macrophage colony stimulating factor (rGM-CSF) (Cytogen, The Netherlands). On day 2, the volume of complete growth medium volume was doubled and on day 5, additional 20 ng mL^{-1} rGM-CSF was added. On day 7, bone marrow dendritic cells were stimulated with PBS (1:250), LPS (10 ng mL^{-1}) or the peptidomimetics (0.5, or 5 μM) or the complexes and the liposomes at siRNA

concentrations of 50 nM (all stimuli buffered to 10 mM HEPES) for 16 h at 37 °C in a humidified CO_2 incubator. Staining of surface markers with the indicated antibodies was performed in the presence of Fc block (2.4 G2) for 30 min on ice. Anti-CD11c (N418) and I-Ad/I-Ed (M5/114) were purchased from eBioscience (San Diego, CA, USA), and anti-CD40 (3/23) and anti-CD86 (GL1) were obtained from BD Biosciences (Breda, The Netherlands). Samples were measured on a FACSCantoII (BD Biosciences, San Jose, CA, USA) and analyzed using the FlowJo software. Ethical approval for the mouse experiment was obtained from the Animal Experiment Committee of Utrecht University, The Netherlands.

2.8. Evaluation of morphology

The morphology of the complexes and the liposomes was determined by transmission electron microscopy (TEM).[17] After negative staining with 2% (w/v) uranyl acetate in water, the particles were visualized by using a Philips CM100 TWIN TEM (Philips, Eindhoven, The Netherlands). Photographs were recorded with a side-mounted Olympus Veleta camera. Further morphological evaluation of the liposomes was carried out by cryo-TEM using a Tecnai G2 20 TWIN instrument (FEI Inc., Hillsboro, OR, USA).[20]

2.9. Heparin decomplexation assay

To evaluate the binding ability of the siRNA–peptidomimetic complexes and liposomes, a heparin decomplexation assay was performed as previously described[21]. Complexes and liposomes were freshly prepared as described above. The complexes were equally distributed over the wells (100 µL per well) of a black, flat-bottomed 96-well plate. To each well, 100 µL of Ribogreen solution (in TE buffer, pH 7.4) was added and incubated for 10 min in the dark at rt. A serial dilution of heparin in RNase-free water containing octyl β-D-glucopyranoside (1 mM) was prepared and 100 µL of each dilution was added followed by incubation for 20 min in the dark at rt. Non-complexed siRNAs treated in a similar way to the nanoparticles and nanoparticles without heparin were included as positive and negative controls, respectively. The decomplexed siRNA was quantified by using the RiboGreen® assay as described above. For comparison, the half-maximal effective concentration (EC_{50}) of heparin decomplexation was analysed.

2.10. Release of siRNA

The release of siRNA was measured in TE buffer using complexes and liposomes, respectively, loaded with EGFP siRNA. Briefly, 20 µL of nanoparticle dispersion was suspended in 1 mL TE buffer in RNase-free Eppendorf tubes and shaken in a water bath (50 rpm) at 37 °C. At given times, samples were taken and analyzed in triplicates. The released siRNA was quantified by using the Ribogreen assay as described above.[15]

2.11. Cell association of siRNA determined by flow cytometry

The cellular uptake of the nanoparticles was quantified by using flow cytometry. The H1299 cells were seeded in 12-well plates (1.5×10^5 cells per well) 24 h before the experiment, which was initiated by incubating the cells with nanoparticles at a concentration of 100 nM Alexa 488-labelled siRNA in serum-free medium at 37 °C for 4 h. Cells were rinsed twice with PBS, trypsinized and diluted with medium. After washing and centrifugation, the cell pellet was resuspended in 200 µL PBS and analyzed by flow cytometry as described above.

2.12. Intracellular siRNA determined by stem-loop qPCR

RNA isolation and purification were performed as previously described.[15] The H1299 EGFP cells were washed with PBS and trypsinized at 48 h post-transfection. The sequences of the stem–loop reverse transcription primers and the PCR primers have been reported previously by Colombo et al.[15] Briefly, a purified RNA amount of 700 ng was reverse transcribed in a total reaction volume of 20 µL that also included a 500 µM deoxynucleotide mix, 20 U Protector RNase Inhibitor, 10 U Transcriptor Reverse Transcriptase, and 1× Transcriptor Reverse Transcriptase buffer (all from Roche, Basel, Switzerland). The RNA template was first denatured and immediately cooled on ice. The reaction mix and the stem–loop primers (11 nM of each) were then added during the cooling phase. The pulsed RT programme consisted of 15 min at 14 °C, 10 min at 42 °C, followed by 25 cycles (15 s at 14 °C, 10 s at 42 °C and 15 s at 65 °C). Subsequently, the mixture was incubated for 5 min at 85 °C for transcriptase inactivation and cooled at 4 °C. The qPCR was performed with a LightCycler 480® (Roche) using the SYBR Green Master mix according to the manufacturer's instructions. An amount of 5 ng DNA was analyzed. The housekeeping gene snoRNA U109 (GenBank ID: AM055742.1) was used for normalization. The PCR programme was 95 °C for 5 min, 37 cycles (95 °C for 15 s, 62 °C for 15 s, 72 °C for 1 s) followed by cooling at 4 °C. The PCR data analyses were performed as previously described.[14]

2.13. Intracellular trafficking of siRNA

The H1299 cells were seeded in 12-well plates (10^5 cells per well) containing a cover slip. After 24 h, the cells were incubated for 12 h with the nanoparticles loaded with Alexa488-labelled siRNA (at 100 nM), then rinsed three times with PBS and incubated for 1 h with Lysotracker DND99 (500 nM, Molecular Probes) to stain the late endosomes and lysosomes. After washing with PBS, the cells were fixed with fresh paraformaldehyde (3% in PBS). In order to stain the nuclei, the cells were incubated with 4′,6-diamidino-2-phenylindole (DAPI, 0.1 µg mL^{-1}) for 5 min and rinsed three times with PBS. After washing, the cover slips were placed on a slide using the Vectashield® mounting medium. The slides were imaged using a Zeiss LSM 710 confocal laser scanning microscope equipped with a Zen2010 module (Carl Zeiss, Jena, Germany).

2.14. Statistics

Values are given as the mean values with standard deviations (SD), n = 3. For the statistics and plotting, PRISM (GraphPad, La Jolla, CA, USA) was used. Statistically significant differences were assessed by an analysis of variance (ANOVA) at a 0.05 significance level and followed by a Tukey's post hoc test.

3. Results and Discussion

3.1. Preparation and physicochemical characteristics of complexes and liposomes

All nanoparticle dispersions prepared in this study are referred to as Pn-C and Pn-L, where Pn, C and L denote (i) the number of sequence repeats in the peptidomimetics, (ii) the complexes, and (iii) the liposomes, respectively. The sequence length of the α-peptide/β-peptoid oligomers was varied from one to four repeats (i.e. P1 to P4, Figure 1A), and their net positive charge was 2, 4, 6, and 8, respectively. The complexes were generally formed via electrostatic interactions between the polycationic peptidomimetics and the highly anionic siRNA, combined with hydrophobic interactions between the palmitoyl chains and probably also the benzyl groups of the peptides. Complexes were formed by mixing the peptidomimetics with siRNA at a specific N/P ratio, which can be expressed as the charge ratio between the peptide nitrogen and the siRNA phosphate groups. An N/P ratio of 2 was chosen for this study because it resulted in small complexes with a low PDI. All peptidomimetics effectively self-assembled with EGFP siRNA to yield complexes of 90–180 nm in diameter (Figure 1B). The complexes were further encapsulated with a lipid membrane bilayer composed of neutral DOPE and anionic CHEMS. The Harashima group has successfully applied these lipids to deliver plasmid DNA, and suggested that this packaging mode was based on electrostatic interactions between DNA, R8 and lipids.[15] We chose a molar ratio of 9:2 between DOPE and CHEMS, as it had been found that this lipid ratio was required for introducing sufficient negative charge to coat the complexes and shield their net positive charge. Expectedly, the diameter of the liposomes (250–400 nm) was larger than the diameter of the complexes (Figure 1B), and the zeta potential of all complex particles became negatively charged as a result of the lipid coating (Figure 1C), indicating that the complexes were in fact coated with a lipid membrane. Also, the zeta potential of the complexes and the liposomes increased with the longer peptidomimetics, and this correlates well with the increased number of cationic charges.

When anionic siRNA was complexed with the cationic peptidomimetics, all complexes showed a high encapsulation efficiency (above 98%, Figure 1C). However, a lower encapsulation efficiency (73%) was observed for P1-L (Figure 1C), only displaying two cationic charges in the peptidomimetics, which apparently is insufficient for forming

a compact particle core. Reduced encapsulation efficiency was also found for P4-L liposomes (63%). A possible explanation could be that anionic lipids may interact more strongly with P4 containing the highest number of cationic charges than with P2 and P3 and influence the assembly of the complexes. P2-L and P3-L showed higher encapsulation efficiency (above 80%) verifying the necessity of optimizing the charge density for these cationic peptidomimetics-based formulations.

3.2. Silencing effect *in vitro*

The siRNA silencing effects of the complexes and the liposomes were tested in H1299 EGFP cells (Figure 2). In general, coating with anionic lipids significantly increased the transfection efficiency, as compared to the corresponding complexes at 100 nM siRNA (N/P = 2, Figure 2A). In addition, P3-L and P4-L (based on the peptidomimetics with the higher charge density) showed a higher silencing effect (~75%) in H1299 EGFP cells than P1-L and P2-L (~35%). There was no significant difference between the silencing effect of P3-L and P4-L ($p > 0.05$). An excess of the cationic component is required to obtain stable particles, whereas a lower cationic charge density and lower N/P ratios are essential to minimize cellular toxicity.[22] Therefore, P3-L was investigated in further detail and compared to the commercial transfection reagent Lip2k. The gene silencing effect was approximately 77% for the P3-L and 86% for Lip2k, respectively, and P3-L showed almost the same effect as Lip2k at 25 nM siRNA (Figure 2B). Even at a low N/P ratio of 1, P3-L effectively formed nanoparticles with EGFP siRNA (ESI, Table 1†), and the P3-L liposomes led to decreased EGFP protein expression in a concentration-dependent manner in a similar way to that seen for Lip2k (Figure 2B). These results suggest that P3-L is an efficient vector for the induction of gene silencing, while the complexes exhibit only a modest silencing efficiency.

A key feature of the lipids used in this mixture is not only their charge, but also their tendency to promote lipid fusion. DOPE is considered a fusogenic lipid,[22] while CHEMS has been used to make liposomes fusogenic as the charge of CHEMS changes at acidic pH.[22] To verify the effects of adding a fusogenic lipid mixture versus adding another lipid mixture, we tested P3-L systems prepared with non-fusogenic lipid mixtures. Expectedly, a low silencing effect (<20%) was observed when we replaced DOPE with the zwitterionic phospholipid dipalmitoylphosphatidylcholine (DPPC), as shown in the ESI, Figure S1.† These results indicate that the coating of the complex surface with a fusogenic lipid mixture plays an essential role in the siRNA silencing process.

3.3. Cell viability

Toxicity is a major concern when a nanocarrier is designed for therapeutic purposes. The cytotoxicity of the complexes and the liposomes was tested by using the MTS/PMS assay. At concentrations of up to 100 nM siRNA, none of the complexes displayed any toxicity (Figure 3A), whereas at higher concentrations of siRNA (i.e. 200 and 400 nM),

all complexes gave rise to cytotoxicity with up to 70% cell death, indicating that the safe dose window of the complexes is narrow. In contrast, minimal toxicity (<5%) was found for all liposome formulations, even at concentrations corresponding to 400 nM siRNA (Figure 3A). The calculated half-maximal inhibitory concentrations (IC_{50}) of the different peptidomimetics infer that the cytotoxicity of the peptidomimetics is increased with oligomer length and thus overall cationic charge (Figure 3B). Furthermore, neither naked EGFP siRNA nor the empty liposome vector showed any cytotoxicity in H1299 cells (ESI, Figure S2†). In addition, Lip2k has been reported to be highly cytotoxic as indicated by its IC_{50} (22.9 μg mL^{-1}) despite its potent transfection efficiency.[11] Therefore, this clearly demonstrates the importance of charge shielding in achieving safe siRNA transfection.[23]

3.4. Immunogenicity *in vitro*

Antigen-presenting cells, such as dendritic cells, recognize pathogens via pattern-recognition receptors. These receptors can recognize peptidoglycan-, RNA- or DNA-associated patterns, which are characteristic of pathogens but absent in eukaryotic cells. TLRs are widely studied pattern-recognition receptors, and in the present study we measured the potential activation of five different human TLRs (TLR2, TLR3, TLR4, TLR7 and TLR9). At low and non-toxic concentrations of peptidomimetics (0.5 and 5 μM), P3-C and P3-L (equivalent to 50 nM siRNA), no TLR activation was observed (Figure 4A and B, and ESI, Figure S3†). At the higher cytotoxic concentrations (Figure 3A), TLR activation could not be determined (results not shown). Activation of bone marrow-derived dendritic cells was assessed by measuring the expression of the maturation markers CD40 and CD86.[19] None of the four peptidomimetics stimulated dendritic cells at concentrations of 0.5 μM; however, P2, P3 and P4 activated the dendritic cells at a concentration of 5 μM (Figure 4C), which cannot be explained by the activation of TLRs. P3-C and P3-L did not show any stimulating effects on the dendritic cells at an siRNA concentration of 50 nM. Together, these results indicate that neither the P3-C complexes nor the P3-L liposomes displayed any apparent immunogenicity. Thus incorporation of the peptidomimetics into complexes and subsequently into liposomes substantially decreased their immunostimulatory capacity.

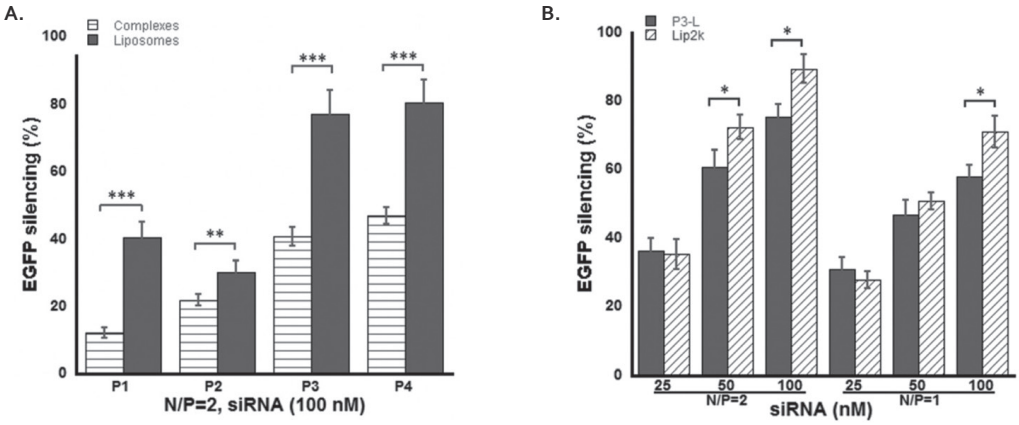

Figure 2 *(A) Silencing effect of the four different complexes and the corresponding liposomes at an N/P ratio of 2 in H1299 EGFP cells. (B) Comparison of P3-L with Lipofectamine 2000 (Lip2k) at N/P ratios of 2 and 1. The weight ratio of Lip2K and siRNA was 3:2 at an N/P of 2. Results are expressed as means ± SD (n = 3). *p < 0.05, **p < 0.01 and ***p < 0.001.*

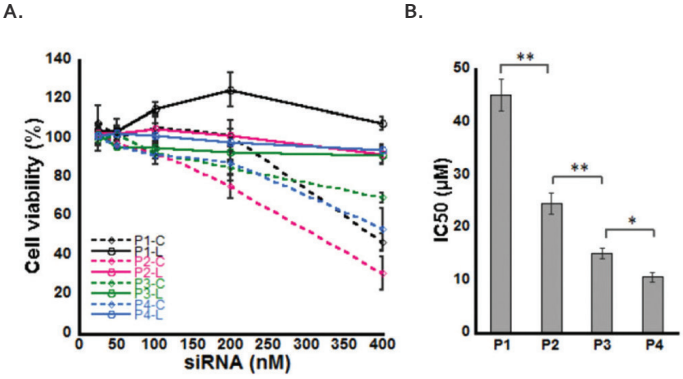

Figure 3 *(A) Effect of complexes and liposomes on the viability of H1299 cells. (B) Effect of the four peptidomimetics (P1–P4) on the viability of H1299 cells. The half-maximal inhibitory concentration (IC_{50}) values were calculated by using a nonlinear regression analysis. Results are expressed as the mean ± SD (n = 3). *p < 0.05 and **p < 0.01.*

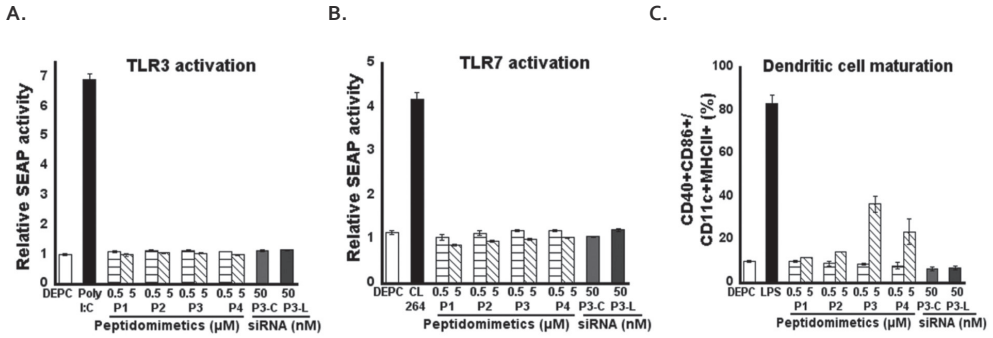

Figure 4 *Reporter cell lines for TLR3 (A) and TLR7 (B) were stimulated with P1–P4 at peptidomimetics concentrations of 0.5 μM, or 5 μM, with P3-C and P3-L at siRNA concentrations of 50 nM or with solvent for 20 h at 37 °C. The activity of the reporter protein SEAP was determined, and the relative expression levels were defined as the sample level divided by the solvent control level. The agonists used for TLR3 and TLR7 were poly I:C and CL264, respectively. DEPC water was used as a negative control. (C) Bone marrow cells were differentiated into dendritic cells (DC) in 7 days with GM-CSF, and where then stimulated with P1–P4 at peptidomimetics concentrations of 0.5 μM, or 5 μM, with P3-C and P3-L at siRNA concentrations of 50 nM or with solvent for 16 h at 37 °C. Lipopolysaccharide (LPS), a stimulant of DC maturation, was used as a positive control, and maturation was determined as the percentage of $CD86^+/CD40^+$ double-positive cells within the $CD11c^+/MHCII^+$ double-positive population. Results are expressed as means ± SD (n = 3) and data are representative of two independent experiments.*

3.5. Morphological evaluation and siRNA release

The morphology of the complexes and the liposomes was analyzed by TEM. The complexes and the liposomes were spherical with a diameter of approximately 90 nm and 250 nm (Figure 5A and B), respectively, which corresponds to the diameters measured by using DLS (Figure 1B). The complexes appeared to have a densely packed structure (Figure 5A). TEM revealed that the ultrastructure of the liposomes is a nuclear core surrounded by one or several concentric lipid membrane bilayers (Figure 5B). Cryo-TEM further confirmed the formation of membrane bilayer(s) enclosing a more electron-dense core, indicating that the complexes are in fact coated with lipid membrane(s) (Figure 5C). Corresponding low-magnification images are presented in ESI, Figure S4.†

When comparing the structure of the complexes before and after membrane coating (Figure 5A and B), it is evident that the complex cores of the liposomes are much larger in size than the uncoated complex particles as a consequence of the lipid coating. Thus we hypothesize that the lipid coating of the complexes results in a looser assembly of the complex core in the liposomes. It has been reported that there is a strong positive correlation between the strength of the association in the siRNA–CPP complexes and their resistance to heparin-induced decomplexation.[21] We therefore performed a heparin

decomplexation analysis to examine this phenomenon. The electrostatic binding of the EGFP siRNA to the peptidomimetic in the P3-L liposome core was compared to that of the uncoated P3-C complex. P3-L displayed a heparin decomplexation EC_{50} value of 29 ± 3 μg mL^{-1}, as compared to 53 ± 5 μg mL^{-1} for P3-C (Figure 5D). These measurements indicate that the lipid coating of the complexes affects the binding affinity between the siRNA and the peptidomimetics. This is in line with our estimate that siRNA is tightly packed with the peptidomimetics in the complex, while the complex core is loosened to some extent upon lipid coating. A possible mechanism for the structural transition of the complexes is that anionic lipids may compete with the negatively charged siRNA for positive electrostatic interaction with the peptidomimetic. Another explanation could be that insertion of the palmitoyl chain of the peptidomimetic into the anionic membrane bilayer may weaken the association between the peptidomimetic and the siRNA in the complex core.

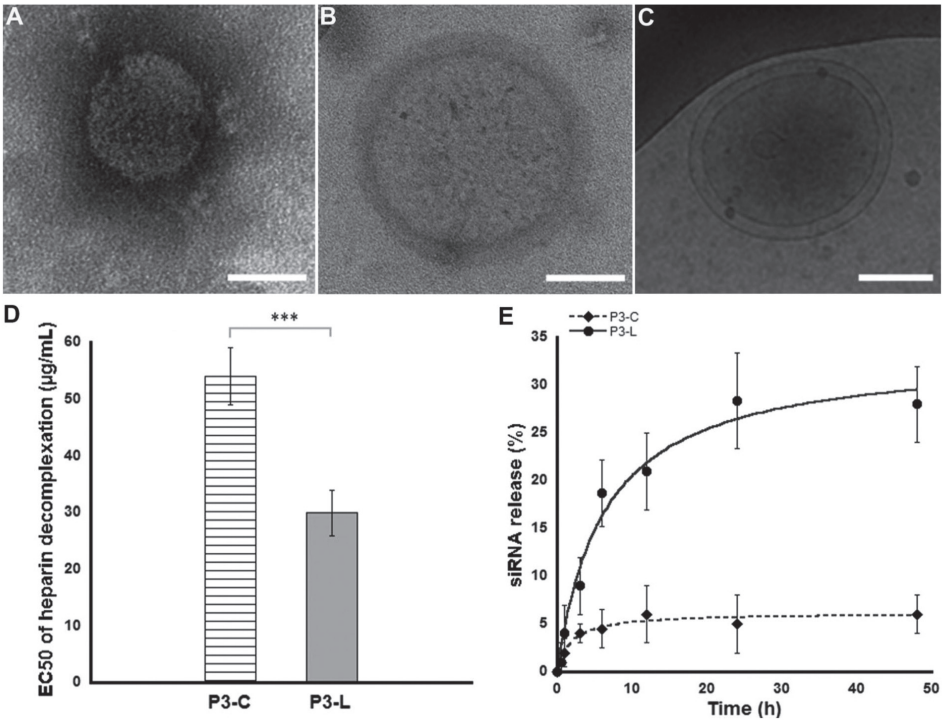

Figure 5 *(A) Representative transmission electron micrograph (TEM) image of a P3-C complex. (B) Representative TEM image of a P3-L liposome showing the nuclear nanocomplex within a lipid bilayer envelope. (C) Representative cryo-TEM image of a P3-L liposome showing the bilayer-core structure. Scale bar = 100 nm. (D) Half-maximal effective concentration (EC_{50}) of heparin decomplexation. (E) siRNA release from complexes and liposomes in TE buffer at pH 7.4 at 37 °C. Results are expressed as the mean ± SD (n = 3), ***p < 0.001*

To further characterize the physicochemical properties, we evaluated the release kinetics for the complexes and the liposomes. A gradual release of siRNA was observed for P3-L, reaching a level of 21% within 12 h. In contrast, siRNA was released more slowly from P3-C: only 7% of total siRNA was released over 48 h (Figure 5E). From the release behavior we found that both curves had an initial linear increase followed by saturation, which happened earlier for P3-C than for P3-L. The observed difference in the release profiles is in line with the transition of the complex structure demonstrated above, and we suggest that the looser structure of the liposome core may contribute to the enhanced siRNA release. Our data are consistent with a previous study, which reported that the most active CPP showed high sensitivity to decomplexation by heparin, indicating the necessity of partial decomplexation for efficient transfection.[21] Thus, it is proposed that a more efficient release of the encapsulated siRNA can explain the enhanced silencing effect of P3-L (Figure 2A).

3.6. Cellular association and intracellular siRNA quantification

Flow cytometric analyses were performed to quantify the association of Alexa488-labeled EGFP siRNA with H1299 cells. The fluorescence intensity in cells treated with naked siRNA showed background fluorescence, while considerable differences in the extent of cellular association were detected for the complexes and the liposomes after 4 h of incubation (Figure 6A). It is well known that positively charged delivery vehicles can facilitate uptake by associating with the negatively charged cellular membranes.[24] As shown in Figure 6B, cationic Lip2k showed a strong association with the cells [mean fluorescence intensity (MFI) 91.0 ± 7.5], and the cellular association of the P3-C complex (MFI 7.0 ± 2.5) was significantly higher ($p = 0.0004$) than that of naked siRNA (MFI 2.2 ± 0.4). Interestingly, the cellular association of negatively charged P3-L (27.1 ± 4.2) was significantly higher ($p = 0.0006$) than that of the positively charged P3-C. These observations may be a consequence of different uptake mechanisms for P3-L particles and P3-C particles. Further studies are needed to elucidate this point. It has been reported that the CPP-based complexes might deliver siRNA to the cells by receptor-mediated endocytosis.[2] Alternatively, both endocytosis and direct fusion between the liposomes and the plasma membrane may be responsible for the entry of functional siRNA into the cytosol.[25]

To better understand the delivery potential of the carriers, we monitored the relative level of siRNA delivered intracellularly by using stem–loop qPCR (Figure 6C). Lip2k, P3-C and P3-L exhibited relative intracellular siRNA uptake patterns similar to the membrane association shown in Figure 5B. In general, the amount of intracellular siRNA delivered by the nanocarriers was directly proportional to their transfection efficiency. Lip2k showed the highest siRNA delivery being 4-fold higher than that of P3-L. However, P3-L showed a comparable siRNA silencing efficiency as Lip2k, indicating that the delivery efficiency of P3-L is higher than that of Lip2k. Our data are in agreement with previous studies,[21]

suggesting that cellular uptake of siRNA is an important, but not sufficient, prerequisite for a high functional transfection.

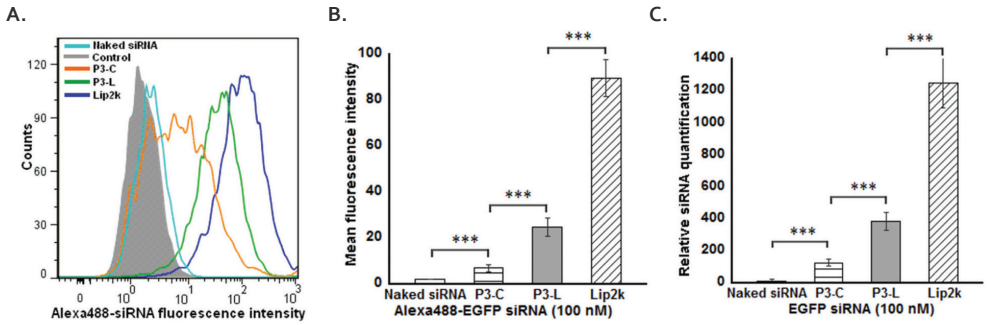

Figure 6 *(A) Representative histograms of flow cytometric analyses demonstrating the cellular association of siRNA after 4 h incubation of H1299 cells with P3-C, P3-L or Lip2k loaded with Alexa488-EGFP siRNA at a concentration of 100 nM. As controls, cells incubated with medium alone and non-complexed siRNA, respectively, were used. (B) Quantitative comparison of nanocarrier-mediated cellular association of Alexa488-EGFP siRNA by flow cytometry. (C) Relative quantification of EGFP siRNA after 48 h transfection with P3-C, P3-L or Lip2k at 100 nM EGFP siRNA using the stem–loop qPCR. Results are expressed as the mean ± SD (n = 3), ***p < 0.001.*

3.7. Subcellular distribution of siRNA and endosomal escape

The intracellular distribution of Alexa488-labeled EGFP siRNA after transfection was visualized by confocal laser scanning microscopy to elucidate the reason for the differential RNAi effects, depending on the particle modification. Considerable differences in the distribution and extent of cellular accumulation were detected between different nanoparticles at a concentration of 100 nM siRNA after 12 h incubation. Naked siRNA displayed an extremely weak fluorescence, whereas Lip2k showed a very strong cellular internalization (Figure 7). For P3-C, a noticeable amount of Alexa488-siRNA was seen in the cytoplasm, while P3-L gave rise to a more extensive cytosolic distribution of labeled siRNA. Visualization of the cellular distribution of Alexa488-labeled siRNA internalized via P3-C and P3-L supported the flow cytometry analyses and cellular siRNA quantification that revealed that P3-L delivered higher amounts of siRNA as compared to P3-C.

It has been reported that nanocarriers can modulate the subcellular drug distribution, eventually resulting in much higher efficacy.[26] An important determinant of siRNA delivery is the efficiency of siRNA escape from the endosomes and the lysosomes into the cytosol.[27] The cationic liposome Lip2k represents one approach for endosomal escape, as shown in Figure 7, and despite the fact that a proportion of Alexa488-siRNA (green) co-localizing with the endosomal/lysosomal marker LysoTracker (red) is evident (yellow or orange

areas), areas of strong green fluorescence are also present in the cells, suggesting that the Lip2k formulation is capable of inducing considerable endolysomal escape. It is proposed that cationic lipids are able to combine with anionic lipids in the endosomal membrane to form ion pairs, thereby destabilizing the endosomal membrane and facilitating the release of siRNA into the cytosol.[28,29] In the case of P3-L treated cells (Figure 7), siRNA only partially co-localized with LysoTracker, indicating that the P3-L particles are capable of escaping lysosomal degradation. Interestingly, it is apparent that siRNA is targeted to the nuclei in the cells incubated with P3-L. A possible mechanism could be that the pH-sensitive fusogenic lipid in the P3-L liposomes may facilitate the delivery of the payload into the cytosol and nucleus.[30] Because CHEMS is acid-sensitive, P3-L may disassemble as a consequence of a structural change of the stable lamellar CHEMS:DOPE liposomes upon reduction of the pH: at reduced pH, CHEMS molecules will change from a cone-like shape to a cylindrical shape due to protonation of the headgroup with a concomitant loss of bilayer-stabilizing properties, and the nonbilayer-forming lipid DOPE will undergo a lamellar-to-hexagonal phase transition, eventually adopting an inverted hexagonal phase that is highly fusogenic, causing membrane destabilization and release of entrapped siRNA.[31] In contrast, reduced cytosolic accumulation of siRNA and a lower silencing effect were observed when we replaced CHEMS with the phospholipid DPPC (ESI, Figure S5†). In addition, cells incubated with P3-C revealed extensive co-localization of siRNA with LysoTracker, suggesting a limited endolysosomal escape of siRNA into the cytosol. Our data are in accordance with the silencing results, which also indicate that the challenge of endosomal escape remains for the development of CPP-mediated siRNA delivery.[2]

These results demonstrate that endosomal/lysosomal escape may be enhanced via modulation of the cellular siRNA distribution as a result of the acid-sensitive anionic lipid-modification on the surface of the nanocomplexes. Therefore, the data suggest that P3-L mediated a higher EGFP silencing primarily by increasing the cellular uptake and mediating a more favorable siRNA release in the cytoplasm. P4-L particles also displayed similar results (data not shown). Our findings are consistent with a recent study, which reported that PepFect6/siRNA–PepFect6 liposomes generated a significant RNAi effect *in vitro*.[32] Although there are marked differences in the experimental conditions for P3-L and PepFect6/siRNA–PepFect6 particles (such as CPP type, cell type, target genes and surface modification), the high cellular uptake, efficient endosomal escape, disintegration of complexes, and potent silencing effect of our liposomes and the PepFect6/siRNA–PepFect6 particles may be attributed to a similarity of the lipid structure coating the nanocomplexes.

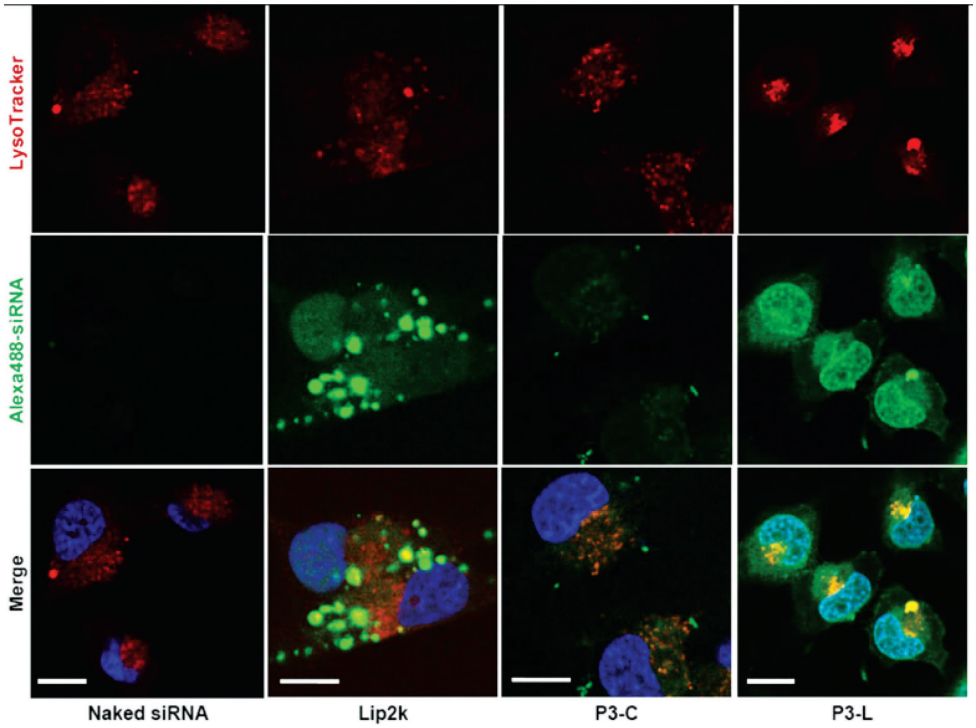

Figure 7 *Representative confocal laser scanning microscopy images of H1299 cells (blue: nuclei) transfected with Lip2k, P3-C and P3-L nanoparticles loaded with 100 nM Alexa488-siRNA. The co-localization patterns of siRNA (green) with LysoTracker (late endosome/lysosome marker, red) 12 h after treatment with nanoparticles show different siRNA distributions. Scale bar = 20 μm.*

4. Conclusions

The optimized anionic liposomes constitute a more effective and robust formulation than the siRNA–peptidomimetic complexes, and show proficient intracellular uptake and endosomal escape. More importantly, the anionic liposomes elicit negligible cytotoxicity and immunogenicity in vitro. Several elements of this study may facilitate future development of oligonucleotide delivery systems. First, the optimization of the length of the peptidomimetics to display an appropriate positive charge not only resulted in small and stable complexes with siRNA at a low N/P ratio, but also reduced the toxicity caused by this polycationic component. This technology for reducing toxicity may be applied to design other cationic peptides or polymers. Second, these results suggest that P3-L liposomes constitute an efficient and biocompatible vector for siRNA delivery with diminished cytotoxicity and immunogenicity, and that the coating lipid

may be extended to other anionic coating agents. Third, although we show that siRNA delivery may be improved *in vitro*, the P3-L nanocarrier may serve as a template for further surface modification with e.g. targeting ligands and functional molecules, especially polyethyleneglycol capable of prolonging the systemic circulation and minimizing adverse immune responses.[27] In summary, such a rational design that addresses safety concerns and ensures effective delivery will aid the translation of engineered peptidomimetic-based nanoparticles to the clinic in the future.

Acknowledgements

We gratefully acknowledge the support from the Innovative Medicines Initiative Joint Undertaking under grant agreement no. 115363 the resources of which are composed of the financial contribution from the European Union's Seventh Framework Programme (FP7/2007-2013) and EFPIA companies' in kind contributions. This project has received funding from the European Union's Seventh Framework Programme for research, technological development and demonstration under grant agreement no. 600207. We are also grateful to the Danish Council for Independent Research and FP7 Marie Curie Actions – COFUND (Grant No. DFF-4093-00292), the Lundbeck Foundation (No. R181-2014-3793) and the Carlsberg Foundation for financial support. We acknowledge the skilled technical assistance of F. Rose, K. J. Vissing, T. Q. Hussein, M. L. Pedersen, S. Rønholt and M. García-Díaz, and we acknowledge the Core Facility for Integrated Microscopy, Faculty of Health and Medical Sciences, University of Copenhagen.

References

1 H. Lv, S. Zhang, B. Wang, S. Cui and J. Yan, Toxicity of cationic lipids and cationic polymers in gene delivery, J. Controlled Release, 2006, 114, 100–109

2 U. Lächelt and E. Wagner, Nucleic Acid Therapeutics Using Polyplexes: A Journey of 50 Years (and Beyond), Chem. Rev., 2015, 115, 11043–11078

3 S. Colombo, X. Zeng, H. Ragelle and C. Foged, Complexity in the therapeutic delivery of RNAi medicines: an analytical challenge, Expert Opin. Drug Delivery, 2014, 11, 1481–1495

4 A. D. Tagalakis, H. D. do Lee, A. S. Bienemann, H. Zhou, M. M. Munye, L. Saraiva, D. McCarthy, Z. Du, C. A. Vink, R. Maeshima, E. A. White, K. Gustafsson and S. L. Hart, Multifunctional, self-assembling anionic peptide-lipid nanocomplexes for targeted siRNA delivery, Biomaterials, 2014, 35, 8406–8415

5 C. Foged, H. Franzyk, S. Bahrami, S. Frokjaer, J. W. Jaroszewski, H. M. Nielsen and C. A. Olsen, Cellular uptake and membrane-destabilising properties of α-peptide/β-peptoid chimeras: lessons for the design of new cell-penetrating peptides, Biochim. Biophys. Acta, 2008, 1778, 2487–2495

6 X. Jing, M. R. Kasimova, A. H. Simonsen, L. Jorgensen, M. Malmsten, H. Franzyk, C. Foged and H. M. Nielsen, Interaction of peptidomimetics with bilayer membranes: biophysical characterization and cellular uptake, Langmuir, 2012, 28, 5167–5175

7 X. Jing, M. Yang, M. R. Kasimova, M. Malmsten, H. Franzyk, L. Jorgensen, C. Foged and H. M. Nielsen, Membrane adsorption and binding, cellular uptake and cytotoxicity of cell-penetrating peptidomimetics with α-peptide/β-peptoid backbone: effects of hydrogen bonding and α-chirality in the β-peptoid residues, Biochim. Biophys. Acta, 2012, 1818, 2660–2668

8 Y. C. Tseng, S. Mozumdar and L. Huang, Lipid-based systemic delivery of siRNA, Adv. Drug Delivery Rev., 2009, 61, 721–731

9 R. J. Lee and L. Huang, Folate-targeted, anionic liposome-entrapped polylysine-condensed DNA for tumor cell-specific gene transfer, J. Biol. Chem., 1996, 271, 8481–8487

10 N. Mignet, C. Richard, J. Seguin, C. Largeau, M. Bessodes and D. Scherman, Anionic pH-sensitive pegylated lipoplexes to deliver DNA to tumors, Int. J. Pharm., 2008, 361, 194–201

11 M. Kapoor and D. J. Burgess, Efficient and safe delivery of siRNA using anionic lipids: Formulation optimization studies, Int. J. Pharm., 2012, 432, 80–90

12 C. Lavigne, K. Slater, N. Gajanayaka, C. Duguay, E. Arnau Peyrotte, G. Fortier, M. Simard, A. J. Kell, M. L. Barnes and A. R. Thierry, Influence of lipoplex surface charge on siRNA delivery: application to the in vitro downregulation of CXCR4 HIV-1 co-receptor, Expert Opin. Biol. Ther., 2013, 13, 973–985

13 W. Ding, F. Wang, J. Zhang, Y. Guo, S. Ju and H. Wang, A novel local anti-colorectal cancer drug delivery system: negative lipidoid nanoparticles with a passive target via a size-dependent pattern, Nanotechnology, 2013, 24, 375101

14 T. Nakamura, H. Akita, Y. Yamada, H. Hatakeyama and H. Harashima, A multifunctional envelope-type nanodevice for use in nanomedicine: concept and applications, Acc. Chem. Res., 2012, 45, 1113–1121

15 S. Colombo, H. M. Nielsen and C. Foged, Evaluation of carrier-mediated siRNA delivery: lessons for the design of a stem-loop qPCR-based approach for quantification of intracellular full-length siRNA, J. Controlled Release, 2013, 166, 220–226

16 Y. Nakamura, K. Kogure, S. Futaki and H. Harashima, Octaarginine-modified multifunctional envelope-type nano device for siRNA, J. Controlled. Release, 2007, 119, 360–367

17 D. Cun, C. Foged, M. Yang, S. Frøkjaer and H. M. Nielsen, Preparation and characterization of poly(DL-lactide-co-glycolide) nanoparticles for siRNA delivery, Int. J. Pharm., 2010, 390, 70–75

18 H. U. Eirheim, C. Bundgaard and H. M. Nielsen, Evaluation of different toxicity assays applied to proliferating cells and to stratified epithelium in relation to permeability enhancement with glycocholate, Toxicol. In Vitro, 2004, 18, 649–657

19 M. B. Lutz, N. Kukutsch, A. L. Ogilvie, S. Rössner, F. Koch, N. Romani and G. Schuler, An advanced culture method for generating large quantities of highly pure dendritic cells from mouse bone marrow, J. Immunol. Methods, 1999, 223, 77–92

[20] P. Nordly, F. Rose, D. Christensen, H. M. Nielsen, P. Andersen, E. M. Agger and C. Foged, Immunity by formulation design: Induction of high CD8+ T-cell responses by poly(I:C) incorporated into the CAF01 adjuvant via a double emulsion method, J. Controlled Release, 2011, 150, 307–317

[21] A. H. van Asbeck, A. Beyerle, H. McNeill, P. H. Bovee-Geurts, S. Lindberg, W. P. Verdurmen, M. Hällbrink, U. Langel, O. Heidenreich and R. Brock, Molecular parameters of siRNA-cell penetrating peptide nanocomplexes for efficient cellular delivery, ACS Nano, 2013, 7, 3797–3807

[22] I. M. Hafez and P. R. Cullis, Cholesteryl hemisuccinate exhibits pH sensitive polymorphic phase behavior, Biochim. Biophys. Acta, 2000, 1463, 107–114

[23] B. Ballarín-González and K. A. Howard, Polycation-based nanoparticle delivery of RNAi therapeutics: adverse effects and solutions, Adv. Drug Delivery Rev., 2012, 64, 1717–1729

[24] V. P. Torchilin, T. S. Levchenko, R. Rammohan, N. Volodina, B. Papahadjopoulos-Sternberg and G. G. D'Souza, Cell transfection in vitro and in vivo with nontoxic TAT peptide–liposome–DNA complexes, Proc. Natl. Acad. Sci. U. S. A., 2003, 100, 1972–1977

[25] J. J. Lu, R. Langer and J. Chen, A novel mechanism is involved in cationic lipid-mediated functional siRNA delivery, Mol. Pharm., 2009, 6, 763–771

[26] X. Zeng, R. Morgenstern and A. M. Nyström, Nanoparticle-directed sub-cellular localization of doxorubicin and the sensitization breast cancer cells by circumventing GST-mediated drug resistance, Biomaterials, 2014, 35, 1227–1239

[27] K. A. Whitehead, R. Langer and D. G. Anderson, Knocking down barriers: advances in siRNA delivery, Nat. Rev. Drug Discovery, 2009, 8, 129–138

[28] I. M. Hafez, N. Maurer and P. R. Cullis, On the mechanism whereby cationic lipids promote intracellular delivery of polynucleic acids, Gene Ther., 2001, 8, 1188–1196

[29] H. Farhood, N. Serbina and L. Huang, The role of dioleoyl phosphatidylethanolamine in cationic liposome mediated gene transfer, Biochim. Biophys. Acta, 1995, 1235, 289–295

[30] I. M. Hafez and P. R. Cullis, Cholesteryl hemisuccinate exhibits pH sensitive polymorphic phase behavior, Biochim. Biophys. Acta, 2000, 1463, 107–114

[31] J. Li, Y. C. Chen, Y. C. Tseng, S. Mozumdar and L. Huang, Biodegradable calcium phosphate nanoparticle with lipid coating for systemic siRNA delivery, J. Controlled Release, 2010, 142, 416–421

[32] A. Mitsueda, Y. Shimatani, M. Ito, T. Ohgita, A. Yamada, S. Hama, A. Gräslund, S. Lindberg, U. Langel, H. Harashima, I. Nakase, S. Futaki and K. Kogure, Development of a novel nanoparticle by dual modification with the pluripotential cell-penetrating peptide PepFect6 for cellular uptake, endosomal escape, and decondensation of an siRNA core complex, Biopolymers, 2013, 100, 698–704

Supplementary Information

Formulation at N/P = 1

EGFP siRNA-loaded complexes and liposomes were prepared at an N/P ratio of 1 by using methods as previously described.[1] Since cationic nanoparticles (and non-complexed cationic peptides) in general affect cell viability,[2,3] we reduced the amount of peptidomimetics applied for complexation with EGFP siRNA (N/P ratio 1). These conditions effectively resulted in nanoscale complexes and liposomes (140-200 nm, Table S1). The results indicate that even though the lower N/P ratio may be advantageous in reducing cationic reagent-mediated cytotoxicity, this could be at the expense of reduced encapsulation efficiency.

Table S1. *Physicochemical characteristics of P3-C complexes and P3-L liposomes encapsulating EGFP siRNA at an N/P = 1.*

Sample	Size (nm)	PDI	Charge (mV)	EE (%)
Complexes	148.5±13.5	0.27±0.01	-28±0.9	77.5±6.2
Liposomes	182.5±4.8	0.27±0.02	-43±1.5	60.3±4.7

P3 denotes the sequence of the α-peptide/β-peptoid with the alternating lysine and arginine residues repeat three times. PDI, polydispersity index; EE, encapsulation efficiency. Values represent mean ± SD (n =3).

Coating with DPPC/CHEMS

In order to verify the effects of coating with fusogenic lipid mixture (DOPE/CHEMS) versus coating with a non- fusogenic lipid mixture, DOPE was replaced with the the zwitterionic lipid dipalmitoylphosphatidylcholine (DPPC), which was used in conjunction with CHEMS for the preparation of liposomes. DPPC/CHEMS liposomes loaded with EGFP siRNA were prepared using the same methods as for the P3-L system. Two different DPPC/CHEMS molar ratios were used (9:2 and 9:4). This resulted in nanoscale liposomes (200-250 nm, results not shown). However, the silencing efficiency of the DPPC/CHEMS-based liposomes was low (< 20% at 100 nM siRNA, Figure S1), suggesting that the helper lipid DOPE is indeed needed for efficient transfection.

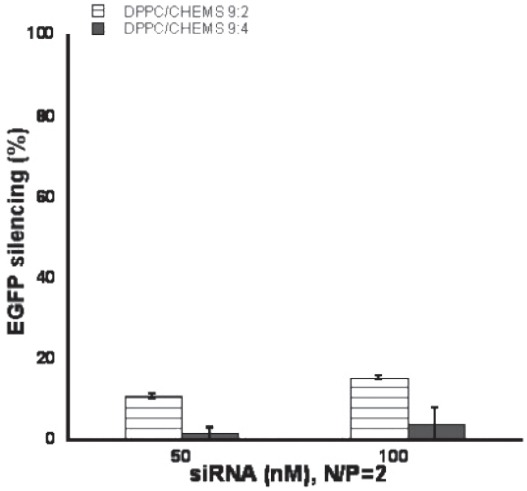

Figure S1. *Silencing effect of the DPPC/CHEMS liposomes at an N/P ratio of 2 in H1299 EGFP cells. Results are expressed as mean ± SD (n = 3).*

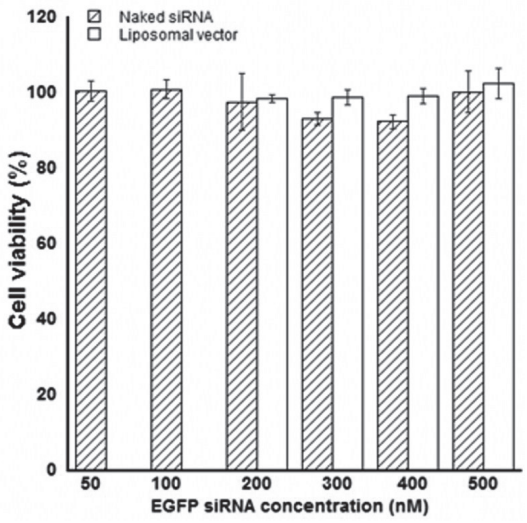

Figure S2. *The cell viability was assessed by using the MTS/PMS assay upon exposure of the human lung cancer cell line H1299 to non-complexed EGFP siRNA or empty liposomal vector at equivalent siRNA concentrations for 48 h. Values represent mean ± SD (n =3).*

Cell viability – siRNA + liposomal vector

As shown in Figure S2, the cell viability was not significantly influenced after exposure to non-complexed EGFP siRNA for 48 h at concentrations ranging from 50 to 500 nM), confirming that EGFP siRNA is non-toxic *in vitro*. It also reveals that the empty liposomal vector without siRNA did not induce cell death at equivalent siRNA concentrations (200 to 500 nM).

TLR activation at low concentrations

At lower concentrations of peptidomimetics (0.5 μM), P3-C and P3-L particles (equivalent to 50 nM siRNA), no Toll- like receptor (TLR) activation wasr observed (Figure S3). The drug delivery systems may possibly inhibit the activation ofthe TLRs *i)* by inhibiting the activation or binding to TLRs,. *ii)* by inhibiting the reporter pathway, and/or *iii)* by causing apoptosis. To exclude these possibilities, the positive control and the drug delivery systems were both added simultaneously and compared to the addition of the positive control + negative control, simultaneously. Not in all cases this possibility could be excluded. Therefore, some of the results of the TLR activation assay were invalid and these have been marked as n.a..

TEM and cryoTEM

From the overview images shown in Figure S4, we found that the P3-L particles show a nuclear nanocomplex (Figure S4, A) within a lipid envelope (Figure S4, B), and cryo-TEM images confirmed the core-structure of the P3-L liposomes (Figure S4, C).

Control DOPE/DPPC liposomes

In order to verify the effects of adding the acidsensitive lipid CHEMS versus adding a neutral stabilizer lipid in the liposomal system, CHEMS was replaced with the neutral stabilizer lipid DPPC, which was used in conjunction with DOPE for the preparation of liposomes. DOPE/DPPC liposomes loaded with EGFP siRNA were prepared using the same methods as for the P3-L particles. Two different DOPE/DPPC molar ratios were used (9:2 and 9:4). Thisresulted in liposomes (200-400 nm, results not shown). However, the silencing effect of these DOPE/DPPC-based liposomes was modest (< 50% at 100 nM siRNA, Figure S5, A), and intracellular trafficking images displayed limited cytosolic accumulation of siRNA (Figure S5, B). The results thus indicate that the anionic CHEMS may be more advantageous for low pH-mediated endosomal/lysosomal escape, as compared to the neutral (zwitterionic) lipid DPPC.

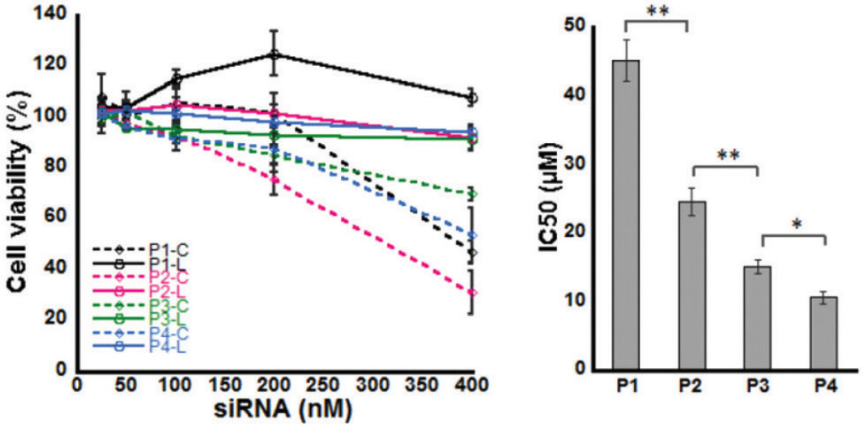

Figure S3. *Effect of the four peptidomimetics P1-P4, P3-C complexes and P3-L liposomes on the activation of Toll-like receptors (TLR2, TLR4 and TLR9), expressed as the relative SEAP activity. DEPC water and PAM3CSK/LPS/ODN were used as negative and positive controls, respectively. Results are expressed as means ± SD (n = 3) and data is representative for two independent experiments.*

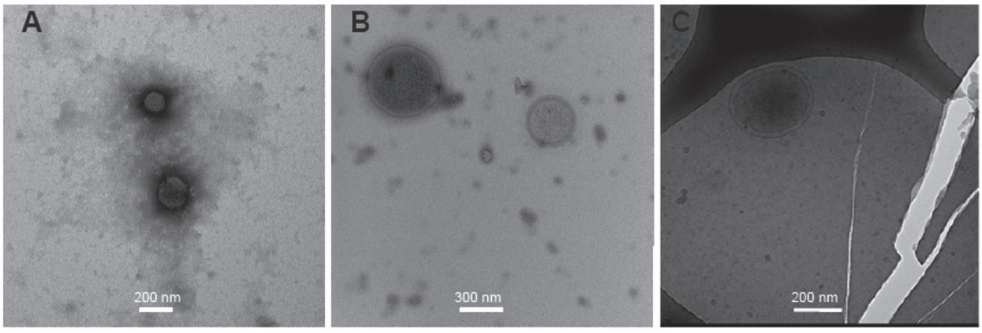

Figure S4. *(A) Representative transmission electron micrograph (TEM) image of the P3-C complexes. (B) Representative TEM image of the P3-L particles. (C) Representative cryo-TEM image of the P3-L liposomes.*

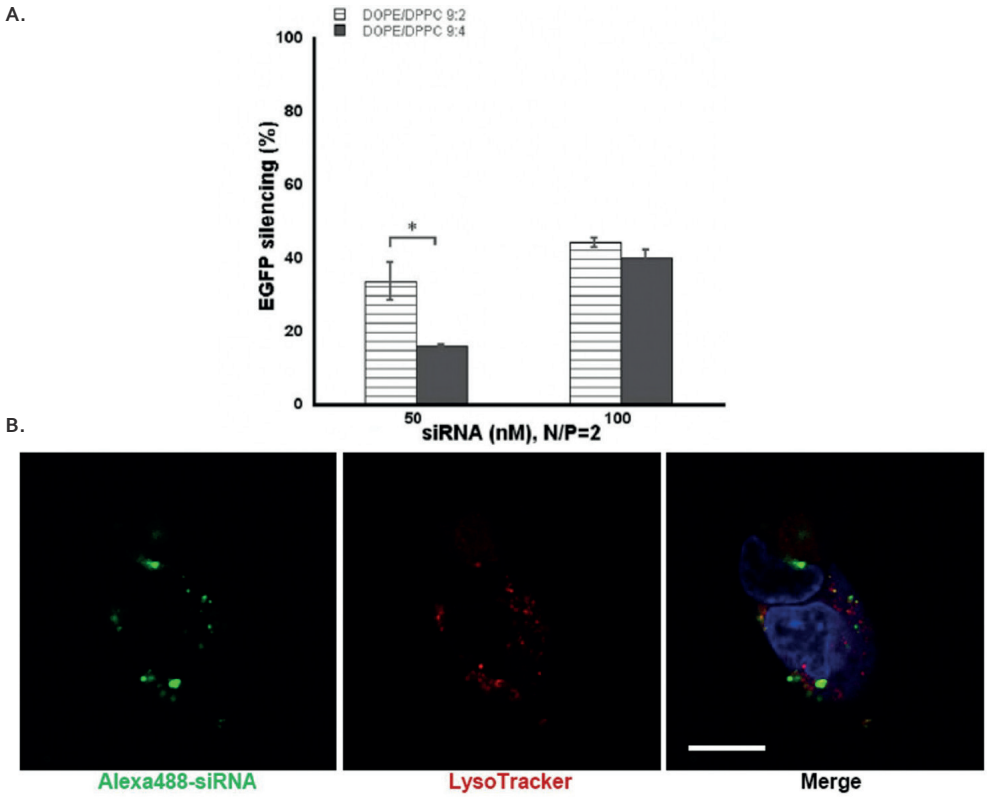

Figure S5. *(A) Silencing effect of the DOPE/DPPC liposomes at an N/P ratio of 2 in H1299 EGFP cells. Results are expressed as mean ± SD (n = 3). *p < 0.05. (B) Representative confocal laser scanning microscopy images of H1299 cells (blue: nuclei) transfected with DOPE/DPPC nanoparticles loaded with 100 nM Alexa488-siRNA. Co-localization of siRNA (green) with LysoTracker (red) 12 h after treatment with nanoparticles. Scale bar = 20 μm.*

References

1 Y. Nakamura, K. Kogure, S. Futaki, H. Harashima, Octaarginine-modified multifunctional envelope-type nano device for siRNA, J. Control. Release, 2007, 119, 360–367.

2 T. Xia, M. Kovochich, M. Liong, J.I. Zink, A.E. Nel, Cationic polystyrene nanosphere toxicity depends on cell- specific endocytic and mitochondrial injury pathways, ACS Nano, 2008, 2, 85-96.

3 B. Ballarín-González, K.A. Howard, Polycation-based nanoparticle delivery of RNAi therapeutics: adverse effects and solutions, Adv. Drug Deliv. Rev. 2012, 64, 1717-1729.

7

Conjugation of Cell-Penetrating Peptides to Parathyroid Hormone Affects Its Structure, Potency, and Transepithelial Permeation

Bioconjugate Chem., 2015, 26 (3), pp 477–488

Mie Kristensen[†]
Anne Marit de Groot[§]
Jens Berthelsen[‡]
Henrik Franzyk[□]
Alice J.A.M. Sijts[§]
Hanne Mørck Nielsen[*†]

[†] Section for Biologics, Department of Pharmacy, Faculty of Health and Medical Sciences, University of Copenhagen, Universitetsparken 2, DK-2100 Copenhagen, Denmark
[‡] Department of International Health, Immunology and Microbiology, Faculty of Health and Medical Sciences, University of Copenhagen, Blegdamsvej 3, DK-2200 Copenhagen, Denmark
[§] Division of Immunology, Department of Infectious Diseases and Immunology, Faculty of Veterinary Medicine, Utrecht University. Yalelaan 1, 3584 CL Utrecht, The Netherlands
[□] Department of Drug Design and Pharmacology, Faculty of Health and Medical Sciences, University of Copenhagen, Universitetsparken 2, DK-2100 Copenhagen, Denmark

Abstract

Delivery of therapeutic peptides and proteins by the use of cell-penetrating peptides (CPPs) as carriers has been suggested as a feasible strategy. The aim of the present study was to investigate the effect of conjugating a series of well-known CPPs to the biologically active part of parathyroid hormone, i.e., PTH(1–34), and to evaluate the effect with regard to secondary structure, potency in Saos-2 cells, immunogenicity, safety, as well as the transepithelial permeation across monolayers by using the Caco-2 cell culture model. Further, co-administration of CPP and PTH(1–34) as an alternative to covalent conjugation was compared with regard to the transepithelial permeation. CPP-conjugated PTH(1–34) fusion peptides were successfully expressed in *Escherichia coli* and purified from inclusion bodies. No clear correlation between the degree of secondary structure of the CPP-conjugated PTH(1–34) fusion peptides and their potency was found, albeit a general decrease in permeation was observed for both N- and C-terminally CPP-conjugated PTH(1–34) as compared to native PTH(1–34). However, attachment of CPP to the N-terminus significantly increased permeation across Caco-2 cell monolayers as compared to the corresponding C-terminally CPP-conjugated PTH(1–34). In addition, the nonaarginine sequence proved to be the only CPP capable of increasing permeation when conjugated to PTH(1–34) as compared to co-administration of CPP and PTH(1–34). This enhancement effect was, however, associated with an unacceptably low level of cell viability. In conclusion, covalent conjugation of CPPs to PTH(1–34) influenced the secondary structure, potency, and transepithelial permeation efficiency of the resulting conjugate, and hence this approach appears not to be favorable as compared to co-administration when optimizing CPP-mediated permeation of PTH(1–34) across an intestinal epithelium.

1. Introduction

Peptides and proteins play important roles as substrates, receptor ligands, downstream signaling molecules, and regulators in a vast number of biological processes, and today they constitute an increasing fraction of drugs used to treat a variety of diseases. Examples comprise use in hormone replacement therapies for, e.g., growth hormone deficiency,[1] and relief of menopausal symptoms in women.[2] Parathyroid hormone (PTH) is an 84-residue protein regulating bone and renal metabolism through its action as a regulator of the extracellular Ca^{2+} level.[3] The N-terminal part comprising 34 residues, i.e., PTH(1–34), is responsible for the pharmacological activity,[4] and today this peptide is used clinically in the treatment of osteoporosis.[5] This disease is characterized by a decreased bone density and associated with a high risk of fractures leading to impaired mobility, pain, and consequently reduced quality of life for the patients. As with the majority of peptide and protein drugs, PTH(1–34) is currently administered via injections, although oral administration is preferred for optimal patient compliance. However, successful oral delivery of peptide and protein drugs involves overcoming a range of challenges due to their susceptibility toward enzymatic degradation, their large molecular size, and thus poor membrane permeation. To circumvent these obstacles, carriers are obviously needed; thus, utilization of cell-penetrating peptides (CPPs) as delivery vehicles appears to be a possible solution, as they have shown promising potential in improving transepithelial delivery of therapeutic peptides and protein drugs[6] either when co-administered with the therapeutic[7-9] or via direct conjugation to the drug.[10, 11]

In the latter case, a CPP is covalently linked to the therapeutic peptide or protein either by chemical synthesis, e.g., as reported for the conjugation of Tat to insulin via the Lys residue B29 in insulin,[10] or by bacterial expression, e.g., as reported for N-terminally CPP-fused α-synuclein.[6, 11-13] The use of an expression host, such as *Escherichia coli* (*E. coli*), enables production of a recombinant fusion peptide, in which gene fragments encoding separate functional parts are translated into a fusion peptide. This approach ensures an inherent proximity of the CPP to the therapeutic peptide or protein, and leads to well-characterized molecules, thus limiting the potential formation of poorly characterized complexes as a result of physical mixing of excess CPP with the therapeutic peptide. However, knowledge regarding the effect of the CPP on the pharmacological activity of the therapeutic peptide or protein as well as the influence of conjugation on the cell-penetrating ability of the CPP has been limited so far.

In order to investigate the effect of direct conjugation of CPPs to a therapeutic peptide, the peptide PTH(1–34) was expressed as fusion peptides with a series of well-known CPPs; namely, penetratin (a 16-mer derived from the Antennapedia homeodomain),[14] $Tat_{(47–57)}$ (a 11-mer derived from the HIV-1 transactivating protein),[15] VP22 (a 34-mer derived from the HSV-1 structural protein),[16] and the synthetic nonaarginine (R9).[17] Both

N- and C-terminally CPP-conjugated PTH(1–34) fusion peptides were expressed, purified, and characterized with respect to secondary structure, immunogenicity, potency, safety, and ability to permeate across Caco-2 cell monolayers. Finally, co-administration of PTH(1–34) and each of the CPPs in a 1:1 molar ratio was explored in order to directly evaluate to which extent a similar amount of free CPP might facilitate permeation in comparison to the covalently CPP-mediated approach for enhancing transepithelial transport of PTH(1–34).

2. Results

2.1. Purification of PTH(1–34) and CPP-PTH(1–34) Fusion Peptides from Inclusion Bodies

In order to obtain the designed recombinant CPP-conjugated PTH(1–34) fusion peptides (Table 1), entry clones encoding sequences of interest were cloned into the pNIC-Bsa4 vector (Supporting Information Figure S1) and expressed as the corresponding histidine (His) tagged peptides in *E. coli*. The His tagging facilitated an initial purification step using immobilized metal ion chromatography (IMAC), and expression together with an adjacent tobacco etch virus (TEV) sequence allowed subsequent removal of the tag by using a TEV-specific protease.

As only three of the target sequences were expressed as soluble peptides (Supporting Information Figure S2), a protocol for the purification from insoluble inclusion bodies (IBs) was developed (Figure 1, top). This newly designed protocol enabled efficient expression of PTH(1–34) and the CPP-conjugated PTH(1–34) fusion peptides into IBs, from which purification was carried out by using IMAC followed by two RP-HPLC purification steps. Between the two latter purification steps, the His tag was cleaved off by a TEV-specific protease, and finally the expected molecular weight was verified by mass spectrometry (MS) as exemplified in Figure 1 (bottom) for the Tat-PTH(1–34) fusion peptide.

In total, PTH(1–34) and seven different CPP-conjugated PTH(1–34) fusion peptides were successfully produced, and isolated with an initial high degree of purity as visualized by a Coomassie-stained sodium dodecyl sulfate polyacrylamide gel electrophoresis (SDS-PAGE) (Figure 2). The penetratin sequence could only be successfully expressed when C-terminally conjugated to PTH(1–34), whereas Tat, VP22, and R9 sequences were all successfully expressed both as N- and C-terminal PTH(1–34) conjugates (Table 1).

2.2 Folding Propensity of PTH(1–34) and Its Fusion Peptides Is Affected by Lipid Bilayers

An α-helical structure is believed to be of importance for retained potency of PTH(1–34)[18] and may also positively affect plasma membrane interactions of the CPPs.[19, 21] Hence, the secondary structure of PTH(1–34) (Figure 3) and of the CPP-conjugated PTH(1–34)

Table 1. *Sequence and Molecular Weight of the Expressed and Purified PTH(1–34) and CPP-Conjugated PTH(1–34) Fusion Peptidesa.*

name	sequence[a]	Calc. Mw (Da)	Mw (Da)
PTH(1–34)	S*SVSEIQLMHNLGKHLNSMERVEWLRKKLQDVHNF	4204.84	4204.19
PTH(1–34)-penetratin	S*SVSEIQLMHNLGKHLNSMERVEWLRKKLQDVHNFRQIKIWFQNRRMKWKK	6433.58	6432.35
PTH(1–34)-Tat	S*SVSEIQLMHNLGKHLNSMERVEWLRKKLQDVHNFYGRKKRRQRRR	5746.67	5746.10
Tat-PTH(1–34)	SS*YGRKKRRQRRRSVSEIQLMHNLGKHLNSMERVEWLRKKLQDVHNF	5833.75	5833.13
PTH(1–34)-VP22	S*SVSEIQLMHNLGKHLNSMERVEWLRKKLQDVHNFDAATATRGRSAASRPTERPRAPARSASRPRRPVG	7773.81	7773.10
VP22-PTH(1–34)	SS*DAATATRGRSAASRPTERPRAPARSASRPRRPVGSVSEIQLMHNLGKHLNSMERVEWLRKKLQDVHNF	7860.89	7864.13
PTH(1–34)-R9	S*SVSEIQLMHNLGKHLNSMERVEWLRKKLQDVHNFRRRRRRRRR	5610.53	5607.08
R9-PTH(1–34)	SS*RRRRRRRRRSVSEIQLMHNLGKHLNSMERVEWLRKKLQDVHNF	5697.60	5694.12

[a]*The CPP sequences are underlined. *N-terminal serine (Ser) residues left on the amino acid sequence encoding PTH(1–34) or on the linked CPP after the His tag was cleaved off by a TEV-specific protease. Nucleotide encoding sequences with an inherent N-terminal Ser residue were ordered without the Ser residue. Calculated molecular weights are obtained from Expasy.org.*

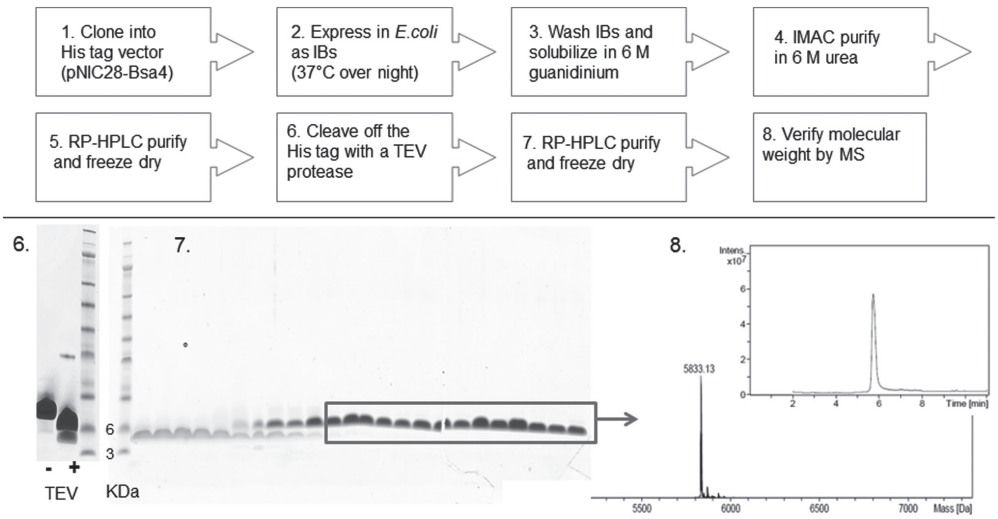

Figure 1. *Representative expression and purification of Tat-PTH(1–34) including flowchart (steps 1–8, top) and experimental results (6–8, bottom) of TEV cleavage (6), RP-HPLC purification (7) and MS (8). IB: Inclusion body.*

fusion peptides (Figure 4) was analyzed by circular dichroism (CD) spectroscopy in the absence or presence of POPC:POPG liposomes as a simplified model for the eukaryote plasma membrane.

In aqueous buffer, PTH(1–34) did not adopt a clearly defined secondary structure, whereas in the presence of POPC:POPG liposomes, its helicity was increased. Similarly, a high helicity was observed in the presence of 20% (v/v) 2,2,2-trifluoroethanol (TFE), which is widely used as an α-helix-inducing agent (Figure 3).

As seen for PTH(1–34), the structures of the CPP-conjugated PTH(1–34) fusion peptides were not clearly defined in aqueous buffer (Supporting Information Figure S3a), whereas in the presence of 20% (v/v) aqueous TFE, all of the fusion peptides adopted an α-helical structure albeit not to the same extend as observed for PTH(1–34) (Supporting Information Figure S3b). In the presence of POPC:POPG liposomes, conjugation of penetratin to the C-terminus of PTH(1–34) (Figure 4a) did not affect the secondary structure as compared to that of native PTH(1–34) (Figure 3), and neither did C-terminal conjugation of Tat (Figure 4b) or N-terminal conjugation of R9 to PTH(1–34) (Figure 4d). On the other hand, a significant difference was observed when comparing the spectra of N- versus C-terminally conjugation of R9 to PTH(1–34) (Figure 4d), whereas only a minor effect of N- versus C-terminal conjugation was observed for the Tat peptide (Figure 4b), and no effect was seen as a result of N- versus C-terminal VP22-conjugation to PTH(1–34) (Figure 4c). CD spectra of the individual CPPs (Supporting Information Figure S4) revealed that only penetratin adopted an α-helical structure in the presence of POPC:POPG liposomes (Supporting Information Figure S4a) in accordance with previous reports.[20, 21]

2.3. Decreased Potency of CPP-Conjugated PTH(1–34) Fusion Peptides

The potencies of the CPP-conjugated PTH(1–34) fusion peptides were evaluated in a cell-based PTH assay, using the PTH receptor-expressing Saos-2 cell line (Supporting Information Figure S5a), and the EC_{50} values for the PTH receptor-mediated cAMP production were determined from the dose–response curves (Table 2).

Upon incubation of conjugates in the concentration range of 1.225 nM–80 μM with Saos-2 cells, none of the fusion peptides gave rise to EC_{50} values comparable to those of expressed unconjugated PTH(1–34) (0.19 ± 0.13 μM) or of a sample of synthetic PTH(1–34) (0.11 ± 0.15 μM) (Supporting Information Figure S5b) included as a reference. Conjugation of Tat to PTH(1–34) overall affected the affinity toward the receptor the least, and only Tat-PTH(1–34) was able to elicit an effect comparable to that of unconjugated PTH(1–34) within the range of concentrations tested. Interestingly, for Tat and VP22 C-terminal conjugation to PTH(1–34) led to lower potencies as compared to the corresponding N-terminal conjugation, whereas the opposite trend was found for conjugation of R9 to PTH(1–34).

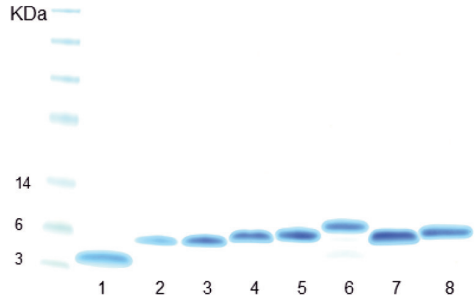

Figure 2. *Coomassie-stained SDS-PAGE gel loaded with purified PTH(1–34) and CPP-PTH(1–34) fusion peptides including a prestained molecular weight marker: 1, PTH(1–34); 2, PTH(1–34)-penetratin; 3, PTH(1–34)-Tat; 4, Tat-PTH(1–34); 5, PTH(1–34)-VP22; 6, VP22-PTH(1–34); 7, PTH(1–34)-R9; 8, R9-PTH(1–34).*

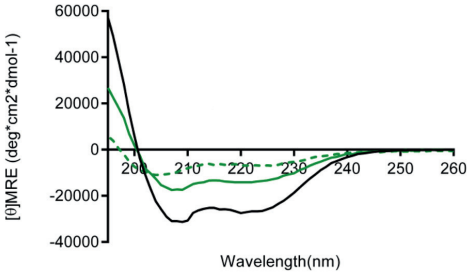

Figure 3. *Circular dichroism spectra of PTH(1–34) recorded at a concentration of 10 μM in aqueous buffer (green dashed line), in the presence of 1 mM POPC:POPG (molar ratio 80:20) liposomes corresponding to a 1:100 peptide to lipid ratio (green solid line), or in 20% (v/v) aqueous TFE (black line).*

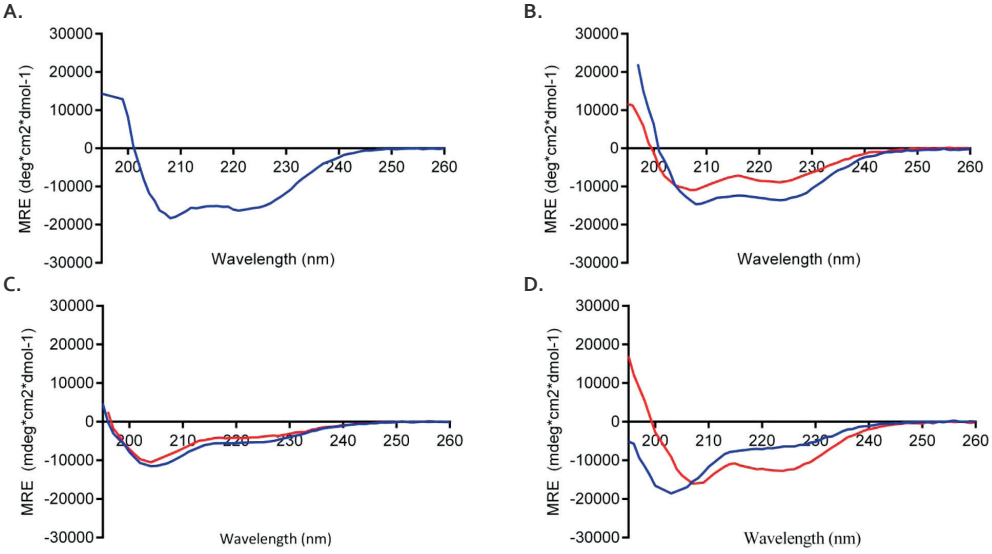

Figure 4. *Circular dichroism spectra of CPP-conjugated PTH(1–34) in the presence of 1 mM POPC:POPG (molar ratio 80:20) liposomes corresponding to a 1:100 peptide to lipid ratio. (a) PTH(1–34)-penetratin (blue), (b) Tat-PTH(1–34) (red) and PTH(1–34)-Tat (blue), (c) VP22-PTH(1–34) (red) and PTH(1–34)-VP22 (blue), (d) R9-PTH(1–34) (red) and PTH(1–34)-R9 (blue). All spectra were recorded at a conjugate concentration of 10 μM.*

2.4. None of the CPP-Conjugated PTH(1–34) Fusion Peptides Induced an *in Vitro* Immune Response

When employing bacterial expression of peptides or proteins for potential therapeutic use, the risk of contamination by endotoxins must be taken into consideration in order to decrease the risk of severe side effects as a result of, e.g., an immune response.[22] Further, the presence of endotoxins might influence the membrane permeation studied in vitro. Hence, the expressed PTH(1–34) and CPP-conjugated PTH(1–34) fusion peptides were tested for a possible immunogenic response using a dendritic cell (DC) maturation assay and a Toll-like receptor (TLR) assay. The native expressed PTH(1–34) showed some immunogenic response, as it gave rise to an up-regulation of maturation markers on murine bone marrow-derived dendritic cells (BMDCs) (Figure 5a) and gave rise to activation of human Toll-like receptor (hTLR) hTLR4 on hTLR4 reporter cells (Figure 5b).

Thus, the expressed PTH(1–34) may be contaminated by trace amounts of endotoxins during its production, whereas none of the CPP-conjugated PTH(1–34) fusion peptides or the synthetic sample of PTH(1–34) resulted in positive responses in any of the immunogenicity assays in the range of concentrations tested (0.15–15 μM) (Figure 5 and Supporting Information Figure S6). This may be explained by the higher polarity of the fusion peptides most likely allows for the complete removal of endoxin contaminants during the HPLC purification step.

2.5. Transepithelial Permeation Is Dependent on the Terminal Positioning of the CPP

The CPP-conjugated PTH(1–34) fusion peptides were evaluated for their ability to permeate an intestinal epithelium *in vitro*. In general, N-terminal CPP conjugation to PTH(1–34) resulted in fusion peptides with a significantly increased permeation as compared to C-terminal CPP conjugation to PTH(1–34) (Figure 5a–c). This trend is further reflected in the calculated apparent permeability coefficients (P_{app}) (Table 3).

Both N- and C-terminal R9-conjugation to PTH(1–34) (Figure 6c) resulted in the highest amount of transported fusion peptide as compared to conjugation of Tat (Figure 6a), VP22 (Figure 6b), and penetratin to PTH(1–34) (Table 3). Moreover, only the R9-conjugates and the N-terminal Tat- and VP22-PTH(1–34) were able to permeate the Caco-2 monolayer in amounts comparable to unconjugated PTH(1–34) co-administered with the individual CPPs in a molar ratio of 1:1 (Table 3). In general, N-terminal conjugation of the CPPs to PTH(1–34) increased the permeation of the fusion peptide significantly as compared to C-terminal conjugation, but only N-terminal R9-conjugation to PTH(1–34) gave rise to increased transepithelial transport as compared to the uncoupled PTH(1–34) control ($P_{app} = (4.64 \pm 1.85) \times 10^{-9}$ cm/s). Due to a possible contamination by endotoxins during the isolation of expressed PTH(1–34) (Figure 5), the synthetic PTH(1–34) was included in the permeation studies as a reference and when co-administered with the

Table 2. *EC_{50} Values Obtained after Incubation of Saos-2 Cells with CPP-PTH(1-34) Fusion Peptides*[a]

	EC_{50} (μM)	
CPP	**CPP-PTH(1–34)**	**PTH(1–34)-CPP**
Penetratin	n.a.	10.76 ± 1.55
Tat	1.58 ± 1.32	4.98 ± 1.30
VP22	14.66 ± 1.63	23.50 ± 1.67
R9	22.59 ± 2.11	6.65 ± 1.25

[a]*Data are presented as mean ± SEM (n = 3).*

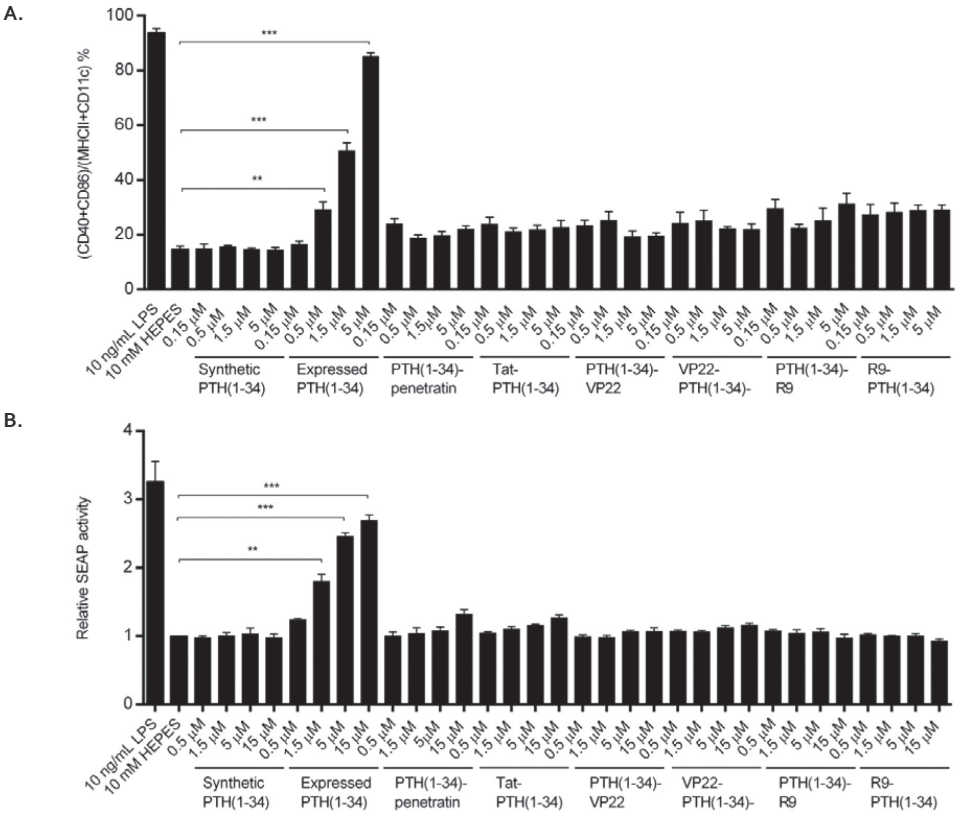

Figure 5. *In vitro immune responses obtained by fluorescence-activated cell sorting (FACS) analysis of expression levels of maturation markers CD40 and CD86 on GM-CSF-differentiated murine bone marrow-derived DCs after incubation with 0.15–15 μM synthetic PTH(1–34), expressed PTH(1–34) or the CPP-PTH(1–34) fusion peptides (a) or analysis of human TLR4 activation on HEK-Blue-hTLR4 cells after incubation with 0.5–15 μM synthetic PTH(1–34), expressed PTH(1–34) or the CPP-PTH(1–34) fusion peptides (b). LPS (10 ng/mL) is included as positive control, while 1 mM HEPES buffer is included as negative control. Data are presented as mean ± SEM (n = 4). Levels of significance are ***: $p < 0.001$ and **: $p < 0.01$.*

CPPs, in order to avoid false positive effects when evaluating the viability of the Caco-2 cells and the integrity of the cell monolayer (Figure 7).

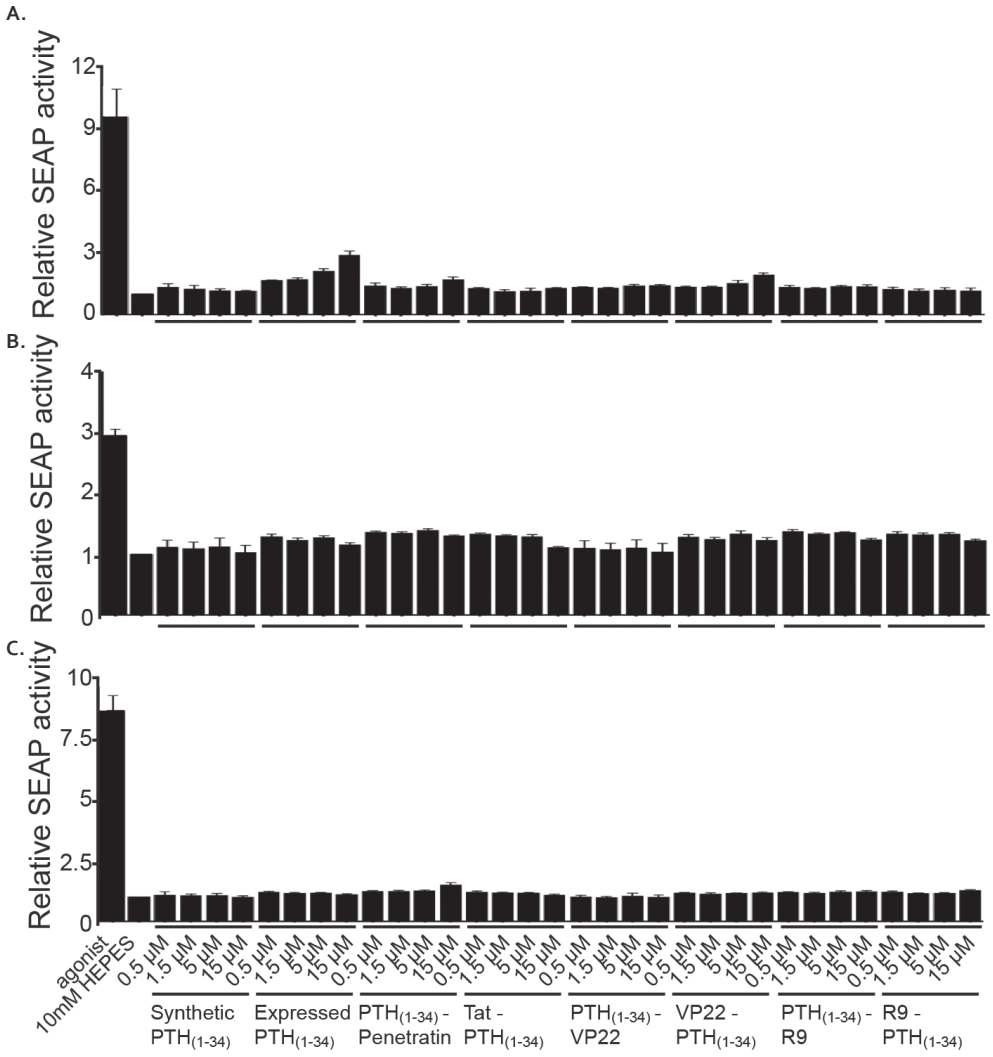

Figure 6. *Permeation of PTH(1–34) after application of 40 µM Tat-conjugated PTH(1–34) (a), 40 µM VP22-conjugated PTH(1–34) (b), or 40 µM R9-conjugated PTH(1–34) (c) across Caco-2 cell monolayers. Red: N-terminal CPP. Blue: C-terminal CPP. Data are presented as mean ± SEM (n = 6). Levels of significance are ***: p < 0.001 and **: p < 0.01.*

Table 3. *Apparent Permeability Coefficient (P_{app}) Determined after Application of CPP-PTH(1–34) Fusion Peptides (40 μM) or Similar Total Concentrations of PTH(1–34) Co-administered with Individual CPPs (Molar Ratio 1:1) across Caco-2 Cell Monolayers*[a]

	P_{app} (10^{-9} cm/s)		
CPP	**CPP-PTH(1–34)**	**PTH(1–34)-CPP**	**Co-administration of CPP and PTH(1–34)**
Penetratin	n.a.	1.62 ± 0.47	3.61 ± 0.88
Tat	2.56 ± 0.46	1.73 ± 0.40	3.60 ± 0.36
VP22	2.23 ± 0.66	0.32 ± 0.12	2.63 ± 0.94
R9	6.03 ± 3.18	3.42 ± 1.02	2.66 ± 0.74

[a]*Data are based on calculations to the end-point and presented as mean ± SEM (n = 6).*

2.6. R9-Coupled PTH(1–34) Fusion Peptides Decrease Cellular Viability

Following each permeation experiment, the cellular viability was assessed in order to determine whether the permeation of the CPP-conjugated PTH(1–34) fusion peptides was associated with decreased cell viability. No decrease in cell viability was observed upon exposure to penetratin-, Tat-, or VP22-conjugated PTH(1–34), while a significant decrease in cell viability was observed for the R9-conjugated fusion peptides, with the C-terminally R9-modified PTH(1–34) being the most toxic to the cells (Figure 7a). In comparison, co-administration of PTH(1–34) with the CPPs in a molar 1:1 ratio did not affect cell viability (Figure 7c). The observations indicated a tendency toward C-terminally CPP-conjugated PTH(1–34) fusion peptides being slightly more toxic to Caco-2 cells in monolayers than the N-terminally CPP-conjugated analogues. However, despite the reduced cell viability observed after exposure to the R9-conjugated PTH(1–34), no effect on the epithelial integrity of the monolayer was observed upon application of any of the fusion peptides (Figure 7b) or as a result of incubation with PTH(1–34) co-administered with the CPPs (Figure 7d).

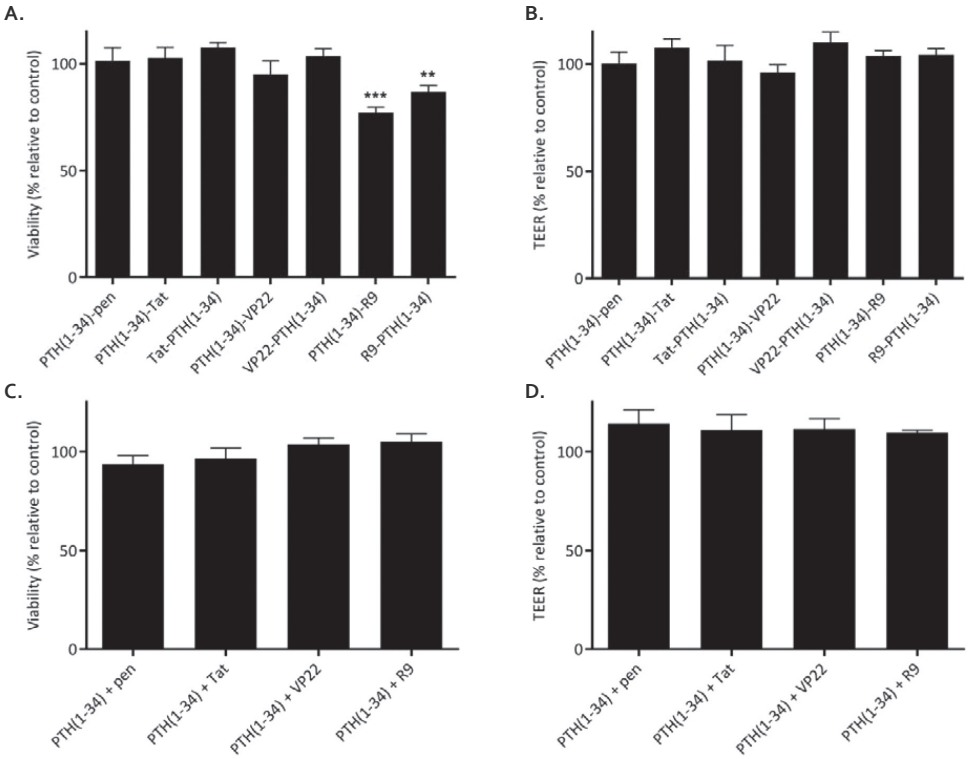

Figure 7. *Cell viability of Caco-2 cells in monolayers after a 3 h permeation study applying 40 µM CPP-conjugated fusion peptide (a) or similar concentrations of PTH(1–34) co-administered with penetratin, Tat, VP22, or R9 (c) and the relative TEER measured after the experiment (b, d). Results are shown as % relative to control (10 mM HEPES in HBSS pH 7.4) ± SEM (n = 6). Levels of significance are ***: p < 0.001 and **: p < 0.01 compared to control.*

3. Discussion

Major progress within the biotechnological area has enabled large-scale expression and purification of recombinant peptides and proteins with a high degree of purity, which makes it possible to establish a tightly controlled high-throughput production of, e.g., dual-function fusion peptides and proteins for therapeutic use. In the present study, CPP-conjugated PTH(1–34) fusion peptides were successfully produced in *E. coli* and purified from IBs in order to study the effect of CPP conjugation on the characteristics of a therapeutic peptide. Thus, the effect of direct conjugation of a CPP to the N- or C-terminus of the therapeutically relevant PTH(1–34) was investigated with respect to structural characteristics, potency, immunogenicity induction, ability to permeate epithelial monolayers, and safety profile.

When producing recombinant peptides and proteins, soluble expression is usually desired in order to avoid time-consuming and complicated solubilization and refolding steps of otherwise insoluble IBs. Overexpression, however, of eukaryotic proteins in *E. coli*, being the most widely used prokaryotic host, often leads to the formation of IBs,[23,24] as was also the case with the expression of PTH(1–34) and of four out of seven of the CPP-conjugated PTH(1–34) fusion peptides produced in the present project. On the other hand, expression of peptides and small proteins into IBs has several advantages: (i) IBs are often expressed in high concentrations, (ii) IBs almost exclusively contain the expressed peptide or protein of interest,[25] (iii) IBs are readily isolated by centrifugation,[26] and (iv) the insoluble aggregates possibly confer protection against enzymatic degradation.[25] For the production of both PTH(1–34) and the CPP-conjugated PTH(1–34) fusion peptides, the expression was therefore deliberately forced into IB production, and a protocol for the solubilization and purification from these was developed (Figure 1, top), and by this method PTH(1–34) and the CPP-conjugated PTH(1–34) fusion peptides were successfully isolated with a high purity (Figure 2).

CD spectra of PTH(1–34) revealed a poorly defined secondary structure in an aqueous buffer, while it adopted an α-helical structure in the presence of both 20% (v/v) aqueous TFE and POPC:POPG liposomes (Figure 3) similarly to previously reported data.[27-29] Moreover, it was shown that the potency of the expressed PTH(1–34) was comparable to the potency of a synthetic PTH(1–34) (Supporting Information Figure S5b). Thus, the newly developed protocol for the purification from IBs is highly suitable for the purification of bioactive molecules. However, the risk of contamination by endotoxins when using a prokaryotic expression host must always be considered, as such trace contaminations may elicit undesired immunogenic responses, which in the present study was actually observed to be the case for the expressed PTH(1–34) (Figure 5).

Regarding the CPP-conjugated PTH(1–34) fusion peptides, CD spectra revealed that the degree of folding into an α-helical secondary structure generally increased in the presence of 20% (v/v) aqueous TFE (Supporting Information Figure S3b) as also observed for PTH(1–34) (Figure 3). In the presence of POPC:POPG liposomes, only C-terminally penetratin- and Tat-conjugated PTH(1–34) and N-terminally R9-conjugated PTH(1–34) were able to fold into an α-helical structure similar to the expressed PTH(1–34) (Figure 4a,b,d). Hence, both the specific sequence and the specific positioning of the CPP influence the overall secondary structure of the CPP-conjugated PTH(1–34) fusion peptide. NMR spectroscopy studies have shown that addition of TFE to solutions of PTH(1–34) stabilizes α-helical structures both at the N- and C-terminus,[27] of which the former positively affects the pharmacological activity *in vivo*.[18] In the present study, the ability to adopt an α-helical structure in the presence of POPC:POPG lipid membranes did not generally correlate with an increased potency of the CPP-conjugated PTH(1–34) fusion peptides as determined *in vitro* (Table 2), since only the N-terminally Tat-conjugated

PTH(1–34) was capable of eliciting a maximum response comparable to that of the expressed PTH(1–34) reference within the range of concentrations tested (Supporting Information Figure S5a). Hence, there is no clear correlation between the ability to adopt an α-helical structure and the potency in vitro of the CPP-conjugated PTH(1–34) fusion peptides.

Tat-PTH(1–34) was found to be the most potent of the CPP-conjugated PTH(1–34) fusion peptides, while both the VP22-conjugates and the R9-PTH(1–34) were less potent (Table 2). VP22 with its 34 residues is the longest of the CPPs employed. Consequently, there may be an upper limit for the length of the CPP sequence conjugated to PTH(1–34) that allows for retaining the potency of the resulting fusion peptide. A short CPP seems, however, not to be the sole determinant for maintaining potency of the therapeutic peptide when conjugated to PTH(1–34), since the Tat-conjugated PTH(1–34) fusion peptides were significantly more potent than the R9-conjugated PTH(1–34) analogue, despite a similar sequence length (i.e., 11 versus 9 residues). Hence, the specific sequence of the CPP also affects potency of the CPP-conjugated PTH(1–34) fusion peptide.

The pharmacologically active PTH(1–34) is composed of two functionally relevant regions interconnected by a flexible linker region.[27] The C-terminal residues 14–34 are involved in receptor binding,[30] whereas the N-terminus is crucial for receptor activation.[31] Although conjugation of a CPP to the C-terminus of PTH(1–34) will keep the N-terminus available for receptor activation, it did not seem to be a general approach for retaining potency of the resulting conjugate (Table 2), supporting the hypothesis that the specific length and amino acid composition of the CPP are both determinants for the overall potency of the fusion peptide. Nevertheless, a clear difference in potency of both the Tat- and the R9-conjugated PTH(1–34) fusion peptides due to N- vs C-terminal attachment was observed. Thus, the specific positioning of the CPP plays a role in the potency of the individual Tat- or R9-conjugated PTH(1–34) fusion peptides, but whether N- or C-terminal conjugation to PTH(1–34) is preferred with respect to achieving the most potent fusion peptide is dependent on the specific CPP.

The CPP-conjugated PTH(1–34) fusion peptides were evaluated for their ability to permeate the Caco-2 cell monolayers (Figure 6). N-Terminal conjugation of the CPPs to PTH(1–34) significantly increased the transepithelial permeation as compared to that seen for the corresponding C-terminally CPP-conjugated PTH(1–34) fusion peptides. Thus, N-terminal R9-conjugation conferred the highest increase in permeation for the PTH(1–34) conjugate (approximately 2- to 3-fold as compared to C-terminally conjugated Tat or VP22; Table 3). With regard to the C-terminally conjugated fusion peptides, R9 was superior in increasing the transepithelial PTH(1–34) permeation as compared to C-terminally conjugated penetratin, Tat and VP22. Exposure to the R9-PTH(1–34) fusion peptides was, however, associated with a decrease in cell viability, with the C-terminally R9-conjugated PTH(1–34) being slightly more toxic than the N-terminal analogues (Figure 7a). This slight cytotoxic effect was, however, not associated with a decrease in the epithelial integrity (Figure 7b). The decrease

in cell viability is most likely caused by irreversible membrane perturbations mediated by the high number of guanidinium groups present in the R9 sequence, an effect previously found to be correlated with an increased number of arginine residues in CPP sequences.[32, 33] Nevertheless, no decrease in cell viability was observed as a result of co-administration of R9 with PTH(1–34) in a 1:1 molar ratio corresponding to the concentrations of the R9-coupled PTH(1–34) fusion peptides (Figure 7c). A plausible explanation of this finding is that complexes are formed by the physical mixing of PTH(1–34) with the CPPs, which shield some of the arginine residues of R9, hence protecting the plasma membrane against an excessively high local concentration of guanidinium groups that might lead to a decreased cell viability. Also, conjugation of R9 to PTH(1–34) may result in longitudinal amphipathicity,[34] thereby causing membrane damage thus explaining the negative effect on viability exerted by the fusion peptides when compared to PTH(1–34) coadministered with R9.

Except for the R9-conjugated PTH(1–34) fusion peptides, the co-administration approach generally resulted in a slightly higher amount of transported PTH(1–34) as compared to the covalent conjugation approach, with penetratin and Tat being superior to both VP22 and R9. Therefore, the inherent proximity of the CPP to the therapeutic peptide as a result of direct conjugation seems not to be an advantage when employing CPPs as transepithelial permeation enhancers for the delivery of a therapeutic peptide such as PTH(1–34). An explanation could be that a possible formation of complexes between the CPP and PTH(1–34) may confer some protection against enzymatic degradation of the CPP, thereby maintaining an intact and functional CPP moiety.

3.1. Conclusions

In conclusion, the present study reveals that it is possible to express and purify a series of CPP-conjugated PTH(1–34) fusion peptides from IBs, and that these samples were nonimmunogenic. While the CPP conjugation to PTH(1–34) generally maintained the propensity to fold into an α-helical structure in the presence of lipid bilayers, the conjugation to a CPP led to a generally decreased potency without any clear dependency on whether conjugation was at the N- or C-terminus of PTH(1–34). By contrast, transepithelial permeation of the compounds revealed that introduction of a CPP at the N-terminus of PTH(1–34) gave rise to increased permeation across Caco-2 monolayers in comparison to C-terminally CPP-conjugated PTH(1–34). In particular R9-modified PTH(1–34) permeated well across the epithelium, and although this was associated with a slight decrease in cell viability, no negative effect on the epithelial membrane integrity could be detected. Further studies are needed to evaluate the potential benefit of conjugation of CPPs to PTH(1–34), with the present study demonstrating the need for more advanced conjugation designs than simple terminal positioning of the CPP.

4. Experimental Procedures

4.1. Materials

Primers were designed using VectorNTI 11 software (Life Technologies, Naerum, Denmark) (Supporting Information Table S1) and cDNA encoding CPP-modified PTH(1–34) fusion peptides were obtained as synthetic genes from GeneArt (Life Technologies, Naerum, Denmark). All enzymes were obtained from New England Biolab (Ipswich, MA, USA). For cloning *E. coli*, Mach1 cells (Life Technologies, Naerum, Denmark) were employed and antibiotics (Sigma-Aldrich, Buchs, Switzerland) were used in the following concentrations: kanamycin 50 μg/mL, chloramphenicol 34 μg/mL. All cells were grown in Terrific Broth (TB) medium (tryptone 12.0 g/L, yeast extract 24.0 g/L, K_2HPO_4 9.4 g/L, KH_2PO_4 2.2 g/L) containing 8 g/L glycerol as a carbon source. For inhibition of enzymatic activity during protein purification Complete Mini EDTA-free protease inhibitor tablets were used (Roche, Hvidovre, Denmark).

Rink amide resin and coupling reagents for solid-phase peptide synthesis of penetratin, Tat and nonaarginine (R9) were purchased from Fluka (Buchs, Switzerland). All amino acid building blocks as well as other solvents and chemicals for peptide synthesis were purchased from Iris Biotech (Merktredwitz, Germany). PTH(1–34) and VP22 were obtained as synthesized peptides from BACHEM (Bubendorf, Schwitzerland) and Selleckchem (Munich, Germany), respectively. All other materials were obtained from Sigma-Aldrich (Buchs, Switzerland).

4.2. Cloning and Expression

Generation of expression constructs: Proteins were expressed using the plasmid pNIC28-Bsa4 (GenBank ID: EF198106) containing an N-terminal hexahistidine tag followed by a TEV protease site (ENLYFQ*SS), two *Bsa*I sites for ligase-independent cloning (LIC) and a *sacB* fragment, which allows for negative selection on sucrose. Sequences of interest were cloned into the vector using LIC as previously described.[35] Briefly, DNA sequences encoding CPP-modified PTH(1–34) fusion peptides of interest and flanked by LIC sites were amplified by PCR, digested with T4 DNA polymerase, and cloned into pNIC28-Bsa4. Successfully transformed vectors were selected on Luria Broth (LB) agar plates containing 50 μg/mL kanamycin and 5% (w/v) sucrose before purification using a Miniprep kit (Macherey-Nagel, Germany). Sequences were verified using an ABI Prism 3700 Analyzer (Life Technologies, Naerum, Denmark) before being transformed into Rosetta expression strains (Millipore, Schwalbach, Germany), which were kept as glycerol stocks for long-term storage at −80 °C.

Protein expression as inclusion bodies: Transformed clones was inoculated in TB medium supplemented with kanamycin (50 μg/mL) and incubated overnight at 37 °C and 180 rpm. Seven mL overnight culture was transferred to 700 mL TB supplemented

with kanamycin (50 μg/mL) in 2 L flasks and incubated at 37 °C and 180 rpm until OD600 reached 1.5. Protein expression was induced by 0.5 mM isopropyl β-d-1-thiogalactopyranoside (IPTG) and continued overnight at 37 °C and 180 rpm.

4.3. Peptide Purification

The overnight culture was centrifuged at 3512 G using a FIBERLite F8–6 × 1000y rotor (Thermo Fisher Scientific, Waltham, MA, USA) in a Sorvall Evolution RC centrifuge (Thermo Fischer Scientific, Waltham, MA, USA) for 10 min at 4 °C, and the pellet was dissolved in lysis buffer (50 mM Tris-HCl, 100 mM NaCl, 10 mM imidazole, 0.5 mM TCEP, 1 Complete Mini EDTA-free protease inhibitor, 50 U/mL benzonase; pH 8) at 4 °C before homogenization using an Emulsiflex-D20B high pressure homogenizer (Avestin, Ottawa, Ontario, Canada). IBs were collected by centrifugation at 18 566 G using a FIBERLite F14–6 × 250y rotor (Thermo Fischer Scientific, Waltham, MA, USA) in a Heraeus X3R Multifuge (Thermo Fischer Scientific, Waltham, MA, USA) for 30 min at 4 °C, and then washed in ice-cold buffer (50 mM Tris-HCl, 100 mM NaCl, 0.5%(v/v) Triton X-100; pH 8) before centrifugation and solubilization (50 mM Tris-HCl, 300 mM NaCl, 10 mM imidazole, 6 M guanidinium chloride; pH 8) overnight at room temperature. Solubilized IBs were isolated by centrifugation at 18,566 G using a FIBERLite F14–6 × 250y rotor (Thermo Fischer Scientific, Waltham, MA, USA) in a Heraeus X3R Multifuge (Thermo Fischer Scientific, Waltham, MA, USA) for 1.5 h at room temperature before filtration through a 0.22 μm PES bottle top filter (MidSci, St. Louis, MO, USA) and purification using a HiTrap Chelating column (GE Healthcare, Broendby, Denmark) coupled to an ÄKTA Xpress system (GE Healthcare, Broendby, Denmark) at room temperature. The column was equilibrated with 10 column volumes (CV) binding buffer (50 mM Tris-HCl, 300 mM NaCl, 10 mM imidazole, 0.5 mM tris(2-carboxyethyl)phophine (TCEP), 6 M urea; pH 8) before sample loading followed by wash in 10 CV wash buffer (50 mM Tris-HCl, 300 mM NaCl, 30 mM imidazole, 0.5 mM TCEP, 6 M urea; pH 8). Peptides were eluted with elution buffer (50 mM Tris-HCl, 300 mM NaCl, 300 mM imidazole, 0.5 mM TCEP, 6 M urea; pH 8) in 2 mL fractions based on the absorbance at 280 nm. Peptide fractions were lyophilized in a Christ Alpha 2–4 LD plus freeze–dryer (Martin Christ Gefriertrocknungsanlagen, Osterode am Harz, Germany) before they were dissolved in 10 mM HEPES pH 7.4 added 0.05% (v/v) trifluoroacetic acid (TFA) and further purified by RP-HPLC (150 × 4.6 mm Phenomenex Jupiter C18 column, 3 μm) by applying a linear gradient of eluent B (acetonitrile (MeCN), 0.05%(v/v) TFA) in eluent A (5% (v/v) MeCN, 0.05% (v/v) TFA, Milli-Q water) increasing from 0% to 100% over 100 min at room temperature. Fractions containing eluted peptide identified based on the absorbance at 280 nm were lyophilized and the N-terminal histidine-tag was cleaved off by incubation with the TEV protease (1 mol TEV to 100 mol target peptide) in TEV buffer (10 mM HEPES, 0.5 mM TCEP; pH 7.4) overnight at 4 °C. Target peptides were separated from

the histidine-tag by RP-HPLC using the same method as described above. Eluted peptide fractions were lyophilized, dissolved in 10 mM HEPES pH 7.4, identified on an Instant Blue Coomassie stained (Expedeon, Cambridgeshire, UK) NuPAGE 4–12% Bis-Tris SDS-PAGE (Life Technologies, Naerum, Denmark), and molecular weights verified by LC-HRMS using a Bruker MicrOTOF-Q II Quadropol MS detector (Bruker, Coventry, UK) and stored at −80 °C until further use.

4.4. Peptide Synthesis

Synthesis of penetratin, Tat, and R9 was carried out as previously described[20] by Fmoc solid-phase peptide synthesis (SPPS) using a MW-assisted automated CEM Liberty synthesizer (CEM, Matthews, NC, USA). The peptides were purified by preparative RP-HPLC (250 × 21.2 mm Phenomenex Luna C18(2) column, particle size: 5 μm). A linear gradient of eluent B (MeCN–water 95:5 with 0.1% (v/v) TFA) in eluent A (MeCN–water 5:95 with 0.1% (v/v) TFA) increasing from 0% to 45% over 25 min was applied at room temperature. The purity of the peptides (>95%) was confirmed by analytical RP-HPLC (150 × 4.6 mm Phenomenex Luna C18(2) column, particle size: 3 μm) with UV detection at 220 nm by using a gradient from 0% to 60% of B over 30 min, while the molecular identity was confirmed by LC-HRMS using a Bruker MicrOTOF-Q II Quadropol MS detector. The peptides were lyophilized and stored at −18 °C until further use. The synthesized peptides are listed in Table 2.

4.5. TLR Activation Assay

Human Toll Like Receptor reporter cell lines (HEK-Blue-hTLRNull1, -hTLR2, -hTLR3, -hTLR4, and -hTLR9 reporter cells) were cultured according to the manufacturer's directions (Invitrogen, Toulouse, France). 25 000 HEK-Blue-hTLRNull1, -hTLR2, or -hTLR3 reporter cells; 12 500 HEK-Blue-hTLR4 cells; or 40 000 HEK-Blue-hTLR9 cells were stimulated with 0.5, 1.5, 5, or 15 μM PTH(1–34) or PTH(1–34)-CPP fusion peptides in a total volume of 100 μL for 20 h at 37 °C in a humidified CO_2 incubator. As positive controls, the following agonists (Invitrogen, Toulouse, France) were used: Pam3SCK (100 ng/mL) for TLR2, LPS-EK (10 ng/mL) for TLR4, ODN2006 (10 μg/mL) for TLR9, Poly(I:C) (5 ug/mL) for TLR3, and TNF-α (100 ng/mL) for TLRNull. To detect secreted reporter protein alkaline phosphatase, 20 μL supernatant was added to 180 μL of QUANTI-Blue substrate (Invitrogen, Toulouse, France) and incubated for 1 h at 37 °C in a humidified CO_2 incubator. Levels of secreted alkaline phosphatase (SEAP) were determined using a Biorad microplate reader at 650 nm. Relative alkaline phosphatase levels were defined as sample level divided by water control level.

4.6. DC Maturation Assay

Dendritic cells were obtained as previously described by Lutz et al.[36] Briefly, bone marrow was flushed from femurs and tibia of CB6F1/CrL mice (6–8 weeks) before they were flushed with culture medium (20 ng/mL murine rGM-CSF (Cytogen, The Netherlands) in Iscove's Modified Dulbecco's Medium supplemented with 5% (v/v) fetal bovine serum (Lonza, Verviers, Belgium), 50 μM 2-mercaptoethanol (Sigma-Aldrich, St. Louis, MO, USA), penicillin, and streptomycin (adapted from Lutz et al.).[36] 450 000 cells were seeded in 1 mL per well in a 12-well plate expanded in culture medium. On day 2, the growth medium volume was doubled, and on day 5, additional 20 ng/mL rGM-CSF was added. On day 7, BMDCs were stimulated with PBS (1:1000), LPS (10 ng/mL), or 1 of the 8 PTH(1–34) test solutions (5, 1.5, 0.5, or 0.15 μM) for 16 h at 37 °C in a humidified CO_2 incubator. Staining of surface markers with the indicated antibodies was performed in the presence of Fc block (2.4G2) for 30 min on ice. Anti-CD11c (N418) and -I-Ad/I-Ed (M5/114) were purchased from eBioscience (San Diego, CA, USA) and anti-CD40 (3/23) and -CD86 (GL1) were obtained from BD Biosciences (Breda, The Netherlands). Samples were measured on a FACSCantoII (BD Biosciences, San Jose, CA, USA) and analyzed with *FlowJo* software (Ashland, OR, USA).

4.7. Liposome Preparation

Anionic unilamellar liposomes (POPC:POPG, 80:20 molar ratio) were prepared for circular dichroism (CD) spectroscopy by the thin film method as previously described.[37] Briefly, dry lipid films were formed in round-bottom flasks under vacuum overnight before they were hydrated for 1 h at room temperature, with vigorous agitation every 10 min, in a buffer containing 10 mM HEPES and 150 mM KCl (pH 7.4) to obtain a final lipid concentration of 20 mM. Upon annealing for 1 h, vesicles were extruded (Lipex Biomembranes Extruder, Vancouver, BC, Canada) 10 times through two stacked polycarbonate filters with 100 nm pore size (Whatman, Herlev, Denmark). For all batches used, the expected vesicle size and polydispersity index (PDI) were verified by dynamic light scattering (DLS) at 25 °C using a Zetasizer Nano ZS (Malvern Optics Instruments, Worcestershire, UK) equipped with a 633 nm laser.

4.8. Secondary Structure Determination

CD spectra of the CPP-modified PTH(1–34) fusion peptides or CPPs alone, in the presence of 20%(v/v) 2,2,2-trifluoroethanol (TFE), or mixed with POPC:POPG liposomes at a fixed peptide to lipid ratio of 1:100 were measured in the range of 180–260 nm on a JASCO spectrophotometer (Easton, MD, USA) using a 1 mm cuvette (Hellma Analytics, Müllheim, Germany). Measurements were performed at 20 °C with 10 μM PTH(1–34), 10 μM CPP-modified PTH(1–34), or 20 μM CPP mixed with 20 μM PTH(1–34) dissolved in Milli-Q water. All spectra were background corrected, transformed into mean residue ellipticity (MRE), and represent an average of 10 scans.

4.9. Cell Culture Models

For potency assessment, Saos-2 cells were obtained from American Type Culture Collection (ATCC, Manassas, VA, USA) and maintained in McCoy's 5A medium (Sigma-Aldrich, Broendby, Denmark) supplemented with 90 U/mL penicillin, 90 µg/mL streptomycin, 2 mM l-glutamine, 0.1 mM nonessential amino acids, and 10% (v/v) fetal calf serum (FCS) (Thermo Fischer Scientific, Slangerup, Denmark). Cells were grown in 5% CO_2 at 37 °C and detached from the culturing flasks at 80% confluence by trypsin-EDTA treatment before being subcultured at a ratio of 1:5 once a week. Before experimental use, 5.0×10^4 cells/well were seeded at in 96-microtiter plates and cultured for 2 days.

For the permeability and viability studies, Caco-2 cells were obtained from American Type Cell Cultures (ATCC, Manassas, VA, USA) and maintained in Dulbecco's Modified Eagle Medium (DMEM) (Sigma-Aldrich, Broendby, Denmark) supplemented with 90 U/mL penicillin, 90 µg/mL streptomycin, 2 mM l-glutamine, 0.1 mM nonessential amino acids, and 10% (v/v) fetal calf serum (FCS) (Thermo Fischer Scientific, Slangerup, Denmark). Cells were grown in 5% CO_2 at 37 °C and detached from the culturing flasks at 80% confluence by trypsin-EDTA treatment before being subcultured at a ratio of 1:5 twice a week. For experimental use 1.0×10^5 cells were grown on polycarbonate membrane inserts (diameter: 12 mm, area: 1.13 cm^2, pore size 0.4 µm) (Corning Costar, Costar, NY, USA) in a 12-well Transwell plate (Corning Costar, Costar, NY, USA) for 20 days.

4.10. Potency Assessment

Saos-2 cells were washed once with phosphate buffered saline (PBS) and incubated with PTH(1–34) and CPP-conjugated PTH(1–34) fusion peptides dissolved in PBS containing 0.1 mM 4-(3-butoxy-4-methoxybenzyl)imidazolidin-2-one) (Sigma-Aldrich, Broendby, Denmark) and 0.5 mM 3-isobutyl-1-methylxanthine (Sigma-Aldrich, Broendby, Denmark) for 1 h at 37 °C with peptide concentrations ranging from 1.225 nM–80 µM. cAMP levels were determined using the bioluminescent cAMP-Glo assay (Promega, Madison, WI, USA) according to the procedure supplied by the manufacturer. Luminescence was measured on a FLUOstar OPTIMA plate reader (BMG Labtech, Offenburg, Germany) for quantification.

4.11. *In Vitro* Permeation Studies

Test samples containing 40 µM CPP-PTH(1–34) fusion peptide or corresponding concentrations of commercially obtained PTH(1–34) mixed with either penetratin, Tat, VP22, or R9 were prepared in Hanks Balanced Salt Solution (HBSS) (Invitrogen, Naerum, Denmark) supplemented with 10 mM HEPES (Applichem, Darmstadt, Germany), and adjusted to pH 7.4 (hHBSS). ^{3}H-mannitol (1 µCi/mL in hHBSS) was included as a control of the integrity of the Caco-2 cell monolayer.

Before initiation of the experiment, the monolayer was washed with 2 × 1 mL hHBSS and subsequently left to equilibrate to room temperature in the last rinsing volume prior to measuring the transepithelial electrical resistance (TEER) followed by equilibration to 37 °C. The hHBSS was removed from the apical and basolateral compartments and the experiment initiated by the addition of 500 µL of the respective test samples before the filter inserts were transferred to new 12-well plates prefilled with 1 mL hHBSS. From wells containing ^{3}H-mannitol, 100 µL samples were withdrawn from the basolateral compartment at time points 0, 30, 60, 90, 120, 150, and 180 min and immediately mixed with 2 mL Ultima Gold (PerkinElmer, Waltham, MA, USA) before being subjected to analysis using a scintillation counter (Packard Tri-Carb 2100 TR, Canberra, Dreieich, Germany). From the wells containing the test samples, 100 µL samples were withdrawn at time points 0, 60, 120, and 180 min and kept on ice until quantification of the amount of permeated PTH(1–34) employing an EIA kit (BACHEM, Bubendorf, Schwitzerland) as described by the manufacturer using the absorbance measured at 450 nm on a FLUOstar OPTIMA plate reader (BMG Labtech, Offenburg, Germany) for quantification. Withdrawn samples were immediately replaced with the same volume of receptor medium.

The apparent permeability coefficient (P_{app}) was calculated by using the equation P_{app} (cm/s) = dQ/dt X 1/(A X C_0) (1) where dQ/dt is the steady state flux, A (1.13 cm^2) is the area of the Caco-2 cell monolayer, and C_0 is the initial donor concentration.

4.12. Viability Assessment

The cellular viability of the Caco-2 cells in the monolayer was determined immediately after each permeability study and assayed using the MTS/PMS assay as previously described.[38] Briefly, the monolayer was incubated with 0.32 mL of a MTS/PMS solution (240 µg/mL MTS, 2.4 µg/mL PMS (Promega, Madison, WI, USA) in hHBSS) for 1.5 h with horizontal shaking (50 rpm, 37 °C). The absorbance of 100 µL samples (n = 2) from each well was subsequently measured at 492 nm on a POLARstar OPTIMA plate reader (BMG Labtech, Offenburg, Germany). The relative viability was calculated by using the equation relative viability (%) = $(A_{sample} - A_{SDS})/(A_{buffer} - A_{SDS})$ X 100% (2) where A_{sample} is the absorbance of the samples, A_{SDS} is the absorbance of the negative control (0.2% (w/v) sodium dodecyl sulfate (SDS)) corresponding to 0% cell viability, and A_{buffer} is the absorbance of the positive control that corresponds to 100% cell viability.

4.13. Data and Statistical Analysis

Data processing was done in *Microsoft Office Excel 2010* and *GraphPad Prism* v 6 (GraphPad Software, San Diego, CA, USA). Statistical analysis was carried out in *GraphPad Prism* v 6 using t test and one way analysis of variance (ANOVA), and data shown as mean ± standard error of mean (SEM) with n representing the number of replicates. The permeation studies were performed using 3 consecutive passages of cells.

References

This article references 38 other publications.

1. Kargi, A. Y. and Merriam, G. R. (2013) Diagnosis and treatment of growth hormone deficiency in adults Nat. Rev. Endocrinol. 9, 335– 345
2. Rozenberg, S., Vandromme, J., and Antoine, C. (2013) Postmenopausal hormone therapy: risks and benefits Nat. Rev. Endocrinol. 9, 216– 227
3. Potts, J. T., jr, Kronenberg, H. M., and Rosenblatt, M. (1982) Parathyroid hormone: chemistry, biosynthesis, and mode of action Adv. Protein Chem. 35, 323– 396
4. Potts, J. T., jr, Tregar, G. W., Keutmann, H. T., Niall, H. D., Sauer, R., Deftos, L. J., Dawson, B. F., Hogan, M. L., and Aurbach, G. D. (1971) Synthesis of a biologically active N-terminal tetratriacontapeptide of parathyroid hormone Proc. Natl. Acad. Sci. U. S. A. 68, 63– 67
5. Lane, J. M., Russell, L. K., and Khan, S. N. (2000) Osteoporosis Clin. Orthop. Relat. Res. 372, 139– 150
6. Kristensen, M., Foged, C., Berthelsen, J., and Nielsen, H. M. (2013) Peptide-enhanced oral delivery of therapeutic peptides and proteins J. Drug Delivery Sci. Technol. 23, 365– 373
7. Morishita, M., Kamei, N., Ehara, J., Isowa, K., and Takayama, K. (2007) A novel approach using functional peptides for efficient intestinal absorption of insulin J. Controlled Release 118, 177– 184
8. Kamei, N., Morishita, M., Eda, Y., Ida, N., Nishio, R., and Takayama, K. (2008) Usefulness of cell-penetrating peptides to improve intestinal insulin absorption J. Controlled Release 132, 21– 25
9. Khafagy, E.-S. and Morishita, M. (2012) Oral biodrug delivery using cell-penetrating peptide Adv. Drug Delivery Rev. 64, 531– 539
10. Liang, J. F. and Yang, V. C. (2005) Insulin-cell penetrating peptide hybrids with improved intestinal absorption efficiency Biochem. Biophys. Res. Commun. 335, 734– 738
11. Patel, L., Wang, J., Kim, K., and Borok, Z. (2009) Conjugation with cationic cell-penetrating peptide increases pulmonary absorption of insulin Mol. Pharmaceutics 6, 492– 503
12. Caldinelli, L., Albani, D., and Pollegioni, L. (2013) One single method to produce native and Tat-fused recombinant human α-synuclein in Escherichia coli BMC Biotechnol. 13, 32
13. Zigoneanu, I. G. and Pielak, G. J. (2012) Interaction of α-synuclein and a cell penetrating fusion peptide with higher eukaryotic cell membranes assessed by ^{19}F NMR Mol. Pharmaceutics 9, 1024– 1029
14. Derossi, D., Calvet, S., Trembleau, A., Brunissen, G. C., and Prochiantz, A. (1996) Cell internalization of the third helix of the Antennapedia homeodomain is receptor-independent J. Biol. Chem. 271, 18188– 18193
15. Frankel, A. and Pabo, C. (1988) Cellular uptake of the tat protein from human immunodeficiency virus Dis. Markers 8, 1189– 1193
16. Elliott, G. and O'Hare, P. (1997) Intercellular trafficking and protein delivery by a herpesvirus structural protein Cell 88, 223– 233
17. Ryser, H. J. and Hancock, R. (1965) Histones and basic polyamino acids stimulate the uptake of albumin by tumor cells in culture Science 150, 501– 503
18. Marx, U. C. (1998) Structure-activity relation of NH2-terminal human parathyroid hormone fragments J. Biol. Chem. 273, 4308– 4316
19. Rydberg, H. A., Matson, M., Amand, H. L., Esbjörner, E. K., and Nordén, B. (2012) Effects of tryptophan content and backbone spacing on the uptake efficiency of cell-penetrating peptides Biochemistry 51, 5531– 5539
20. Bahnsen, J. S., Franzyk, H., Sandberg-Schaal, A., and Nielsen, H. M. (2013) Antimicrobial and cell-penetrating properties of penetratin analogs: Effect of sequence and secondary structure Biochim. Biophys. Acta 1828, 223– 232
21. Christiaens, B., Grooten, J., Reusens, M., Joliot, A., Goethals, M., Vandekerckhove, J., Prochiantz, A., and Rosseneu, M. (2004) Membrane interaction and cellular internalization of penetratin peptides Eur. J. Biochem. 271, 1187– 1197

22. Schellekens, H. (2002) Bioequivalence and the immunogenicity of biopharmaceuticals Nat. Rev. Drug Discovery 1, 457– 462
23. Kane, J. F. and Hartley, D. L. (1988) Formation of recombinant protein inclusion bodies in Escherichia coli Tibtech. 6, 95– 101
24. Georgiou, G., Telford, J. N., Shuler, M. L., and Wilson, D. B. (1986) Localization of inclusion bodies in Escherichia coli overproducing beta-lactamase or alkaline phosphatase Appl. Environ. Microbiol. 52, 1157– 1161
25. Singh, S. M. and Panda, A. K. (2005) Solubilization and refolding of bacterial inclusion body proteins J. Biosci. Bioeng. 99, 303– 310
26. Taylor, G., Hoare, M., Gray, D. R., and Marston, F. A. O. (1984) Size and density of inclusion bodies Nat. Biotechnol. 4, 553– 557
27. Pellegrini, M., Royo, M., Rosenblatt, M., Chorev, M., and Mierke, D. F. (1998) Addressing the tertiary structure of human parathyroid hormone-(1–34) J. Biol. Chem. 273, 10420– 10427
28. Strickland, L. A., Bozzato, R. P., and Kronis, K. A. (1993) Structure of human parathyroid hormone(1–34) in the presence of solvents and micelles Biochemistry 32, 6050– 6057
29. Marx, U. C., Adermann, K., Bayer, P., Forssmann, W. G., and Rösch, P. (2000) Solution structures of human parathyroid hormone fragments hPTH(1–34) and hPTH(1–39) and bovine parathyroid hormone fragment bPTH(1–37) Biochem. Biophys. Res. Commun. 267, 213– 220
30. Caulfield, M. P., McKee, R. L., Goldman, M. E., Duong, L. T., Fisher, J. E., Gay, T. C., DeHaven, P. A., Levy, J. J., Roubini, E., Nutt, R. F., Chorev, M., and Rosenblatt, M. (1990) The bovine renal parathyroid hormone (PTH) receptor has equal affinity for two different amino acid sequences: the receptor binding domains of PTH and region Endocrinology 127, 83– 87
31. McKee, M. D. and Murray, T. M. (1985) Binding of intact parathyroid hormone to chicken renal plasma membranes Endocrinology 117, 1930– 1939
32. Tünnemann, G., Ter-Avetisyan, G., Martin, G. M., Stoockl, M., Hermann, A., and Cardoso, C. (2008) Live-cell analysis of cell penetration ability and toxicity of oligo-arginines J. Pept. Sci. 14, 469– 476
33. Bendifallah, N., Rasmussen, F. W., Zachar, V., Ebbesen, P., Nielsen, P. E., and Koppel (2006) Evaluation of cell-penetrating peptides (CPPs) as vehicles for intracellular delivery of antisense peptide nucleic acid (PNA) Bioconjugate Chem. 17, 750– 758
34. Pujals, S., Fernández-Carneado, J., López-Iglesias, C., Kogan, M. J., and Giralt, E. (2006) Mechanistic aspects of CPP-mediated intracellular drug delivery: Relevance of CPP self-assembly Biochim. Biophys. Acta 1758, 264– 279
35. Savitsky, P., Bray, J., Cooper, C. D. O., Marsden, B. D., Mahajan, P., Burgess-Brown, N. A., and Gileadi, O. (2010) High-throughput production of human proteins for crystallization: the SGC experience J. Struct. Biol. 172, 3– 13
36. Lutz, M. B., Kukutsch, N., Ogilvie, A. L. J., Rössner, R., Koch, F., Romani, N., and Schuler, G. (1999) An advanced culture method for generating large quantities of highly pure dendritic cells from mouse bone marrow J. Immunol. Methods 223, 77– 92
37. Foged, C., Franzyk, H., Bahrami, S., Frokjaer, S., Jaroszewski, J. W., Nielsen, H. M., and Olsen, C. A. (2008) Cellular uptake and membrane-destabilising properties of alpha-peptide/beta-peptoid chimeras: lessons for the design of new cell-penetrating peptides Biochim. Biophys. Acta 1778, 2487– 2495
38. Cory, A. H., Owen, T. C., Barltrop, J. A., and Cory, J. G. (1991) Use of an aqueous soluble tetrazolium/ formazan assay for cell growth assays in culture Cancer Commun. 3, 207– 212

Supporting Information

Overview of the primers and the plasmid used for cloning, data on soluble expression, CD spectra of the fusion peptides in aqueous buffer and TFE, CD spectra of the CPPs alone, dose–response plots after incubation of fusion peptides with Saos-2 cells, and data on immune response causing TLR2-, TLR3-, or TLR9-activation. This material is available free of charge via the Internet at http://pubs.acs.org.

Table S1. *Overview of primers used for the cloning of PTH(1-34) and the CPP-conjugated PTH(1-34) fusion peptides. FW: forward, RV: reverse.*

Name	Sequence
PTH(1-34) FW	tacttccaatcctcgGTTAGCGAAATTCAGCTGATGCATAATCTGG
PTH(1-34) RV	tatccacctttactgttaAAAGTTATGCACATCCTGCAGTTTTTTACGCAG
PTH(1-34)-penetratin FW	tacttccaatcctcgGTTAGCGAAATTCAGCTGATGCATAATCTGG
PTH(1-34)-penetratin RV	tatccacctttactgttaTTTTTTCCATTTCATACGACGGTTCTGAAACC
PTH(1-34)-Tat FW	tacttccaatcctcgGTTAGCGAAATTCAGCTGATGCATAATCTGG
PTH(1-34)-Tat RV	tatccacctttactgttaACGTCTACGCTGCCTACGTTTTTTGC
Tat-PTH(1-34) FW	tacttccaatcctcgTACGGTCGTAAAAAACGTCGTCAGCG
Tat-PTH(1-34) RV	tatccacctttactgttaAAAATTATGCACATCCTGCAGTTTTTTGCGCAG
PTH(1-34)-VP22 FW	tacttccaatcctcgGTTAGCGAAATTCAGCTGATGCATAATCTGG
PTH(1-34)-VP22 RV	tatccacctttactgttaACCAACCGGACGACGCGGAC
VP22-PTH(1-34) FW	tacttccaatcctcgGATGCAGCAACCGCAACCCGTG
VP22-PTH(1-34) RV	tatccacctttactgttaAAAGTTATGCACATCCTGCAGTTTTTTACGCAG
PTH(1-34)-R9 FW	tacttccaatcctcgGTTAGCGAAATTCAGCTGATGCATAATCTGG
PTH(1-34)-R9 RV	tatccacctttactgttaACGACGCCTTCTCCGGCGC
R9-PTH(1-34) FW	tacttccaatcctcgAGACGTAGGCGCCGGAGAAGG
R9-PTH(1-34)-RV	tatccacctttactgttaAAAGTTATGCACATCCTGCAGTTTTTTACGCAG

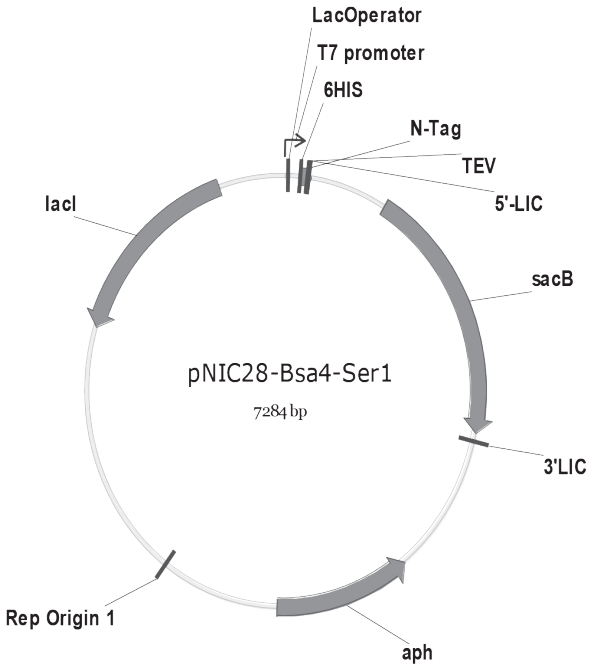

Figure S1. *pNIC28-Bsa4-Ser1 plasmid used for the cloning of PTH(1-34) and the CPP-conjugated PTH (1-34) fusion peptides.*

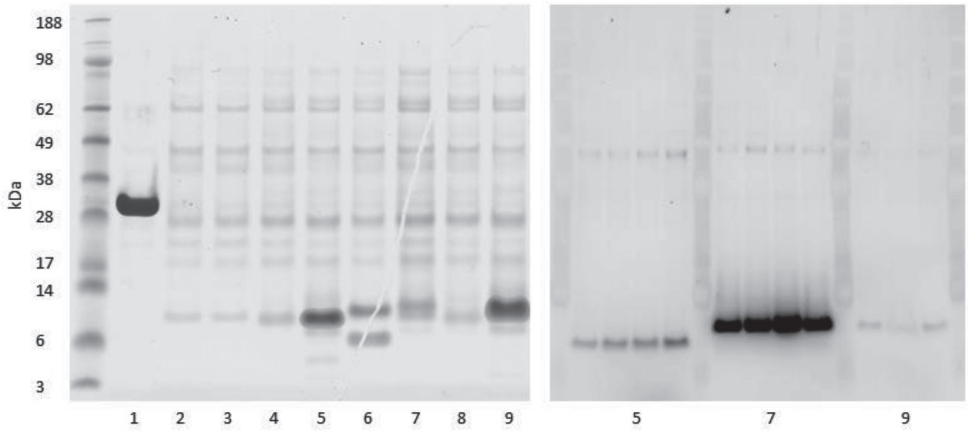

Figure S2. *Left: Coomassie-stained SDS-page gel loaded with soluble expressed and IMAC-purified PTH (1-34) and CPP-conjugated PTH(1-34) fusion peptides next to a pre-stained molecular weight marker. Right: Western blot with detection of soluble expressed and IMAC-purified CPP-conjugated PTH(1-34) fusion peptides by an anti-His antibody. 1: GFP control, 2: PTH(1-34), 3: PTH(1-34)-penetratin, 4: PTH(1-34)-Tat, 5: Tat-PTH(1-34), 6: PTH(1-34)-VP22, 7: VP22-PTH(1-34), 8: PTH(1-34)-R9, 9: R9-PTH(1-34).*

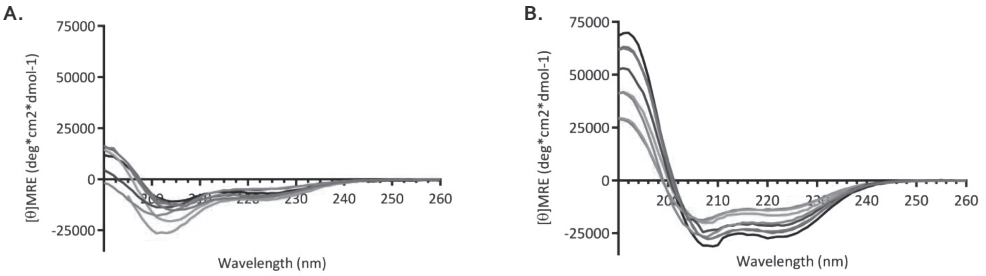

Figure S3. *Circular dichroism spectra of 10 µM PTH(1-34) and 10 µM CPP-conjugated PTH(1-34) fusion peptides in aqueous buffer solution (a) or in the presence of 20% aqueous TFE (b). PTH(1-34): black, PTH(1-34)-penetratin: grey, PTH(1-34)-Tat: dark green, Tat-PTH(1-34): light green, PTH(1-34)-VP22: dark blue, VP22-PTH(1-34): light blue, PTH1-34)-R9: red, R9-PTH(1-34): light red.*

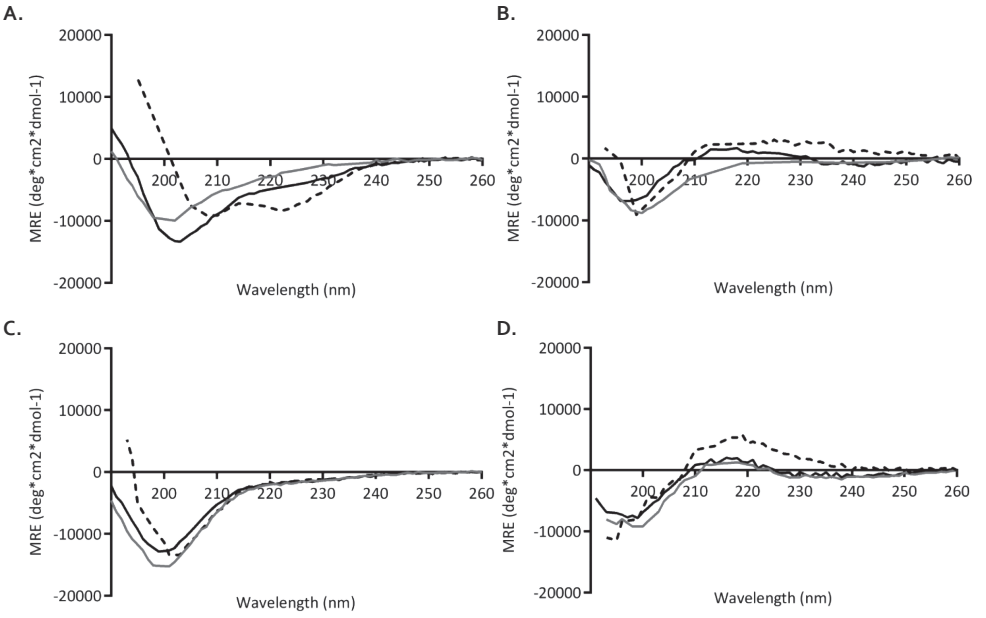

Figure S4. *Circular dichroism spectra of 20 µM CPP in aqueous buffer solution (grey), in the presence of 20%(v/v) aqueous TFE (black), or 1 mM POPC:POPG (molar ratio 80:20) liposomes corresponding to a 1:100 peptide to lipid ratio (black dash). (a): Penetratin, (b): Tat, (c): VP22, (d): R9.*

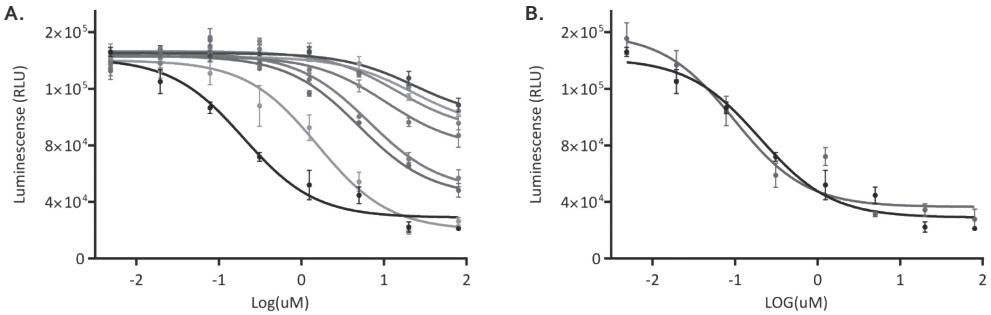

Figure S5. *Dose-response plots obtained after incubation of Saos-2 cells with 1.225 nM - 80 µM expressed PTH(1-34) or CPP-conjugated PTH(1-34) fusion peptides (a) or with 1.225 nM - 80 µM expressed PTH(1-34) or synthetic PTH(1-34) (b). Expressed and purified PTH(1-34): Black, synthetic PTH(1-34): Brown, PTH(1-34)-penetratin: Grey, PTH(1-34)-Tat: Dark green, Tat-PTH(1-34): Light green, PTH(1-34)-VP22: Dark blue, VP22-PTH(1-34): Light blue, PTH81-34)-R9: Red, R9-PTH(1-34): Light red. Data are presented as mean ± SEM (n = 3).*

Figure S6.

A.

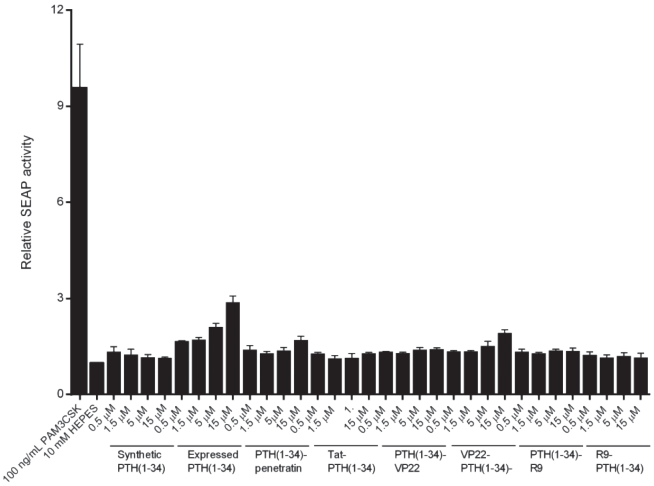

B.

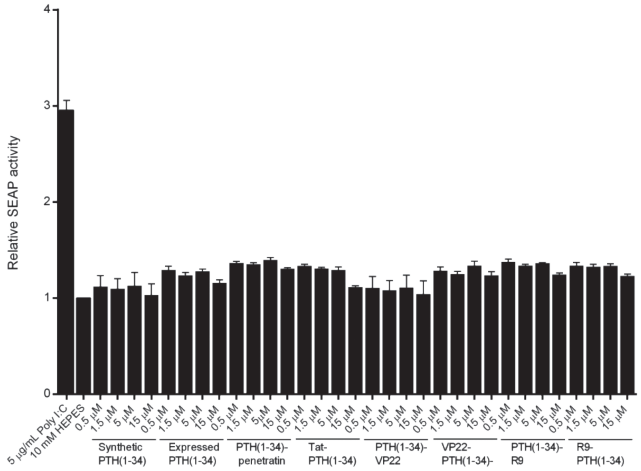

C.

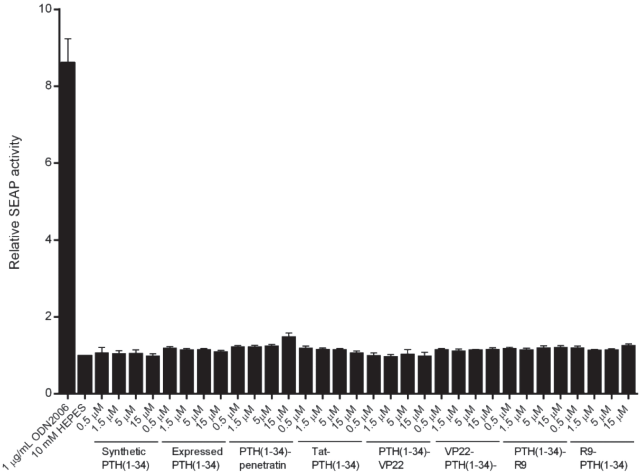

Figure S6. *Test for in vitro immune response by FACS analysis of human TLR2 activation on HEK-Blue™-hTLR2 cells (a), TLR3 activation on HEK-Blue™-hTLR3 cells (b), or TLR9 activation on HEK-Blue™-hTLR9 cells after incubation with 0.5-15 µM synthetic PTH(1-34), expressed PTH(1-34) or CPP-conjugated PTH(1-34) fusion peptides. 100 ng/mL PAM3CSK, 5 ng/mL Poly I:C, or 1 µg/mL ODN2006 are included as positive controls, respectively, and 1 mM HEPES buffer is included as negative control. Data are presented as mean ± SEM (n = 4).*


8

Summarizing Discussion

Immunogenicity of therapeutic biopharmaceuticals

Biopharmaceutical (BP) proteins offer several therapeutic advantages compared to classical small molecule synthetic drugs.[1] For example, the complexity of their structure compared to small molecule drugs offers BP high specificity at receptor level, letting them effectively intervene in disease pathways. Consequently, the number of biotechnology-derived proteins that are used as therapeutic agents is steadily increasing. Unfortunately, these products may induce unwanted immune responses. Their recognition by and triggering of the immune system they induce can be influenced by various factors, including patient- and disease-related factors as well as product-related factors. Therefore, assays to determine immunogenicity are required, and the clinical significance of immunogenicity should be analyzed. Production of anti-drug antibodies (ADA) against therapeutic proteins is common.[2] However, the immunological response is complex and, in addition to antibody formation, T cell activation or innate immune responses could contribute to potential adverse effects, which may range from: without any clinical significance to a severe life threatening situation. Therefore, it is essential to study the potential immunological effects and the associated clinical consequences of BP administration. This is currently done by determining the presence of antibodies, and if epitopes are recognized, the affinity of the antibodies, isotype and amount of antibodies induced, and ability of immune complexes to activate complement.

In general, the risk of immunogenicity has consequences for both the efficacy and safety of a therapeutic. For example, so called "neutralizing antibodies" may bind to (or near) the active site of a pharmacological compound and thereby eliminate ("neutralize") its active site, which is directly linked to loss of efficacy. Non-neutralizing antibodies (binding to a non-active or non-essential site) are generally expected to have less clinical consequences, but they can influence efficacy indirectly by decreasing availability or accessibility. Safety concerns regarding immunogenicity include serious acute immune effects such as anaphylaxis due to cytokine storm in an allergic (IgE dependent) manner or in a non-allergic manner. Several antibody based BPs may induce rare but severe reactions upon first infusion, including those cytokine storms.[3] In addition, cross-reactivity from BP-specific ADA's to an endogenous counterpart is observed, leading to increase of symptoms when administrating BP-based therapeutics.

The assessment of immunogenicity, and specifically ADA formation, is tested in clinical trials, and the guidelines on immunogenicity from the European medicine agency reflect on the procedures necessary for proper assessment.[4, 5] Unfortunately, the predictive value of non-clinical studies for evaluation of immunogenicity of a biological medicinal product in humans is not that high. This is believed to result from differences between human and animal immune systems and to immunogenicity of human proteins in animals. As an example, a target molecule that had a different distribution over effector cells between

rodents and nonhuman primates versus humans led to life threatening situations in first clinical trials.[6,7] Because of the low predictive value, non-clinical studies aimed at predicting immunogenicity in humans are normally not required. However, novel assessment models could be of value in selecting lead compounds for further development. In the before mentioned case updated peripheral blood mononuclear cell assays could in hindsight identify the toxicity of the therapeutic,[8] showing the value of preclinical testing.

In this thesis the immunogenicity was assessed of BPs in the research stage of development. Development of BP focused on reducing delivery- and targeting-bottlenecks, and on pre-clinical validation of biocompatibility and bioavailability.[9] Therefore, immunogenicity assessment in part II of this thesis was aimed at selecting lead compounds that do not raise concerns in preclinical- and *in vitro*- phase studies. Combining specific human innate receptor assays, with more general murine antigen presenting cell assays, will give a translational step towards preclinical testing.

In general, when performing immunogenicity assays, it is of importance that studies are supplied with material, sufficiently representative of the medicinal product that is going to be placed on the market, also with respect to impurities or contaminants that could be present in non-clinical samples. In **Chapter 7**, we tested the immunogenicity of parathyroid hormone (PTH), produced in a microbacterial system. Without proper purification, BP produced by such technology will activate the immune system due to contamination with microbial products. This was indeed the case for PTH expressed using a bacterial expression system, while the other bacterially expressed PTH conjugates and the synthetic produced PTH were non-activating. Therefore, to avoid false positive test results, it is recommended in the immunogenicity assessment guidelines that products that are identical or closely related to the desired end product are assessed.[4,5] In addition, also the comparability of the manufacturing process is subjected to guidelines.[10]

Immunogenicity of siRNA based biopharmaceuticals

Not only proteins and peptides have changed the drug field as new BPs, but also nucleic acid structures hold promise for treatment of human disease. Especially small interfering RNAs (siRNA) are important players in RNA interference, as they can potentially silence any (viral) gene in the body. They activate the RNA induced silencing complex and specifically bind messenger RNA structures. This results in the inhibition of transcription leading to reduced protein expression.[11] Although they seem very promising, several challenges have come to light. Next to their size and negative charge, that is not favorable for passive transport over a membrane, they are susceptible to degradation by nucleotides.[12] Next to that, they can activate the innate immune system, because their double stranded structure, which mimics viral origin, can be recognized and could induce inflammation.[13]

Fortunately, multiple possibilities for chemical modifications of the backbone of the RNA structures have been identified that may reduce immunogenicity, and also siRNA enzymatic degradation.[12] The siRNAs delivered in **Chapter 5** and **6** were modified at the 2'-*O*-position of the ribonucleotides by addition of a methyl group (2'-O-Methyl modification). Indeed no activation of innate immune cells was observed for naked siRNA (data not shown), indicating that the siRNAs used in these chapters are not immunogenic by themselves.

Delivery of biopharmaceuticals and immunogenicity

While BPs have contributed to human healthcare already to a large extent, there are still drawbacks in their use. To overcome the challenges faced, such as low membrane and tissue crossing, and rapid enzymatic degradation (necessitating administration via repeated intravenous injection), drug delivery systems (DDS) are developed. These delivery systems, which can be lipid, polymer, peptide, or otherwise based, allow for prolonged circulation times, enhanced uptake by cells, or protection from enzymatic degradation of the BP structure, and thus for a decrease in number and amount of administration doses of the BP. This reduction in doses can reduce immunogenicity of the BP, because there will be less repeated contacts with the immune system. On the other hand, when a chronical disease is targeted with the BP, potential immunogenicity can be just delayed.

Furthermore, DDS can shield proteins from extracellular recognition by immune cells. However, the use of DDS can have indirect effects on enhancing immunogenicity to BP/DDS combination. Proteins that are used for stabilization of BPs may be recognized by the immune system and for instance induce DDS specific ADA's. These can lead to reduced efficacy of enhanced safety risks. However, not only proteins, but also lipids, and saccharides can trigger humoral immune responses. However, class switching of antibodies and affinity maturation, enhancing antibody efficacy, generally occurs when T cell help (which is activated by proteins only) is provided.

An direct effect on enhancing immunogenicity of the BP can als0 be induces by the repetitive polymer structure of lipids and polysaccharides, used in DDS. These repetitive structures can be recognized as foreign by for instance innate receptors, like Toll-like receptors (TLRs), inducing pro-inflammatory cytokines, necessary for induction of immune response. Furthermore, while the use of for instance poly(DL-lactic-co-glycolic acid) (PLGA) nanoparticles enhances uptake of BP by phagocytic cells,[14, 15] this enhanced interaction and permeability of the cell membrane for membrane crossing can also lead to increased cell cytotoxicity.[16, 17] Therefore, the combination of DDS and BP should not be more immunogenic that the BP itself. Therefore, not only the immunogenicity BPs on, but also immunogenicity of the BP/DDS combination should be assessed.

Delivery systems in this thesis

The utilization of cell-penetrating peptides (CPP) has shown promising in improving transepithelial delivery of therapeutic peptides and proteins.[18-20] In **Chapter 7**, the conjugation of four different CPPs to PTH, however, affected both the secondary structure, and therefore the potency and permeation of the BP. Therefore, terminal covalent conjugation of the selected CPPs does not seem favorable over direct co-delivery of CPPs with PTH. Further studies have already been performed in co-administration of the CCP penetratin with either PTH or Insulin. In these studies, enhanced permeation of epithelial cells was found, with even a further enhanced effect at lower pH [personal communication]. This is favorable over effects at high/neutral pH, because the target organs of both BPs are in the GI-track where low pH values are observed[21]. The first *in vitro* immunogenicity studies on this co-administration delivery strategy showed immunocompatibility of the CPP penetratin when combined the BPs PTH or Insulin, compared to PTH or Insulin only [in preparation]. This shows that the DDS/BP combination is not more immunogenic that the BP only. And, further *in vivo* efficacy results are currently under investigation in animals. Together this shows that conjugation is not always more effective than co-administration of CPP.

CPPs have not only been proposed for peptide and protein delivery, but also for siRNA delivery. A series of proteolytically stable peptidomimetics with promising membrane-destabilization and cell-penetrating properties[22-25] were shown to complex with siRNA into well-defined nano-self-assemblies in **Chapter 6**. The resulting nanocomplexes were coated with anionic lipids to prevent the challenges faced by cationic vectors, giving rise to net anionic liposomes. The optimized anionic liposomes mediated a high silencing effect. More importantly, they did not display any noticeable cytotoxicity or immunogenicity *in vitro*. In contrast, the corresponding nanocomplexes, without anionic lipids, displayed a reduced silencing effect and had a narrower safety window regarding toxicity. The findings in this study could be extrapolated to the design of future delivery systems. Three optimization steps could be learned and included in future design: (i) fine tuning the length and repetition of the cationic vector, resulting in a stable complex with low toxicity is recommended, (ii) coating with anionic lipids results in an efficient and biocompatible delivery method with low cytotoxicity and immunogenicity *in vitro*, (iii) the formed liposomes can be modified with extra functional molecules. These could circumvent delivery challenges encountered in vivo, such as surface modification with PEG to enhance circulation time,[26] but also targeting ligands could be introduced for specific tumor delivery.

Like Chapter 6, where delivery systems are based on nanocomplexes from anionic lipidoids and cationic peptidomimetics, **Chapter 5** also focuses on hybrid delivery system to deliver siRNA across cell membranes. It has recently been shown that

encapsulation of siRNA in lipid-polymer hybrid nanoparticles (LPNs) based on PLGA and cationic lipid-like materials (called lipidoids) remarkably enhances intracellular delivery of siRNA as compared to siRNA delivery with LPNs modified with dioleoyltrimethylammoniumpropane (DOTAP) as the lipid component [Thanki et al submitted]. However, potential lipid-mediated immune modulation remains unexplored. Preliminary immunogenicity assessments were done and when testing the lipidoids and DOTAP for innate immune receptor activating properties, we found that lipidoids, but not DOTAP are agonists for human TLR4. Furthermore, the lipidoids activated murine antigen-presenting cells *in vitro*. This agonistic effect was further confirmed *in silico* using a prediction model based on crystal structure of the lipidoids and TLR4 related molecules. TLR activation by lipidoids could potentially have effect on immunosafety, and therefore the lipidoids by themselves are not suitable for clinical use. However, by combining lipidoids with PLGA into hybrid LPNs (as DDS for delivery of siRNA), TLR4 activation was abrogated, showing that particle engineering prevented lipidoid-induced TLR4 activation. TLR4 activation *was* measured for lipidoids formulated as stable nucleic acid lipid particles (SNALP), which is the reference formulation for siRNA delivery.[27, 28] Thus, the LPN did not activate TLR4, while the SNALP still showed TLR4 activation, however it is unclear what caused the observed difference. Although the presence of PLGA in the nanoparticle formulation of the LPN could have a direct diminishing effect on recognition of the lipidoid, we hypothesized that the design and structure of the particles were the reason for the observed difference in immune activation. The lipidoids are embedded in the outer layer of the SNALPs, forming a more liposome related structure. This structure could permit contact of lipidoids with the LPS binding protein (LBP), which isolates LPS and transports it to TLR4/MD2.[29, 30] In comparison to SNALP, LPN incorporate lipidoids more tightly in their outer layers, making them less accessible for LBP. For further studies on lipid-based particle engineering, we recommend to include assessment of LBP binding ability as criterion for definition of potential immune activating properties.[31]

Intracellular delivery of biopharmaceuticals

DDS are used to overcome delivery challenges of the BPs as they protect the BP structure from fast degradation and moreover, they facilitate membrane crossing. How this membrane crossing and subsequent cytosolic delivery exactly works is still not know, Multiple hypothesis have been put forward to explain these effects.[32]

The first hypothesis postulates that cationic polymer based DDS escape the endosome according to the 'proton sponge' hypothesis. This is also called the pH-buffering effect, because polymers such as polyethylenimine have protonatable residues at physiological pH.[33] After endocytosis, during maturation of the endosomes protons are translocated

from the cytosol to the endosome for acidification of endosomal compartment. The protonatable secondary amine groups of certain cationic polymers bind the attracted protons, preventing acidification of these compartments. This buffering capacity serves two purposes: it inhibits the activity of lysosomal nucleases that would otherwise degrade nucleic acids and it will change the osmolarity of the vesicles resulting in endosomal swelling and rupture.[34]

The second hypothesis is the 'flip-flop' mechanism proposed for cationic lipid based DDS. The cationic, positively charged lipid forms lipoplexes with the negatively charged nucleic acids resulting in a net positive complex. Lipoplexes will be entrapped inside early endosomes and here the electrostatic interaction between the cationic lipid from the DDS and the anionic lipids present at the cytoplasmic side of the endosomal membrane will take place. The anionic lipids will fuse into the cationic lipids of the DDS resulting in release of the nucleic acids into the cytosol.[35-37] In **Chapter 6**, endosomal escape was investigated to a certain extent. For the cationic lipofectamine 2000 the flip-flop fusion method was proposed. But the anionic liposomes, used in the peptidomimetics-siRNA complex, were based on pH sensitive lipids. Their endosomal escape mechanism is proposed to be based on structural changes of the lipid layers, going from a bilayer to a nonbilayer that eventually allows release of cargo into the cytosol.[38]

A next hypothesis is that CPPs could either open transient pores in the lipid bilayer membrane and the endosome by mimicking the disruptive properties of fusogenic sequences of viral fusion proteins[39] or otherwise destabilization of the endosomal membrane occurs due to conformational changes of the CPPs. In addition, direct translocation and paracellular translocation have been proposed as mechanisms underlying intracellular delivery of cargo by CPPs.[40, 41] The escape mechanism of the CPP DDS used in **Chapter 7** was not directly assessed in this thesis. Some additional preliminary data suggest both tight junction - and endocytic-related transport of penetratin-mediated delivery of PTH [personal communication].

Immunogenicity of BP-based dermally delivered vaccines

An immune response against BPs is the desired effect when BPs are developed for vaccination purposes and, in this case, immunogenicity is an important characteristic of the BP. The protective effect of most vaccines on the market depends on the induction of antibodies, i.e. a humoral response comprising neutralizing antibodies necessary to clear pathogens. However, for intracellular pathogens, and especially to protect against highly variable, mutating pathogens that replicate intracellularly, a cellular cytotoxic T cell response is needed to clear infection once the intruder has entered the intracellular spaces of the infected host. Many vaccines under investigation are based on recombinant proteins

or subunits of pathogens, because of high safety and lower production costs compared to live or attenuated vaccines.[42] However, the induction of a cellular immune response towards a subunit vaccine is challenging, because a protein needs to be transported over the cellular membrane in order to facilitate intracellular processing, which is necessary for the induction of a cytotoxic T cell response. The use of delivery systems such as PLGA based nanoparticles[43] or the use of adjuvants like TLR agonists[44, 45] can enhance T cell responses towards protein, and will be discussed on page 8 (of the discussion). In the next paragraph, we will first discuss DNA vaccines, which have been intensively studied and have been shown to promote both cellular and humoral immune responses.[46]

DNA based vaccination

DNA vaccination strategies have shown much progress since the first finding of direct gene expression in vivo after DNA vector injection.[47] After spontaneous gene transfection of cells of an immunized individual, pDNA is transcribed and translated into immunogenic proteins that, after processing, can elicit an immune response. Delivering DNA vaccines was originally investigated via intramuscular route,[47] however, the skin also has great potential as immunization site for vaccines.[48] Methods to overcome the skin's outer barrier (the stratum corneum) for delivery of DNA vaccines include Gene-gun injection, electroporation[49] or tattooing. Tattooing is a procedure that involves solid vibrating needle(s) that repeatedly punctures the skin, wounding both the epidermis and the upper dermis in the process and causing cutaneous inflammation followed by healing,[50] a process that is thought to contribute to immunogenicity. Delivering DNA vaccines by tattooing has shown already potential in multiple murine immunization studies.[51-53] In **Chapter 4**, we used DNA tattoo to immunize mice with antigen cDNA and we further aimed to enhance immunogenicity of vaccine antigens. Modulation of antigen processing of the encoded proteins, by equipping them with sequences that enhance proteolytic liberation of contained cytotoxic T cell epitopes, represents a strategy to enhance vaccine efficacy. Epitopes that were identified in the *Mycobacterium tuberculosis* vaccine antigen H56 were altered in order to increase immunogenicity. First, fusion of antigen cDNA to cDNA of tetanus toxin fragment C or Ubiquitin led to enhancement of epitope specific $CD8^+$ T cells. This is most likely due to the $CD4^+$ T cell help generated by epitopes present in TTFC[54-56] and due to modified degradation kinetics for the ubiquitin-fused antigen.[57] Second, changing the amino acids flanking the epitopes on the C terminus to enhance epitope liberation from its flanking sequences, led to enhancement of specific $CD8^+$ T cell responses. Such strategies to enhance immunogenicity of cDNA vaccine encoded antigens by modulation of antigen processing could be applied in further vaccine design.

Microneedles for dermal immunizations with protein-based vaccines

Another method to circumvent the skin barrier is the use of microneedles. Microneedles provide the possibility of minimally invasive vaccination compared to tattooing. There are other benefits in using microneedles compared to traditional hypodermic needles, like possible painless vaccination, the requirement of less trained personnel and reduced contamination risk.[58] Nowadays a wide variety of these microneedles exist, including coated, dissolving, porous, and hollow microneedles.[59-61]

In **chapter 3**, hollow microneedles were used and they have the ability to inject a wide variety of fluids into the skin at different pressure-driven flow rates.[62, 63] These hollow microneedles offer the highest precision in dose delivery regarding volume, flow rate and depth among all microneedle types. Furthermore, they offer the possibility to screen the potency of multiple formulations without time-consuming design, preparation, and loading of different microneedles arrays. For the precise injection of fluids through hollow microneedles an applicator is necessary, and a hollow microneedle and applicator are designed for laboratory settings.[63-65] The use of short hypodermic needles are already tested in clinical trials,[66] but the road to self-administration of hollow microneedles is still further away.

Other microneedles are more often array-structured, containing multiple needles on an array that could potentially be self-applied, with an easy to use applicator that allows for skin penetration by MNA. Coated microneedle arrays (MNA) have vaccine formulations coated by adsorption on the surface of the microneedles[67] and upon skin penetration would release the coating in the skin.[68] Surfactants and thickening agents have to be used to facilitate effective coating of antigens on microneedle arrays.[69, 70] However, these agents and the coating procedure could hamper the immunogenicity of the vaccine formulations and extra stabilizers like trehalose and dextran should be added to reduce the damage on the BP structure.[71] However, the thick coating layer, necessary to achieve high vaccine dose, could hamper the skin penetration ability.

Next to coated, also dissolving microneedle arrays are developed for vaccination. Safe and inert polymers or sugars are often used for the production of these needles and vaccine formulations are embedded in the matrix of this structure. After skin piercing, the microneedle array tips dissolve in the skin, releasing the vaccine formulation in the skin over time.[72-74] However, some challenges are encountered in designing dissolving microneedles: dissolving of the needles can be time consuming,[75, 76] it is difficult to only load the dissolving microneedle tips for reduced vaccine residue,[77, 78] and polymers used for dissolving microneedles lack piercing strength compared to materials used for coated microneedles.

The most recent microneedle based delivery system are nanoporous microneedles. They have an interconnected porous structured network throughout the MNA.[79] This allows for loading of formulation in the matrix of the MNA by absorption and release of the formulation after skin piercing occurs via diffusion.[80, 81] Via an easy foil penetration method, tip loading was achieved in **Chapter 2,** resulting in reduced formulation residue and fast diffusion in the skin. Furthermore, absorption of the formulation is favorable over adsorption on the surface by for instance solid microneedles, because the former method does not require any additional chemical interactions that could reduce immunogenicity of the compound. The materials used for porous microneedles have strength for skin piercing,[61] but a balance needs to be found to be porous enough for loading of BPs and strong enough for piercing.[82, 83]

The field of microneedles has grown over the last decade and a variety of different needles exist for vaccine delivery in the skin. Each microneedle types has its advantages and disadvantages, and in this thesis we attributed to the field by exploring 2 needle types. In chapter 2, we showed fully characterized the new nanoporous microneedles and showed for the first time the immunological potential of nanoporous microneedles for known vaccine antigens. In chapter 3 we elaborated on the immune responses that could be induced using hollow microneedles.

Adjuvants in dermal immunization with protein-based vaccines

As mentioned before (page 6), in order to induce a cellular immune response towards a protein or subunit based vaccine multiple strategies can be applied. These strategies include the use of DNA vaccination, as described above, but also the use of drug delivery system such as nanocarriers or adjuvants like TLR agonists. Antigen loaded - PLGA based nanoparticles enhance antigen uptake by antigen presenting cells and they contribute to a prolonged presentation of the vaccine antigen at the cell surface,[15, 84] leading to activation of a cellular immune response. Relatively little is known about the immune responses elicited by nanoparticulated vaccines when administered intradermally using minimal invasive microneedles. Only a few papers have combined these approaches.[85-90] In two of these studies the skin was pretreated with microneedles that allowed for formulation crossing over the stratum corneum. Subsequently, N-trimethyl chitosan based nanoparticles were topically applied. This immunization regimen was shown to lead to specific IgG titers.[85, 86] Two next studies immunized with pDNA, either coated on or loaded in nanoparticles. pDNA-coated nanoparticles were in this study also applied after pretreatment of the skin with microneedles, and resulted in detectable antigen specific serum IgG titers.[87] In the second study, pDNA particles were delivered using dissolving microneedle arrays, however immune responses were not assessed.[88] The use of a protein loaded nanoparticles

as vaccine antigens delivered via microneedles was assessed even fewer.[89, 90] DeMuth *et al.* prepared dissolving microneedle arrays loaded with PLGA nanoparticles containing the model antigen ovalbumin, and showed that the vaccine antigen gradually was released, over a number of weeks.[89] Only Zaric *et al.* showed the immune potency of combining intradermal injection using microneedles and PLGA nanoparticles for subunit vaccine delivery.[90] They induced a robust protective cytotoxic T cell response after immunization using dissolving microneedles. Although a solid begin with the use of nanoparticles for microneedle based intradermal delivery has been made, other microneedle types and nanoparticles should be assessed to address the full potential of combing these strategies.

TLR agonist as adjuvant in intradermal immunization with protein-based vaccines

Vaccine antigen uptake and presentation to T cells only, is not sufficient for the induction of naïve T cells. Costimulation and cytokine secretion by antigen-presenting cells, which can be induced via innate receptors, are necessary for sufficient signal to prime a naïve T cell. TLRs from the innate immune system are, among others, receptors that contribute to the recognition of foreign structures. A variety of dendritic cells in the dermis and epidermis, which have been shown to contribute to immune activation after intradermal immunization,[91, 92] express TLRs. Multiple intradermal immunization studies using different needles have shown added effects of different TLR agonists based adjuvants.[93, 94] For this reason, in **Chapter 2**, the TLR7 agonist imiquimod was added to antigens loaded in nanoporous microneedles. However, following prime boost immunization, overall antibody titers against DT and TT in mice either immunized with full antigen doses, or with half of the antigen dose adjuvanted in imiquimod, were equally high. Based on these results, one may argue that imiquimod may allow for lower antigen doses to be used. However, further immunization studies with different antigen dilutions must point out if there was an added effect of imiquimod, or that half the dose of the antigen itself gives rise to equal antibody titers.

In the above mentioned study, none of the vaccine antigens were encapsulated in nanoparticles. In **Chapter 3,** we combined the approach of nanoparticulation of the antigen and using TLR agonist as adjuvants. Mice were immunized with a model vaccine antigen encapsulated in PLGA nanoparticles with and without TLR3 agonist as adjuvant. A cytotoxic T cell response was indeed induced and showed protection against an intracellular bacterium. Here we contributed to the field of nanoparticles for vaccine delivery in the skin using microneedles, showing the use of a different microneedle type, the induction of endogenous T cell responses and the protectiveness of those T cells against an intracellular bacterium.

Future perspectives

The differences in immune activation that we observe in this thesis provide different opportunities for the field of advanced drug delivery formulations. If aiming for delivery of an antiviral, an antitumor drug, or designing for vaccination, immune activation (within the safe range) is a desired outcome. The immune stimulating effects of unmodified RNA in combination with SNALPs have been described and the lipidoid-mediated immune activating effect of the SNALPs are likely to contribute to effective antiviral therapy. And moreover, PLGA nanoparticles designed for vaccination actively enhanced immune activation towards the BP delivered. On the other side, LPN, CPPs, and siRNA-peptidomimetic nano-self-assemblies all showed immune compatibility, which is necessary for therapeutic delivery. Taken together, the different possibilities for the design of drug delivery systems provide a range of opportunities to modify and engineer drug delivery system to promote a specific, desirable outcome.

References

1 Walsh G. Biopharmaceuticals and biotechnology medicines: an issue of nomenclature. Eur J Pharm Sci. 2002;15(2):135-8.

2 Shankar G, Pendley C, Stein K. A risk-based bioanalytical strategy for the assessment of antibody immune responses against biological drugs. Nat Biotechnol. 2007;25(5):555-61.

3 Hansel T, Kropshofer H, Singer T, Mitchell J, George AJT. The safety and side effects of monoclonal antibodies. Nat Rev Drug Discov. 2010;9(4):325-38.

4 Committee for Medicinal Products for Human Use (CHMP). Guideline on Immunogenicity assessment of biotechnology-derived therapeutic proteins. European Medicine Agency; 2008. Report No.: EMEA/CHMP/BMWP/14327/2006.

5 Committee for Medicinal Products for Human Use (CHMP). Guideline on Immunogenicity assessment of biotechnology-derived therapeutic proteins. European Medicine Agency; 2015. Report No.: EMEA/CHMP/BMWP/14327/2006 Rev. 1.

6 Hünig T. The rise and fall of the CD28 superagonist TGN1412 and its return as TAB08: a personal account. FEBS J. 2016;283(18):3325-34.

7 Suntharalingam G, Perry M, Ward S, Brett S, Castello Cortes A, Brunner M, et al. Cytokine storm in a phase 1 trial of the anti-CD28 monoclonal antibody TGN1412. N Engl J Med. 2006;355(10):1018-28.

8 Vessillier S, Eastwood D, Fox B, Sathish J, Sethu S, Dougall T, et al. Cytokine release assays for the prediction of therapeutic mAb safety in first-in man trials--Whole blood cytokine release assays are poorly predictive for TGN1412 cytokine storm. J Immunol Methods. 2015;424:43-52.

9 Collaboration on the optimization of macromolecular pharmaceutical access to cellular targets [Internet].; 2017 [].

10 Committee for Proprietary Medicinal Products (CPMP). Comparability of biotechnological/biological products subject to changes in their manufacturing process. EMEA / European Medicine Agency; 2005. Report No.: CPMP/ICH/5721/03.

11 Elbashir SM, Harborth J, Lendeckel W, Yalcin A, Weber K, Tuschl T. Duplexes of 21-nucleotide RNAs mediate RNA interference in cultured mammalian cells. Nature. 2001;411(6836):494-8.

12 Bennett CF, Swayze E. RNA targeting therapeutics: molecular mechanisms of antisense oligonucleotides as a therapeutic platform. Annu Rev Pharmacol Toxicol. 2010;50:259-93.

13 Whitehead K, Dahlman J, Langer R, Anderson D. Silencing or stimulation? siRNA delivery and the immune system. In: UNITED STATES: Annual Reviews; 2011. p. 77-96.

14 Shen H, Ackerman A, Cody V, Giodini A, Hinson E, Cresswell P, et al. Enhanced and prolonged cross-presentation following endosomal escape of exogenous antigens encapsulated in biodegradable nanoparticles. Immunology. 2006;117(1):78-88.

15 Waeckerle Men Y, Allmen EU, Gander B, Scandella E, Schlosser E, Schmidtke G, et al. Encapsulation of proteins and peptides into biodegradable poly(D,L-lactide-co-glycolide) microspheres prolongs and enhances antigen presentation by human dendritic cells. Vaccine. 2006;24(11):1847-57.

16 Zhao L, Seth A, Wibowo N, Zhao C, Mitter N, Yu C. Nanoparticle vaccines. Vaccine. 2014;32(3):327-37.

17 Jiskoot W, Randolph T, Volkin D, Middaugh CR, Schoeneich C, Schöneich C, et al. Protein instability and immunogenicity: roadblocks to clinical application of injectable protein delivery systems for sustained release. J Pharm Sci. 2012;101(3):946-54.

18 Kristensen M, Foged C, Berthelsen J, Nielsen HM. Peptide-enhanced oral delivery of therapeutic peptides and proteins. Journal of drug delivery science and technology. 2013;23(4):365-73.

19 Kamei N, Morishita M, Eda Y, Ida N, Nishio R, Takayama K. Usefulness of cell-penetrating peptides to improve intestinal insulin absorption. J Control Release. 2008;132(1):21-5.

20 Khafagy ES, Morishita M. Oral biodrug delivery using cell-penetrating peptide. Adv Drug Deliv Rev. 2012;64(6):531-9.

21 Kristensen M, Nielsen HM. Cell-Penetrating Peptides as Carriers for Oral Delivery of Biopharmaceuticals. Basic & clinical pharmacology & toxicology. 2016;118(2):99-106.

22 Foged C, Franzyk H, Bahrami S, Frokjaer S, Jaroszewski J, Nielsen H, et al. Cellular uptake and membrane-destabilising properties of alpha-peptide/beta-peptoid chimeras: lessons for the design of new cell-penetrating peptides. Biochim Biophys Acta. 2008;1778(11):2487-95.

23 Jing X, Kasimova M, Simonsen A, Jorgensen L, Malmsten M, Franzyk H, et al. Interaction of peptidomimetics with bilayer membranes: biophysical characterization and cellular uptake. Langmuir. 2012;28(11):5167-75.

24 Jing X, Yang M, Kasimova M, Malmsten M, Franzyk H, Jorgensen L, et al. Membrane adsorption and binding, cellular uptake and cytotoxicity of cell-penetrating peptidomimetics with a-peptide/ß-peptoid backbone: effects of hydrogen bonding and a-chirality in the ß-peptoid residues. Biochim Biophys Acta. 2012;1818(11):2660-8.

25 Tseng Y, Mozumdar S, Huang L. Lipid-based systemic delivery of siRNA. Adv Drug Deliv Rev. 2009;61(9):721-31.

26 Han H, Lee A, Hwang T, Song C, Seong H, Hyun J, et al. Enhanced circulation time and antitumor activity of doxorubicin by comblike polymer-incorporated liposomes. J Control Release. 2007;120(3):161-8.

27 Akinc A, Zumbuehl A, Goldberg M, Leshchiner E, Busini V, Hossain N, et al. A combinatorial library of lipid-like materials for delivery of RNAi therapeutics. Nat Biotechnol. 2008;26(5):561-9.

28 Love K, Mahon K, Levins C, Whitehead K, Querbes W. Lipid-like materials for low-dose, in vivo gene silencing (vol 107, pg 1864, 2010). Proc Natl Acad Sci U S A. 2010;107(21):9915-.

29 Schumann RR, Leong SR, Flaggs GW, Gray PW, Wright SD, Mathison JC, et al. Structure and function of lipopolysaccharide binding protein. Science. 1990;249(4975):1429-31.

30 Vesy CJ, Kitchens RL, Wolfbauer G, Albers JJ, Munford RS. Lipopolysaccharide-binding protein and phospholipid transfer protein release lipopolysaccharides from gram-negative bacterial membranes. Infect Immun. 2000;68(5):2410-7.

31 Dentener MA, Vreugdenhil ACE, Hoet PHM, Vernooy JHJ, Nieman FHM, Heumann D, et al. Production of the acute-phase protein lipopolysaccharide-binding protein by respiratory type II epithelial cells: implications for local defense to bacterial endotoxins. Am J Respir Cell Mol Biol. 2000;23(2):146-53.

32 Liang W, Lam JKW. Endosomal Escape Pathways for Non-Viral Nucleic Acid Delivery Systems. In: Ceresa B, editor. Molecular Regulation of Endocytosis. InTech; 2012. p. Chapter 17.

33 Godbey WT, Wu KK, Mikos AG. Poly(ethylenimine) and its role in gene delivery. J Control Release. 1999;60(2-3):149-60.

34 BOUSSIF O, LEZOUALCH F, SCHERMAN D, Behr JP, Zanta MA, Mergny MD, et al. A versatile vector for gene and oligonucleotide transfer into cells in culture and in vivo: polyethylenimine. Proc Natl Acad Sci U S A. 1995;92(16):7297-301.

35 ZHOU X, HUANG L. DNA transfection mediated by cationic liposomes containing lipopolylysine: characterization and mechanism of action. Biochim Biophys Acta. 1994;1189(2):195-203.

36 Zelphati O, Szoka FC. Intracellular distribution and mechanism of delivery of oligonucleotides mediated by cationic lipids. Pharm Res. 1996;13(9):1367-72.

37 Zelphati O, Szoka FC. Mechanism of oligonucleotide release from cationic liposomes. Proc Natl Acad Sci U S A. 1996;93(21):11493-8.

38 Li J, Chen Y, Tseng Y, Mozumdar S, Huang L. Biodegradable calcium phosphate nanoparticle with lipid coating for systemic siRNA delivery. J Control Release. 2010;142(3):416-21.

39 Melikov K, Chernomordik LV. Arginine-rich cell penetrating peptides: from endosomal uptake to nuclear delivery. Cell Mol Life Sci. 2005;62(23):2739-49.

40 Palm C, Jayamanne M, Kjellander M, Hallbrink M, Hällbrink M. Peptide degradation is a critical determinant for cell-penetrating peptide uptake. Biochim Biophys Acta. 2007;1768(7):1769-76.

41 Kristensen M, Nielsen H. Cell-penetrating peptides as tools to enhance non-injectable delivery of biopharmaceuticals. Tissue Barriers. 2016;4(2):e1178369-.

42 Perrie Y, Mohammed A, Kirby D, McNeil S, Bramwell V. Vaccine adjuvant systems: enhancing the efficacy of sub-unit protein antigens. Int J Pharm. 2008;364(2):272-80.

[43] Waeckerle Men Y, Groettrup M. PLGA microspheres for improved antigen delivery to dendritic cells as cellular vaccines. Adv Drug Deliv Rev. 2005;57(3):475-82.

[44] Manicassamy S, Pulendran B. Modulation of adaptive immunity with Toll-like receptors. Semin Immunol. 2009 8;21(4):185-93.

[45] Kawai T, Akira S. The role of pattern-recognition receptors in innate immunity: update on Toll-like receptors. Nat Immunol. 2010;11(5):373-84.

[46] Kutzler M, Weiner D. DNA vaccines: ready for prime time? Nat Rev Genet. 2008;9(10):776-88.

[47] Wolff JA, Malone RW, Williams P, CHONG W, Acsadi G, Jani A, et al. Direct gene transfer into mouse muscle in vivo. Science. 1990;247(4949 Pt 1):1465-8.

[48] Levin C, Perrin H, Combadiere B. Tailored immunity by skin antigen-presenting cells. Hum Vaccin Immunother. 2015;11(1):27-36.

[49] Hirao L, Wu L, Khan A, Satishchandran A, Draghia Akli R, Weiner D. Intradermal/subcutaneous immunization by electroporation improves plasmid vaccine delivery and potency in pigs and rhesus macaques. Vaccine. 2008;26(3):440-8.

[50] Gopee N, Cui Y, Olson G, Warbritton A, Miller B, Couch L, et al. Response of mouse skin to tattooing: use of SKH-1 mice as a surrogate model for human tattooing. Toxicol Appl Pharmacol. 2005;209(2):145-58.

[51] Bins AD, Jorritsma A, Wolkers MC, Hung CF, Wu TC, Schumacher TNM, et al. A rapid and potent DNA vaccination strategy defined by in vivo monitoring of antigen expression. Nat Med. 2005;11(8):899-904.

[52] Pokorna D, Rubio I, Muller M. DNA-vaccination via tattooing induces stronger humoral and cellular immune responses than intramuscular delivery supported by molecular adjuvants. Genet Vaccines Ther. 2008 feb 7;6:4.

[53] Chiu Y, Sampson J, Jiang X, Zolla Pazner S, Kong X. Skin Tattooing As A Novel Approach For DNA Vaccine Delivery. Journal of Visualized Experiments (JoVE). 2012(68).

[54] Stevenson F, Rice J, Ottensmeier C, Thirdborough S, Zhu D. DNA fusion gene vaccines against cancer: from the laboratory to the clinic. Immunol Rev. 2004;199(1):156-80.

[55] Panina-Bordignon P, Tan A, Termijtelen A, Demotz S, Corradin G, Lanzavecchia A. Universally immunogenic T cell epitopes: promiscuous binding to human MHC class II and promiscuous recognition by T cells. Eur J Immunol. 1989;19(12):2237-42.

[56] Oosterhuis K, Aleyd E, Vrijland K, Schumacher T, Haanen J. Rational design of DNA vaccines for the induction of human papillomavirus type 16 E6- and E7-specific cytotoxic T-cell responses. Hum Gene Ther. 2012;23(12):1301-12.

[57] Ebstein F, Lehmann A, Kloetzel P. The FAT10- and ubiquitin-dependent degradation machineries exhibit common and distinct requirements for MHC class I antigen presentation. Cell Mol Life Sci. 2012;69(14):2443-54.

[58] van der Maaden K, Jiskoot W, Bouwstra J. Microneedle technologies for (trans)dermal drug and vaccine delivery. J Control Release. 2012;161(2):645-55.

[59] Kim Y, Park J, Prausnitz M. Microneedles for drug and vaccine delivery. Adv Drug Deliv Rev. 2012;64(14):1547-68.

[60] Larraneta E, McCrudden MTC, Courtenay A, Donnelly R, Larrañeta E. Microneedles: A New Frontier in Nanomedicine Delivery. Pharm Res. 2016;33(5):1055-73.

[61] van der Maaden K, Luttge R, Vos P, Bouwstra J, Kersten G, Ploemen I. Microneedle-based drug and vaccine delivery via nanoporous microneedle arrays. Drug Deliv Transl Res. 2015;5(4):397-406.

[62] Quinn H, Kearney M, Courtenay A, McCrudden MTC, Donnelly R. The role of microneedles for drug and vaccine delivery. Expert Opin Drug Deliv. 2014;11(11):1769-80.

[63] Van Der Maaden K, Trietsch SJ, Kraan H, Varypataki EM, Romeijn S, Zwier R, et al. Novel hollow microneedle technology for depth-controlled microinjection-mediated dermal vaccination: A study with polio vaccine in rats. Pharm Res. 2014;31(7):1846-54.

[64] Schipper P, van der Maaden K, Romeijn S, Oomens C, Kersten G, Bouwstra J, et al. Determination of Depth-Dependent Intradermal Immunogenicity of Adjuvanted Inactivated Polio Vaccine Delivered by Microinjections via Hollow Microneedles. Pharm Res. 2016;33(9):2269-79.

65 Schipper P, van der Maaden K, Romeijn S, Oomens C, Kersten G, Jiskoot W, et al. Repeated fractional intradermal dosing of an inactivated polio vaccine by a single hollow microneedle leads to superior immune responses. J Control Release. 2016.

66 Beran J, Ambrozaitis A, Laiskonis A, Mickuviene N, Bacart P, Calozet Y, et al. Intradermal influenza vaccination of healthy adults using a new microinjection system: a 3-year randomised controlled safety and immunogenicity trial. BMC Med. 2009;7:13-.

67 Gill H, Prausnitz M. Coated microneedles for transdermal delivery. J Control Release. 2007;117(2):227-37.

68 Matriano J, Cormier M, Johnson J, Young W, Buttery M, Nyam K, et al. Macroflux microprojection array patch technology: a new and efficient approach for intracutaneous immunization. Pharm Res. 2002;19(1):63-70.

69 Cormier M, Johnson B, Ameri M, Nyam K, Libiran L, Zhang D, et al. Transdermal delivery of desmopressin using a coated microneedle array patch system. J Control Release. 2004;97(3):503-11.

70 Chen X, Prow T, Crichton M, Jenkins DWK, Roberts M, Frazer I. Dry-coated microprojection array patches for targeted delivery of immunotherapeutics to the skin. J Control Release. 2009;139(3):212-20.

71 Kim Y, Quan F, Compans R, Kang S, Prausnitz M. Formulation and coating of microneedles with inactivated influenza virus to improve vaccine stability and immunogenicity. J Control Release. 2010;142(2):187-95.

72 Raphael A, Crichton M, Chen X, Fernando GJP, Prow T. Targeted, needle-free vaccinations in skin using multilayered, densely-packed dissolving microprojection arrays. Small. 2010;6(16):1785-93.

73 Sullivan S, Koutsonanos D, Del Pilar Martin M, Lee J, Zarnitsyn V, Compans RW, et al. Dissolving polymer microneedle patches for influenza vaccination. Nat Med. 2010;16(8):915-20.

74 Wendorf J, Ghartey Tagoe E, Williams S, Enioutina E, Singh P, Cleary G. Transdermal delivery of macromolecules using solid-state biodegradable microstructures. Pharm Res. 2011;28(1):22-30.

75 Park J, Allen M, Prausnitz M. Polymer microneedles for controlled-release drug delivery. Pharm Res. 2006;23(5):1008-19.

76 Kim M, Jung B, Park J. Hydrogel swelling as a trigger to release biodegradable polymer microneedles in skin. Biomaterials. 2012;33(2):668-78.

77 Fukushima K, Ise A, Morita H, Hasegawa R, Ito Y, Sugioka N, et al. Two-layered dissolving microneedles for percutaneous delivery of peptide/protein drugs in rats. Pharm Res. 2011;28(1):7-21.

78 Chu L, Choi S, Prausnitz M. Fabrication of dissolving polymer microneedles for controlled drug encapsulation and delivery: Bubble and pedestal microneedle designs. J Pharm Sci. 2010;99(10):4228-38.

79 Liu L, Kai H, Nagamine K, Ogawa Y, Nishizawa M. Porous polymer microneedles with interconnecting microchannels for rapid fluid transport. RSC Advances. 2016;6(54):48630-5.

80 Bystrova S, Luttge R. Micromolding for ceramic microneedle arrays. Microelectronic Engineering. 2011 8;88(8):1681-4.

81 Verhoeven M, Bystrova S, Winnubst L, Qureshi H, de Gruijl T. Applying ceramic nanoporous microneedle arrays as a transport interface in egg plants and an ex-vivo human skin model. Microelectronic engineering. 2012;98:659-62.

82 Ji J, Tay FEH, Miao J, Iliescu C. Microfabricated microneedle with porous tip for drug delivery. J Micromech Microengineering. 2006;16(5):958-64.

83 Klyshko A, Balucani M, Ferrari A. Mechanical strength of porous silicon and its possible applications. Superlattices and microstructures. 2008;44(4-5):374-7.

84 Shen H, Ackerman A, Cody V, Giodini A, Hinson E, Cresswell P, et al. Enhanced and prolonged cross-presentation following endosomal escape of exogenous antigens encapsulated in biodegradable nanoparticles. Immunology. 2006;117(1):78-88.

85 Bal S, Slutter B, Jiskoot W, Bouwstra J, Slütter B. Small is beautiful: N-trimethyl chitosan-ovalbumin conjugates for microneedle-based transcutaneous immunisation. Vaccine. 2011;29(23):4025-32.

86 Kumar A, Li X, Sandoval M, Rodriguez BL, Sloat B. Permeation of antigen protein-conjugated nanoparticles and live bacteria through microneedle-treated mouse skin. International journal of nanomedicine. 2011;6.

[87] Kumar A, Wonganan P, Sandoval M, Li X, Zhu S, Cui Z. Microneedle-mediated transcutaneous immunization with plasmid DNA coated on cationic PLGA nanoparticles. J Control Release. 2012;163(2):230-9.

[88] McCaffrey J, McCrudden C, Ali A, Massey A, McBride J, McCarthy HO, et al. Transcending epithelial and intracellular biological barriers; a prototype DNA delivery device. J Control Release. 2016;226:238-47.

[89] Demuth PC, Garcia-Beltran WF, Ai-Ling ML, Hammond PT, Irvine DJ. Composite dissolving microneedles for coordinated control of antigen and adjuvant delivery kinetics in transcutaneous vaccination. Advanced Functional Materials. 2013;23(2):161-72.

[90] Zaric M, Lyubomska O, Touzelet O, Poux C, Al Zahrani S, Fay F, et al. Skin dendritic cell targeting via microneedle arrays laden with antigen-encapsulated poly-D,L-lactide-co-glycolide nanoparticles induces efficient antitumor and antiviral immune responses. ACS Nano. 2013;7(3):2042-55.

[91] Fehres C, Garcia Vallejo J, Unger WWJ, van Kooyk Y. Skin-resident antigen-presenting cells: instruction manual for vaccine development. Front Immunol. 2013;4:157-.

[92] Zaric M, Lyubomska O, Poux C, Hanna ML, McCrudden MT, Malissen B, et al. Dissolving microneedle delivery of nanoparticle-encapsulated antigen elicits efficient cross-priming and th1 immune responses by murine langerhans cells. J Invest Dermatol. 2015;135(2):425-34.

[93] Varypataki E, van der Maaden K, Bouwstra J, Ossendorp F, Jiskoot W. Cationic liposomes loaded with a synthetic long peptide and poly(I:C): a defined adjuvanted vaccine for induction of antigen-specific T cell cytotoxicity. AAPS J. 2015;17(1):216-26.

[94] Weldon W, Zarnitsyn V, Esser ES, Taherbhai M, Koutsonanos D, Vassilieva E, et al. Effect of adjuvants on responses to skin immunization by microneedles coated with influenza subunit vaccine. PLoS ONE. 2012;7(7):e41501-.

9

Addendum

- **Abbreviations**
- **Samenvatting in het Nederlands**
- **Dankwoord / Acknowledgements**
- **CV**
- **List of publications**

Abbreviations

ADA	anti-drug antibody
AP1	activator protein 1
APC	antigen presenting cell
BM-APC	bone marrow derived APC
BP	biopharmaceutical
CD	cluster of differentiation
DDS	drug delivery system
dLN	draining lymph node
DNA	deoxyribonucleic acid
DOTAP	dioleoyl trimethylammonium propane
DT	diphtheria toxin
DTP	diphtheria, tetanus, polio vaccine
ID	intradermal injection
IgG	immunoglobulin G
IMQ	imiquimod
LBP	LPS binding protein
Lf	limits of flocculation
LPN	lipid-polymer hybrid nanoparticle
LPS	lipopolysaccharide
MHC	major histocompatibility complex
MNA	microneedle array
NFkB	nuclear factor kappa-light-chain-enhancer of activated B cells
NP	nanoparticle
npMNA	nanoporous MNA
pAPC	professional antigen presenting cell
PLGA	poly(DL-lactic-co-glycolic acid)
PRR	pathogen recognition receptor
PTH	parathyroid hormone
RNA	ribonucleic acid
SC	subcutaneous injection
siRNA	small interfering RNA
SNALP	stable nucleic acid lipid particles
TLR	Toll-like Receptor
TNFa	tumor necrosis factor alfa
TT	tetanus toxin

Aflevering en immunogeniciteit van biofarmaceutica voor vaccinatie en voor therapie

Al het leven bestaat uit kleine cellen; dit kan één cel zijn (zoals sommige bacteriën) of miljarden cellen (zoals mensen). De bouwstenen van cellen worden eiwitten genoemd en deze bestaan er in vele soorten en maten. Het DNA in de cel bevat de codering voor al deze eiwitten. Wanneer eiwitten en DNA-structuren gebuikt worden als medicijn om processen in de cel aan te passen spreek je van biofarmaceutica: biologisch verwante farmaceutica gebruikt als medicijnen.

Dit proefschrift beschrijft het onderzoek naar zowel de aflevering van biofarmaceutische eiwitten en DNA-structuren in het lichaam, als naar de potentie van deze biofarmaceutische eiwitten en DNA-structuren om het afweersysteem te activeren (immunogeniciteit). Activatie van het afweersysteem is handig als je deze eiwitten en DNA-structuren wilt gebruiken voor vaccinatiedoeleinden, maar als je ze wilt gebruiken als medicijn of therapie is het niet handig en soms zelf gevaarlijk als ze worden herkend en opgeruimd door het afweersysteem.

Deel 1: Huidvaccinatie

Deel 1 van dit proefschrift focust specifiek op het gebruik van biofarmaceutica voor vaccinatie, in het bijzonder huidvaccinatie. De meeste, reeds bestaande vaccins worden afgeleverd met een spuit en naald in de spier of subcutaan (net onder de huid in het bindweefsel). De huid biedt zelf echter ook veel mogelijkheden voor het inbrengen van vaccinaties. De huid is erg groot en makkelijk bereikbaar, maar bevat bovenal veel sensorische afweercellen. Dit zijn cellen die de omgeving screenen op lichaamsvreemde stoffen en deze stoffen afvoeren om te voorkomen dat we ziek worden. Zo zal een goed sensorisch systeem er bij een klein wondje voor zorgen dat je geen infectie krijgt. Natuurlijk kunnen we bij vaccinaties ook gebruik maken van deze sensorische cellen in de huid. Als deze sensorische cellen namelijk kleine hoeveelheden ziekteverwekker tegenkomen, kunnen ze een afweergeheugen helpen opbouwen en kan er sneller toegeslagen worden wanneer er een gevaarlijke hoeveelheid ziekteverwekker het lichaam binnenkomt.

Om deze sensorische cellen te bereiken moet echter eerst het buitenste laagje van de huid (het stratum corneum) omzeild worden, bijvoorbeeld door daar met een naaldstructuur doorheen te prikken. Voor huidvaccinaties moet de naald lang en sterk genoeg zijn om door de bovenste laag te prikken zonder dat de huid meebuigt, maar kort genoeg om in de huid te blijven en niet door te dringen naar het bindweefsel. In de huid zitten immers de meeste sensorische afweer cellen. Bovendien bereik je op deze manier ook de pijnsensoren niet. Deze korte naalden worden micronaalden genoemd, omdat ze een lengte hebben van honderden micrometers, maar kleiner dan een millimeter. Wanneer de naald door de bovenste laag heen heeft geprikt, kan het vaccin de huid binnendringen.

Hier kunnen de sensorische cellen de kleine stukjes ziekteverwekker herkennen en meenemen naar de lymfeknopen. In de lymfeknopen wordt vervolgens ziekteverwekker-specifieke immuniteit verworven, door het activeren van verschillende componenten van het immuunsysteem, waaronder de productie van antistoffen, maar ook de activatie van cellen die geïnfecteerde cellen kunnen doden (killercellen) en cellen die bij deze processen kunnen helpen (helpercellen). Deze specifieke afweerspelers zorgen voor de opruiming van de ziekteverwekker bij een mogelijke volgende keer dat deze het lichaam binnendringt. Er wordt in de wetenschap onderzoek gedaan naar meerdere soorten micronaalden. Deze kunnen verschillen in materiaal, sterkte, lengte, werkwijze en allerlei andere variabelen. En alhoewel een aantal naalden al wel veelbelovende antistoffen in diermodellen kan opwekken na vaccinatie, is er nog geen micronaald op de markt voor het vaccineren van mensen. In dit proefschrift dragen wij bij aan het vaststellen van het optimaal gebruik van deze micronaalden en onderzoeken wij de werking van de geïnduceerde afweerreactie.

Dit proefschrift:

In **hoofdstuk 2** wordt een nieuw type micronaald ontwikkeld, beschreven en toegepast: de nanoporeuze micronaald. De naalden die ontwikkeld zijn bestaan uit keramisch, poreus materiaal genaamd alumina, waar in de holtes van het materiaal het vaccin kan worden opgenomen. In dit hoofdstuk laten we zien dat deze naaldjes beladen kunnen worden met eiwitten van de difteriebacterie (difterietoxine) en de tetanusbacterie (tetanustoxine), eiwitten die ook in de humane vaccins worden gebruikt. De dosis die achterblijft in de huid nadat de naaldjes door de huid zijn geprikt en daar 20 minuten hebben gezeten is bepaald. Bovendien laten we de succesvolle productie van antistoffen zien in een muismodel na huidvaccinatie met deze beladen micronaalden. De huidvaccinatie met micronaalden induceert net zoveel antistoffen als de subcutane vaccinatie in het bindweefsel. Dit laat de potentie van dit nieuwe type nanoporeuze micronaalden zien.

In **hoofdstuk 3** is er minder gefocust op de inductie van antistoffen, maar juist op de inductie van immuuncellen, zowel helpercellen als killercellen. Voor de bescherming tegen en opruiming van ziekteverwekkers die zich in de cel bevinden (zoals virussen of een aantal specifieke bacteriën) is de aanwezigheid van specifieke killercellen nodig. Dit in tegenstelling tot ziekteverwekkers buiten de cel (het grootste deel van de bacteriën), waar met name de aanwezigheid van de eerder genoemde antistoffen nodig zijn voor bescherming. Voor de activatie van deze killercellen (CD8 T cellen) is het nodig dat de vaccineiwitten ook in de cel terechtkomen. Dit gebeurt met eiwitten niet vanzelf en hiervoor kan gebruik gemaakt worden van nanopartikels. Dit zijn structuren die als envelopje kunnen fungeren voor de eiwitten die gebruikt worden als vaccin, zodat deze door de wand van de cel afgeleverd kunnen worden in de cel. In dit hoofdstuk hebben we het modelvaccin OVA gebruikt en deze geladen in nanopartikels gemaakt van de stof PLGA. Deze partikels zijn via micronaalden ingebracht in de huid van muizen.

Het gebruikte naaldtype is de holle micronaald, welke in structuur het meest lijkt op een traditionele naald, maar dan op microschaal. Na vaccinatie werden inderdaad killercellen gevonden specifiek voor de vaccineiwitten. Bovendien ontwikkelden de muizen die gevaccineerd zijn met een combinatie van het vaccineiwit en een hulpstof in de PLGA-envelopjes een bepaalde groep aan killercellen die bescherming bood tegen de bacterie waar het vaccineiwit van afkomstig was. Dit hoofdstuk laat de toepasbaarheid van deze PLGA-envelopjes zien in huidvaccinatie.

In **hoofdstuk 4** wordt ook huidvaccinatie bestudeerd, maar nu vaccinaties gebaseerd op DNA. Als DNA afgeleverd wordt in de huid, dan zal een groep huidcellen dit DNA omzetten in eiwitten. Vervolgens worden deze eiwitten in stukjes geknipt door de sensorische cellen van het afweersysteem, alvorens ze aan de uitvoerende cellen van het afweersysteem worden gepresenteerd. In hoofdstuk 4 worden manieren voorgesteld om het in stukjes knippen van de vaccineiwitten efficiënter te maken. Op twee manieren is geprobeerd om de 'schaar' in de cel makkelijker en efficiënter het interessante stukje van het vaccin uit te laten knippen: de ene manier is het aanpassen van de stukken die net naast het interessante deel van het vaccin zitten; de andere manier is het toevoegen van extra DNA van een hulpeiwitaan het vaccin. Beide manieren resulteerden in meer ziekteverwekker-specifieke killer (CD8 T) cellen.

Deel 2: Immunogeniciteit bij therapeutisch gebruik

Deel 2 van het proefschrift gaat over het gebruik van biofarmaceutica voor therapeutisch gebruik. Een groot deel van deze medicijnen heeft pas therapeutisch effect, wanneer ze in de cel worden afgeleverd. Eerder genoemde afleveringssystemen, zoals nanopartikels, kunnen biofarmaceutica door de wand van de cel brengen en in de cel afleveren. Een nadeel van deze nanopartikels is echter dat ze sneller worden gezien als lichaamsvreemd, dus als niet van de mens zelf. Indien dit gebeurt, kan het afweersysteem een afweerreactie op gang brengen. Deze afweerreactie kan meerdere effecten op het medicijn hebben: het kan zorgen voor verminderde beschikbaarheid van het biofarmaceuticum doordat deze wordt opgeruimd door het afweersysteem, maar er kunnen ook hevige bijwerkingen ontstaan door een misplaatste, acute afweerreactie. Het is dus erg belangrijk dat van tevoren wordt bepaald of er een risico is op het activeren van het afweersysteem (immunogeniciteit). Het is wettelijk verplicht om dit in klinische studies bij mensen te onderzoeken voordat een medicijn op de markt mag worden gebracht. Omdat het niet haalbaar is om voor alle potentiële kandidaatmedicijn in de onderzoekspijplijn een klinische studie op te zetten, is het testen van immunogeniciteit in een eerder stadium wenselijk, bijvoorbeeld door gebruik te maken van diermodellen. Het onderzoeken van medicijnen *in vivo* (zoals in diermodellen, *in vivo* = in levenden) kan duidelijkheid verschaffen in verschillende processen, zoals de distributie van het middel door het lichaam, de effectiviteit van het medicijn en ook de immunogeniciteit van de biofarmaceutica. Echter, ook voor dit type

onderzoek geldt dat het ethisch, tijdtechnisch en financieel niet mogelijk is om te testen voor alle biofarmaceutica uit elke optimalisatiestap binnen de medicijnontwikkeling. Het nóg vroeger kunnen identificeren van mogelijke risico's is daarom noodzakelijk. Het gebruik van proefopzetten in het laboratorium, ook wel *in vitro* experimenten genoemd (*in vitro* = in glas (plastic)), als eerste linie voor de beoordeling van immunogeniciteit is daarom een uitkomst. Effecten van de biofarmaceutica op het gehele, complexe afweersysteem zijn moeilijk na te bootsen *in vitro*. De effecten op het activeren van de initiële sensorische afweercellen kunnen echter wel worden nagebootst. Op deze manier kunnen prominente kandidaatmedicijnen vroeg worden geselecteerd voor verder onderzoek.

Dit proefschrift:

In hoofdstukken 5-7 worden drie verschillende afleveringssystemen ontwikkeld. Naast de ontwikkeling door farmaceutisch georiënteerde partneronderzoekers, zijn deze afleveringssystemen beoordeeld op de mate waarin ze de sensorische cellen van het immuunsysteem kunnen activeren. De sensorische cellen van het afweersysteem kunnen lichaamsvreemde stoffen herkennen via receptoren aan de buitenkant van de cel. Als de sensorisch cel een stof inderdaad als lichaamsvreemd beoordeelt, dan zal de cel een transformatie ondergaan waarin er nieuwe markers op de oppervlakte verschijnen en er kleine signaalstofjes worden uitgescheiden door de cel. Via twee type *in vitro* experimenten kan de activatie van deze sensorische afweercellen worden geanalyseerd; het eerste type is de TLR-proef, waarbij gekeken wordt naar de activatie van de specifieke 'TLR'-receptoren die op het celoppervlak zitten; een tweede proef is de APC-proef, waarbij naar de transformatie van de sensorische afweercel (APC) wordt gekeken.

In **hoofdstuk 6 en 7** worden twee nieuwe afleveringssystemen voor therapeutische medicijnen onderzocht en beschreven. Deze afleveringssystemen lieten volledige immuun-compatibiliteit zien, wat wil zeggen dat deze afleveringssystemen dezelfde immunogeniciteit vertonen als het medicijn zelf. In hoofdstuk 6 wordt een afleverings-systeem bestemd voor de aflevering van DNA-structuren beschreven dat bestaat uit peptide-polymeer hybride nanopartikels die als envelopjes fungeren. In hoofdstuk 7 wordt gebruik gemaakt van verschillende peptiden (stukjes eiwit) die door de wand van de cel kunnen dringen voor de aflevering van therapeutische hormonen. In **hoofdstuk 5** werd een elders beschreven lipide-polymeer hybride combinatie gebruikt voor de afgifte van de DNA-structuren. Behalve dat het lipidedeel van deze envelop resulteerde in de activatie van de TLR-receptor (een nieuwe bevinding op zichzelf), laat hoofdstuk 5 ook zien dat het combineren van de lipidestructuren met een polymeer in een hybride partikel resulteerde in immuuncompatibiliteit van het afleveringssysteem. In deze hoofdstukken worden dus drie verschillende afleveringssystemen beschreven met lage immunogeniciteit.

Tot slot:

In dit proefschrift hebben we bijgedragen aan het vaststellen van het optimaal gebruik van nieuwe micronaalden voor vaccinatie in de huid. Hierbij blijken nanoporeuze micronaalden een geschikte optie voor vaccinatie met subunit vaccins. Daarnaast hebben we beoordeeld dat nanopartikels van toevoeging kunnen zijn in huidvaccinatie, waarbij ook naar de werking en verdeling van de geïnduceerde afweerrespons gekeken.

Verder is er onderzocht dat drie nieuwe afleveringssystemen voor biofarmaceutica lage immunogeniciteit vertonen en daarmee immuuncompatibel zijn. Op deze manier kunnen prominente kandidaatvaccins vroeg worden geselecteerd voor verder onderzoek.

Dankwoord / Acknowledgements

Aan het einde van het hele traject neem ik graag de mogelijkheid om iedereen te bedanken voor de bijdrages aan dit proefschrift.

Als allereerste **Alice**, bedankt voor eigenlijk alles. Maar specifiek je kunde! En ook je bereikbaarheid en je snelheid. En als we het werk even zat waren, de gezellige verhalen over thuis. Dank je voor de mogelijkheid om in Utrecht te komen werken en vooral de samenwerking. En daarbij wil ik natuurlijk ook **Femke** en **Willem** bedanken voor de mogelijkheid, de begeleiding. Femke, ook voor het weten wat je wanneer moet zeggen. Jij kunt zowel relativeren als aanmoedigen tegelijkertijd. En Willem voor het zijn van mijn promotor en de mogelijkheid tot promoveren en daarbij je optimisme.

Ik zou ook graag alle leden van mijn **beoordelingscommissie** bedanken. Prof.dr. Wim Jiskoot, prof.dr. Henk Haagsman, prof.dr. Aletta Kraneveld, prof.dr. Marca Wauben en dr. Enrico Mastrobattista: dank voor het investeren van tijd en moeite in het lezen en beoordelen van mijn proefschrift. En wat een voorrecht dat ik met de meeste van jullie op een manier (buiten het proefschrift) heb mogen samenwerken. En ook dank aan de extra leden van mijn **promotiecommissie**.

De grote stapel aan samenwerkingen die ik aanging, die op mijn pad kwamen of die mij aangeboden werden, waren allemaal, naast een logistieke en mentale uitdaging, ontzettend leuk om te doen. Al deze samenwerkingen zorgden ervoor dat ik over een heel breed gebied allerlei dingen heb mogen leren, maar bovenal dat ik ontzettend veel mensen heb ontmoet en die zou ik hier graag voor willen bedanken.

The research was conducted in the COMPACT consortium. I would like to thank the whole **consortium**. And more specific, special thanks for both **Steve** and **Arwyn** as leaders from WP3 with the longest and still most efficient TC's. I learned many things in WP3. Also a thank you to **Claus-Michael**, van het zeer gezellige WP6, waar de F2F in Noorwegen me nog lang bij zal blijven. En natuurlijk dank aan **Enrico**, niet alleen als academisch leider van het consortium, maar ook als Team Utrecht. Daarnaast ook de COMPACT samenwerkingen met Copenhagen en Leiden. From Copenhagen, I would particularly like to thank **Kaushik** and **Camilla**: thanks for the fruitful collaboration described in chapter 5. From Leiden, thanks to **Juha** and **Joke**, with later on much help from **Guangsheng**. Thank you all for the very pleasant collaboration. After long days of T cell transfers, I was pleased to perfect my anaesthetic skills while you managed the scary buttons, and I was happy to handle them myself in the last few (well actually quite many) experiments. Thanks for the collaboration in Chapter 3. Binnen COMPACT had ik ook lotgenoten, de mede AiO's. **Erik**, **Neda, Steffi** en **Remi**, dank jullie wel voor de gezelligheid en morele ondersteuning tijdens de COMPACT meetings. En soms toevallig nog een co-publicatie! Maar ook nog andere COMPACT members, o.a. **Mie**, **Stine** and **Xianghui**: many thanks for the collaborations in chapter 6 and 7.

Ook buiten COMPACT bleken mijn TLR's een basis voor vruchtbare grond. **Maarten, Jan-Jaap** en **Marijke**; wat ben ik blij en trots dat ik heb kunnen bijdragen aan jullie mooie manuscripten. Ik heb ontzettend veel van jullie en jullie onderwerpen geleerd; van moedermelk tot ijzer, tot smerige bacteriën, ik voel me bijna een echte all rounder. Dank voor de samenwerkingen en zeker ook de gezelligheid.

En het laatste adoptiepaper waar ik veel van geleerd heb en een erg prettige samenwerking heb gehad. **Koen**, bedankt voor die fijne productieve samenwerking.

Ik heb bij de Immuno's van de UU een heerlijke tijd gehad waar ik ook veel mensen graag wil bedanken. Als eerste de alumni SAIO's **Anouk, Lindert, Susan** en **Evelien**. We hebben veel gezelligheid gehad samen: lunchen, congressen, borrels, feestjes en tennispartijtjes. En hartstikke handig om even af te mogen kijken! Bedankt! Maar ook de huidige SAIO's **Manon, Peter, Charlotte, New, Andreja** en **Irene**. Een hoop gezelligheid, borrels, gespreken en koffiewandelingetjes. En natuurlijk ook de andere **sAiO's** op het lab! Allemaal veel succes met het afronden en bedankt!

Bedankt analisten uit de groep en daarbij zeker **Irene** en **Peter** voor de kennis, hulp en gezelligheid die daarbij gepaard ging. **Daphne**, na 5 jaar kamergenoot nog nooit een werkinhoudelijk gesprek gehad (best knap), maar des te meer gezelligheid! Even omdraaien om bij te kletsen schoot toch vaak door in een lang gesprek. Beste labuitje ever, toch **Ruurd**?! En natuurlijk dankjewel aan alle anderen van de **Immuno-afdeling** voor de leuke tijd. Doen jullie voorzichtig met de tosti's?

En mijn studententeam: **Tom**, **Laura** en **Djai**. Wat was ik blij dat jullie mij kwamen helpen met de DDS'en testen. Karaoke met pizza, taart en tompoucen of een halve liter Bullit. Ik heb veel van jullie geleerd en hopelijk jullie ook wat van mij. Maar vooral was het ook erg gezellig. Veel succes bij jullie eigen loopbanen.

En ook bedankt aan de I&I boefjes **Bart** en **Annemarie**. Oei Oei Oei, leren valsspelen van de beste. Dank voor de burgers, biertjes en bovenal lol. Gelukkig hebben we de foto's nog!

Naast alle vakinhoudelijke hulp en support is er buiten de wetenschap ook een hoop steun geweest. En ik zou ook graag alle lieve vrienden bedanken voor het plezier en de steun in de afgelopen tijd. Natuurlijk de **Otto's** voor alle gezelligheid, verkleedpartijen en vooral de groepsdruk! Werd ik daar bijna de grote roze verliezer van het promotiespel. En graag willen we ook deodorant en de toiletten bedanken voor de nodige afleiding. Oh nee, verkeerde dankwoord. Bedankt Ali, Birk, Emma, Stephan en Wouter! Bedankt ook aan **Bestuur 08-09**. Met wassende manen en saunabezoekjes werd de (bio)medische taal afgewisseld. Dank voor de support. En thanks **Negens en Nivten**, volgend weekend weer bij mij?! Trouwens, dips op spelen met zwart. Ook **Willeke, Lisanne** en **Jasper**, thanks voor de vriendschap en dank jullie voor jullie interesse en steun in dat rare onderzoek.

Lieve **Mam** en **Pap**, dank jullie wel voor jullie mateloze vertrouwen en optimisme. Zelfs als ik geen zin had om uit te wijden bleven jullie geïnteresseerd. En bereid om even op en neer naar de Uithof te gaan, zondag of niet. Ook dank jullie wel **Opa** en **Oma**, **Meike** en **Irene**. Ik hoop dat hoofdstuk 9 wat inzicht geeft in het werk van de afgelopen jaren.

En bijna als laatste mijn paranimfen! **Emma** en **Anouk**, wat fijn dat jullie mij willen begeleiden en ondersteunen op de laatste dag van mijn PhD. Anouk, vanaf dag 1 waren we kamergenootjes, groepsgenootjes, labgenootjes, lotgenootjes. Dat gaat uiteraard gepaard met een opgebouwde vriendschap en veel gezelligheid. Waar het begon als analistje spelen bij elkaars experimenten (die 1e tattoo, ik weet het nog goed), hebben we ook geprobeerd samenwerkingen op te zetten. Waar die initieel niet zo van de grond kwamen, sta je uiteindelijk toch mooi op drie van de zes hoofdstukken als auteur! Emma, bedankt eigenlijk voor de algemene vriendschap al meer dan 10 jaar. Maar uiteraard ook specifiek de laatste jaren waar dat op werk gerelateerd vlak ook extra intensief werd. De overstap naar Utrecht maakte de frequentie nog hoger. Dank je wel voor je werkinhoudelijk bijdrage, je statistiekhulp, het thuiswerken met Leo en zeker de stok achter de deur. 't Is weer tijd voor koffie, bij jou of bij mij dit keer?

Als allerlaatste lieve **Karel**. Promoveren doe je niet alleen, en zonder jou had ik het gewoonweg niet gekund of gered. Dank je wel loef, voor alles.

Curriculum Vitae

Anne Marit de Groot was born on June 2nd, 1988 in Naarden, The Netherlands. In September 2006 she started her university education at the VU University in Amsterdam. In 2010 she obtained her Bachelor of Science degree in biomedical sciences. In 2012 she obtained her Master of Science degree in biomedical sciences with the specialisation Infectious Diseases and the specialisation Immunology. During her masters she conducted an internship in 2010 at the VU medical centre at the department of Medical Microbiology and Infection Prevention under supervision of prof. dr. Wilbert Bitter on the characterization of a chaperone protein for the type VII protein secretion pathway. In 2011, she conducted an internship at Sanquin – Research at the department of Blood Cell Research in the group of prof. dr. Taco Kuijpers on a splice variant of Fcγ-Receptors. And she performed a final literature thesis in 2012 at Academic Medical Centre in Amsterdam at the department of Experimental Virology on immunology of HIV vaccine clinical trials. In August 2012, she started as a PhD candidate at Utrecht University at the department of Infectious diseases and Immunology in the group of prof. dr. Willem van Eden in the lab of dr. Alice J.A.M. Sijts and also under supervision of dr. Femke Broere. She studied the delivery and immunogenicity of biopharmaceuticals and drug delivery systems. This with a goal of application for both vaccination and therapeutic use. The research conducted during her PhD is described in this thesis.

List of Publications

Zonneveld MI, Fernandez-Gutierrez M*, **de Groot AM*,** van Herwijnen MJC, Kleinjan M, Capel T, Sijts EJAM, Taams LS, Garssen J, de Jong EC, Klerebezem M, Nolte-'t Hoen ENM, Redegeld FA, Wauben MHM, *Maternal EV delivered via milk create a window of opportunity for the regulated development of the infant gastrointestinal tract and immune system,* to be submitted

de Groot AM*, Platteel ACM*, Kuijt N, Kooten PJS, Vos, PJ, Sijts EJAM, van der Maaden K, *Nanoporous microneedle arrays to efficiently induce antibody responses against diphtheria and tetanus toxoid,* in review

de Groot AM*, Thanki K*, Gangloff M, Falkenberg E, Zeng X, van Bijnen DCJ, van Eden W, Frankzyk H, Nielsen HM, Broere F, Gay NJ, Foged C, Sijts EJAM, *Overcoming lipidoid-mediated TLR4 activation with lipidoid-polymer nanoparticles:* In silico *modelling and* in vitro *test,* in review

de Groot AM*, Du G*, Mönkäre J, Platteel ACM, Broere F, Bouwstra JA, Sijts EJAM, *Hollow microneedle-mediated intradermal delivery of model vaccine antigen-loaded PLGA nanoparticles elicits protective T cell-mediated immunity to an intracellular bacterium,* Journal of Controlled Release, 28 November 2017, 266:27-35

Coorens M, Schneider VAF, **de Groot AM**, van Dijk A, Meijerink M, Wells J, Scheenstra M, Veldhuizen EJA, Haagsman HP, *Cathelicidins inhibit E. coli-induced TLR2 and TLR4 activation in a viability-dependent manner.* J Immunol. 2017 Aug 15;199(4):1418-1428

Verhoef JJF, **de Groot AM**, van Moorsel M, Ritsema J, Beztsinna N, Maas C, Schellekens H*, Iron nanomedicines induce Toll-like receptor activation, cytokine production and complement activation*, Biomaterials. 2017 march; 119:68-77

Platteel ACM, **de Groot AM**, Keller C, Andersen P, Ovaa H, Kloetzel PM, Mishto M, Sijts EJAM *Strategies to enhance immunogenicity of cDNA vaccine encoded antigens by modulation of antigen processing* Vaccine. 2016 sept 30; 34 (42):5132-5140

Zeng X, **de Groot AM**, Sijts AJ, Broere F, Oude Blenke E, Colombo S, van Eden W, Franzyk H, Nielsen HM, Foged C. *Surface coating of siRNA-peptidomimetic nano-self-assemblies with anionic lipid bilayers: enhanced gene silencing and reduced adverse effects in vitro* Nanoscale. 2015 Nov 19;7(46):19687-98.

Kristensen M, **de Groot AM**, Berthelsen J, Franzyk H, Sijts A, Nielsen HM. *Conjugation of cell-penetrating peptides to parathyroid hormone affects its structure, potency, and transepithelial permeation*. Bioconjug Chem. 2015 Mar 18;26(3):477-88

Barberá A, Lorenzo N, Garrido G, Mazola Y, Falcón V, Torres AM, Hernández MI, Hernández MV, Margry B, **de Groot AM**, van Roon J, van der Zee R, Broere F, van Eden W, Padrón G, Domínguez Mdel C. *APL-1, an altered peptide ligand derived from human heat-shock protein 60, selectively induces apoptosis in activated CD4+ CD25+ T cells from peripheral blood of rheumatoid arthritis patients.* Int Immunopharmacol. 2013 Dec;17(4):1075-83.

Daleke MH*, van der Woude AD*, Parret AH, Ummels R, **de Groot AM**, Watson D, Piersma SR, Jiménez CR, Luirink J, Bitter W, Houben EN. *Specific chaperones for the type VII protein secretion pathway.* J Biol Chem. 2012 Sep 14;287(38):31939-47